Universiteit
Leiden
The Netherlands

Dietary modulation of adipose tissue and cardiometabolic health

Kuipers, E.N.

Citation
Kuipers, E. N. (2019, September 25). *Dietary modulation of adipose tissue and cardiometabolic health*. Retrieved from https://hdl.handle.net/1887/78662

Version:	Publisher's Version
License:	Licence agreement concerning inclusion of doctoral thesis in the Institutional Repository of the University of Leiden
Downloaded from:	https://hdl.handle.net/1887/78662

Note: To cite this publication please use the final published version (if applicable).

Cover Page

Universiteit Leiden

The handle http://hdl.handle.net/1887/78662 holds various files of this Leiden University dissertation.

Author: Kuipers, E.N.
Title: Dietary modulation of adipose tissue and cardiometabolic health
Issue Date: 2019-09-25

DIETARY MODULATION OF ADIPOSE TISSUE AND CARDIO-METABOLIC HEALTH

Eline Kuipers

Dietary modulation of adipose tissue and cardiometabolic health

Eline N. Kuipers

Dietary modulation of adipose tissue and cardiometabolic health
©2019, Eline N. Kuipers

Cover design: Malou-Amber (www.malou-amber.com)
Layout and printed by: Optima Grafische Communicatie (www.ogc.nl)
ISBN: 978-94-6361-266-1

All rights are reserved. No part of this thesis may be transformed, reproduced or transmitted in any form and by any means without prior permission of the author.

Dietary modulation of adipose tissue and cardiometabolic health

Proefschrift

ter verkrijging van
de graad van Doctor aan de Universiteit Leiden,
op gezag van Rector Magnificus Prof. mr. C.J.J.M. Stolker,
volgens besluit van het College voor Promoties
te verdedigen op woensdag 25 september 2019
klokke 16.15 uur

door

Eline Nathalie Kuipers

geboren te Groningen
in 1990

Promotor	Prof. dr. P.C.N. Rensen
Copromotor	Dr. M.R. Boon
Leden promotiecommissie	Prof. dr. J.A.P. Willems van Dijk
	Prof. dr. M. van der Stelt
	Prof. dr. R. Shiri-Sverdlov (MUMC, Maastricht)
	Prof. dr. R.H. Houtkooper (AUMC, Amsterdam)

The work described in this thesis was performed at the Department of Medicine, Division of Endocrinology, Leiden University Medical Center, Leiden, The Netherlands, and at the Einthoven Laboratory for Experimental Vascular Medicine, Leiden, The Netherlands.

Eline Kuipers was supported by a grant of the Rembrandt Institute of Cardiovascular Science (RICS) to Riekelt H. Houtkooper and Mariëtte R. Boon.

Financial support by the Dutch Heart Foundation and the Netherlands Association for the Study of Obesity (NASO) for the publication of this thesis is gratefully acknowledged. The research described in this thesis was supported by a grant of the Dutch Heart Foundation (2014B002 CVON ENERGISE).

TABLE OF CONTENTS

CHAPTER 1	General introduction and outline	7
CHAPTER 2	Pyruvate dehydrogenase complex plays a central role in brown adipocyte energy expenditure and fuel utilization during short-term beta-adrenergic activation	25
CHAPTER 3	Generation of conditionally immortalized murine and human brown pre-adipocytes with preserved adipogenic capacity	51
CHAPTER 4	IL-37 expression reduces lean body mass in mice by reducing food intake	79
CHAPTER 5	A single day of high fat diet feeding induces lipid accumulation and insulin resistance in brown adipose tissue in mice	97
CHAPTER 6	High fat diet increases circulating endocannabinoids accompanied by increased synthesis enzymes in adipose tissue	123
CHAPTER 7	Quercetin lowers plasma triglycerides accompanied by white adipose tissue browning in diet-induced obese mice	147
CHAPTER 8	General discussion and future perspectives	171
CHAPTER 9	Addendum	199
	Summary	201
	Nederlandse samenvatting	205
	List of publications	211
	Curriculum vitae	213
	Dankwoord	215

1

GENERAL INTRODUCTION AND OUTLINE

In the ancient times, when the hunters and gatherers were living, periods of food scarcity were very common. It was, therefore, advantageous to have efficient mechanisms of energy storage in the body. After all, it was uncertain when the next meal would be available. This is in sharp contrast to the current modern 24-hour society we are currently living in with food readily available. The body has not adapted to this excessive presence of nutrients and still efficiently stores excessive energy. This increased storage of nutrients, together with the fact that we have adapted a more sedentary lifestyle, led to a dramatic increase in people suffering from obesity. The world health organization (WHO) defines overweight and obesity as having a body mass index (BMI, kg/m^2) equal or over 25 or 30, respectively. In 2015, over 600 million adults were obese world-wide. Obesity has a great impact on society as it contributes to the development of several diseases including type 2 diabetes (T2D), cardiovascular diseases, and even cancer [1]. More specifically, having a high BMI (>25) was estimated to contribute to 4 million deaths globally with cardiovascular diseases being the leading cause [2, 3]. These numbers are expected to further increase in the coming years [4, 5]. Only recently, obesity has been proposed to be a chronic relapsing disease with food being the pathological agent [6].

OBESITY: RESULT OF A POSITIVE ENERGY BALANCE

Obesity results from a long-term positive energy balance, defined as an energy imbalance, with energy intake exceeding energy expenditure. This results in excessive storage of sugar and fat in the form of triglycerides, in adipose tissue and eventually also in other organs and tissues. Triglycerides consist of three fatty acids (FA) attached to a glycerol backbone. Triglyceride-derived FA are, besides glucose, the most important energy source of our body and are transported within triglyceride-rich lipoproteins to metabolically active tissues including heart, skeletal muscle as well as white adipose tissue (WAT) and brown adipose tissue (BAT). The parenchymal cells of these tissues synthesize lipoprotein lipase (LPL) that is translocated to the luminal side of endothelial cells lining the blood vessels within tissues, and which cleaves off the FA from the triglyceride molecules. This is followed by FA uptake by FA transporters such as cluster of differentiation 36 (CD36) and FA binding protein (FABP) into (cardio)myocytes and adipocytes (**Fig. 1**). Central in the uptake of glucose and lipids is the anabolic hormone insulin, which is released by the pancreas upon a rise in plasma glucose or FA levels. For instance, insulin stimulates adipocytes to enhance translocation of LPL and glucose transporter type 4 (GLUT4) towards the cell surface and thereby increases the uptake of triglyceride-derived FA and glucose, respectively [7, 8]. Once taken up, in most cell types the FA and glucose are burnt into CO_2 to concomitantly generate the body's usable

energy source adenosine triphosphate (ATP). ATP is required for many cellular processes, such as contraction of (cardio)myocytes in heart and skeletal muscles.

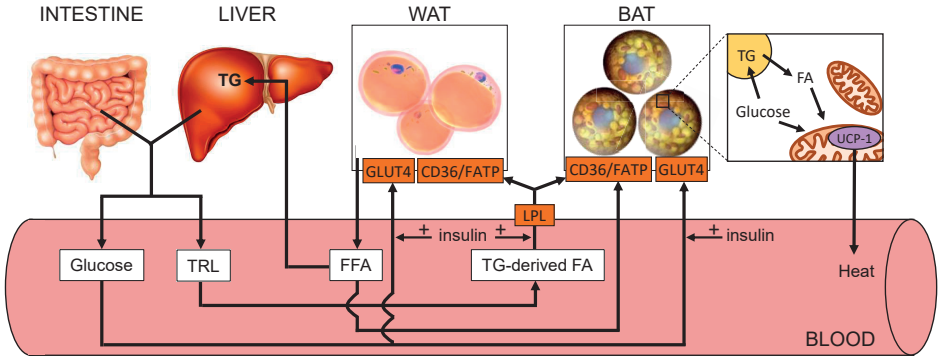

Figure 1. Schematic representation of glucose and lipid fluxes between intestine, liver, white and brown adipose tissue. See text for explanation. BAT, brown adipose tissue; CD36, cluster of differentiation 36; FA, fatty acid; FATP, fatty acid transport protein; FFA, free fatty acid; GLUT4, glucose transporter type 4; LPL, lipoprotein lipase; TG, triglyceride; TRL, triglyceride-rich lipoprotein; UCP-1, uncoupling protein-1; WAT, white adipose tissue.

TYPES OF ADIPOSE TISSUES

In case of a positive energy balance, triglycerides are primarily stored in the adipose tissue depot. White adipose tissue (WAT) is the most abundant form of adipose tissue in the body and can be divided into different subcutaneous and visceral depots [9]. Morphologically, the adipocytes within WAT are characterized by a large lipid droplet, with a few mitochondria that together with the nucleus reside in the small volume of cytoplasm that surrounds the lipid droplet. Adipose tissue is not only composed of adipocytes but also contains a so-called 'stromal-vascular fraction (SVF)' which consists of blood cells, endothelial cells and adipocyte precursor cells (pre-adipocytes) [10]. WAT plays a central role in the regulation of energy metabolism. First, WAT has the capacity to store excessive glucose and FA in the form of triglycerides *via* two processes: hyperplasia and hypertrophy. Hyperplasia involves the maturation of pre-adipocytes into mature adipocytes resulting in an increased number of adipocytes and only occurs in childhood and adolescence [11]. In fact the number of fat cells stays rather constant after the age of 20 years [11]. Hypertrophy refers to the expansion of the size of mature adipocytes, and is the process *via* which WAT stores excessive nutrients in adulthood. Thus, adipocyte number and morphology can alter in response to energy balance depending on the stage of life. Secondly, during energy shortage, the FA within stored triglycerides can be liberated from white adipocytes *via* intracellular lipolysis, using adipose triglyceride lipase (ATGL) and hormone-sensitive lipase (HSL), to fuel other organs. On the long term,

this will result in shrinkage of the adipocytes and weight loss. Besides its function in energy storage, WAT is also an important endocrine organ because it synthesizes and secretes several factors (generally called 'adipokines'), such as leptin, adiponectin, cytokines and chemokines [10]. *Via* these signals, WAT influences a range of metabolic processes like satiety, lipid and glucose homeostasis.

Besides WAT, there is also the functionally and morphologically distinct brown adipose tissue (BAT) depot. BAT is located in the interscapular and subscapular region in rodents and human babies [12] and primarily in the neck region, above the clavicles and around the aorta in human adults [13-15]. Rodent studies have shown that besides brown adipocytes in the classical depots, there are also brown-like adipocytes scattered within WAT called beige, brite or recruitable adipocytes. These beige cells tend to have low basal uncoupling protein-1 (UCP-1, function described below) expression, which however is highly induced upon activation [16]. Although several studies suggest that human BAT is mainly composed of beige adipocytes [17, 18], for simplicity it will be referred to as BAT. BAT volume in adults has been estimated to range from 50 mL to 300 mL [19], whereas WAT can comprise 20% of the total body weight [20]. In contrast to the unilocular white adipocytes, brown adipocytes possess multiple small lipid droplets and many mitochondria. In fact, the many mitochondria give BAT its brownish color. BAT is also distinct from WAT in another respect. The mitochondria of brown adipocytes contain the protein UCP-1 within their inner mitochondrial membrane, which 'uncouples' the electron transport chain from ATP synthesis. This feature enables BAT to burn FA to generate heat in a process called 'adaptive thermogenesis', described in more detail below [12]. BAT has become a 'hot' research topic since five research groups independently showed the presence of active BAT in adult humans in 2009 [13-15, 21, 22]. BAT activity, as assessed with [^{18}F]fluorodeoxyglucose positron emission tomography-computed tomography ([^{18}F]FDG PET/CT) which is the current 'gold' standard to determine BAT activity in humans, appears to be negatively associated with BMI [13]. Because of this association and BAT's capacity to take up and combust large amounts of glucose and triglyceride-derived FA from the circulation [23, 24], BAT has since been regarded as a target to combat adiposity and related diseases. Furthermore, it has become clear that alike WAT, BAT also secretes factors called 'batokines' [25] that are able to influence systemic energy metabolism. Also similar to WAT, lipid deposition within BAT increases during the development of obesity, which results in BAT whitening and BAT dysfunction [26]. This is a process that is not completely understood but may be beneficial to prevent in order to enhance the contribution of BAT to energy metabolism in obesity. To this end, more research is needed to elucidate what happens to BAT in the early stages of overweight or obesity development, which up till now is still largely unknown.

THERMOGENESIS BY BAT

Since active BAT is able to take up and combust large amounts of glucose and triglycerides from the circulation, BAT activation is regarded as a novel potential target for therapy of adiposity and related cardiometabolic disorders [27]. The physiological activator of BAT is cold, which leads to the release of the neurotransmitter norepinephrine (also called 'noradrenaline') from sympathetic nerve endings in the vicinity of brown adipocytes. Norepinephrine binds to adrenergic receptors on the cell membrane of the brown adipocytes and thereby activates an intracellular cascade of events that, amongst others, results in the liberation of FA from the intracellular lipid droplets [28]. The released FA enter the mitochondria and *via* β-oxidation generate substrates for the citric acid cycle, which in the end activate the electron transport chain to build up a proton gradient over the mitochondrial inner membrane, which normally generates ATP *via* activating ATP synthase. In brown and beige adipocytes, the presence of UCP-1 uncouples the proton gradient, resulting in heat production (**Fig. 1**) [12, 29]. Prolonged BAT activation depletes the intracellular lipid droplets from triglycerides and these therefore have to become replenished *via* the uptake of triglyceride-derived FA and glucose from the circulation [24, 30]. Again, insulin appears central in this process as insulin signaling is required for uptake of triglyceride-derived FA [31] and glucose [32] by BAT (**Fig. 1**). Liver and muscle cells are also able to oxidize glucose and FA. Energy metabolism within these cells follow the principles of Randle, where the intermediate metabolites of glucose oxidation inhibits FA oxidation and vice versa [33]. On the contrary, active BAT takes up both substrates and concomitantly activates their oxidation pathways, as well as triglyceride storage pathways [34, 35]. Therefore, it remains to be studied what the fate of these substrates is once taken up by BAT and on which substrate activated BAT primarily depends.

THE ENDOCANNABINOID SYSTEM

Adipose tissues are not the only contributors to energy balance. The brain and nervous system also vividly interact with other organs, including the heart and skeletal muscles, in order to impact on whole body metabolism. One of the best known modulators of energy balance is the endocannabinoid system (ECS) [36]. This system is comprised of the two main endocannabinoids 2-arachidonoylglycerol (2-AG) and anandamide (*N*-arachidonoyl-ethanolamine, AEA), their G protein-coupled receptors cannabinoid receptor 1 (CB1R) and 2 (CB2R), and the enzymes responsible for the endocannabinoid synthesis and degradation. The CB1R is widely expressed, including in the brain and on WAT and BAT, whereas the CB2R is primarily expressed on immune cells [37]. Activation of the

ECS results, amongst others, in increased food intake, increased motivation to consume palatable food, increased lipid accumulation in WAT, and reduced thermogenesis in BAT [36]. In obesity, circulating endocannabinoid levels have been shown to be increased, in both mice [38, 39] and humans [40, 41]. However, the specific organs that are responsible for the rise in endocannabinoid levels in obesity have not been elucidated as yet [42]. Importantly, blocking the endocannabinoid system, by using the inverse CB1R agonist rimonabant, has proven to be a very effective approach to combat obesity [43]. Obese patients who received rimonabant for 12 months showed reduced body weight, reduced waist circumference and improved blood lipid and glucose levels. However, psychiatric side effects of rimonabant, likely due to effects on the centrally located CB1R, led to the withdrawal of this drug from the market in 2008 [44]. Recently, several preclinical studies have been focusing on specifically targeting peripheral endocannabinoid receptors, to circumvent the unwanted central side effects of ECS inhibition while preserving (a part of) the beneficial metabolic effects [45-47]. Besides targeting endocannabinoid receptors, regulating local levels of endocannabinoids in the periphery by interfering with the activity of the enzymes involved in their biosynthesis and degradation is regarded a more direct approach.

METABOLIC CONSEQUENCES OF OBESITY

Storage of triglycerides in WAT is not harmful by itself, but the metabolic consequences of excessive storage in case of obesity, such as insulin resistance resulting in hyperglycemia and hyperlipidemia, ultimately leading to type 2 diabetes and cardiovascular diseases, can pose a health risk. In obesity, increased storage of lipids in white adipocytes will lead to hypertrophy, hypoxia and eventually to cell death, and subsequently to the recruitment of immune cells such as monocytes that maturate into macrophages [48]. The hypertrophic adipocytes and macrophages release the pro-inflammatory cytokines tumor necrosis factor α (TNF-α) and interleukin-6 (IL-6). These cytokines can directly interfere in the insulin signaling cascade resulting in insulin resistance [49], leading to dyslipidemia and hyperglycemia, which can contribute to the development of T2D [50]. When the adipose tissue has reached saturation of its expansion capacity, lipids will overflow and accumulate in other organs such as muscle and the liver where intracellular FA will interfere with the local insulin sensitivity [51]. Additionally, insulin resistant adipocytes have increased intracellular lipolysis, which leads to an increased flux of free FA to the liver as substrate for hepatic VLDL-triglyceride production [52]. This, together with enhanced VLDL production as a result of reduced hepatic insulin sensitivity, causes dyslipidemia [53]. The dyslipidemia is further increased by reduced VLDL catabolism

since insulin resistance reduces the expression and translocation of LPL in peripheral tissues [54].

Several studies suggest that, besides elevated circulating levels of low-density lipoprotein (LDL), elevated levels of remnants of triglyceride-rich lipoproteins (*i.e.* chylomicrons and VLDL), are a risk factor for atherosclerosis [55, 56]. Both the uptake of triglyceride-derived FA from the circulation by LPL expressing organs and exchange of triglycerides from VLDL with cholesteryl esters from high-density lipoproteins (HDL) by the action of the cholesteryl ester transfer protein (CETP) results in the formation of atherogenic cholesterol-enriched particles [57]. Atherosclerosis development is initiated by local inflammation and the retention of pro-atherogenic cholesterol-rich lipoproteins, for which triglyceride-rich lipoproteins are precursors, in the vessel wall. In more detail, monocytes are recruited from the circulation, which thereby differentiate into macrophages. Macrophages scavenge oxidatively modified and aggregated lipoproteins thereby turning into foam cells, which augment the inflammatory response. The atherosclerotic plaque grows because of further recruitment of immune cells and increased deposition of cholesterol within macrophages in the vessel wall [58-60]. Eventually, the plaque can rupture, resulting in formation of a thrombus that can occlude vessels that provide oxygen to *e.g.* the heart or brain, leading to a cardiovascular event, *i.e.* myocardial infarction or stroke, respectively.

Taken together, the adverse cardiometabolic consequences of excessive storage of lipids in WAT and lipid deposition in other organs shows that research should focus on developing therapeutic strategies to prevent and treat these unbeneficial metabolic effects.

THERAPEUTIC STRATEGIES TO COMBAT OBESITY AND RELATED METABOLIC DISORDERS

Current treatment strategies

Since obesity results from a long term positive energy balance, therapeutic strategies aim to tilt the balance in the opposite direction by decreasing energy intake and/or increasing energy expenditure. Current treatment options that have proven to be effective in obesity can be subdivided into lifestyle intervention, pharmacotherapy and bariatric surgery [61]. Although lifestyle interventions that are aimed at decreasing dietary intake in combination with enhancing physical activity are effective on the short term, the adherence of patients is very low with drop-out rates of participants up to 80% [62]. With respect to pharmacotherapy, the most widely prescribed weight-management medication, at least in the US, is phentermine, a norepinephrine-releasing agent that primarily suppresses food intake. Also the glucagon-like peptide-1 (GLP-1) analogue liraglutide,

which is widely prescribed for the treatment of T2D, has been approved by the FDA as an anti-obesity drug because of its favorable satiety profile [63, 64]. Orlistat, a pancreatic lipase inhibitor that reduces the uptake of fat by the intestine, is commonly used in Europe [65]. Although phentermine, liraglutide and orlistat are effective in inducing weight loss, use of either therapeutic is often reported to cause adverse events [66]. The third and most effective method to treat obesity, albeit with higher risk and selective eligibility, is bariatric surgery. This procedure aims at reducing the size of the stomach and in the case of gastric bypass surgery also partly bypassing the small intestines [61]. Taken together, current treatment methods are either not effective on the long-term, often cause adverse events or are invasive.

Brown(ing) adipose tissue

As outlined above, both preclinical and clinical studies indicate a pivotal role for BAT in whole-body metabolism. Rodent studies have shown that BAT activation increases energy expenditure and whole-body insulin sensitivity, and decreases fat mass, plasma lipid levels and atherosclerosis development [24, 57]. Moreover, increasing whole body BAT mass in mice, by performing BAT transplantation, improves glucose tolerance and causes a complete reversal of high-fat diet-induced insulin resistance [67]. In humans, cold exposure increases BAT activity, as measured by increased uptake of [^{18}F]FDG by PET/CT, increases energy expenditure in lean [68] and obese individuals [69] and even decreases fat mass in healthy lean participants [68]. Moreover, cold exposure increases insulin sensitivity in healthy individuals [70] and in patients with T2D [71]. Besides activating the classical BAT depots, cold exposure also induces the expression of beige adipocyte markers in WAT in mice [72] and humans [73]. In addition, pharmacological agents, *via* enhancing sympathetic outflow (*i.e.* centrally mediated) or *via* direct activation of adipocytes (*e.g.* adrenergic receptor agonists and agents that enhance NO availability) are being studied for their potency to activate BAT and/or induce browning of WAT [19, 74]. Taken together, these studies indicate the potential of BAT activation and browning of WAT in the search for novel strategies to combat obesity and its related disorders by increasing energy expenditure.

Anti-inflammatory agents

Because of the profound link between inflammation, obesity and T2D, anti-inflammatory agents are extensively studied for their therapeutic effectiveness to treat these diseases. Salsalate, an anti-inflammatory drug belonging to the salicylate class of drugs, is applied in the clinic to treat pain and inflammation caused by rheumatoid arthritis (RA). Interestingly, salsalate improves glucose and lipid homeostasis in T2D patients [75] and increases energy expenditure in healthy subjects [76]. Moreover, salsalate also activates BAT as shown in mice [77]. Thus, targeting inflammation might also have beneficial

effects on BAT and/or browning [78]. Whereas salsalate inhibits the transcription of many inflammatory cytokines, other therapeutics target the functionality of specific circulating pro-inflammatory cytokines. Approaches targeting TNF-α and IL-6 have been extensively studied in the context of insulin resistance with controversial results [79]. In contrast to the numerous studies on the role and therapeutic potential of inhibiting pro-inflammatory cytokines [79], the potential application of anti-inflammatory cytokines such as interleukin-37 (IL-37) are still underexplored. Interestingly, mice with transgenic IL-37 expression were shown to be protected from diet-induced obesity and obesity-associated inflammation and insulin resistance [80]. However, the precise mechanism of action leading to these beneficial metabolic effects is not entirely known and requires further study.

Dietary compounds

A more recent research topic in the search for therapeutic strategies to combat obesity is the application of dietary components. There is a variety of dietary components that exert beneficial effects on plasma lipid and glucose levels and that are able to activate BAT and/or increase browning of WAT [81]. Polyphenols are the most extensively studied dietary components and these can be found in, amongst others, fruits and vegetables [82]. For instance, the polyphenol capsaicin activates transient receptor potential vanilloid channel 1 (TRPV1), which is present on many metabolic tissues, and thereby increases fat oxidation, improves insulin sensitivity and decreases body fat mass in animal models [83]. Moreover, capsaicin has been shown to activate BAT in mice and men [19]. Another well-studied polyphenol is resveratrol which has been shown to induce browning in obese mice [84], and to improve lipid metabolism and reduce atherosclerosis in hypercholesterolemic mice [85]. Although clinical studies into the beneficial metabolic effects of resveratrol are less consistent, trials with T2D patients imply an anti-diabetic effect of resveratrol [86]. Finally, quercetin, which belongs to the polyphenol subclass of flavonoids, has been shown to attenuate body weight [87] and lipid deposition in WAT [88] in rodents on a high-fat diet. Moreover, dietary quercetin supplementation lowers plasma triglyceride levels in mice [89] and in humans [90]. Of note, recent *in vitro* experiments showed that quercetin induces browning of white adipocytes [91]. However, the mechanism behind the triglyceride-lowering effect of quercetin, including a potential role for browning, remains to be studied.

OUTLINE OF THIS THESIS

As is evident from this chapter (**Chapter 1**), obesity and its related T2D and cardiovascular diseases are multifactorial diseases that form a great health risk. Obesity results

from a long-term energy imbalance, where energy intake exceeds expenditure. Current methods to treat obesity are either not effective on the long term or are invasive with a relatively high risk as with bariatric surgery. Increasing energy expenditure *via* activation of BAT seems a promising novel tool. A better understanding of the pathophysiology of diet-induced obesity on BAT function and whole body metabolism is thus a prerequisite for the development of novel compounds that would activate BAT and thereby target these metabolic pathologies. Therefore, we aimed to address four key objectives in this thesis: 1) to generate *in vitro* brown adipocyte models for mice and humans to study and better understand brown adipocyte metabolism and potential species differences, 2) to gain more insight into the effect and underlying mechanisms of the anti-inflammatory cytokine IL-37 on the energy balance, 3) to study the effect of diet-induced obesity on BAT function and the ECS, and 4) to study the therapeutic potential of the dietary compound quercetin on triglyceride metabolism, with emphasis on BAT and WAT.

To address the first key objective, we used an already available murine brown adipocyte cell line (T37i) and generated new immortalized murine and human brown preadipocyte cell lines. Since activated BAT is thought to primarily burn FA to produce heat, while taking up glucose, free FA and triglyceride-derived FA from the circulation, the fate of these substrates within the adipocytes has not entirely been elucidated. Therefore, the aim of **Chapter 2** was to assess the effect of β3-adrenergic receptor activation on metabolic fluxes in T37i murine brown adipocytes. Current cell culture models for brown adipocytes constitutively express oncoproteins that drive proliferation that at the same time might inhibit differentiation capacity. To overcome this caveat, in **Chapter 3** we aimed to generate murine and human brown preadipocyte cell lines that were conditionally immortalized, to relieve these cells from oncoprotein expression during differentiation.

Inflammation plays an important role in the development of obesity-induced insulin resistance. Research has primarily focused on the role of pro-inflammatory cytokines in this pathophysiology and only recently attention was drawn to the anti-inflammatory cytokine IL-37. IL-37 transgenic mice have been shown to be protected from obesity and obesity-associated inflammation and insulin resistance. However, the mechanism behind the beneficial metabolic effects of IL-37 was not entirely known. In **Chapter 4**, to address key objective 2, we therefore studied the effect IL-37 on the energy balance in more detail.

To meet our third objective, we performed two studies in which mice were fed a high-fat diet in order to study the pathophysiology of diet-induced obesity on BAT and the ECS. Long-term high-fat diet feeding leads to whitening and dysfunctional BAT. However what happens to BAT on a short-term of high-fat diet feeding, and thus what the sequence of events is that causes BAT dysfunction on the long-term is unknown. In **Chapter 5** we aimed to determine how rapid BAT dysfunction occurs upon high-fat diet feeding and what the related mechanisms are. The ECS is seen as a potential therapeutic

target since its tone is elevated in obesity. However, more insight is needed in how fast and in which organs the dysregulation of the ECS sets off, in order to be able to develop novel and more specific therapeutics. In **Chapter 6** we investigated the circulating endocannabinoid levels and the gene expression of enzymes involved in endocannabinoid synthesis and degradation in several metabolic tissues of mice that were fed a high-fat diet ranging from one day up to 18 weeks.

Although the pathophysiology of dyslipidemia in obesity is multifactorial, the hallmark of dyslipidemia in obesity is elevated plasma triglyceride levels [53]. Quercetin has been shown to reduce plasma triglyceride levels in mice and humans, whereas the mechanism remained elusive. To meet our last key objective, we investigated the underlying mechanism for the quercetin-induced lowering of plasma triglycerides in **Chapter 7**.

Finally, the results from these studies and their implications will be discussed in **Chapter 8**.

REFERENCES

1. Knight, J. A. Diseases and disorders associated with excess body weight. *Ann Clin Lab Sci* **2011**, 41, (2), 107-21.
2. The GBD 2015 Obesity Collaborators Health Effects of Overweight and Obesity in 195 Countries over 25 Years. *N Engl J Med* **2017**, 377, (1), 13-27.
3. http://www.who.int/features/factfiles/obesity/en/.
4. Finkelstein, E. A.; Khavjou, O. A.; Thompson, H.; Trogdon, J. G.; Pan, L.; Sherry, B.; Dietz, W. Obesity and severe obesity forecasts through 2030. *Am J Prev Med* **2012**, 42, (6), 563-70.
5. Preston, S. H.; Stokes, A.; Mehta, N. K.; Cao, B. Projecting the effect of changes in smoking and obesity on future life expectancy in the United States. *Demography* **2014**, 51, (1), 27-49.
6. Bray, G. A.; Kim, K. K.; Wilding, J. P. H. Obesity: a chronic relapsing progressive disease process. A position statement of the World Obesity Federation. *Obes Rev* **2017**, 18, (7), 715-723.
7. Goldberg, I. J.; Eckel, R. H.; Abumrad, N. A. Regulation of fatty acid uptake into tissues: lipoprotein lipase- and CD36-mediated pathways. *J Lipid Res* **2009**, 50 Suppl, S86-90.
8. Furtado, L. M.; Somwar, R.; Sweeney, G.; Niu, W.; Klip, A. Activation of the glucose transporter GLUT4 by insulin. *Biochem Cell Biol* **2002**, 80, (5), 569-78.
9. Cinti, S. The adipose organ. *Prostaglandins Leukot Essent Fatty Acids* **2005**, 73, (1), 9-15.
10. Coelho, M.; Oliveira, T.; Fernandes, R. Biochemistry of adipose tissue: an endocrine organ. *Arch Med Sci* **2013**, 9, (2), 191-200.
11. Spalding, K. L.; Arner, E.; Westermark, P. O.; Bernard, S.; Buchholz, B. A.; Bergmann, O.; Blomqvist, L.; Hoffstedt, J.; Naslund, E.; Britton, T., et al. Dynamics of fat cell turnover in humans. *Nature* **2008**, 453, (7196), 783-7.
12. Cannon, B.; Nedergaard, J. Brown adipose tissue: function and physiological significance. *Physiol Rev* **2004**, 84, (1), 277-359.
13. van Marken Lichtenbelt, W. D.; Vanhommerig, J. W.; Smulders, N. M.; Drossaerts, J. M.; Kemerink, G. J.; Bouvy, N. D.; Schrauwen, P.; Teule, G. J. Cold-activated brown adipose tissue in healthy men. *N Engl J Med* **2009**, 360, (15), 1500-8.
14. Cypess, A. M.; Lehman, S.; Williams, G.; Tal, I.; Rodman, D.; Goldfine, A. B.; Kuo, F. C.; Palmer, E. L.; Tseng, Y. H.; Doria, A., et al. Identification and importance of brown adipose tissue in adult humans. *N Engl J Med* **2009**, 360, (15), 1509-17.
15. Virtanen, K. A.; Lidell, M. E.; Orava, J.; Heglind, M.; Westergren, R.; Niemi, T.; Taittonen, M.; Laine, J.; Savisto, N. J.; Enerback, S., et al. Functional brown adipose tissue in healthy adults. *N Engl J Med* **2009**, 360, (15), 1518-25.
16. Chechi, K.; van Marken Lichtenbelt, W.; Richard, D. Brown and beige adipose tissues: phenotype and metabolic potential in mice and men. *J Appl Physiol (1985)* **2018**, 124, (2), 482-496.
17. Xue, R.; Lynes, M. D.; Dreyfuss, J. M.; Shamsi, F.; Schulz, T. J. Clonal analyses and gene profiling identify genetic biomarkers of the thermogenic potential of human brown and white preadipocytes. *Nat Med* **2015**, 21, (7), 760-8.
18. Shinoda, K.; Luijten, I. H.; Hasegawa, Y.; Hong, H.; Sonne, S. B.; Kim, M.; Xue, R.; Chondronikola, M.; Cypess, A. M.; Tseng, Y. H., et al. Genetic and functional characterization of clonally derived adult human brown adipocytes. *Nat Med* **2015**, 21, (4), 389-94.
19. Ruiz, J. R.; Martinez-Tellez, B.; Sanchez-Delgado, G.; Osuna-Prieto, F. J.; Rensen, P. C. N.; Boon, M. R. Role of Human Brown Fat in Obesity, Metabolism and Cardiovascular

Disease: Strategies to Turn Up the Heat. *Prog Cardiovasc Dis* **2018**, 61, (2), 232-245.
20. Boon, M. R.; Bakker, L. E.; Meinders, A. E.; van Marken Lichtenbelt, W.; Rensen, P. C.; Jazet, I. M. [Brown adipose tissue: the body's own weapon against obesity?]. *Ned Tijdschr Geneeskd* **2013**, 157, (20), A5502.
21. Zingaretti, M. C.; Crosta, F.; Vitali, A.; Guerrieri, M.; Frontini, A.; Cannon, B.; Nedergaard, J.; Cinti, S. The presence of UCP1 demonstrates that metabolically active adipose tissue in the neck of adult humans truly represents brown adipose tissue. *FASEB J* **2009**, 23, (9), 3113-20.
22. Saito, M.; Okamatsu-Ogura, Y.; Matsushita, M.; Watanabe, K.; Yoneshiro, T.; Nio-Kobayashi, J.; Iwanaga, T.; Miyagawa, M.; Kameya, T.; Nakada, K., et al. High incidence of metabolically active brown adipose tissue in healthy adult humans: effects of cold exposure and adiposity. *Diabetes* **2009**, 58, (7), 1526-31.
23. Khedoe, P. P.; Hoeke, G.; Kooijman, S.; Dijk, W.; Buijs, J. T.; Kersten, S.; Havekes, L. M.; Hiemstra, P. S.; Berbee, J. F.; Boon, M. R., et al. Brown adipose tissue takes up plasma triglycerides mostly after lipolysis. *J Lipid Res* **2015**, 56, (1), 51-9.
24. Bartelt, A.; Bruns, O. T.; Reimer, R.; Hohenberg, H.; Ittrich, H.; Peldschus, K.; Kaul, M. G.; Tromsdorf, U. I.; Weller, H.; Waurisch, C., et al. Brown adipose tissue activity controls triglyceride clearance. *Nat Med* **2011**, 17, (2), 200-5.
25. Villarroya, F.; Cereijo, R.; Villarroya, J.; Giralt, M. Brown adipose tissue as a secretory organ. *Nat Rev Endocrinol* **2017**, 13, (1), 26-35.
26. Shimizu, I.; Aprahamian, T.; Kikuchi, R.; Shimizu, A.; Papanicolaou, K. N.; MacLauchlan, S.; Maruyama, S.; Walsh, K. Vascular rarefaction mediates whitening of brown fat in obesity. *J Clin Invest* **2014**, 124, (5), 2099-112.
27. Poher, A. L.; Altirriba, J.; Veyrat-Durebex, C.; Rohner-Jeanrenaud, F. Brown adipose tissue activity as a target for the treatment of obesity/insulin resistance. *Front Physiol* **2015**, 6, 4.
28. Townsend, K. L.; Tseng, Y. H. Brown fat fuel utilization and thermogenesis. *Trends Endocrinol Metab* **2014**, 25, (4), 168-77.
29. Fedorenko, A.; Lishko, P. V.; Kirichok, Y. Mechanism of fatty-acid-dependent UCP1 uncoupling in brown fat mitochondria. *Cell* **2012**, 151, (2), 400-13.
30. Hoeke, G.; Kooijman, S.; Boon, M. R.; Rensen, P. C.; Berbee, J. F. Role of Brown Fat in Lipoprotein Metabolism and Atherosclerosis. *Circ Res* **2016**, 118, (1), 173-82.
31. Heine, M.; Fischer, A. W.; Schlein, C.; Jung, C.; Straub, L. G.; Gottschling, K.; Mangels, N.; Yuan, Y.; Nilsson, S. K.; Liebscher, G., et al. Lipolysis Triggers a Systemic Insulin Response Essential for Efficient Energy Replenishment of Activated Brown Adipose Tissue in Mice. *Cell Metab* **2018**, 28, (4), 644-655.e4.
32. Roberts-Toler, C.; O'Neill, B. T.; Cypess, A. M. Diet-induced obesity causes insulin resistance in mouse brown adipose tissue. *Obesity (Silver Spring)* **2015**, 23, (9), 1765-70.
33. Hue, L.; Taegtmeyer, H. The Randle cycle revisited: a new head for an old hat. *Am J Physiol Endocrinol Metab* **2009**, 297, (3), E578-91.
34. Labbe, S. M.; Caron, A.; Bakan, I.; Laplante, M.; Carpentier, A. C.; Lecomte, R.; Richard, D. In vivo measurement of energy substrate contribution to cold-induced brown adipose tissue thermogenesis. *FASEB J* **2015**, 29, (5), 2046-58.
35. Yu, X. X.; Lewin, D. A.; Forrest, W.; Adams, S. H. Cold elicits the simultaneous induction of fatty acid synthesis and beta-oxidation in murine brown adipose tissue: prediction from differential gene expression and confirmation in vivo. *FASEB J* **2002**, 16, (2), 155-68.
36. Mazier, W.; Saucisse, N.; Gatta-Cherifi, B.; Cota, D. The Endocannabinoid System: Pivotal Orchestrator of Obesity and Metabolic

Disease. *Trends Endocrinol Metab* **2015**, 26, (10), 524-37.

37. Cota, D. CB1 receptors: emerging evidence for central and peripheral mechanisms that regulate energy balance, metabolism, and cardiovascular health. *Diabetes Metab Res Rev* **2007**, 23, (7), 507-17.
38. D'Eon, T. M.; Pierce, K. A.; Roix, J. J.; Tyler, A.; Chen, H.; Teixeira, S. R. The role of adipocyte insulin resistance in the pathogenesis of obesity-related elevations in endocannabinoids. *Diabetes* **2008**, 57, (5), 1262-8.
39. Pati, S.; Krishna, S.; Lee, J. H.; Ross, M. K.; de La Serre, C. B.; Harn, D. A., Jr.; Wagner, J. J.; Filipov, N. M.; Cummings, B. S. Effects of high-fat diet and age on the blood lipidome and circulating endocannabinoids of female C57BL/6 mice. *Biochim Biophys Acta* **2018**, 1863, (1), 26-39.
40. Bluher, M.; Engeli, S.; Kloting, N.; Berndt, J.; Fasshauer, M.; Batkai, S.; Pacher, P.; Schon, M. R.; Jordan, J.; Stumvoll, M. Dysregulation of the peripheral and adipose tissue endocannabinoid system in human abdominal obesity. *Diabetes* **2006**, 55, (11), 3053-60.
41. Engeli, S.; Bohnke, J.; Feldpausch, M.; Gorzelniak, K.; Janke, J.; Batkai, S.; Pacher, P.; Harvey-White, J.; Luft, F. C.; Sharma, A. M., et al. Activation of the peripheral endocannabinoid system in human obesity. *Diabetes* **2005**, 54, (10), 2838-43.
42. Hillard, C. J. Circulating Endocannabinoids: From Whence Do They Come and Where are They Going? *Neuropsychopharmacology* **2018**, 43, (1), 155-172.
43. Despres, J. P.; Golay, A.; Sjostrom, L. Effects of rimonabant on metabolic risk factors in overweight patients with dyslipidemia. *N Engl J Med* **2005**, 353, (20), 2121-34.
44. Sam, A. H.; Salem, V.; Ghatei, M. A. Rimonabant: From RIO to Ban. *J Obes* **2011**, 2011, 432607.
45. Boon, M. R.; Kooijman, S.; van Dam, A. D.; Pelgrom, L. R.; Berbee, J. F.; Visseren, C. A.; van Aggele, R. C.; van den Hoek, A. M.; Sips, H. C.; Lombes, M., et al. Peripheral cannabinoid 1 receptor blockade activates brown adipose tissue and diminishes dyslipidemia and obesity. *FASEB J* **2014**, 28, (12), 5361-75.
46. Argueta, D. A.; DiPatrizio, N. V. Peripheral endocannabinoid signaling controls hyperphagia in western diet-induced obesity. *Physiol Behav* **2017**, 171, 32-39.
47. Tam, J.; Cinar, R.; Liu, J.; Godlewski, G.; Wesley, D.; Jourdan, T.; Szanda, G.; Mukhopadhyay, B.; Chedester, L.; Liow, J. S., et al. Peripheral cannabinoid-1 receptor inverse agonism reduces obesity by reversing leptin resistance. *Cell Metab* **2012**, 16, (2), 167-79.
48. Kalupahana, N. S.; Moustaid-Moussa, N.; Claycombe, K. J. Immunity as a link between obesity and insulin resistance. *Mol Aspects Med* **2012**, 33, (1), 26-34.
49. Dandona, P.; Aljada, A.; Bandyopadhyay, A. Inflammation: the link between insulin resistance, obesity and diabetes. *Trends Immunol* **2004**, 25, (1), 4-7.
50. Wellen, K. E.; Hotamisligil, G. S. Inflammation, stress, and diabetes. *J Clin Invest* **2005**, 115, (5), 1111-9.
51. Tchernof, A.; Despres, J. P. Pathophysiology of human visceral obesity: an update. *Physiol Rev* **2013**, 93, (1), 359-404.
52. Olefsky, J. M.; Glass, C. K. Macrophages, inflammation, and insulin resistance. *Annu Rev Physiol* **2010**, 72, 219-46.
53. Klop, B.; Elte, J. W.; Cabezas, M. C. Dyslipidemia in obesity: mechanisms and potential targets. *Nutrients* **2013**, 5, (4), 1218-40.
54. Schofield, J. D.; Liu, Y.; Rao-Balakrishna, P.; Malik, R. A.; Soran, H. Diabetes Dyslipidemia. *Diabetes Ther* **2016**, 7, (2), 203-19.
55. Kannel, W. B.; Vasan, R. S. Triglycerides as vascular risk factors: new epidemiologic insights. *Curr Opin Cardiol* **2009**, 24, (4), 345-50.
56. Nordestgaard, B. G.; Varbo, A. Triglycerides and cardiovascular disease. *Lancet* **2014**, 384, (9943), 626-635.

57. Berbee, J. F.; Boon, M. R.; Khedoe, P. P.; Bartelt, A.; Schlein, C.; Worthmann, A.; Kooijman, S.; Hoeke, G.; Mol, I. M.; John, C., et al. Brown fat activation reduces hypercholesterolaemia and protects from atherosclerosis development. *Nat Commun* **2015**, 6, 6356.
58. Libby, P. Inflammation in atherosclerosis. *Nature* **2002**, 420, (6917), 868-74.
59. Schaftenaar, F.; Frodermann, V.; Kuiper, J.; Lutgens, E. Atherosclerosis: the interplay between lipids and immune cells. *Curr Opin Lipidol* **2016**, 27, (3), 209-15.
60. Steinberg, D. Atherogenesis in perspective: hypercholesterolemia and inflammation as partners in crime. *Nat Med* **2002**, 8, (11), 1211-7.
61. Heymsfield, S. B.; Wadden, T. A. Mechanisms, Pathophysiology, and Management of Obesity. *N Engl J Med* **2017**, 376, (3), 254-266.
62. Moroshko, I.; Brennan, L.; O'Brien, P. Predictors of dropout in weight loss interventions: a systematic review of the literature. *Obes Rev* **2011**, 12, (11), 912-34.
63. Isaacs, D.; Prasad-Reddy, L.; Srivastava, S. B. Role of glucagon-like peptide 1 receptor agonists in management of obesity. *Am J Health Syst Pharm* **2016**, 73, (19), 1493-507, 10.2146/ajhp150990.
64. Brown, E.; Cuthbertson, D. J.; Wilding, J. P. Newer GLP-1 receptor agonists and obesity-diabetes. *Peptides* **2018**, 100, 61-67.
65. Yumuk, V.; Tsigos, C.; Fried, M.; Schindler, K.; Busetto, L.; Micic, D.; Toplak, H. European Guidelines for Obesity Management in Adults. *Obes Facts* **2015**, 8, (6), 402-24.
66. Yanovski, S. Z.; Yanovski, J. A. Long-term drug treatment for obesity: a systematic and clinical review. *JAMA* **2014**, 311, (1), 74-86.
67. Stanford, K. I.; Middelbeek, R. J.; Townsend, K. L.; An, D.; Nygaard, E. B.; Hitchcox, K. M.; Markan, K. R.; Nakano, K.; Hirshman, M. F.; Tseng, Y. H., et al. Brown adipose tissue regulates glucose homeostasis and insulin sensitivity. *J Clin Invest* **2013**, 123, (1), 215-23.
68. Yoneshiro, T.; Aita, S.; Matsushita, M.; Kayahara, T.; Kameya, T.; Kawai, Y.; Iwanaga, T.; Saito, M. Recruited brown adipose tissue as an antiobesity agent in humans. *J Clin Invest* **2013**, 123, (8), 3404-8.
69. Hanssen, M. J.; van der Lans, A. A.; Brans, B.; Hoeks, J.; Jardon, K. M.; Schaart, G.; Mottaghy, F. M.; Schrauwen, P.; van Marken Lichtenbelt, W. D. Short-term Cold Acclimation Recruits Brown Adipose Tissue in Obese Humans. *Diabetes* **2016**, 65, (5), 1179-89.
70. Chondronikola, M.; Volpi, E.; Borsheim, E.; Porter, C.; Annamalai, P.; Enerback, S.; Lidell, M. E.; Saraf, M. K.; Labbe, S. M.; Hurren, N. M., et al. Brown adipose tissue improves whole-body glucose homeostasis and insulin sensitivity in humans. *Diabetes* **2014**, 63, (12), 4089-99.
71. Hanssen, M. J.; Hoeks, J.; Brans, B.; van der Lans, A. A.; Schaart, G.; van den Driessche, J. J.; Jorgensen, J. A.; Boekschoten, M. V.; Hesselink, M. K.; Havekes, B., et al. Short-term cold acclimation improves insulin sensitivity in patients with type 2 diabetes mellitus. *Nat Med* **2015**, 21, (8), 863-5.
72. Igarashi, Y.; Nawaz, A.; Kado, T.; Bilal, M.; Kuwano, T.; Yamamoto, S.; Sasahara, M.; Jiuxiang, X.; Inujima, A.; Koizumi, K., et al. Partial depletion of CD206-positive M2-like macrophages induces proliferation of beige progenitors and enhances browning after cold stimulation. *Sci Rep* **2018**, 8, (1), 14567.
73. Finlin, B. S.; Memetimin, H.; Confides, A. L.; Kasza, I.; Zhu, B.; Vekaria, H. J.; Harfmann, B.; Jones, K. A.; Johnson, Z. R.; Westgate, P. M., et al. Human adipose beiging in response to cold and mirabegron. *JCI Insight* **2018**, 3, (15).
74. Villarroya, F.; Vidal-Puig, A. Beyond the sympathetic tone: the new brown fat activators. *Cell Metab* **2013**, 17, (5), 638-43.

75. Goldfine, A. B.; Silver, R.; Aldhahi, W.; Cai, D.; Tatro, E.; Lee, J.; Shoelson, S. E. Use of salsalate to target inflammation in the treatment of insulin resistance and type 2 diabetes. *Clin Transl Sci* **2008**, 1, (1), 36-43.
76. Meex, R. C.; Phielix, E.; Moonen-Kornips, E.; Schrauwen, P.; Hesselink, M. K. Stimulation of human whole-body energy expenditure by salsalate is fueled by higher lipid oxidation under fasting conditions and by higher oxidative glucose disposal under insulin-stimulated conditions. *J Clin Endocrinol Metab* **2011**, 96, (5), 1415-23.
77. van Dam, A. D.; Nahon, K. J.; Kooijman, S.; van den Berg, S. M.; Kanhai, A. A.; Kikuchi, T.; Heemskerk, M. M.; van Harmelen, V.; Lombes, M.; van den Hoek, A. M., et al. Salsalate activates brown adipose tissue in mice. *Diabetes* **2015**, 64, (5), 1544-54.
78. van den Berg, S. M.; van Dam, A. D.; Rensen, P. C.; de Winther, M. P.; Lutgens, E. Immune Modulation of Brown(ing) Adipose Tissue in Obesity. *Endocr Rev* **2017**, 38, (1), 46-68.
79. Esser, N.; Paquot, N.; Scheen, A. J. Anti-inflammatory agents to treat or prevent type 2 diabetes, metabolic syndrome and cardiovascular disease. *Expert Opin Investig Drugs* **2015**, 24, (3), 283-307.
80. Ballak, D. B.; van Diepen, J. A.; Moschen, A. R.; Jansen, H. J.; Hijmans, A.; Groenhof, G. J.; Leenders, F.; Bufler, P.; Boekschoten, M. V.; Muller, M., et al. IL-37 protects against obesity-induced inflammation and insulin resistance. *Nat Commun* **2014**, 5, 4711.
81. Mele, L.; Bidault, G.; Mena, P.; Crozier, A.; Brighenti, F.; Vidal-Puig, A.; Del Rio, D. Dietary (Poly)phenols, Brown Adipose Tissue Activation, and Energy Expenditure: A Narrative Review. *Adv Nutr* **2017**, 8, (5), 694-704.
82. Cherniack, E. P. Polyphenols: planting the seeds of treatment for the metabolic syndrome. *Nutrition* **2011**, 27, (6), 617-23.
83. Panchal, S. K.; Bliss, E.; Brown, L. Capsaicin in Metabolic Syndrome. *Nutrients* **2018**, 10, (5).
84. Wang, S.; Liang, X.; Yang, Q.; Fu, X.; Rogers, C. J.; Zhu, M.; Rodgers, B. D.; Jiang, Q.; Dodson, M. V.; Du, M. Resveratrol induces brown-like adipocyte formation in white fat through activation of AMP-activated protein kinase (AMPK) alpha1. *Int J Obes (Lond)* **2015**, 39, (6), 967-76.
85. Berbee, J. F.; Wong, M. C.; Wang, Y.; van der Hoorn, J. W.; Khedoe, P. P.; van Klinken, J. B.; Mol, I. M.; Hiemstra, P. S.; Tsikas, D.; Romijn, J. A., et al. Resveratrol protects against atherosclerosis, but does not add to the antiatherogenic effect of atorvastatin, in APOE*3-Leiden.CETP mice. *J Nutr Biochem* **2013**, 24, (8), 1423-30.
86. de Ligt, M.; Timmers, S.; Schrauwen, P. Resveratrol and obesity: Can resveratrol relieve metabolic disturbances? *Biochim Biophys Acta* **2015**, 1852, (6), 1137-44.
87. Kobori, M.; Masumoto, S.; Akimoto, Y.; Oike, H. Chronic dietary intake of quercetin alleviates hepatic fat accumulation associated with consumption of a Western-style diet in C57/BL6J mice. *Mol Nutr Food Res* **2011**, 55, (4), 530-40.
88. Panchal, S. K.; Poudyal, H.; Brown, L. Quercetin ameliorates cardiovascular, hepatic, and metabolic changes in diet-induced metabolic syndrome in rats. *J Nutr* **2012**, 142, (6), 1026-32.
89. Hoek-van den Hil, E. F.; Keijer, J.; Bunschoten, A.; Vervoort, J. J.; Stankova, B.; Bekkenkamp, M.; Herreman, L.; Venema, D.; Hollman, P. C.; Tvrzicka, E., et al. Quercetin induces hepatic lipid omega-oxidation and lowers serum lipid levels in mice. *PLoS One* **2013**, 8, (1), e51588.
90. Sahebkar, A. Effects of quercetin supplementation on lipid profile: A systematic review and meta-analysis of randomized controlled trials. *Crit Rev Food Sci Nutr* **2017**, 57, (4), 666-676.
91. Lee, S. G.; Parks, J. S.; Kang, H. W. Quercetin, a functional compound of onion peel, remodels white adipocytes to brown-like adipocytes. *J Nutr Biochem* **2017**, 42, 62-71.

2

PYRUVATE DEHYDROGENASE COMPLEX PLAYS A CENTRAL ROLE IN BROWN ADIPOCYTE ENERGY EXPENDITURE AND FUEL UTILIZATION DURING SHORT-TERM BETA-ADRENERGIC ACTIVATION

Eline N. Kuipers*, Ntsiki M. Held*, Michel van Weeghel, Jan Bert van Klinken, Simone W. Denis, Marc Lombès, Ronald J. Wanders, Frédéric M. Vaz, Patrick C.N. Rensen, Arthur J. Verhoeven, Mariëtte R. Boon, Riekelt H. Houtkooper

Scientific Reports (2018); 22: 9562

ABSTRACT

Activation of brown adipose tissue (BAT) contributes to total body energy expenditure through energy dissipation as heat. Activated BAT increases the clearance of lipids and glucose from the circulation, but how BAT accommodates large influx of multiple substrates is not well defined. The purpose of this work was to assess the metabolic fluxes in brown adipocytes during β3-adrenergic receptor (β3-AR) activation.T37i murine preadipocytes were differentiated into brown adipocytes and we used Seahorse respirometry employing a set of specific substrate inhibitors in the presence or absence of β3-AR agonist CL316,243. The main substrate used by these brown adipocytes were fatty acids, which were oxidized equally during activation as well as during resting condition. [U-^{13}C]-glucose tracer-based metabolomics revealed that the flux through the TCA cycle was enhanced and regulated by pyruvate dehydrogenase (PDH) activity. Based on ^{13}C-tracer incorporation in lipids, it appeared that most glucose was oxidized *via* TCA cycle activity, while some was utilized for glycerol-3-phosphate synthesis to replenish the triglyceride pool. Collectively, we show that while fatty acids are the main substrates for oxidation, glucose is also oxidized to meet the increased energy demand during short term β3-AR activation. PDH plays an important role in directing glucose carbons towards oxidation.

INTRODUCTION

One of the major health threats of today's society is obesity. Obesity develops as a consequence of a long-term positive energy balance and is associated with the onset and progression of dyslipidaemia, type 2 diabetes, cardiovascular disease, and certain types of cancer [1]. Brown adipose tissue (BAT) in adult humans is involved in non-shivering thermogenesis and thereby contributes to whole body energy expenditure [2–5]. The functional relevance of BAT activity in adult humans has been underscored in recent years as repeated BAT activation through cold exposure reduces body fat [6], and improves insulin sensitivity in lean [7, 8], obese [9] and type 2 diabetic individuals [10]. BAT activation is therefore regarded as a novel therapy to treat obesity and related metabolic disorders [11].

The therapeutic potential of BAT activation originates from its potent metabolic oxidative capacity that is due to a high number of mitochondria that express uncoupling protein 1 (UCP-1). UCP-1 activity allows BAT mitochondria to uncouple respiration from ATP production and generate heat instead [12]. Physiologically, this thermogenic function is induced by cold exposure which results in enhanced sympathetic outflow towards brown adipocytes and binding of noradrenaline to the β3-adrenergic receptor (β3-AR) on brown adipocytes. BAT activation induces the release of internally stored substrate pools as well as the uptake of vast amounts of circulating glucose and lipids [13–17]. Despite the large influx of glucose in activated brown adipocytes, fatty acids are suggested to be the preferred substrates during thermogenesis [12], in line with high fatty acid oxidation upon BAT activation in mice [16] and in humans [18]. These fatty acids are released by lipolysis but also originate from the uptake of circulating lipids. Interestingly, inhibition of lipolysis reduces the uptake of glucose and lipids significantly and results in a dampened thermogenic response [15, 17]. It has therefore been suggested that substrate uptake is high in activated brown adipocytes to replenish the intracellular lipid pool [17, 19]. This metabolic effect in BAT has primarily been studied through PET-CT tracer studies and gene expression arrays, which counterintuitively showed concomitant increased expression of glycolysis, β-oxidation, glycogen and fatty acid synthesis gene [13, 17, 20–22]. This implies that substrate utilization in BAT is regulated in a different way as compared to that of liver and muscle, which typically follow the principles of the Randle or glucose-fatty acid cycle. These principles are based on the idea that substrates compete for their oxidation due to inhibitory effects of intermediate metabolites [23]. For example, during fatty acid oxidation the levels of acetyl-CoA increase. The rise of this intermediary metabolite has an inhibitory effect on enzymes involved in glucose oxidation. The BAT-specific regulation allowing simultaneous uptake, storage and oxidation of glucose and fatty acids is poorly understood.

In this study, we used the T37i murine brown adipocyte cell line to determine metabolic fluxes of the most common substrates glucose, fatty acids and glutamine during short-term β3-AR activation. We used a set of specific inhibitors to selectively inhibit either the uptake or oxidation of substrates and determined the contribution of these substrates to cellular oxygen consumption using Seahorse respirometry. Furthermore, we applied ^{13}C-stable isotope tracer-based metabolomics to examine the detailed metabolic wiring in these brown adipocytes. We found that pyruvate dehydrogenase plays a central role in directing glucose to oxidative metabolism during acute activation in brown adipocytes, while glucose is also utilized to replenish the intracellular triglyceride pool after long-term stimulation.

MATERIALS AND METHODS

Cell culture of T37i brown adipocytes and Oil-Red-O staining

T37i cells were cultured and differentiated as described previously [24, 25]. In brief, cells were kept in maintenance culture in DMEM/F12 Glutamax supplement (Life technologies) containing 10% FBS (BioWhittaker), 100 IU/mL penicillin and 10mg/mL streptomycin (Life technologies) until passage 37. For differentiation, cells were kept at complete confluency and after two days 2 nM triiodothyronine (Sigma-Aldrich) and 2 µM insulin (Sigma-Aldrich) was added to the medium for 9 days. During differentiation, medium was replaced every two days and cells were used for experiments between differentiation day 10-12. Oil-Red-O (Sigma-Aldrich) staining was performed to evaluate lipid droplet accumulation. In short, cells were washed with PBS and fixed in 10% (v/v) formalin for 1 h, rinsed in 60% (v/v) isopropanol for 5 min, and stained with filtered 60% Oil-Red-O solution for 15 min. Excess of Oil Red O was removed and cells were maintained in demineralized water during imaging.

Gene expression and protein content in T37i cells

Total RNA was isolated with TRIreagent (Sigma-Aldrich) according to the manufacturer's instructions including addition of DNase treatment (Promega). cDNA synthesis was performed with 1 µg RNA using the QuantiTect Reverse Transcription Kit (QIAGEN). LightCycler 480 SYBR Green I Master (Roche) was used for qPCR analysis, primers are listed in **Table 1**. Data were analyzed with Light Cycler 480 software release 1.5 and LinRegPCR version 2015.3, as previously described [26].

For protein extraction, T37i cells were lysed in RIPA buffer (50 mM Tris-HCl pH 7.4, 150 mM NaCl, 0.1% (w/v) sodium dodecyl sulfate, 0.5% (w/v) sodium deoxycholate, 1% (v/v) Triton X-100) with addition of Complete mini protease inhibitor cocktail (Roche) and Phosphatase Inhibitor Cocktail 2 and 3 (Sigma-Aldrich). Samples were lysed by tip

Table 1. Primer sequences of forward and reverse primers for qPCR

Gene	Accession	Forward primer	Reverse primer
Actb	NM_007393	AACCGTGAAAAGATGACCCAGAT	CACAGCCTGGATGGCTACGTA
Cidea	NM_007702	ATCACAACTGGCCTGGTTACG	TACTACCCGGTGTCCATTTCT
Dio2	NM_010050	GGCCGTCGGTCCTTCCTT	TCCCAGCTGTGTACATGCCTCAAT
Gapdh	NM_008084	GGGGCTGGCATTGCTCTCAA	TTGCTCAGTGTCCTTGCTGGGG
Ppia	NM_008907	CAAATGCTGGACCAAACACAA	GCCATCCAGCCATTCAGTCT
Prdm16	NM_027504	CAGCACGGTGAAGCCATTC	GCGTGCATCCGCTTGTG
Ucp1	NM_009463	ACGTCCCCTGCCATTTACTGTCA	GGCCGTCGGTCCTTCCTT

sonication and protein concentration was measured using the BCA protein assay kit (Pierce). For immunoblot analysis, lysates were diluted in NuPAGE LDS Sample Buffer and Sample Reducing Agent (Life Technologies) and heated to 70°C. Protein extracts were separated on pre-cast NuPAGE 4-12% gradient Bis-Tris gels (Life Technologies), and transferred to a nitrocellulose membrane. Membranes were blocked with 3% BSA (in PBS containing 0.1% (v/v) Tween-20), and incubated overnight at 4°C with the following primary antibodies: total PDHE1α (#ab67592, Abcam), phospho-Ser232 PDHE1α (#AP1063, Calbiochem) and HSP60 (#4870, Cell Signaling). The immunoreactive bands were detected with HRP-linked secondary antibodies (Goat anti-rabbit, Goat anti-mouse, DAKO) and ECL prime western blotting detection reagent (Amersham) and imaged with the ImageQuant LAS4000 (GE Healthcare). Quantification of bands was performed using Bio-Rad Quantity one 4.6.6 software.

Oxygen consumption

Oxygen consumption rate (OCR) and extracellular acidification rate (ECAR) was measured using the Seahorse XF96 analyzer (Seahorse Bioscience). T37i cells were plated at differentiation day 9 in 96-well Seahorse plates at a density of 60,000 cells per well and incubated overnight under normal cell culture conditions. The following day, medium was replaced by DMEM (Sigma, D5030) containing 17.5 mM glucose (Sigma-Aldrich), 1 mM sodium pyruvate (Lonza), and 2 mM L-Glutamine (Life technologies). Basal respiration was measured three times followed by six measurements after addition of 10 μM β3-AR agonist CL316,243 (Tocris) to induce brown adipocyte activation. ATP-coupled respiration and the maximal respiration were determined by the addition of 1.5 μM oligomycin and 1.5 μM FCCP (Sigma-Aldrich), respectively. OCR was corrected for non-mitochondrial respiration determined by simultaneous addition of 2.5 μM antimycin A and 1.25 μM rotenone (Sigma-Aldrich).

Glycolytic function was determined in DMEM medium (Sigma, D5030) containing 2 mM L-Glutamine (Life technologies) according to Seahorse XF Glycolysis stress test manufacturer instructions. In brief, basal ECAR was measured three times followed by six

measurements after sequential addition of (a) 10 µM CL316,243 or vehicle (medium), (b) 10 mM glucose, (c) 1.5 µm oligomycin and (d) 100 mM 2-deoxy-glucose (Sigma-Aldrich).

Substrate dependency and reserve capacity were determined according the Seahorse XF Mito Fuel Flex Test user guide protocol. Briefly, after measuring basal OCR and after addition of 10 µM CL316,243 or vehicle; 100 µM POCA (sodium 2-[5-(4-chlorophenyl)-pentyl] oxirane- 2-carboxylate), a CPT1 inhibitor (kind gift from BYK Gulden Pharmazeutica); 3 µM BPTES (Bis-2-(5-phenylacetamido-1,3,4-thiadiazol-2-yl)ethyl sulfide), a glutaminase inhibitor (Sigma-Aldrich) and 2 µM UK5099, an inhibitor of the mitochondrial pyruvate transporter (Sigma-Aldrich) were subsequently injected and OCR was determined six times. Data were analysed using Seahorse XF Mito Fuel Flex test report data analysis.

All ECAR and OCR values were adjusted for cell input using the CyQUANT Cell Proliferation Assay Kit (Thermo Fischer Scientific) according to the manufacturer's instruction. The final measurement point after each compound addition was always used for quantification.

Pyruvate oxidation

Pyruvate oxidation was determined by measuring the release of $^{14}CO_2$ from [1-^{14}C]-pyruvate [27]. At differentiation day 9, cells were seeded at a density of 500,000 cells in a glass liquid scintillation vial under normal cell culture conditions. The following day, cells were washed twice with DPBS prior to a 1 h incubation in Dulbecco's PBS (Life Technologies) supplemented with 500 µM [1-^{14}C]-pyruvate (specific activity: 0.55 mCi/mmol) (Perkin Elmer) combined with 10 µM CL316,243 or vehicle (PBS). A centre well containing 2 M NaOH was placed to trap CO_2. After 1 h of shaking at 37°C, medium was acidified with 2.6 M perchloric acid to stop the reaction. After 3 h of trapping, the $^{14}CO_2$ collected in the centre well was counted by liquid scintillation. Pyruvate oxidation flux was determined by the amount of pyruvate oxidized to CO_2 normalized to protein content.

Isotopic labelling of polar metabolites

Cells were differentiated in 6-well plates. At differentiation day 10, a time course incubation was started in DMEM without glucose, pyruvate, glutamine and phenol red (Life technologies) with addition of 17.5 mM [U-^{13}C]-glucose (Cambridge Isotope Laboratories)in combination with 10 µM CL316,243 or vehicle (medium). Samples were harvested by two-phase methanol-water/chloroform extraction as described [28]. Briefly, medium was removed, cells were washed twice with ice-cold 0.9% NaCl, and metabolism was quenched by the addition of 1 mL ice-cold methanol-water (1:1, v/v). Cells were removed from the well by scraping and collected in a centrifuge tube. One mL of chloroform was added to the mixture, followed by tip sonication and centrifugation at 10,000 *x g* for 10 min. The organic phase of the extraction was collected for lipidomic analysis (see below). After collection of the aqueous phase, the organic phase

and insoluble pellet were re-extracted with 1 mL methanol-water (1:1, v/v). The aqueous phases of both extractions were collected and evaporated. The metabolite residue was dissolved in 100 µL 60% (v/v) methanol and analyzed by ultra-high-pressure liquid chromatography system (Thermo Scientific) with a SeQuant ZIC-cHILIC column (100 x 2.1 mm, 3 µm particle size, Merck, Darmstadt, Germany) coupled to a Thermo Q Exactive Plus Orbitrap mass spectrometer (Thermo Scientific). The column was kept at 15°C and the flow rate was 0.250 mL/min. The mobile phase was composed of (A) 9/1 acetonitrile/water with 5 mM ammonium acetate; pH 6.8 and (B) 1/9 acetonitrile/water with 5 mM ammonium acetate; pH 6.8, respectively. The LC gradient program was: beginning with 100% (A) hold 0-3 min; ramping 3-20 min to 36% (A); ramping from 20-24 min to 20% (A); hold from 24-27 min at 20% (A); ramping from 27-28 min to 100% (A); and re-equilibrate from 28-35 min with 100% (A). Data were acquired in full-scan negative ionization mode. Data interpretation was performed using the Xcalibur software (Thermo Scientific). ^{13}C enrichment was calculated based on mass distribution isotopomer analysis (MIDA), all results were corrected for their natural ^{13}C abundance by solving the associated set of linear equations for each metabolite using non-negative least squares [29].

Non-stationary metabolic flux analysis

Non stationary metabolic flux analysis was based on the algorithm described in [30]. In short, the carbon transition model of the TCA cycle (**Table 2**) was converted into a set of linear ordinary differential equations describing the time dynamics of the corresponding Elementary Metabolite Units (EMUs) using an in-house pipeline developed in MATLAB (The MathWorks, Natick, USA). Subsequently, the flux and metabolite concentrations were estimated by minimizing the sum of the squared residuals of the measured MID time data with respect to the model prediction using the Levenberg-Marquardt algorithm.

Table 2. Carbon transition model used for non-stationary metabolic flux analysis

Substrate	Reaction	Product
citrate(abcdef)	➔	alpha-ketoglutarate(abdef) + CO_2(c)
pyruvate(abc)	➔	acetyl-CoA(ab) + CO_2(c)
acetyl-CoA(ab) + fumarate_malate(cdef)	➔	citrate(bacdef)
alpha-ketoglutarate(abcde)	➔	succinate(abcd) + CO_2(e)
alpha-ketoglutarate(abcde)	➔	succinate(dcba) + CO_2(e)
succinate(abcd)	➔	fumarate_malate(abcd)
fumarate_malate(abcd)	➔	succinate(abcd)
pyruvate(abc) + CO_2(d)	➔	fumarate_malate(dabc)
pyruvate(abc) + CO_2(d)	➔	fumarate_malate(cbad)

Isotopic labelling of lipids

The aforementioned organic phase was processed according to the lipodomic sample preparation work flow described previously [31], with minor modifications. A mixture of internal standards for multiple lipid classes was added to 250 µL of the organic phase. The internal standard mixture (all lipids from Avanti Polar Lipids) contained the following lipid concentrations: 7.5 nmol of phosphatidylserine PS(14:0)$_2$; 3.0 nmol of phosphatidylcholine PC(14:0)$_2$ and sphingomyelin SM(d18:1/12:0); 0.75 nmol of diacylglycerol DAG(14:0)$_2$, triacylglycerol TAG(14:0)$_3$, cholesteryl ester CE(14:0), phosphatidylinositol PI(14:0)$_2$, phosphatidylethanolamine PE(14:0)$_2$, phosphatidic acid PA(14:0)$_2$, Lysophosphatidylcholine LPC(14:0); 0.3 nmol of bis(monoacylglycero)phosphate BMP(14:0)$_2$; 0.15 nmol of cardiolipin CL(14:0)$_4$, phosphatidylglycerol PG(14:0)$_2$, lysophosphatidylglycerol LPG(14:0), lyso-phosphatidylethanolamine LPE(14:0) and lysophosphatidic acid LPA(14:0). After addition of internal standard mixture, the organic phase was evaporated under nitrogen flow. The lipid extract was dissolved in 100 µL of methanol/chloroform (1:1, v/v) and analyzed as described [31]. In brief, samples were injected onto a LiChrospher silica-60 (5 µm) HPLC column (Merck) coupled to a Thermo Q Exactive Plus Orbitrap mass spectrometer (Thermo Scientific). Data were acquired in negative and positive scan mode and processed using in-house developed metabolomics pipeline written in the R programming language. The identified peaks were normalized to the intensity of the internal standard for each lipid class. ^{13}C enrichment in selected lipids was calculated based on MIDA, all results were corrected for their natural ^{13}C abundance by solving the associated set of linear equations for each metabolite using non-negative least squares [29].

Statistical analysis

Groups were compared using a two-tailed Student's t-test or one-way ANOVA with *post hoc* Bonferroni correction using GraphPad Prism (GraphPad Software v5.0). $P<0.05$ was considered statistically significant. Data are displayed as mean ± SD or SEM, as indicated in the figure legends.

RESULTS

T37i brown preadipocytes adapt to a BAT bioenergetic profile during differentiation

To characterize substrate utilization in brown adipocytes upon acute β3-adrenergic activation, we utilized the T37i brown preadipocyte cell line [24, 25]. Prior to differentiation these cells have a fibroblast-like phenotype (**Fig. 1A**). T37i cells differentiated into brown adipocytes after at least nine days of exposure to insulin and triiodothyronine

(T3). Successful differentiation was characterized by multilocular lipid droplets and induction of the thermogenic gene program (**Fig. 1B-C**), confirming the brown adipocyte phenotype.

Inducibility of the β3-adrenergic response serves as ultimate evidence of differentiation into mature brown adipocyte. To determine this, we used Seahorse respirometry to measure oxygen consumption rate (OCR) in the presence of vehicle or the β3-AR agonist CL316,243. First, we determined the mitochondrial bioenergetic profile by recording res-

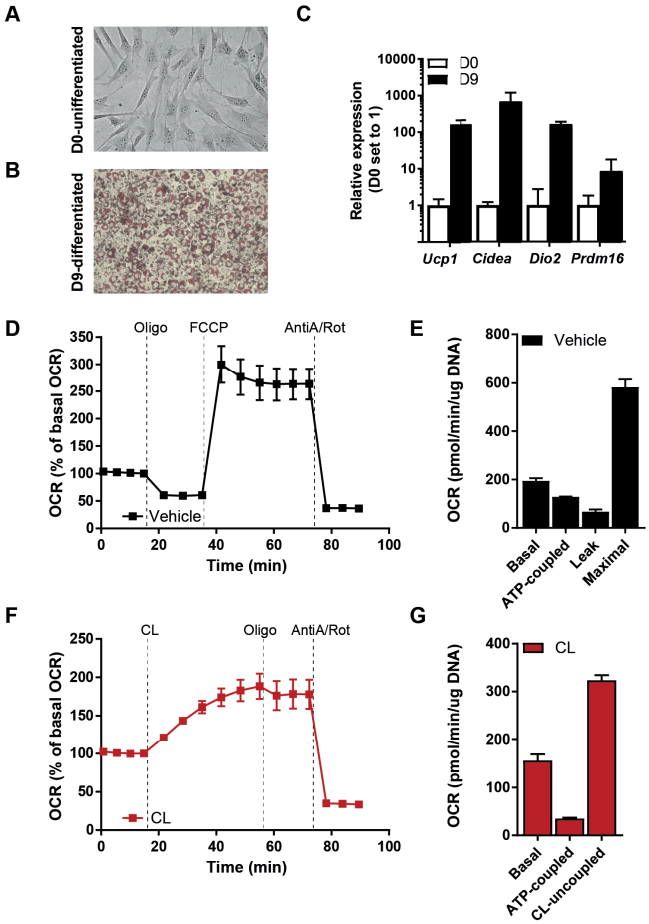

Figure 1. T37i bioenergetic profile during differentiation and β3-AR stimulation. (A-B) Oil-Red-O stained phase contrast images of undifferentiated (A) and differentiated (B) T37i cells. (C) Induction of mRNA expression of brown adipocyte genes after differentiation at day 9 relative to expression at day 0. (D) Oxygen consumption rate (OCR) of differentiated cells and (E) quantification of basal respiration, ATP-coupled and leak respiration after successive addition of 1.5 μM oligomycin, maximum respiration induced by 2 μM FCCP, corrected for non-mitochondrial respiration calculated after addition of 1.25 μM rotenone and 2.5 μM antimycin A. (F) OCR after CL316,243 and oligomycin addition and (G) quantification of basal, ATP coupled and CL-uncoupled respiration. Data is presented as average of three experiments ± SEM.

piration under basal, ATP coupled, oligomycin-inhibited (leak) and maximal (uncoupled) conditions (**Fig. 1D**). Without β3-AR stimulation, the ATP-coupled and leak respiration represented 66% and 34% of the basal respiration rate, respectively. The chemical uncoupler FCCP induced maximal respiration to 334% of basal respiration (**Fig. 1E**). CL316,243 also induced uncoupled respiration but the response was less pronounced and acute compared to FCCP (**Fig. 1F**). CL316,243 reduced the ATP coupled respiration to 20% of basal OCR (**Fig. 1G**). These data confirm that T37i is a bona fide BAT model that displays a high mitochondrial activity and a robust β3-AR response [32].

β3-AR activation improves metabolic flexibility in brown adipocytes

Substrate availability and utilization dictate the mitochondrial respiratory capacity. Our first approach to determine substrate utilization under basal conditions and upon β3-AR activation was to measure respiration in the presence of glutamine oxidation, fatty acid oxidation and glucose oxidation inhibitors. The effect of a single substrate inhibitor on respiration determines how much this respiration is dependent on a given substrate—a parameter known as substrate dependency. Glutamine dependency was determined by the response to BPTES, an inhibitor of glutaminase [33]. Fatty acid oxidation dependency was estimated with POCA, a CPT1 inhibitor [34]. Finally, glucose oxidation dependency was determined by the sensitivity to UK5099, which is an inhibitor of the mitochondrial pyruvate carrier [35]. The substrate dependency was calculated as a percentage of the total reduction in OCR when all three inhibitors were administered.

When comparing these three substrates it was evident that addition of BPTES hardly affected the OCR and hence that glutamine oxidation contributes the least to mitochondrial respiration (**Fig. 2A**). The T37i brown adipocytes were most sensitive to inhibition of fatty acid oxidation, indicating that they primarily depend on fatty acid oxidation to maintain mitochondrial respiration (**Fig. 2B**). This strong reliance on fatty acid oxidation was not further induced by β3-AR activation. It is worth noting that the substrate dependency was not influenced by β3-AR stimulation, *i.e.* resting and activated cells rely predominantly on fatty acid oxidation, although the respiration rates were obviously higher after CL316,243 treatment (**Fig. 2D**).

Next, we treated the differentiated T37i cells with combinations of two of the above-mentioned inhibitors. The residual respiration after the addition of two inhibitors marks the capacity to operate on a single substrate—a parameter known as reserve capacity (**Fig. 2E-G**). As these brown adipocytes depend most on fatty acid oxidation, this pathway also had the largest reserve capacity (**Fig. 2H**). This highlights that fatty acid oxidation could compensate for the loss of glutamine and glucose oxidation in both rest and activated state (**Fig. 2H**). The reserve capacity of glutamine oxidation was and that of glucose oxidation was marginal during rest (**Fig. 2H, G**). However, upon β3-AR stimulation the reserve capacity of these substrates, especially of glucose oxidation,

was markedly induced (**Fig. 2H**). Taken together, this suggests that brown adipocytes strongly rely on fatty acid oxidation but are metabolically more flexible in their substrate utilization upon β3-AR activation.

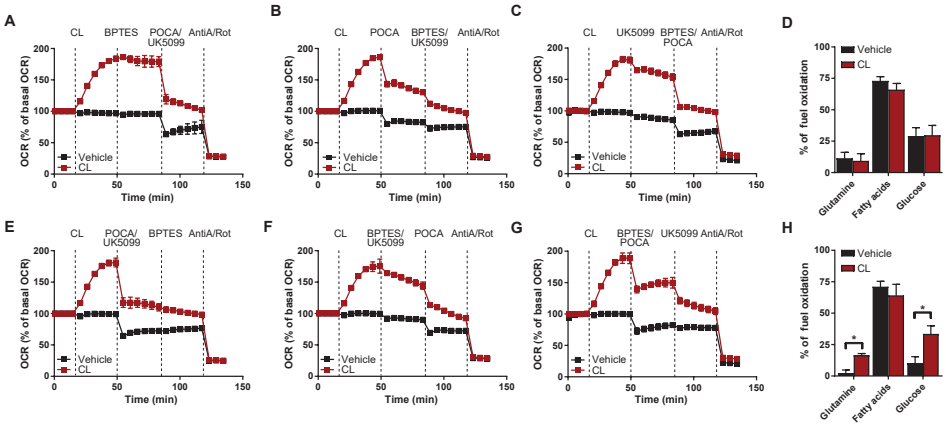

Figure 2. β3-AR activation improves metabolic flexibility in brown adipocytes. Representative OCR trace showing substrate dependence for maintaining respiration based on individual inhibitor addition strategies. Substrate oxidation dependence was determined for (A) glutamine with BPTES, (B) fatty acids with POCA and (C) glucose with UK5099. (D) Quantification of substrate dependence highlights that both resting and activated T37i adipocytes predominantly rely on fatty acid utilization to sustain OCR. Representative OCR trace showing (E) glutamine, (F) fatty acid and (G) glucose reserve capacity for maintenance of respiration after simultaneous addition of two inhibitors. (H) Quantification of substrate reserve capacity in resting and activated T37i cells. Glutamine and glucose oxidation reserved capacity is induced in CL316,243 stimulated cells. Line graphs show mean ± SD of 6 wells of one representative experiment. Data in bar graphs are presented as mean ± SEM of four experiments; *P<0.05 (unpaired Student's t-test).

Increased glycolytic flux contributes to uncoupled respiration in activated brown adipocytes

Despite the large influx of glucose during activation, glucose has been suggested to play a minor role in BAT oxidative capacity [12]. For the T37i cells, glucose was indeed the second preferred substrate, although activated cells could increase the oxidation of glucose markedly if necessary. To establish whether the reduction of ATP-coupled respiration after β3-AR activation (**Fig. 1E,G**) increases the glycolytic rate, we measured the extracellular acidification rate (ECAR) as an indicator of glycolysis. Indeed, addition of CL316,243 induced glycolysis maximally, as it could not be further induced by the addition of glucose or oligomycin (**Fig. 3A-B**). We next evaluated whether glycolysis contributes to uncoupled respiration by β3-AR stimulation. Uncoupled oxygen consumption without adrenergic activation was measured after addition of oligomycin, followed by addition of CL316,243 in combination with glucose or the glycolysis inhibitor 2-deoxy-glucose (2DG) (**Fig. 3C**). The capacity to induce uncoupled respiration was

blunted when glycolysis was inhibited (**Fig. 3D**), supporting the notion that glucose utilization contributes to β3-AR induced uncoupled respiration in brown adipocytes.

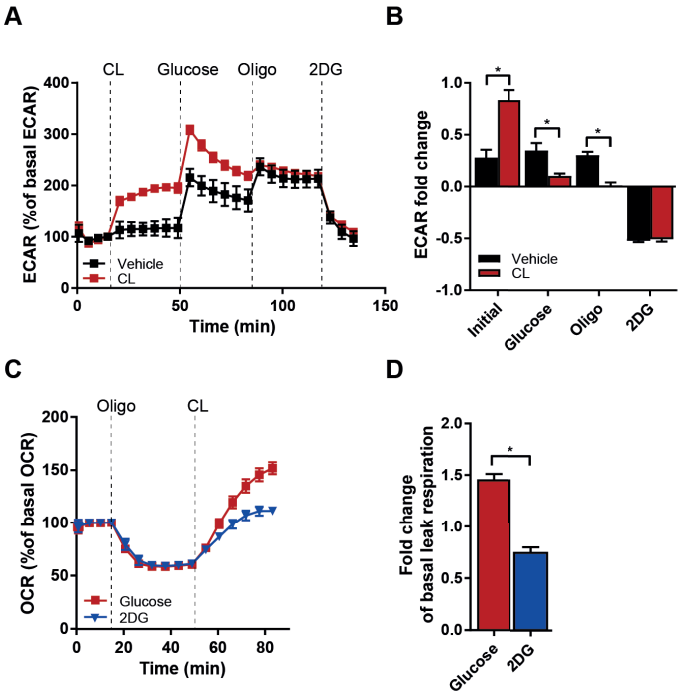

Figure 3. Increased glycolytic flux contributes to uncoupled respiration in activated brown adipocytes. (A) Extracellular acidification rate (ECAR) of vehicle and CL316,243-stimulated cells in response to 10 mM glucose, 1.5 μM oligomycin and 100 mM 2-deoxy-D-glucose (2DG). (B) ECAR fold change compared to basal ECAR shows increased initial glycolytic flux but unchanged glycolytic capacity. (C) Oxygen consumption rate (OCR) of cells under basal conditions, after addition of 1.5 μM oligomycin and 10 μM CL316,243 combined with 10 mM D-glucose (in red) or with 100 mM 2DG (in blue). (D) 2DG significantly reduces uncoupled respiration in activated brown adipocytes. Line graphs show a representative experiment with mean ± SD of 12 wells. Data in bar graphs are presented as mean ± SEM of three experiments; *P<0.05 (unpaired Student's t-test).

The glucose carbon flux into the TCA cycle is stimulated in β3-AR activated brown adipocytes

Fatty acids are an important carbon source of T37i cells, but upon β3-AR stimulation glucose uptake and glycolysis are greatly induced. Inhibition of glycolysis affects uncoupled respiration indicating that glucose is oxidized to contribute to uncoupled respiration (**Fig. 3C-D**). Gene expression studies show that short- and long-term cold-induced BAT activation increases expression of genes involved in glycolysis, the pentose phosphate pathway, fatty acid oxidation but also of fatty acid synthesis [20–22]. To assess through which pathways glucose is preferentially utilized during short-term β3-adrenergic acti-

vation, we incubated cells with [U-^{13}C]-glucose in the presence of CL316,243 or vehicle. We reconstructed metabolic flux distribution by measuring 13C-labeled metabolites using untargeted metabolomics after 30 min up to 7 h. First, we focused on labelling in glycolysis and pentose phosphate pathway (PPP) intermediates after acute activation. The PPP gives rise to NADPH that is required for lipid synthesis and glutathione antioxidant defense system, two processes suggested to be upregulated upon BAT activation [20]. Indeed, ^{13}C-labeling in PPP intermediates appeared to be increased after 30 min of β3-AR activation (**Suppl. Table 1**). Possibly, the increased PPP activity in activated brown adipocytes caused the observed decrease in labelling in glycolytic intermediates (**Suppl. Table 1**). However, after ≥ 2 h, labeling of glycolytic and PPP intermediates were equal in vehicle and CL316,243 treated cells (**Suppl. Table 1**). Interestingly, despite the initial reduced label incorporation in pyruvate, TCA cycle intermediates were rapidly labelled following [U-^{13}C]-glucose incubation. The rate of label incorporation in TCA cycle intermediates was greatly enhanced from 30 min up to 7 h after β3-AR stimulation (**Fig. 4A**). To estimate the flux through the TCA cycle we performed non-stationary flux analysis on the ^{13}C label incorporation mass isotopomer distribution (MID) time patterns (**Fig. 4B-C**). Metabolic flux analysis showed that the overall TCA activity was increased upon β3-AR activation. Pyruvate entered the TCA cycle *via* pyruvate dehydrogenase (PDH) and pyruvate carboxylase (PC) activity which were both increased upon β3-AR activation (**Fig. 4D-E**). It appears that the overall flux of glucose metabolism is increased after β3-AR activation.

Short-term β3-adrenergic activation stimulates pyruvate dehydrogenase activity without stimulating *de novo* lipogenesis

It has been suggested that glucose enters the TCA cycle merely to be exported to the cytoplasm as citrate to act as a building block for *de novo* lipogenesis [19]. Glucose oxidation is tightly regulated at the level of PDH, and increased PDH activity is associated with *de novo* lipogenesis [36, 37]. Metabolic flux analysis estimated a 2.5-fold increase in PDH flux (**Fig. 4D-E**). To estimate this flux through PDH from our flux distribution measurements, we measured the ratio of ^{13}C-labeled citrate to ^{13}C-labeled phosphoenolpyruvate (PEP). This ratio was markedly increased in the CL316,243-activated cells which is indeed indicative of increased PDH flux. This allows carbons to enter the TCA cycle more rapidly in the activated state (**Fig. 4A**). The activity of PDH is regulated by phosphorylation and is influenced by many factors including mitochondrial redox status, intracellular ATP, pyruvate and acetyl-CoA levels [38]. The phosphorylated PDH is inactive, preventing pyruvate conversion to acetyl-CoA. Stimulation with CL316,243 resulted in a short-term dephosphorylation of PDH which peaked after 15-60 min of stimulation (**Fig. 5B**). Indeed, in this time window pyruvate oxidation rate was doubled (**Fig. 5C**), accounting for the strong glucose driven respiration after CL316,243 (**Fig. 2C, G-H**). Interestingly, 1 h

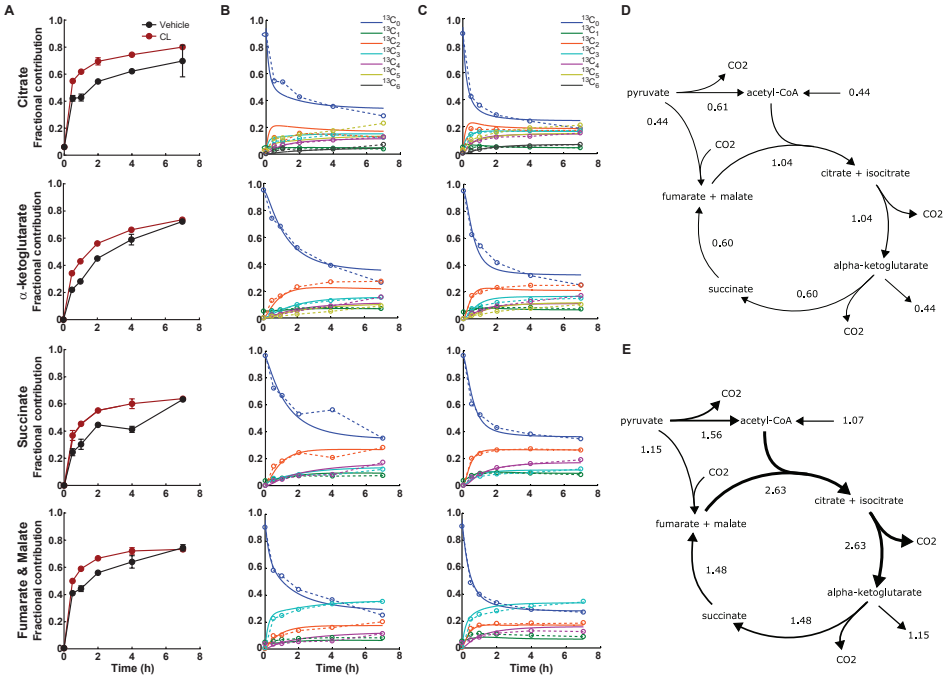

Figure 4. Increased glucose oxidation through TCA cycle activity after β3-AR activation. (A) Time course incubation with [U-^{13}C]-glucose results in increased labelling of tricarboxylic acid (TCA) cycle intermediates at early time points after CL316,243 activation, suggesting increased TCA flux. (B) The measured MID data in dotted lines and predicted MID data in solid lines of vehicle-treated cells and (C) CL316,243-treated cells. (D) Results of non-stationary metabolic flux analysis of cells after vehicle and (E) β3-AR stimulation. The flux values have unit [/hr] and are normalized to the alpha-ketoglutarate/glutamate concentration. Data represent mean ± SD of two separate experiments.

stimulation with CL316,243 increased PDH activity to a similar extent as 1 h stimulation with the established PDH activator dichloroacetate (DCA), which activates PDH through the inhibition of PDH kinase [39].

Our combined data support the idea that glucose acutely serves as a substrate to maintain oxygen consumption through increased PDH activity. At the same time, we aimed to establish whether glucose also enters lipogenesis. To do this, we examined the labelling pattern of the three most abundant triglycerides (TG)—TG(48:3), TG(50:3) and TG(54:3)—after incubation with [U-^{13}C]-glucose using our lipidomics platform [31,40]. Glucose can contribute to TG synthesis by (1) producing glycerol-3-phosphate *via* glycolysis and thereby providing the TG backbone [41]; and/or (2) acetyl-CoA generation required for *de novo* fatty acid synthesis (**Fig. 6A**) [19, 42]. We analysed the TG species of vehicle or CL316,243-stimulated cells for after 1 and 6 h (**Fig. 6B-D**). The most abundant TGs followed a similar labelling pattern, which was particularly enriched with $^{13}C_3$ indicating incorporation of three ^{13}C atoms likely through glycerol. This effect was

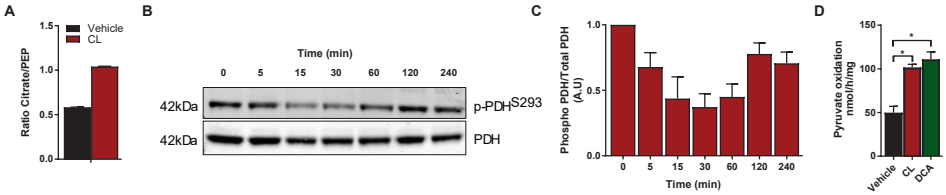

Figure 5. β3-AR stimulation increases glucose flux through PDH. (A) Increased ratio of ^{13}C-labeled citrate over ^{13}C-labeled phosphoenolpyruvate (PEP) after 30 min CL316,243 activation suggests increased flux through pyruvate dehydrogenase (PDH). (B) Western blot showing reduced PDH phosphorylation at serine-293, which is indicative for PDH activation. (C) The ratio of the quantified phosphorylated PDH E1-α serine-293 over the total PDH E1-α. (D) Upon 1 h CL316,243 stimulation pyruvate oxidation (using [1-^{14}C]-pyruvate as substrate) is increased to a level that is similar as 1 h stimulation with the established PDH activator dichloroacetate (DCA). Data in (A) is mean ± SD of duplicate experiments, and (B-C) represent mean ± SEM of triplicates; *P<0.05 (one-way ANOVA, Bonferroni corrected).

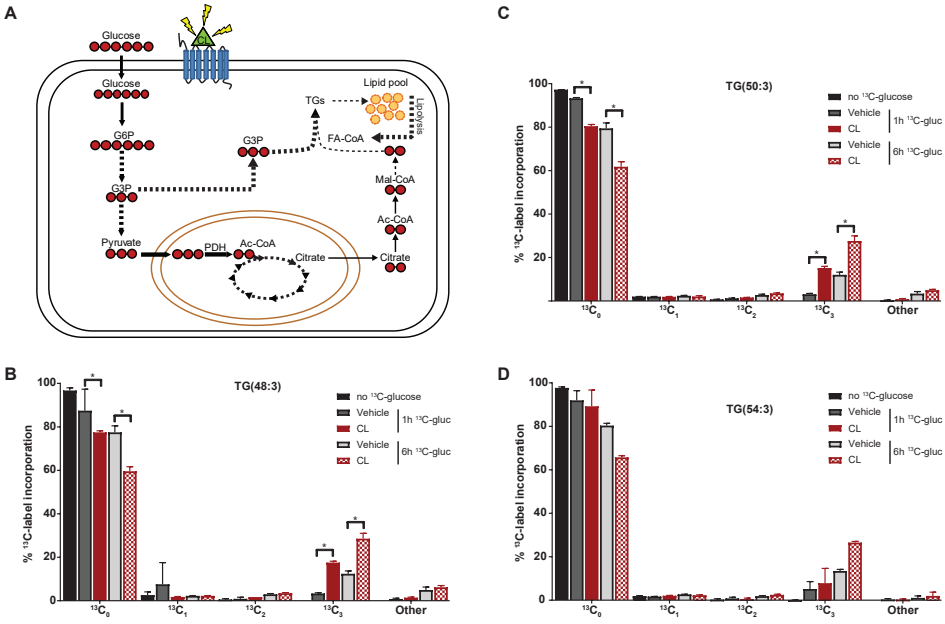

Figure 6. Short-term β3-AR stimulation increases fatty acid re-esterification. (A) Schematic illustration of label incorporation scenarios in lipids. Ac-CoA, acetyl-CoA; G6P, glucose-6-phosphate; G3P, glycerol-3-phosphate; FA-CoA, fatty acyl-CoA; mal-CoA, malonyl-CoA; PDH, pyruvate dehydrogenase. Solid lines and dashed lines indicate direct and indirect fluxes. Isotope profile of the three most abundant triglycerides (B) TG(48:3), (C) TG(50:3) and (D) TG(54:3) after 0, 1 and 6 hours of CL316,243 or vehicle stimulation. Incorporation of even carbons ($^{13}C_{[nx2]}$) is relatively low, while the $^{13}C_3$ is increased over time suggesting glycerol incorporation in TG. CL316,243 induces glycerol incorporation significantly after 1 and especially after 6 hours. Bars represent mean ± SD of three biological replicates samples; *P<0.05 (one-way ANOVA, Bonferroni corrected).

even more pronounced in activated brown adipocytes (**Fig. 6B-D**). The incorporation of $^{13}C_2$-labeled acetyl-CoA—after malonyl-CoA conversion and incorporation leading to $^{13}C_{[n\times2]}$-labelled TG —was relatively minor (**Fig. 6B-D**). Altogether, our results suggest that short-term β3-AR stimulation specifically induces glycolysis and glucose oxidation which is mediated by increased PDH activity. While the overall increased TCA cycle activity sustains increased respiration rates, the increased flux through PDH does not seem to induce *de novo* lipogenesis as glucose-derived acetyl-CoA is sparsely incorporated in TGs. Rather the increased glycolytic flux favours glycerol production required for esterification of fatty acids.

DISCUSSION

Brown adipose tissue activation is classically accompanied by increased uptake of glucose and lipids from the circulation. The induced uptake of glucose and lipids is such a key event that it is often used as a proxy for BAT activation [43, 44]. The mechanism underlying simultaneous glucose and lipid uptake and utilization is not fully understood, despite being at the core of BAT function and its therapeutic potential. In the present study, we investigated substrate utilization by brown adipocytes during short-term β3-AR activation. We show that brown adipocytes indeed oxidize fatty acids and glucose simultaneously. β3-AR activation induced partitioned glucose utilization, *i.e.* allowing coinciding glucose oxidization and glucose utilization for alternative metabolic pathways, such as glycerol synthesis.

It has been suggested that the purpose of the increased influx of glucose is not to meet the direct increase in energy demand. Rather, it may be utilized as a building block for lipid synthesis to replenish the lipid pool for later usage [20, 44]. Our data indicate that glucose is the second preferred substrate, but glucose oxidation is clearly induced upon β3-AR activation. In mice, glucose uptake and glycolysis are upregulated during BAT activation presumably to compensate for the loss of ATP due to UCP-1-mediated uncoupling [45]. During short-term activation, the increased glycolytic rate did not only give rise to increased lactate levels (**Fig. 3C**), but also a considerable amount of glucose was oxidized into CO_2 and thereby contributed to uncoupled respiration (**Fig. 5D**). It has been recently shown that UCP-1 KO mice have diminished uncoupled respiration after β3-AR activation but glucose uptake and glycolysis were stimulated to similar extent as in the WT [46, 47]. It is therefore likely that next to glucose oxidation, β3-AR stimulation also induces glucose metabolism to partly channel glucose to alternative pathways. Proposed alternative pathways are the pentose phosphate pathway, glycerol synthesis and *de novo* fatty acid synthesis [20–22]. We observed only a transient increase in PPP activity and therefore focused on TGs and fatty acid synthesis.

β-adrenergic signalling induces lipolysis *via* hormone sensitive lipase and adipose triglyceride lipase [48]. Genetic and pharmacological inhibition of lipolysis hampers UCP-1-mediated uncoupling [49], and thereby promotes cold intolerance in mice [17, 50, 51] and humans [13]. With this in mind, it was postulated that fatty acids derived from intracellular lipid droplets are the main fuel source for brown adipocytes that must be continuously replenished. Our lipidomics analysis shows that incubation with [U-^{13}C]-glucose predominantly gives rise to $^{13}C_3$-labeled TGs. This is supportive of glucose conversion into glycerol which is subsequently used for TG synthesis [41]. This is in contrast to previous suggestions that glucose is primarily ending up in complex lipids through *de novo* fatty acid synthesis [19]. Such *de novo* lipogenesis would require glucose conversion to acetyl-CoA, after which these two-carbon units are utilized as the building blocks to elongate fatty acid chains. If such a scenario were true, we would have found TGs with two, four, six or more even ^{13}C-labeled TGs (**Fig. 6A**). This is not the case suggesting that glucose is primarily entering the TG pool *via* glycerol, even though it is still possible that differences in growth phase, glucose concentration, intracellular lipid content, or specific cellular context affects the metabolic phenotype in BAT [52, 53].

Very recently, the principle that lipolysis is required for BAT activation has been challenged [54, 55]. The loss of thermoregulation upon whole body or adipose-specific loss of lipolysis underlines the importance of fatty acids as a substrate for thermogenesis [15, 17, 50, 51]. However, by selectively inhibiting BAT lipolysis only, it was shown that BAT can be very flexible in its substrate utilization leading to increased uptake of circulating substrates. The increased uptake of exogenous substrates was especially induced during cold exposure or specific β3-AR stimulation [54, 55]. We have seen this plasticity of brown adipocyte metabolism as well. When using a combination of inhibitors that prevent glucose and fatty acid oxidation, we found an increase in glutamine oxidation. Similarly, when glutamine and fatty acid oxidation were inhibited, glucose oxidation was elevated. This flexibility in substrate utilization was induced after β3-AR activation. The loss of fatty acid oxidation and the rise of intracellular fatty acids can activate peroxisome proliferator activated receptor (PPAR) signaling [56], and thereby contribute to metabolic plasticity to meet the increase energy demands during BAT activation.

Glucose metabolism is regulated at multiple levels. Pyruvate is a key metabolite in glucose metabolism as it lies at the crossroads of glycolysis and TCA cycle activity. Pyruvate is an important substrate to maintain the high respiration rates during uncoupled respiration. Inhibition of pyruvate entrance into mitochondria has previously shown to attenuate noradrenaline-induced uncoupled respiration [57]. Likewise, inhibition of glycolysis and thus the reduction of pyruvate levels attenuated uncoupled respiration after β3-AR stimulation (**Fig. 3A**). Pyruvate supports TCA cycle activity through decarboxylation by PDH or carboxylation by PC [58]. Our metabolic flux analysis estimated an increase in flux through both enzymes. PDH is considered as a gatekeeper for glucose utilization and

energy metabolism [58, 59]. PDH senses intermediate metabolites —such as pyruvate and acetyl-CoA— and the NAD^+/NADH redox state to control glucose metabolism and maintain optimal energy homeostasis [38]. In proliferating cells, genetic deletion of PDH could be compensated by increased uptake of lipids and increased glutamine utilization that is alternatively metabolized to contribute to lipid synthesis [59]. This underlines the plasticity of cellular metabolism as well as the contribution of PDH in this process. We observed an induction of PDH activity upon β3-AR stimulation resulting in increased pyruvate oxidation which was similar to the maximal level reached by stimulation with PDH agonist DCA. Activating PDH may therefore favor BAT metabolism to allow optimal thermogenesis.

Collectively, our data demonstrate that glycolysis and glucose oxidation contribute to uncoupled respiration, despite that fatty acids are the main fuel for brown adipocytes. Glucose metabolism appeared to be heavily regulated upon β3-AR stimulation. We identified PDH as a gatekeeper for glucose utilization that directs most glucose towards oxidation to maintain uncoupled respiration. The accompanying increase of PC activity to convert pyruvate to oxaloacetate replenishes the TCA cycle during this high PDH activity. Oxaloacetate could also act as a precursor for glyceroneogenesis, which is the formation of glycerol-3-phosphate *via* phosphoenolpyruvate carboxykinase activity [41, 60], and thereby allow part of the glucose to be directed to glycerol synthesis and storage of free fatty acids as TGs in lipid droplets as substrates for future use. Pharmacological targeting of the PDH holds potential as a novel strategy to potentiate BAT function.

FUNDING

This work is financially supported by Rembrandt Institute for Cardiovascular Science (RHH & MRB) and The Netherlands Cardiovascular Research Initiative: an initiative with support of the Dutch Heart Foundation (CVON2014-02 ENERGISE). RHH is funded by an ERC Starting grant (no. 638290) and a ZonMw VIDI grant (no. 917.15.305).

REFERENCES

1. Bray GA, Bellanger T. Epidemiology, Trends, and Morbidities of Obesity and the Metabolic Syndrome. *Endocrine* **2006**, 29, (1), 109-118.
2. van Marken Lichtenbelt WD, Vanhommerig JW, Smulders NM, Drossaerts JMAFL, Kemerink GJ, Bouvy ND, Schrauwen P, Teule GJJ. Cold-Activated Brown Adipose Tissue in Healthy Men. *N Engl J Med* **2009**, 360, (15), 1500-1508.
3. Saito M, Okamatsu-ogura Y, Matsushita M, Watanabe K, Yoneshiro T, Nio-kobayashi J, Iwanaga T, Miyagawa M, Kameya T, Nakada K, et al. High Incidence of Metabolically Active Brown Adipose Effects of Cold Exposure and Adiposity. *Diabetes* **2009**, 58, (7), 1526-1531.
4. Virtanen KA, Lidell ME, Orava J, Heglind M, Westergren R, Niemi T, Taittonen M, Laine J, Savisto N-J, Enerbäck S, et al. Functional Brown Adipose Tissue in Healthy Adults. *N Engl J Med* **2009**, 360, (15), 1518-1525.
5. Zingaretti MC, Crosta F, Vitali A, Guerrieri M, Frontini A, Cannon B, Nedergaard J, Cinti S. The presence of UCP1 demonstrates that metabolically active adipose tissue in the neck of adult humans truly represents brown adipose tissue. *FASEB J* **2009**, 23, (9), 3113-3120.
6. Yoneshiro T, Aita S, Matsushita M, Kayahara T, Kameya T, Kawai Y, Iwanaga T, Saito M, Cannon B, Nedergaard J, et al. Recruited brown adipose tissue as an antiobesity agent in humans. *J Clin Invest* **2013**, 123, (8), 3404-3408.
7. Chondronikola M, Volpi E, Børsheim E, Porter C, Annamalai P, Enerbäck S, Lidell ME, Saraf MK, Labbe SM, Hurren NM, et al. Brown Adipose Tissue Improves Whole Body Glucose Homeostasis and Insulin Sensitivity in Humans. *Diabetes* **2014**, 63, (12), 4089-4099.
8. Lee P, Smith S, Linderman J, Courville AB, Brychta RJ, Dieckmann W, Werner CD, Chen KY, Celi FS. Temperature-Acclimated Brown Adipose Tissue Modulates Insulin Sensitivity in Humans. *Diabetes* **2014**, 63, (11), 3686-3698.
9. Hanssen MJW, van der Lans AAJJ, Brans B, Hoeks J, Jardon KMC, Schaart G, Mottaghy FM, Schrauwen P, van Marken Lichtenbelt WD. Short-term Cold Acclimation Recruits Brown Adipose Tissue in Obese Humans. *Diabetes* **2016**, 65, (5), 1179-1189.
10. Hanssen MJW, Hoeks J, Brans B, van der Lans A a JJ, Schaart G, van den Driessche JJ, Jörgensen J a, Boekschoten M V, Hesselink MKC, Havekes B, et al. Short-term cold acclimation improves insulin sensitivity in patients with type 2 diabetes mellitus. *Nat Med* **2015**, 21, (7), 6-10.
11. Scheele C, Nielsen S. Metabolic regulation and the anti-obesity perspectives of human brown fat. *Redox Biol* **2017**, 12, (3), 770-775.
12. Cannon B, Nedergaard J. Brown adipose tissue: function and physiological significance. *Physiol Rev* **2004**, 84, (1), 277-359.
13. Ouellet V, Labbé SM, Blondin DP, Phoenix S, Guérin B, Haman F, Turcotte EE, Richard D, Carpentier AC. Brown adipose tissue oxidative metabolism contributes to energy expenditure during acute cold exposure in humans. *J Clin Invest* **2012**, 122, (2), 545-552.
14. Bartelt A, Bruns OT, Reimer R, Hohenberg H, Ittrich H, Peldschus K, Kaul MG, Tromsdorf UI, Weller H, Waurisch C, et al. Brown adipose tissue activity controls triglyceride clearance. *Nat Med* **2011**, 17, (2), 200-205.
15. Blondin DP, Frisch F, Phoenix S, Guérin B, Turcotte ÉE, Haman F, Richard D, Carpentier AC. Inhibition of Intracellular Triglyceride Lipolysis Suppresses Cold-Induced Brown Adipose Tissue Metabolism and Increases Shivering in Humans. *Cell Metab* **2017**, 25, (2), 438-447.

16. Berbée JFP, Boon MR, Khedoe PPSJ, Bartelt A, Schlein C, Worthmann A, Kooijman S, Hoeke G, Mol IM, John C, et al. Brown fat activation reduces hypercholesterolaemia and protects from atherosclerosis development. *Nat Commun* **2015**, 6,(10) , 6356.
17. Labbe SM, Caron A, Bakan I, Laplante M, Carpentier AC, Lecomte R, Richard D. In vivo measurement of energy substrate contribution to cold-induced brown adipose tissue thermogenesis. *FASEB J* **2015**, 29, (5), 2046-2058.
18. Bakker LEH, Boon MR, van der Linden RAD, Arias-Bouda LP, van Klinken JB, Smit F, Verberne HJ, Jukema JW, Tamsma JT, Havekes LM, et al. Brown adipose tissue volume in healthy lean south Asian adults compared with white Caucasians: a prospective, case-controlled observational study. *Lancet Diabetes Endocrinol* **2014**, 2, (3), 210-217.
19. Irshad, Z.; Dimitri, F.; Christian, M.; Zammit, V. A. Diacylglycerol acyltransferase 2 links glucose utilization to fatty acid oxidation in the brown adipocytes. *J Lipid Res* **2017**, 58, (1), 15-30.
20. Hao Q, Yadav R, Basse AL, Petersen S, Sonne SB, Rasmussen S, Zhu Q, Lu Z, Wang J, Audouze K, et al. Transcriptome profiling of brown adipose tissue during cold exposure reveals extensive regulation of glucose metabolism. *Am J Physiol Endocrinol Metab* **2015**, 308, (5), E380-92.
21. Marcher A-B, Loft A, Nielsen R, Vihervaara T, Madsen JGS, Sysi-Aho M, Ekroos K, Mandrup S. RNA-Seq and Mass-Spectrometry-Based Lipidomics Reveal Extensive Changes of Glycerolipid Pathways in Brown Adipose Tissue in Response to Cold. *Cell Rep* **2015**, 13, (9), 2000-2013.
22. Yu XX, Lewin DA, Forrest W, Adams SH. Cold elicits the simultaneous induction of fatty acid synthesis and B-oxidation in murine brown adipose tissue : prediction from differential gene expression and confirmation in vivo. *FASEB J* **2002**, 16, (2), 155-168.
23. Hue L, Taegtmeyer H. The Randle cycle revisited. *Am J Physiol - Endocrinol Metab* **2009**, 297, , 578-591.
24. Nakae J, Cao Y, Oki M, Orba Y, Sawa H, Kiyonari H, Iskandar K, Suga K, Lombes M, Hayashi Y. Forkhead transcription factor FoxO1 in adipose tissues regulates energy storage and expenditure. *Diabetes* **2008**, 57, (3), 563-576.
25. Zennaro MC, Le Menuet D, Viengchareun S, Walker F, Ricquier D, Lombès M. Hibernoma development in transgenic mice identifies brown adipose tissue as a novel target of aldosterone action. *J Clin Invest* **1998**, 101, (6), 1254-1260.
26. Ramakers C, Ruijter JM, Lekanne Deprez RH, Moorman AFM. Assumption-free analysis of quantitative real-time polymerase chain reaction (PCR) data. *Neurosci Lett* **2003**, 339, (1), 62-66.
27. Borud O, Pettersen JE. Normal 2-aminobutyrate oxidation and increased valine oxidation in fibroblasts deficient in pyruvate dehydrogenase. *J Inherit Metab Dis* **1982**, 5, (1), 55-57.
28. Sapcariu SC, Kanashova T, Weindl D, Ghelfi J, Dittmar G, Hiller K. Simultaneous extraction of proteins and metabolites from cells in culture. *MethodsX* **2014**, 1, (7) , 74-80.
29. Fernández-Fernández M, Rodríguez-González P, García Alonso JI. A simplified calculation procedure for mass isotopomer distribution analysis (MIDA) based on multiple linear regression. *J Mass Spectrom* **2016**, 51, (10), 980-987.
30. Young JD, Walther JL, Antoniewicz MR, Yoo H, Stephanopoulos G. An elementary metabolite unit (EMU) based method of isotopically nonstationary flux analysis. *Biotechnol Bioeng* **2008**, 99, (3), 686-699.
31. Herzog K, Pras-Raves ML, Vervaart MAT, Luyf ACM, van Kampen AHC, Wanders RJA, Waterham HR, Vaz FM. Lipidomic analysis of fibroblasts from Zellweger spectrum disorder patients identifies disease-specif-

ic phospholipid ratios. *J Lipid Res* **2016**, 57, (8), 1447-1454.
32. Viengchareun S, Caron M, Auclair M, Kim MJ, Frachon P, Capeau J, Lombès M, Lombès A. Mitochondrial toxicity of indinavir, stavudine and zidovudine involves multiple cellular targets in white and brown adipocytes. *Antivir Ther* **2007**, 12, (6), 919-929.
33. Robinson MM, Mcbryant SJ, Tsukamoto T, Rojas C, Ferraris DV, Hamilton SK, Hansen JC, Curthoys NP. Novel mechanism of inhibition of rat kidney-type glutaminase by bis-2-(5-phenylacetamido-1,2,4-thiadiazol-2-yl)ethyl sulfide (BPTES). *Biochem J* **2007**, 406, (3), 407-414.
34. Wolf HPO, Eistetter K, Ludwig G. Phenylalkyloxirane carboxylic acids, a new class of hypoglycaemic substances: Hypoglycaemic and hypoketonaemic effects of sodium 2-[5-(4-chlorophenyl)-pentyl]-oxirane-2-carboxylate (B 807-27) in fasted animals. *Diabetologia* **1982**, 22, (6), 456-463.
35. Hildyard JCW, Ämmälä C, Dukes ID, Thomson SA, Halestrap AP. Identification and characterisation of a new class of highly specific and potent inhibitors of the mitochondrial pyruvate carrier. *Biochim Biophys Acta - Bioenerg* **2005**, 1707, (2-3), 221-230.
36. McCormack JG, Denton RM. Evidence that fatty acid synthesis in the interscapular brown adipose tissue of cold-adapted rats is increased in vivo by insulin by mechanisms involving parallel activation of pyruvate dehydrogenase and acetyl-coenzyme A carboxylase. B*iochem J* **1977**, 166, (3), 627-630.
37. Moura MAF, Kawashita NH, Brito SMRC, Kettelhut IC, Migliorini RH. Effect of cold acclimation on brown adipose tissue fatty acid synthesis in rats adapted to a high-protein, carbohydrate-free diet. *Metabolism* **2001**, 50, (12), 1493-1498.
38. Patel MS, Korotchkina LG. Regulation of the pyruvate dehydrogenase complex. *Biochem Soc Trans* **2006**, 34, (2), 217.
39. Bonnet S, Archer SL, Allalunis-Turner J, Haromy A, Beaulieu C, Thompson R, Lee CT, Lopaschuk GD, Puttagunta L, Bonnet S, et al. A Mitochondria-K+ Channel Axis Is Suppressed in Cancer and Its Normalization Promotes Apoptosis and Inhibits Cancer Growth. *Cancer Cell* **2007**, 11, (1), 37-51.
40. Houtkooper RH, Rodenburg RJ, Thiels C, Lenthe H van, Stet F, Poll-The BT, Stone JE, Steward CG, Wanders RJ, Smeitink J, et al. Cardiolipin and monolysocardiolipin analysis in fibroblasts, lymphocytes, and tissues using high-performance liquid chromatography-mass spectrometry as a diagnostic test for Barth syndrome. *Anal Biochem* **2009**, 387, (2), 230-237.
41. Brito MN, Brito N a, Brito SR, Moura M a, Kawashita NH, Kettelhut IC, Migliorini RH. Brown adipose tissue triacylglycerol synthesis in rats adapted to a high-protein, carbohydrate-free diet. *Am J Physiol* **1999**, 276, (4 Pt 2), R1003-9.
42. Trayhurn P. Fatty acid synthesis in mouse brown adipose tissue the influence of environmental temperature on the proportion of whole-body fatty acid synthesis in brown adipose tissue and the liver. *Biochim Biophys Acta - Lipids Lipid Metab* **1981**, 664, (3), 549-560.
43. Chen KY, Cypess AM, Laughlin MR, Haft CR, Hu HH, Bredella MA, Enerbäck S, Kinahan PE, Lichtenbelt W van M, Lin FI, et al. Brown Adipose Reporting Criteria in Imaging STudies (BARCIST 1.0): Recommendations for Standardized FDG-PET/CT Experiments in Humans. *Cell Metab* **2016**, 24, (2), 210-222.
44. Hoeke G, Kooijman S, Boon MR, Rensen PCN, Berbée JFP. Role of Brown Fat in Lipoprotein Metabolism and Atherosclerosis. *Circ Res* **2016**, 118, (1), 173-182.
45. Lee PL, Jung SM, Guertin DA. The Complex Roles of Mechanistic Target of Rapamycin in Adipocytes and Beyond. *Trends Endocrinol Metab* **2017**, 28, (5), 319-339.

46. Olsen JM, Csikasz RI, Dehvari N, Lu L, Sandström A, Öberg AI, Nedergaard J, Stone-Elander S, Bengtsson T. β3-Adrenergically induced glucose uptake in brown adipose tissue is independent of UCP1 presence or activity: Mediation through the mTOR pathway. *Mol Metab* **2017**, 6, (6), 611-619.
47. Hankir MK, Kranz M, Keipert S, Weiner J, Andreasen SG, Kern M, Patt M, Klöting N, Heiker JT, Brust P, et al. Dissociation Between Brown Adipose Tissue 18 F-FDG Uptake and Thermogenesis in Uncoupling Protein 1–Deficient Mice. *J Nucl Med* **2017**, 58, (7), 1100-1103.
48. Zechner R, Zimmermann R, Eichmann TO, Kohlwein SD, Haemmerle G, Lass A, Madeo F. FAT SIGNALS - Lipases and lipolysis in lipid metabolism and signaling. *Cell Metab* **2012**, 15, (3), 279-291.
49. Li Y, Fromme T, Schweizer S, Schöttl T, Klingenspor M. Taking control over intracellular fatty acid levels is essential for the analysis of thermogenic function in cultured primary brown and brite/beige adipocytes. *EMBO Rep* **2014**, 15, (10), 1069-1076.
50. Ahmadian M, Abbott MJ, Tang T, Hudak CSS, Kim Y, Bruss M, Hellerstein MK, Lee HY, Samuel VT, Shulman GI, et al. Desnutrin/ATGL is regulated by AMPK and is required for a brown adipose phenotype. *Cell Metab* **2011**, 13, (6), 739-748.
51. Haemmerle G, Lass A, Zimmermann R, Gorkiewicz G, Meyer C, Rozman J, Heldmaier G, Maier R, Theussl C, Eder S, et al. Defective Lipolysis and Altered Energy Metabolism in Mice Lacking Adipose Triglyceride Lipase. *Science* **2006**, 312, (5774), 734-737.
52. Yao CH, Fowle-Grider R, Mahieu NG, Liu GY, Chen YJ, Wang R, Singh M, Potter GS, Gross RW, Schaefer J, et al. Exogenous Fatty Acids Are the Preferred Source of Membrane Lipids in Proliferating Fibroblasts. *Cell Chem Biol* **2016**, 23, (4), 483-493.
53. Young JD. Metabolic flux rewiring in mammalian cell cultures. *Curr Opin Biotechnol* **2013**, 24, (6), 1108-1115.
54. Shin H, Ma Y, Chanturiya T, Cao Q, Wang Y, Kadegowda AKG, Jackson R. Lipolysis in Brown Adipocytes Is Not Essential for Cold-Induced Thermogenesis in Mice. *Cell Metab* **2017**, 26, (5), 1-14.
55. Schreiber R, Diwoky C, Schoiswohl G, Schrauwen P, Haemmerle G, Zechner R, Schreiber R, Diwoky C, Schoiswohl G, Feiler U, et al. Cold-Induced Thermogenesis Depends on ATGL- Mediated Lipolysis in Cardiac Muscle, but Not Brown Article Cold-Induced Thermogenesis. *Cell Metab* **2017**, 26, (5), 1-11.
56. Mottillo EP, Bloch AE, Leffs T, Granneman JG. Lipolytic products activate peroxisome proliferator-activated receptor (PPAR) a and g in brown adipocytes to match fatty acid oxidation with supply. *J Biol Chem* **2012**, 287, (30), 25038-25048.
57. Cannon B, Nedergaard J. The Physiological Role of Pyruvate Carboxylation in Hamster Brown Adipose Tissue. *Eur J Biochem* **1979**, 94, (2), 419-426.
58. Gray LR, Tompkins SC, Taylor EB. Regulation of pyruvate metabolism and human disease. *Cell Mol Life Sci* **2014**, 71, (14), 2577-2604.
59. Rajagopalan KN, Egnatchik RA, Calvaruso MA, Wasti AT, Padanad MS, Boroughs LK, Ko B, Hensley CT, Acar M, Hu Z, et al. Metabolic plasticity maintains proliferation in pyruvate dehydrogenase deficient cells. *Cancer Metab* **2015**, 3, (1), 7.
60. Moura MAF, Festuccia WTL, Kawashita NH, Garófalo MAR, Brito SRC, Kettelhut IC, Migliorini RH. Brown adipose tissue glyceroneogenesis is activated in rats exposed to cold. *Pflugers Arch Eur J Physiol* **2005**, 449, (5), 463-469.

SUPPLEMENTARY APPENDIX

Supplementary table 1. Fractional contribution of ^{13}C- glucose corrected for natural abundance in pentose phosphate pathway (PPP) and glycolytic intermediates upon vehicle or CL316,243 time course stimulation

	Metabolite	0.5 h		1 h		2 h		4 h		7 h	
		Veh	CL	Veh	CL	Veh	CL	Veh	CL	Veh	CL
PPP	R5P	0.118	0.049	0.135	0.057	0.173	0.140	0.273	0.277	0.481	0.430
	ER-4P	0.800	0.765	0.756	0.930	0.917	0.956	0.947	1.000	0.996	0.977
	SED-7P	0.815	0.688	0.803	0.756	0.922	0.843	0.939	0.928	0.954	0.956
Glycolysis	G6P	0.825	0.682	0.775	0.767	0.881	0.801	0.881	0.903	0.915	0.894
	G3P/DHAP	0.746	0.624	0.716	0.643	0.818	0.841	0.884	0.815	0.976	0.916
	BPG	0.755	0.532	0.681	0.671	0.868	0.789	0.911	0.940	0.986	0.949
	PG	0.751	0.507	0.686	0.635	0.872	0.777	0.872	0.940	0.966	0.945
	PEP	0.721	0.528	0.669	0.638	0.847	0.768	0.893	0.930	0.942	0.947
	Pyruvate	0.771	0.694	0.742	0.762	0.859	0.830	0.891	0.900	0.916	0.916
	Lactate	0.776	0.740	0.775	0.795	0.856	0.840	0.868	0.886	0.911	0.902

Supplementary table 2 related to figure 4. Fractional distribution of isotopologues corrected for natural abundance used to determine metabolite labeling as shown in Figure 4A

	Fractional distribution									
	0.5 h		1 h		2 h		4 h		7 h	
Metabolite	Veh	CL	Veh	CL	Veh	CL	Veh	CL	Veh	CL
Citrate $^{13}C_0$	0.579	0.451	0.573	0.382	0.454	0.305	0.378	0.256	0.303	0.199
Citrate $^{13}C_1$	0.003	0.015	0.011	0.033	0.019	0.032	0.020	0.033	0.020	0.032
Citrate $^{13}C_2$	0.126	0.191	0.098	0.184	0.159	0.186	0.151	0.176	0.131	0.178
Citrate $^{13}C_3$	0.096	0.138	0.094	0.157	0.113	0.158	0.141	0.167	0.123	0.167
Citrate $^{13}C_4$	0.060	0.083	0.067	0.093	0.083	0.119	0.101	0.125	0.125	0.150
Citrate $^{13}C_5$	0.116	0.102	0.120	0.122	0.146	0.155	0.173	0.189	0.230	0.209
Citrate $^{13}C_6$	0.019	0.021	0.037	0.030	0.026	0.044	0.034	0.054	0.068	0.065
α-Ketoglutarate $^{13}C_0$	0.780	0.659	0.718	0.571	0.550	0.439	0.411	0.338	0.278	0.264
α-Ketoglutarate $^{13}C_1$	0.013	0.032	0.023	0.050	0.046	0.063	0.061	0.069	0.056	0.061
α-Ketoglutarate $^{13}C_2$	0.132	0.175	0.166	0.202	0.235	0.236	0.273	0.253	0.278	0.254
α-Ketoglutarate $^{13}C_3$	0.044	0.070	0.055	0.092	0.093	0.114	0.122	0.138	0.146	0.147
α-Ketoglutarate $^{13}C_4$	0.020	0.041	0.026	0.055	0.050	0.093	0.086	0.127	0.153	0.171
α-Ketoglutarate $^{13}C_5$	0.011	0.023	0.013	0.031	0.026	0.054	0.047	0.076	0.088	0.104
Succinate $^{13}C_0$	0.755	0.632	0.697	0.547	0.554	0.448	0.587	0.398	0.367	0.361
Succinate $^{13}C_1$	0.015	0.048	0.026	0.068	0.051	0.077	0.047	0.076	0.060	0.067
Succinate $^{13}C_2$	0.145	0.203	0.184	0.240	0.247	0.265	0.210	0.275	0.286	0.266
Succinate $^{13}C_3$	0.050	0.056	0.048	0.062	0.076	0.079	0.076	0.091	0.116	0.117
Succinate $^{13}C_4$	0.035	0.061	0.044	0.083	0.073	0.130	0.080	0.160	0.171	0.190
Fumarate $^{13}C_0$	0.590	0.500	0.557	0.410	0.440	0.333	0.360	0.279	0.256	0.268
Fumarate $^{13}C_1$	0.022	0.054	0.030	0.067	0.043	0.069	0.052	0.069	0.056	0.065
Fumarate $^{13}C_2$	0.110	0.160	0.113	0.184	0.149	0.197	0.172	0.198	0.205	0.200
Fumarate $^{13}C_3$	0.242	0.226	0.260	0.258	0.313	0.286	0.357	0.323	0.365	0.340
Fumarate $^{13}C_4$	0.035	0.060	0.040	0.081	0.055	0.115	0.059	0.132	0.118	0.127
Malate $^{13}C_0$	0.625	0.510	0.573	0.419	0.480	0.365	0.401	0.316	0.267	0.284
Malate $^{13}C_1$	0.047	0.110	0.066	0.119	0.077	0.111	0.090	0.098	0.092	0.084
Malate $^{13}C_2$	0.087	0.128	0.092	0.153	0.125	0.165	0.147	0.172	0.203	0.176
Malate $^{13}C_3$	0.211	0.200	0.235	0.237	0.272	0.261	0.311	0.299	0.337	0.348
Malate $^{13}C_4$	0.030	0.053	0.034	0.072	0.046	0.098	0.051	0.115	0.101	0.108
Glutamate $^{13}C_0$	0.784	0.666	0.722	0.579	0.556	0.451	0.419	0.347	0.287	0.272
Glutamate $^{13}C_1$	0.013	0.031	0.024	0.049	0.047	0.063	0.062	0.070	0.057	0.062
Glutamate $^{13}C_2$	0.129	0.171	0.163	0.201	0.232	0.233	0.269	0.251	0.276	0.254
Glutamate $^{13}C_3$	0.044	0.069	0.053	0.089	0.091	0.111	0.120	0.135	0.145	0.145
Glutamate $^{13}C_4$	0.020	0.040	0.025	0.052	0.049	0.090	0.085	0.123	0.149	0.166
Glutamate $^{13}C_5$	0.011	0.023	0.013	0.030	0.026	0.052	0.045	0.073	0.086	0.101

3

GENERATION OF CONDITIONALLY IMMORTALIZED MURINE AND HUMAN BROWN PRE-ADIPOCYTES WITH PRESERVED ADIPOGENIC CAPACITY

Eline N. Kuipers*, Jia Liu*,
Hetty C.M. Sips,
Jennifa C. Mariadasan,
Andrea D. van Dam,
Constantinos Christodoulides,
Fredrik Karpe, Guang-Qian Zhou,
Mariëtte R. Boon,
Patrick C.N. Rensen,
Antoine A.F. de Vries,
Sander Kooijman

In preparation

ABSTRACT

Brown adipose tissue (BAT) is a potential target to treat cardiometabolic disorders because of its capacity to take up and combust glucose and fatty acids for thermoregulation. Its cellular and molecular investigation in humans is hampered by the limited availability of cell material and the heterogeneity of BAT between and within individuals. In this study, monoclonal lines of conditionally immortalized brown preadipocytes (iBPAs) of both mouse and human origin were generated. Conditional immortalization was achieved by doxycycline-controlled expression of simian virus 40 large T antigen with a Tet-On system. In the presence of doxycycline, both the murine and human cell lines showed long-term proliferation capacity with a cell doubling time of approx. 24 h. Shutdown of large T expression by removal of doxycycline and concomitant exposure to an adipogenic differentiation cocktail, resulted in the acquirement of brown adipocyte properties in cells of both species. This was evidenced by the accumulation of multilocular lipid droplets, the upregulation of brown adipocyte markers including uncoupling protein 1 and the induction of lipolysis and oxygen consumption following adrenergic stimulation. Notably, shutdown of large T expression prior to the onset of differentiation appeared to be only critical to induce adipogenesis in the human iBPAs, while their murine counterparts showed adipogenesis upon exposure to the adipogenic differential cocktail regardless of large T expression. We suggest that conditionally iBPAs represent an easy-to-use model for fundamental and applied research into BAT.

INTRODUCTION

Activation of brown adipose tissue (BAT) represents a therapeutic tool to reduce cardiometabolic disease by enhancing energy expenditure with increased clearance of circulating glucose and lipids [1-3]. Cold is the physiological activator of BAT, upon which the sympathetic nerves that innervate BAT release noradrenaline (NA) that binds to β-adrenergic receptors on the cell membrane of brown adipocytes [4]. This promotes intracellular lipolysis leading to liberated fatty acids being directed towards the mitochondria for oxidation. This process produces heat in the presence of uncoupling protein 1 (UCP-1), which is uniquely expressed by brown/beige adipocytes [5-10]. In order to replenish the intracellular lipid pools, BAT takes up large amounts of triglyceride-derived fatty acids and glucose from the circulation.

In recent years many (pharmacological) approaches have been identified to promote BAT activity, at least in rodents. The development of fundamental and applied research into human BAT is hampered by the lack of high-throughput brown adipocyte cell culture models. The use of (primary) brown (pre-)adipocytes, obtained from biopsies, has important constraints: the amount of available cells is limited and there is a large heterogeneity of human BAT not only between subjects but also within one subject depending on the anatomical location from where the biopsy is taken [11]. Moreover, mature adipocytes are post-mitotic and lipid-laden causing them to be very fragile and of low buoyant density. As a consequence, it is challenging to bring mature adipocytes into culture because they float and require ceiling culturing to adhere [12]. Therefore, the formation of sufficient brown adipocytes for experiments requires proliferation and differentiation of adipocyte precursors.

To overcome these problems, a number of different mouse brown preadipocyte (BPA) lines have been generated such as HB2 [13], HIB 1B [14, 15] and T37i [16]. HB2 cells are brown preadipocytes isolated from the interscapular BAT of p53 knockout mice, while HIB 1B and T37i cells were derived from transgenic mice expressing the simian virus 40 (SV40) large T (LT) antigen using constitutively active, lineage-restricted promoters to drive transgene expression. These cell lines have been helpful in increasing our understanding of adipocyte biology. However, the absence of the cellular gatekeeper protein p53 or the constitutive expression of oncoproteins limits their usefulness as model systems to study the properties of BAT. In addition, in order to study human brown adipocyte function, Shinoda *et al.* [17] and Xue *et al.* [18] generated human BPA lines by transducing the stromal vascular fraction of human supraclavicular adipose tissues with retroviral vectors encoding SV40 LT antigen and hTERT (*i.e.* the catalytic subunit of telomerase), respectively. Following adipogenic differentiation, these cells express *UCP1* and respond to stimulation with noradrenaline and forskolin with an increase in lipolysis

and mitochondrial respiration. These human BPA lines have been successfully used to identify BAT-specific genes and to investigate their function.

We postulated that generating conditionally immortalized monoclonal BPA (iBPA) lines is the next step towards the development of a high-throughput model for human brown adipocytes. The reasons for this were as follows: 1) Previous constitutive expression of oncoproteins such as SV40 LT to immortalize cells may affect the differentiation capacity of brown adipocytes through interactions of LT with pocket proteins (in particular the retinoblastoma protein [pRB]) and with the tumor suppressor protein p53 [19, 20]. 2) Proliferation and differentiation are two opposing processes that generally do not occur simultaneously. In other words, continuous proliferation pressure due to permanent immortalization may reduce the differentiation capacity of BPAs. 3) The adipogenic capacity of existing BPA lines has been shown to be rapidly lost with increasing passage numbers [13].

These drawbacks prompted us to generate iBPA lines of both mouse and human origin by using a lentiviral vector (LV) expressing LT in a doxycycline (dox)-dependent manner to control cell proliferation [21, 22]. The resulting monoclonal cell lines were characterized in terms of their dox-dependent LT expression level and proliferation capacity and their ability to undergo adipogenic differentiation using multilocular lipid droplet formation and expression of BAT marker genes as read-out systems. Finally, the effects of adrenergic stimulation on glycerol secretion, *Ucp1*/*UCP1* mRNA expression and oxygen consumption rate of adipogenically differentiated iBPAs were studied.

MATERIALS AND METHODS

Lentiviral vector (LV) production

LV particles were produced as detailed before [22]. The molecular structure of the shuttle plasmids used for LV production are depicted in **Suppl. Fig. 1**. The construction of these plasmids is described in the Suppl. Materials and Methods.

Isolation and culture of primary mouse and human BPAs

Mouse tissue was collected in accordance with the Institute's Guide for the Care and Use of Laboratory Animals and had received approval from the Animal Experiments Committee of the Leiden University Medical Center (LUMC). Prior to the collection of human BAT, patients scheduled for surgery in the thyroid region gave written informed consent for taking biopsies and the procedure was approved by the Medical Ethical Committee of the Oxford Centre for Diabetes and performed in accordance with the principles of the revised Declaration of Helsinki.

Primary mouse BPAs were isolated from pooled interscapular BAT depots of 5 male, 5-week-old C57Bl/6J mice (Charles River Laboratories International, Wilmington, MA). Human primary BPAs were isolated from biopsies obtained from four patients (**Suppl. Table 1**). Biopsies of adipose tissue of brown-red color were obtained from an area close to the isthmus region of the thyroid gland. Isolated tissue was minced with a scissor into 3- to 4-mm pieces, washed once with DMEM/F-12 GlutaMAX (Thermo Fisher Scientific; catalogue number: 10565018) and cells were separated by incubation in DMEM/F-12 GlutaMAX containing 1 mg/mL collagenase type I (Thermo Fisher Scientific; catalog number: 17018029) at 37°C for 45 min. The resulting cell suspensions were filtered through a 200-µm pore-sized nylon filter (Sefar, Lochem, the Netherlands; catalogue number: 03-200/39) and the cells were pelleted by low-speed centrifugation. The cell pellets were suspended in red blood cell lysis buffer (Thermo Fisher Scientific; catalogue number: 00433357) and incubated for 5 min (Thermo Fisher Scientific; catalogue number: 00433357) at room temperature with occasional shaking. After pelleting, the cells were suspended in growth medium (DMEM/F-12 GlutaMAX supplemented with 10% heat-inactivated fetal bovine serum (FBS), 100 U/mL penicillin and 100 µg/mL streptomycin) for *in vitro* culture. Growth medium was replaced the following day and then every other day.

Transduction of primary BPAs and generation of lines of conditionally immortalized mouse and human BPAs

The primary mouse BPAs at population doubling (PD) 2 and human BPAs at approximately PD 6 were transduced with the plasmids LV.iHsEEF1A1.SV40-LT-*ts*A58.WHVPRE and LV.iHsUBC.LT-*ts*A58.WHVPRE (see Suppl. Materials and Methods), respectively. The next day, the inoculum was replaced by growth medium containing 100 ng/mL dox (Sigma-Aldrich) to induce LT expression. The cells were subsequently given fresh growth medium with dox every other day. After 1 week of culture, the transduced cells were trypsinized and plated at a low density of approx. 10-20 cells/cm^2 to allow formation of single-cell clones. Two to three weeks later, individual cell colonies were picked and separately expanded in the presence of dox.

Culture, differentiation and adrenergic stimulation of mouse and human iBPAs

Mouse and human iBPA clones were cultured in growth medium supplemented with 100 ng/mL dox. Growth medium was replaced every other day and cells were split 1:8 after reaching approximately 70% confluency. For differentiation of the mouse iBPAs, cells were grown confluent in 2% gelatin (Sigma-Aldrich; catalogue number: G9391)-coated wells and 2 days later exposed to growth medium containing 5.6 nM bovine insulin (Sigma-Aldrich; catalogue number: I0305000), 126 µM sodium ascorbate (Sigma-Aldrich; catalogue number: A-7631), 1 µM of the peroxisome proliferator-activated receptor γ (PPARγ) agonist rosiglitazone (Sigma-Aldrich; catalogue number: R2408) and

10 mM HEPES (adjusted to pH 7.40 with NaOH). This medium was replaced every other day for up to 14 days. For differentiation of the human iBPAs, cells were grown confluent in 2% gelatin-coated wells. After reaching confluence, the medium was replaced by growth medium without dox. Two days later, differentiation was induced by growth medium supplemented with 150 nM human insulin (Sigma-Aldrich; catalogue number: I9278), 1 µM dexamethasone (Sigma-Aldrich; catalogue number: D2915), 1 µM rosiglitazone, 1 nM triiodothyronine (T3, Sigma-Aldrich; catalogue number: T6397), 500 µM 3-isobutyl-1-methylxanthine (IBMX, Sigma-Aldrich; catalogue number: I7018) and 125 µM Indomethacin (Sigma-Aldrich; catalogue number: I7378), which was refreshed after 48 hours and replaced on day 4 by growth medium supplemented with 150 nM insulin, 1 nM T3, and 1 µM rosiglitazone. The latter medium was replaced every other day up to day 16. Exposing the murine and human iBPA clones to these differentiation cocktails will be referred to as culturing under adipogenic culture/differentiation conditions.

The various clones were screened for their adipogenic capacity, *i.e.* their ability to develop multilocular lipid droplets and to express the BAT marker gene *Ucp1*/*UCP1*. Every other day during the differentiation process of the selected mouse and human iBPAs, pictures were taken to capture cellular morphology using the ZOE fluorescent cell imager (Bio-Rad, Hercules, CA) and cells were collected in Tripure (Roche Life Science, Almere, the Netherlands) for RNA isolation and gene expression analysis as described below (n=4 cultures per time point and experimental group).

Differentiated iBPAs (at differentiation day 14 and 16 for the mouse and human iBPAs, respectively) were stimulated with 1 µM noradrenaline (Sigma-Aldrich; catalogue number: A7257) or vehicle for 8 hours. Subsequently, supernatant was collected for colorimetric determination of glycerol production (Instruchemie, Delfzijl, the Netherlands) and cells were lysed in TriPure. All data was generated using cells that underwent 40-50 PDs.

Analysis of cell proliferation

To draw growth curves, the primary mouse BPAs and conditionally immortalized murine cells were subcultured 1:4 and 1:8 on reaching confluency so that each passage corresponded to 2 and 3 PDs, respectively. To assess their proliferation rate and dependence on the activity of SV40 LT antigen, the mouse iBPAs were cultured at low density in medium with or without 100 ng/mL dox. At different days after culture initiation, cells were collected in medium and counted using an Accuri flow cytometer (BD Biosciences, Breda, the Netherlands).

Western blotting

Western blotting was carried out as detailed before [23] with primary mouse monoclonal antibodies directed against LT (1:2,000; Santa Cruz Biotechnology, Dallas, TX; catalogue

number: sc-147) or glyceraldehyde 3-phosphate dehydrogenase (GAPDH; loading control; 1:100,000; Merck Millipore, Burlington, MA; catalogue number: MAB374) and goat anti-mouse IgG secondary antibodies linked to horseradish peroxidase (1:15,000; Santa Cruz Biotechnology). Data was analyzed by Quantity One software (Bio-Rad Laboratories) using the GAPDH signals for normalization purposes.

RNA isolation and reverse transcription-quantitative PCR (RT-qPCR) analysis

Total RNA was isolated using TriPure Isolation reagent according to the manufacturer's protocol. cDNA synthesis was performed using M-MLV reverse transcriptase (Promega Benelux, Leiden, the Netherlands; catalogue number: M1705), random primers, dNTPs and RNasin ribonuclease inhibitor (all from Promega Benelux) and 1 µg of input RNA. Real-time quantitative PCR was carried out on a CFX96 Real-time PCR machine (Bio-Rad Laboratories) using GoTaq qPCR master mix (Promega Benelux; catalogue number: A6002). mRNA expression of the mouse iBPAs was normalized to that of the ribosomal protein-encoding reference gene *Rplp0*, also known as *36b4*. mRNA expression of the human iBPAs was normalized to reference gene *LRP10*. The primer pairs used for mouse and human iBPAs are listed in **Tables 1 and 2**, respectively. The forward and reserve primer of each primer pair were located in different exons except for the primers of murine *Pparg*.

Table 1. Nucleotide sequences of primer pairs used for RT-qPCR of murine mRNAs

Gene	Forward primer	Reverse primer
Fabp4	ACACCGAGATTTCCTTCAAACTG	CCATCTAGGGTTATGATGCTCTTCA
Lpl	CCCTAAGGACCCCTGAAGAC	GGCCCGATACAACCAGTCTA
Pparg	GTGCCAGTTTCGATCCGTAGA	GGCCAGCATCGTGTAGATGA
Ppargc1α	TGCTAGCGGTTCTCACAGAG	AGTGCTAAGACCGCTGCATT
Prdm16	ACTTTGGATGGGAGCAGATG	CTCCAGGCTCGATGTCCTTA
Rplp0	GGACCCGAGAAGACCTCCTT	GCACATCACTCAGAATTTCAATGG
Ucp1	TCAGGATTGGCCTCTACGAC	TGCATTCTGACCTTCACGAC

Table 2. Nucleotide sequences of primer pairs used for RT-qPCR of human mRNAs

Gene	Forward primer	Reverse primer
FABP4	CCTTTAAAAATACTGAGATTTCCTTCA	GGACACCCCCATCTAAGGT
LPL	TCAACTGGATGGAGGAGGAGT	CAGGAGAAAGACGACTCGGG
LRP10	CAGACTGTCACCATCAGGTTC	GAGAGGGGAGCGTAGGGTTA
PPARG	GTCGTGTCTGTGGAGATAAAGC	AACAGCTTCTCCTTCTCGGC
PPARGC1A	TGCATGAGTGTGTGCTCTGT	GCACACTCGATGTCACTCCA
PRDM16	CACGAGTGCAAGGACTGC	TGTGGATGACCATGTGCTG
UCP1	ACCGCAGGGAAAGAAACAGC	TCAGATTGGGAGTAGTCCCT

Oxygen consumption

Oxygen consumption rate was measured using the Seahorse XF96 analyzer (Agilent Technologies, Santa Clara, CA). Mouse and human iBPAs were cultured and differentiated in Seahorse cell culture plates as described in the section 'Culture, differentiation and adrenergic stimulation of mouse and human iBPAs'. One hour prior to the oxygen consumption measurement, the differentiation medium was replaced by Seahorse XF Base Medium (Agilent; catalogue number: 102353-100) containing 5 mM glucose (Sigma-Aldrich; catalogue number: G8769), 0.5 mM sodium pyruvate (Life Technologies Europe; catalogue number: 11370-070), 1x GlutaMAX (Life technologies Europe; catalogue number: 35050061) and 10% FBS (Life Technologies Europe). Basal respiration was measured three times followed by six measurements after addition of 1 μM noradrenaline or vehicle.

Oxygen consumption rate values were adjusted for cell input using the CyQUANT Cell Proliferation Assay Kit (Thermo Fischer Scientific; catalogue number: C7026) according to the manufacturer's instruction. The last measurement point before compound addition was used for quantification.

Statistical analysis

Data are represented as means ± standard error of the mean (SEM). Effect of adrenergic stimuli on iBPAs was analyzed by Student's t-test. GraphPad Prism version 6.0 (GraphPad Software, La Jolla, CA) was used for all calculations. Differences at P values < 0.05 were considered statistically significant.

RESULTS

Generation of conditionally immortalized mouse BPAs

Mouse primary BPAs were isolated from the pooled interscapular BAT depots of 5 mice and transduced with an LV conferring dox-dependent expression of the SV40 LT (Suppl. **Fig.1**). Immunocytological staining (**Fig. 1A**) and western blotting (**Fig. 1B**) showed LT expression in the transduced BPAs but not in primary BPAs following the exposure of both cell types to dox. Primary BPAs gradually stopped proliferating after about 18 PDs (**Fig. 1C**), whereas the transduced LT-expressing BPAs kept proliferating for at least 60 PDs without showing any obvious decrease in their proliferative capacity (**Fig. 1C**).

Low-density cultures of the LT-expressing murine BPAs were used for isolating single-cell clones, which were picked and numbered in order of appearance. From over 50 rapidly growing cell clones, clone #6 was selected to further study the long-term dox-dependent proliferation capacity of iBPAs since it was one of the most adipogenic clones (see below). LT expression of clone #6 cells before (day 0) and 2, 4, 6 and 8 days

after dox removal was analyzed by immunocytological staining and western blotting. Clone #6 displayed dox-inducible LT expression; LT was highly expressed in the presence of dox, and LT levels gradually declined in its absence, being no longer detectable 6 days after dox removal (**Fig. 1D, E and F**). Consistent with these findings iBPAs showed

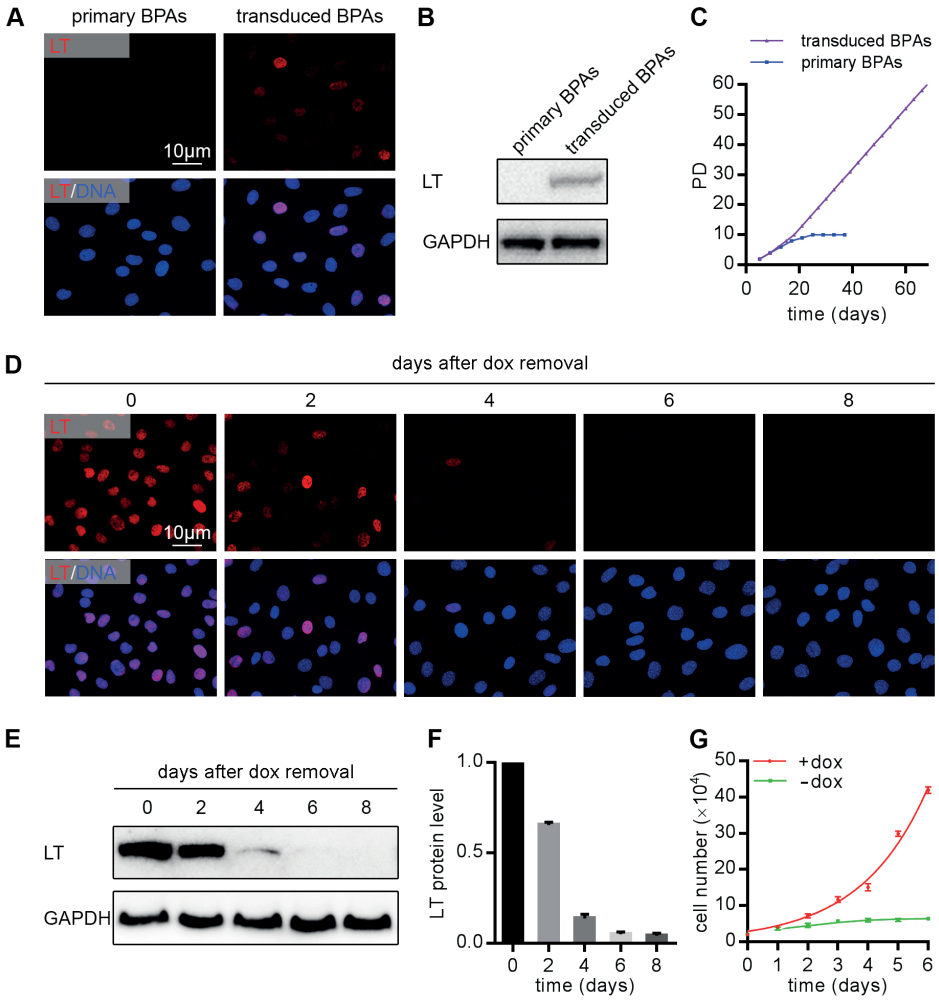

Figure 1. Conditional immortalization of mouse BPAs. (A, B) Confirmation of LT expression in dox-exposed transduced BPAs (18 PDs) by immunocytological staining (A) and western blotting (B). In both cases, dox-treated primary BPAs that underwent 18 PDs served as negative controls. Cell nuclei were visualized by Hoechst 33342 (blue) and stained for LT (red). (C) Growth curves of primary BPAs and transduced BPAs. Cells were cultured in the presence of dox. (D-F) Analysis by immunocytology (D) and western blotting (E, F) of LT expression in clone #6 iBPAs before (day 0) and at 2, 4, 6 and 8 days after dox removal. (G) Quantification of cell numbers in cultures of clone #6 iBPAs exposed for the indicated days to medium with or without dox. BPA, brown preadipocyte; LT, large T; dox, doxycycline; PD, population doubling; GAPDH, glyceraldehyde 3-phosphate dehydrogenase.

dox-inducible proliferation capacity as shown by immunostaining for the cellular proliferation marker Ki-67, which was no longer detectable 6 days after dox removal (**Suppl. Fig.2**). In the presence of dox, cells proliferated with an average doubling time of approx. 24 hours, whereas in the absence of dox, the cell number slightly increased up to day 4 and then remained constant (**Fig. 1G**). The small increase in the number of iBPAs during the first 4 days after dox removal is likely due to the slow decline of the LT expression level following transgene silencing. Taken together, the expression of LT enabled BPAs to continuously proliferate and bypass senescence.

Mouse iBPAs possess adipogenic capacity

In order to assess their adipogenic capacity, cells from each clone were cultured in growth medium and when these clonal preadipocyte cell lines reached 100% confluence (day 0), dox was removed from the culture medium at which time point the cells were induced to differentiate to brown adipocytes under adipogenic culture conditions for 14 days (**Fig. 2A**). Cells from clones #6 and #7 exhibited the highest differentiation capacity based on the extent of lipid droplet formation and highest *Ucp1* expression level (data not shown). To better characterize the adipogenic potential of these two clones, microscopic images of cell cultures subjected to adipogenic differentiation conditions were taken every two days (**Fig. 2B**). The cells of both clones gradually accumulated small lipid droplets acquiring the multilocular phenotype typical for brown adipocytes and after 14 days of adipogenic differentiation > 90% of the cells was lipid-laden (**Fig. 2B**). Interestingly, proliferation pressure (*i.e.* the presence of dox) did not seem to reduce the adipogenic potential of mouse iBPAs (**Fig. 2B**).

Mouse iBPAs were further analyzed by RT-qPCR to assess the expression of brown adipocyte markers during adipogenesis without proliferation pressure (*i.e.* in absence of dox). Expression of the unique BAT marker *Ucp1* showed a robust induction starting at day 4 of adipogenic differentiation for both clones (**Fig. 3A**). The *Ucp1* mRNA level peaked at differentiation day 12 for clone #6 and at differentiation day 10 for clone #7 (**Fig. 3A**). The transcriptional coactivators PR domain containing 16 (*Prdm16*) and peroxisome proliferator-activated receptor gamma coactivator 1-α (*Ppargc1α*), the peroxisome proliferator-activated receptor γ (*Pparg*), fatty acid binding protein 4 (*Fabp4*) and lipoprotein lipase (*Lpl*) followed similar patterns of expression, *i.e.* expression of all these markers was induced from the start of adipogenic differentiation and, peaked at differentiation day 12, except for *Lpl* that showed bimodal expression (**Fig. 3A**). Based on these data, we conclude that conditionally immortalized murine BPAs possess adipogenic capacity and that optimal differentiation of iBPAs is reached at 12-14 days after initiation of adipogenesis.

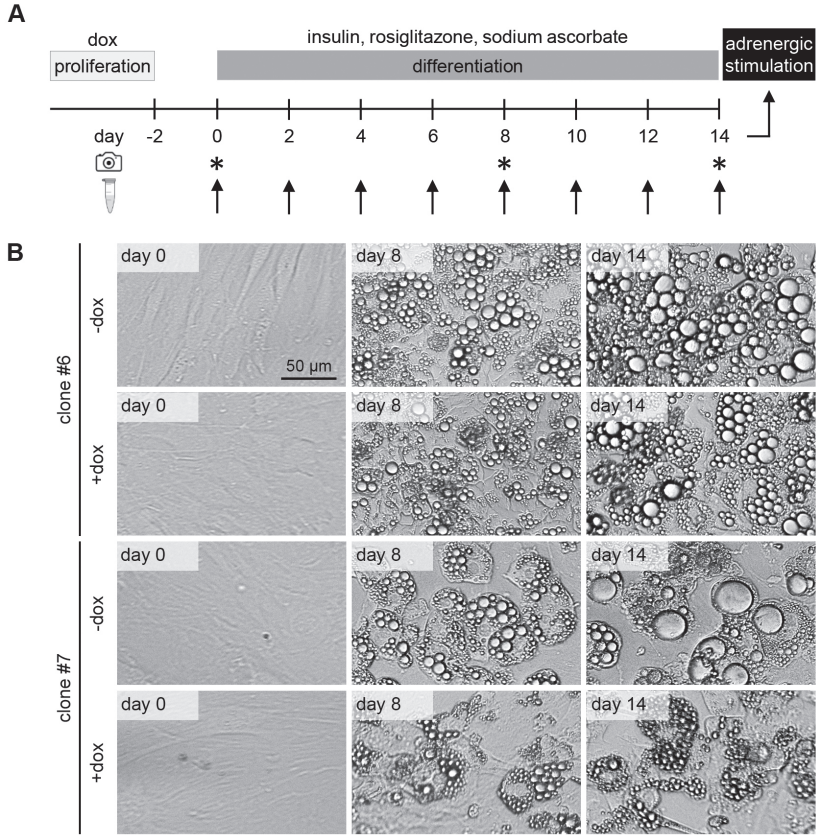

Figure 2. Adipogenic capacity of mouse iBPAs. (A) Protocol used to differentiate mouse iBPAs into brown adipocytes. (B) Phase-contrast images showing the morphological changes associated with the adipogenic differentiation of murine clone #6 and #7 iBPAs in the presence or absence of dox. iBPA, conditionally immortalized brown preadipocyte; PD, population doubling; dox, doxycycline.

Noradrenaline activates adipogenically differentiated mouse iBPAs

To investigate the response of adipogenically differentiated iBPAs to adrenergic stimulation, the cells were stimulated with the non-selective adrenergic agonist noradrenaline [24] upon which glycerol release was quantified and *Ucp1* expression was determined. As expected, the glycerol concentration in the culture medium was significantly increased after 8 hours of stimulation with noradrenaline (17.6-fold, $P<0.001$ for clone #6; 21.3-fold, $P<0.001$ for clone #7) pointing to increased intracellular lipolysis (**Fig. 3B**). Consistent with the increased lipolysis, *Ucp1* expression was significantly increased after noradrenaline stimulation in both clones (+3.3-fold, $P<0.001$ for clone #6; 2.2-fold, $P<0.05$ for clone #7, **Fig. 3C**). Furthermore, oxygen consumption was measured using Seahorse respirometry before and after the addition of noradrenaline. Both clones acutely increased their oxygen consumption rate in response to noradrenaline (up to

+67% for clone #6 and +78% for clone #7 from the basal respiration rate, **Fig. 3D and E**). Together, these data demonstrate that the differentiated mouse iBPAs are responsive to adrenergic stimulation.

Human iBPAs possess adipogenic capacity only after shutdown of LT expression

Human primary BPAs were isolated from a biopsy taken from an area close to the isthmus region of the thyroid gland and monoclonal cell lines of human BPAs were generated in a similar fashion as for the mouse iBPAs (**Suppl. Fig. 1**). From patient 1, clones #2 and #3 were selected for further characterization as they exhibited the highest proliferative capacity, lipid droplet formation and *UCP1* expression. They were cultured under adipogenic culture conditions in the absence or presence of dox to relieve or exert proliferation pressure (**Fig. 4A**). Consecutive microscopic images taken two days apart revealed that cells from both clones gradually accumulated small lipid droplets only in the absence of dox (**Fig. 4B**). After 16 days of differentiation in the absence of dox 80-90% of the cells were lipid-laden, while cells cultured in the presence of dox did not show any signs of lipid droplet formation (**Fig. 4B**).

Since dox negatively impacted on the formation of lipid droplets by the human iBPAs as determined by microscopy, we next analyzed the expression patterns of brown adipocyte markers by RT-qPCR in both clones cultured in both the absence and presence of dox (**Fig. 4C**). The expression of UCP-1 increased starting at day 4 of adipogenic differentiation for both clones cultured without dox (-dox), whereas the *UCP1* expression of cells cultured in the presence of dox remained constant and low (+dox). *UCP1* expression of clone #3 peaked at day 14 of adipogenic differentiation and at this time point was more than 4 times higher than the *UCP1* expression of clone #2. *PRDM16* mRNA levels took an unexpected course being similar at differentiation day 0 and lower at differentiation day 16, with a peak in *PRDM16* mRNA levels at differentiation day 8 of clone #3 in the absence of dox. When the cells were cultured in the absence of dox, *PPARGC1A*, *FABP4* and *LPL* expression robustly increased between differentiation day 4 and 8, after which *PPARGC1A* expression stabilized at a somewhat lower level. *FABP4* and *LPL* expression further increased after differentiation day 8, peaking around differentiation day 10-12 and day 10-14, respectively. When the cells were cultured in the presence of dox, expression of these three markers did not significantly change/increase during the entire differentiation period. Lastly, *PPARG* expression showed a similar induction during the first 4 days of adipogenic differentiation under all culture conditions. Subsequently, *PPARG* expression of clone #3 cultured without dox further increased and peaked at differentiation day 8. In contrast, *PPARG* expression of clone #2 cultured without dox remained fairly stable while in both clones cultured in the presence of dox *PPARG* expression declined again. Based on these data, we conclude that conditionally immortalized human BPAs

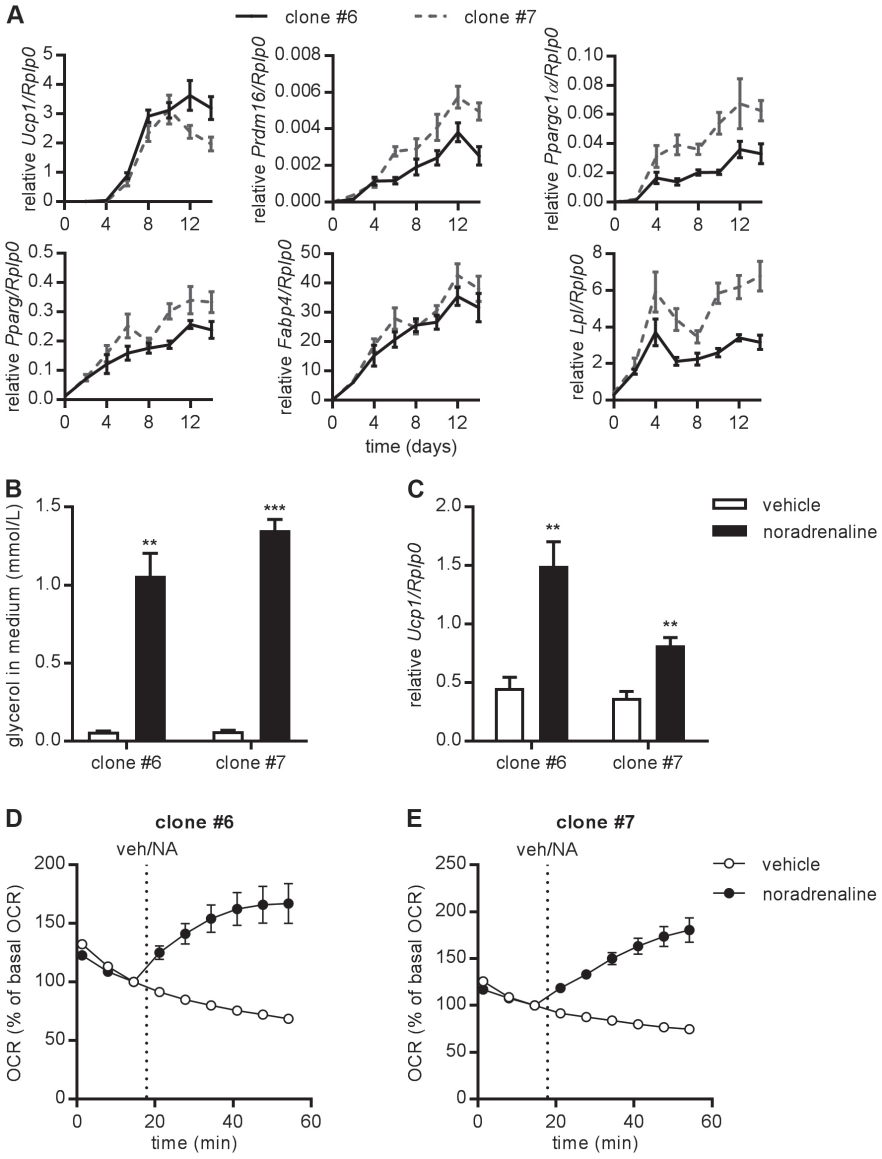

Figure 3. Genetic profiles and functional properties of adipogenically differentiated mouse iBPAs. (A) RT-qPCR analysis of *Ucp1*, *Prdm16*, *Ppargc1a*, *Pparg*, *Fabp4* and *Lpl* gene expression in clone #6 and #7 mouse iBPAs on the indicated days of adipogenic differentiation normalized to *Rplp0* expression. (B-E) Effect of adrenergic stimulation on clone #6 and #7 mouse iBPAs. Both clones were stimulated with 1 μM noradrenaline for 8 hours, at differentiation day 12, after which glycerol in the culture medium (B) and *Ucp1* mRNA levels in the cells (C) were measured. Oxygen consumption rate in adipogenically differentiated mouse iBPAs upon injection of vehicle or noradrenaline using Seahorse respirometry (D, E). Data are means ± SEM (n=4 in A, B, C, D; n=7-12 in D, E). ** P<0.01; *** P<0.001. iBPA, conditionally immortalized brown preadipocyte; RT-qPCR, reverse transcription-quantitative polymerase chain reaction; OCR, oxygen consumption rate; veh, vehicle.

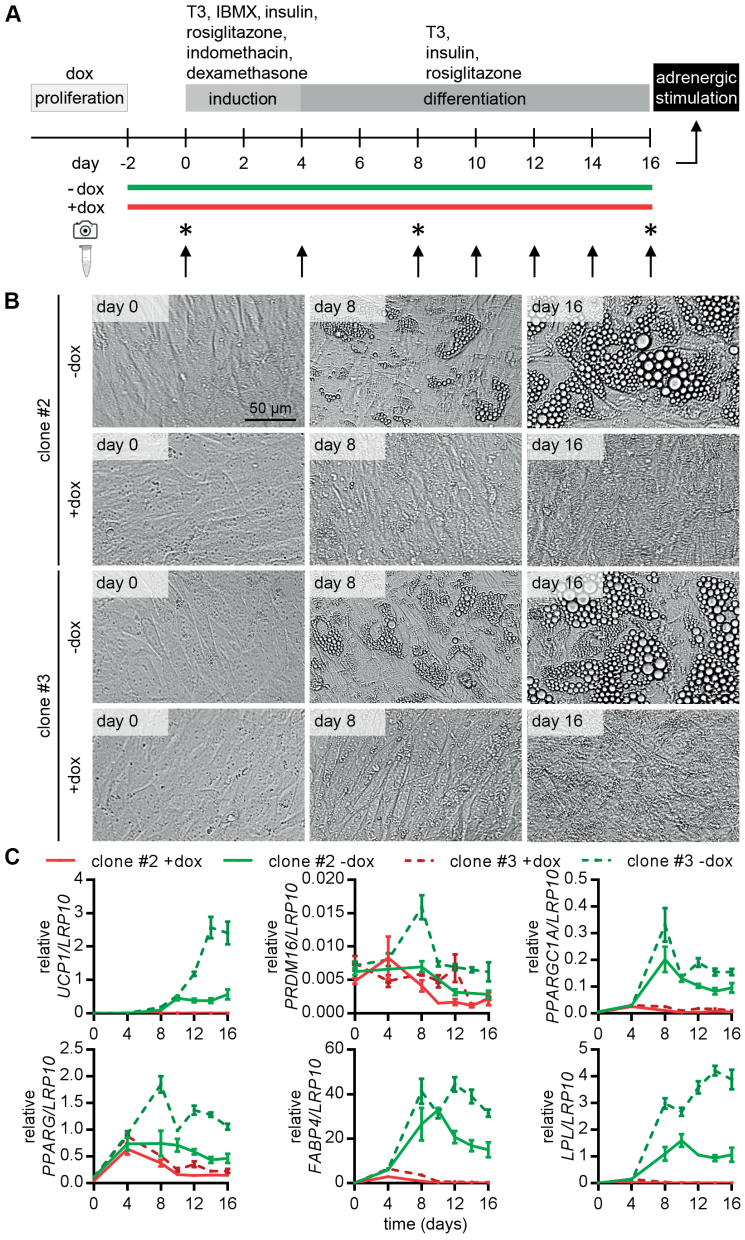

Figure 4. Adipogenic capacity of human iBPAs. (A) Protocol used to differentiate human iBPAs into brown adipocytes. (B) Phase-contrast images showing the morphological changes induced by adipogenic stimulation of clone #2 and #3 human iBPAs cultured with (+dox) and without (-dox) continuous proliferation pressure. (C) RT-qPCR analysis of *UCP1*, *PRDM16*, *PPARGC1A*, *PPARG*, *FABP4* and *LPL* gene expression in clone #2 and #3 human iBPAs on the indicated days of culturing under adipogenic culture conditions with and without dox. Expression levels were normalized to *LRP10* expression. Data are means ± SEM (n=4). iBPA, conditionally immortalized brown preadipocyte; dox, doxycycline; RT-qPCR, reverse transcription-quantitative polymerase chain reaction; T3, triiodothyronine; IBMX, 3-isobutyl-1-methylxanthine.

were able to adapt a multilocular phenotype and a gene expression pattern compatible with brown adipocytes only in the absence of dox and that optimal differentiation is reached at 14-16 days after initiation of adipogenesis.

Noradrenaline activates adipogenically differentiated human iBPAs

Similar to the mouse iBPAs, we also investigated the response of adipogenically differentiated human iBPAs to adrenergic stimulation. Stimulation of differentiated iBPAs with noradrenaline increased the glycerol concentration in the culture medium with +43% ($P<0.01$, **Fig. 5A**) and +200% ($P<0.001$, **Fig. 5A**) over basal values for clone #2 and clone #3, respectively. Although *UCP1* expression levels were lower in clone #2 compared to clone #3, noradrenaline stimulation increased *UCP1* expression in both clones (clone #2: +292%, $P<0.05$ and clone #3: +198%, $P<0.05$, **Fig. 5B**). Also, oxygen consumption rate was increased in both clones in response to noradrenaline stimulation (up to +106% for clone #2 and +93% for clone #3 from the basal respiration rate, **Fig. 5C-D**).

Subsequently, monoclonal cell lines from BAT biopsies of three other adult humans were generated by conditional immortalization as described above. One clone was selected from each patient based on its differentiation capacity and *UCP1* expression to investigate their response to adrenergic stimulation. During adipogenic culture conditions, clones from all three patients showed an increase in *UCP1* expression from differentiation day 4 onwards with the clone from patient 4 reaching the higher level of *UCP1* mRNA (**Fig. 5E**). Moreover, all three clones also showed increased glycerol release (**Fig. 5F**) and *UCP1* expression (**Fig. 5G**) 8 hours following noradrenaline stimulation. Together, these data demonstrate that differentiated human iBPAs derived from different patients are responsive to adrenergic stimulation.

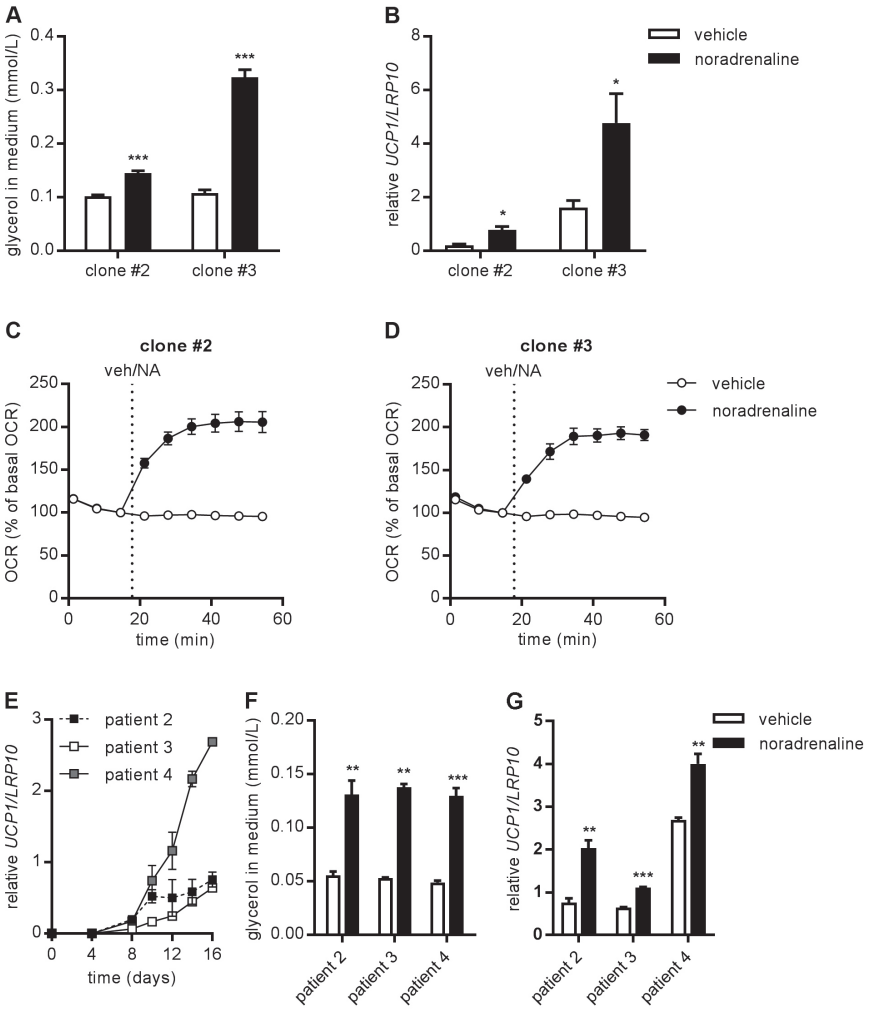

Figure 5. Functional properties of adipogenically differentiated human iBPAs. (A-D) Effect of adrenergic stimulation on clone #2 and #3 human iBPAs. Both clones were stimulated with 1 µM noradrenaline for 8 hours, at differentiation day 16, after which glycerol in the culture medium (A) and *UCP1* mRNA levels in the cells (B) were measured. Oxygen consumption rate in adipogenically differentiated human iBPAs upon injection of vehicle or noradrenaline using Seahorse respirometry (C, D). RT-qPCR analysis of *UCP1* expression (E) during adipogenic differentiation in human iBPA clones derived from 3 additional patients (*i.e.* patients 2-4). Effect of adrenergic stimulation on human iBPA clones from patients 2, 3 and 4 (F, G). These clones were stimulated with 1 µM noradrenaline for 8 hours, at differentiation day 16, and glycerol in the culture medium (F) and *UCP1* mRNA levels in the cells (G) were measured. Data are means ± SEM (n=4 in A, B; n=10-12 in C, D; n=3 in E, F, G). * P<0.05; ** P<0.01; *** P<0.001. iBPA, conditionally immortalized brown preadipocyte; OCR, oxygen consumption rate; veh, vehicle; RT-qPCR, reverse transcription-quantitative polymerase chain reaction.

DISCUSSION

In this study, we used a system enabling the robust and tightly controlled expansion of monoclonal populations of mouse and human BPAs by endowing the cells with a dox-regulated SV40 LT expression. The presence of dox in the culture medium induced LT expression and caused rapid iBPA expansion, while removing dox released the proliferation pressure and prepared the cells for subsequent adipogenic differentiation. Our iBPA lines have adipogenic capacity and respond to adrenergic stimulation with an increase in lipolytic activity and oxygen consumption.

Permanent immortalization of murine BPAs has been proven to be a useful tool for studying brown adipocyte biology and responses to pharmacological treatments [13-16, 25]. However, these cells generally display a rapid loss of robust adipogenic capacity upon repeated cell divisions [13], limiting their applicability in high-throughput assays. Also, several important differences have been observed between murine and human BAT [26], which may limit the usefulness of immortalized murine BPAs as a model system for human brown adipocytes. Hence, the permanent immortalization of human BPAs was pursued, which yielded disparate cell lines [17, 18, 27] rather than providing standardized and ready-to-use cell clones that could be massively expanded without a substantial loss of adipogenic differentiation. In favorable contrast, our mouse and human iBPA lines retained full adipogenic capacity for at least 64 PDs, thereby providing abundant cell sources for high-throughput studies. Another limitation of non-conditionally immortalized BPAs is the potential influence of permanent expression of immortalization genes on the differentiation potential of BPAs or on the phenotype of the brown adipocytes derived from the immortalized cells. Conditional immortalized mouse BPAs have been generated using the temperature-sensitive LT mutant *ts*A58 [28]. However, even at the non-permissive temperature of 39°C, the binding of LT-*ts*A58 to p53 is only partially inhibited whereas its ability to repress pRB remains unaltered [29]. Lastly, immortalization of cells without clonal selection might result in unstable cell lines, since faster proliferating cells will overgrow the slower proliferating cells and thereby change the composition of the lines over serial passaging. On the other hand, using clonal selection may introduce selection bias since the fastest proliferating clones might not automatically give the best differentiating clones. Our monoclonal iBPA lines proved easy to culture and exhibited controlled expression of immortalization genes. Altogether, these assets provide a clear advantage in the assessment of differentiation stage-dependent gene expression profiles over existing models.

Gene expression profiles of mouse and human iBPA during differentiation showed several similarities with rising mRNA expression levels of the genes encoding *UCP1*, *PPARGC1A*, *FABP4* and *LPL*. Interestingly, while in murine iBPAs *PRDM16* expression was induced during adipogenic differentiation, this was not the case for the human iBPAs.

PRDM16 is a known transcriptional coregulator of BAT development and is suggested to repress white adipocyte gene expression and to promote the expression of beige/brown adipocyte genes [30, 31]. Using mouse adipocytes, Ohno *et al.* [32] have shown that PRDM16 is required for PPARγ agonist-induced brown adipogenesis. In line with this finding and considering the fact that *UCP1* is a target gene of PRDM16, it might be expected that the mRNA expression patterns of *UCP1* and *PRDM16* would follow a similar trend. Indeed, others have reported a strong correlation between *PRDM16* expression and *UCP1* expression in human brown adipocytes from the perirenal depot [33]. Nonetheless, even though our human iBPA do not show a clear adipogenic differentiation-dependent increase in *PRDM16* expression, they efficiently differentiate into multilocular brown adipocytes that are responsive to adrenergic stimulation. Perhaps, PRDM16 activity during the differentiation of our human iBPAs is post-transcriptionally regulated. However, since to date most studies on the regulation of BAT formation have been performed in mice and given the differences between murine and human BAT, additional studies are required to determine the precise role of PRDM16 and other factors in human brown adipogenesis.

We found that continuous LT expression, as induced by dox, inhibited the adipogenic differentiation of the human BPAs, whereas the presence of dox in the culture medium did not inhibit adipogenesis of the mouse BPAs. Previously dox has been shown to negatively impact on mitochondrial function [34, 35], which could theoretically impact differentiation capacity. However, since the concentration of dox used in our iBPA cultures (*i.e.* 100 µg/µL) was well below the concentration shown to disturb mammalian mitochondrial function [35] and the mouse iBPAs readily differentiated into brown adipocytes at this concentration, it is more likely that another mechanism is underlying the discrepancy between mouse and human cells. Since the preadipocytes were isolated from young mice versus from middle-aged humans, perhaps the age of the preadipocytes affects the capacity to differentiate under continuous proliferation pressure. Moreover, two different promoters were used to drive LT expression in murine and human BPAs and this may have resulted in different expression levels of LT, thereby contributing to differences in the adipogenic differentiation potential between dox-exposed murine and human iBPAs. The interspecies difference may also be caused by less pronounced effects of the pRB pathway on human cells compared to mouse adipocytes with respect to adipogenesis. Several studies have shown that inactivation of the pRB pathway inhibits white adipogenesis but facilitates brown adipogenesis in mice [20, 36, 37], whereas no correlation was found between *RB1*, the gene encoding pRB, and *UCP1* gene expression in human adipose tissue [38].

To immortalize human BPAs, Shinoda *et al.* [17] previously used a retrovirus which contains a UTR promoter-driven LT gene without intron, while our human iBPAs were generated using a lentiviral vector that contains an HsUBC promoter-driven LT gene with

intron. Pre-mRNA that contains the intron, *via* alternative splicing, gives rise to LT, 17kT and small tumor antigen (ST) [39, 40]. The lack of the intron results in depletion of small tumor antigen [39]. ST contains a cellular protein phosphatase 2A (PP2A) binding region which inhibits the pro-apoptotic activity of PP2A, thereby increasing the viability of cells [41, 42]. Xue *et al.* [18] used a comparable transfection method but LT was replaced by hTERT. A clear advantage of our cells is the proliferation speed and capacity. The cell lines of Xue *et al.* [18] exhibit slow proliferation speed and very limited PD, while Shinoda *et al.* [17] showed no data on proliferation capacity. We were able to generate murine and human cell lines from one clone that retain adipogenic capacity until at least PD 64.

Our iBPA cell lines provide many opportunities for future research. The mouse iBPA clone #6 retained full adipogenic capacity for at least 64 PDs, implying that > 10^{18} brown adipocytes could be generated from a single preadipocyte. This provides an abundant cell source for fundamental and applied research [43]. The tightly controlled LT expression/proliferation used in this study provided a safeguard against tumor development and creates an opportunity for this iBPAs to become a transplantable cell source. In addition, our iBPAs could be used to further explore the recently proposed hypothesis that mature brown adipocytes of mice retain proliferative capacity *in vivo* [44, 45], although the mechanism(s) involved is/are largely unknown. It will hence be of interest to investigate what happens when adipogenically differentiated iBPAs are re-exposed to dox. If this would cause them to start dividing again, it might (i) provide a good model system to gain more insight into the pathways involved in BAT hyperplasia and (ii) allow dox-dependent regulation of the size of the BAT compartment *in vivo*. Besides, a better understanding of the species-specific role of LT and pRB in adipogenesis will help to further understand the mechanisms of brown adipogenesis as well as the conversion of white into brown adipocytes and *vice versa*. iBPAs are unique in their ability to vary the timing of LT expression and therefore vary the pocket protein activity in relation to the moment of adipogenic stimulation. This property makes iBPAs particularly attractive for studying the role of cell cycle regulators including those directly targeted by LT in BPA differentiation.

In conclusion, we established lines of conditionally immortalized mouse and human BPAs with long-term proliferation ability and adipogenic capacity. Following adipogenesis, these cells display a multilocular lipid droplet appearance as well as a gene expression signature and metabolic capacity akin to brown adipocytes. The generated cell lines have many potential applications and can, for example, be used to investigate BPA proliferation and differentiation, brown (pre)adipocyte metabolism and regulation of *Ucp1*/*UCP1* activity and thermogenesis, for brown (pre)adipocyte-based disease modelling, BPA transplantation studies and drug development.

ACKNOWLEDGEMENTS

The authors also thank Kevin Brewster and Trea Streefland (LUMC, Dept. Internal Medicine, Div. Endocrinology) for their valuable technical assistance.

FUNDING

This work was supported by the Netherlands Heart Institute (grant 230.148-04 to A.A.F.V); the Royal Netherlands Academy of Arts and Sciences (Chinese Exchange Programme grant 10CDP007 to A.A.F.V); the research programme More Knowledge with Fewer Animals (MKMD; grant 114022503 to A.A.F.V); a research grant from the Rembrandt Institute of Cardiovascular Science; the Dutch Diabetes Foundation (grant 2015.81.1808 to M.R. Boon); the Dutch Heart Foundation (grant 2017T016 to S. Kooijman) and the European Foundation for the Study of Diabetes (EFSD Rising Star Fellowship Programme to S. Kooijman). J.L. was supported by the Chinese Scholarship Council.

REFERENCES

1. Bartelt, A.; Bruns, O. T.; Reimer, R.; Hohenberg, H.; Ittrich, H.; Peldschus, K.; Kaul, M. G.; Tromsdorf, U. I.; Weller, H.; Waurisch, C., et al. Brown adipose tissue activity controls triglyceride clearance. *Nat Med* **2011**, 17, (2), 200-5.
2. van den Berg, R.; Kooijman, S.; Noordam, R.; Ramkisoensing, A.; Abreu-Vieira, G.; Tambyrajah, L. L.; Dijk, W.; Ruppert, P.; Mol, I. M.; Kramar, B. A, et al. Diurnal Rhythm in Brown Adipose Tissue Causes Rapid Clearance and Combustion of Plasma Lipids at Wakening. *Cell Rep* **2018**, 22, (13), 3521-3533.
3. Hoeke, G.; Kooijman, S.; Boon, M. R.; Rensen, P. C.; Berbée, J. F. Role of brown fat in lipoprotein metabolism and atherosclerosis. *Circ Res* **2016**, 118, (1), 173-82.
4. Cannon, B.; Nedergaard, J. Brown adipose tissue: function and physiological significance. *Physiol Rev* **2004**, 84, (1), 277-359.
5. Townsend, K.; Tseng, Y. H. Brown adipose tissue: Recent insights into development, metabolic function and therapeutic potential. *Adipocyte* **2012**, 1, (1), 13-24.
6. Schulz, T. J.; Tseng, Y. H. Brown adipose tissue: development, metabolism and beyond. *Biochem J* **2013**, 453, (2), 167-78.
7. Zhang, H.; Schulz, T. J.; Espinoza, D. O.; Huang, T. L.; Emanuelli, B.; Kristiansen, K.; Tseng, Y. H. Cross talk between insulin and bone morphogenetic protein signaling systems in brown adipogenesis. *Mol Cell Biol* **2010**, 30, (17), 4224-33.
8. Kajimura, S.; Seale, P.; Kubota, K.; Lunsford, E.; Frangioni, J. V.; Gygi, S. P.; Spiegelman, B. M. Initiation of myoblast to brown fat switch by a PRDM16-C/EBP-beta transcriptional complex. *Nature* **2009**, 460, (7259), 1154-8.
9. Seale, P.; Bjork, B.; Yang, W.; Kajimura, S.; Chin, S.; Kuang, S.; Scime, A.; Devarakonda, S.; Conroe, H. M.; Erdjument-Bromage, H., et al. PRDM16 controls a brown fat/skeletal muscle switch. *Nature* **2008**, 454, (7207), 961-7.
10. Cannon, B.; Nedergaard, J. Developmental biology: Neither fat nor flesh. *Nature* **2008**, 454, (7207), 947-8.
11. Kiefer, F. W. The significance of beige and brown fat in humans. *Endocr Connect* **2017**, EC-17-0037.
12. Zhang, J.; Thomas, T. Z.; Kasper, S.; Matusik, R. J. A small composite probasin promoter confers high levels of prostate-specific gene expression through regulation by androgens and glucocorticoids in vitro and in vivo. *Endocrinology* **2000**, 141, (12), 4698-4710.
13. Irie, Y.; Asano, A.; Canas, X.; Nikami, H.; Aizawa, S.; Saito, M. Immortal brown adipocytes from p53-knockout mice: differentiation and expression of uncoupling proteins. *Biochem Biophys Res Commun* **1999**, 255, (2), 221-5.
14. Kozak, U. C.; Held, W.; Kreutter, D.; Kozak, L. P. Adrenergic regulation of the mitochondrial uncoupling protein gene in brown fat tumor cells. *Mol Endocrinol* **1992**, 6, (5), 763-72.
15. Klaus, S.; Choy, L.; Champigny, O.; Cassard-Doulcier, A. M.; Ross, S.; Spiegelman, B.; Ricquier, D. Characterization of the novel brown adipocyte cell line HIB 1B. Adrenergic pathways involved in regulation of uncoupling protein gene expression. *J Cell Sci* **1994**, 107 (Pt 1), 313-9.
16. Zennaro, M. C.; Le Menuet, D.; Viengchareun, S.; Walker, F.; Ricquier, D.; Lombes, M. Hibernoma development in transgenic mice identifies brown adipose tissue as a novel target of aldosterone action. *J Clin Invest* **1998**, 101, (6), 1254-60.
17. Shinoda, K.; Luijten, I. H.; Hasegawa, Y.; Hong, H.; Sonne, S. B.; Kim, M.; Xue, R.; Chondronikola, M.; Cypess, A. M.; Tseng, Y. H., et al. Genetic and functional characterization of clonally derived adult human

brown adipocytes. *Nat Med* **2015**, 21, (4), 389-94.

18. Xue, R.; Lynes, M. D.; Dreyfuss, J. M.; Shamsi, F.; Schulz, T. J.; Zhang, H.; Huang, T. L.; Townsend, K. L.; Li, Y.; Takahashi, H. , et al. Clonal analyses and gene profiling identify genetic biomarkers of the thermogenic potential of human brown and white preadipocytes. *Nat Med* **2015**, 21, (7), 760-8.
19. Molchadsky, A.; Ezra, O.; Amendola, P. G.; Krantz, D.; Kogan-Sakin, I.; Buganim, Y.; Rivlin, N.; Goldfinger, N.; Folgiero, V.; Falcioni, R., et al. p53 is required for brown adipogenic differentiation and has a protective role against diet-induced obesity. *Cell Death Differ* **2013**, 20, (5), 774-83.
20. Hansen, J. B.; Jørgensen, C.; Petersen, R. K.; Hallenborg, P.; De Matteis, R.; Bøye, H. A.; Petrovic, N.; Enerbäck, S.; Nedergaard, J.; Cinti, S., et al. Retinoblastoma protein functions as a molecular switch determining white versus brown adipocyte differentiation. *Proc Natl Acad Sci U S A* **2004**, 101, (12), 4112-7.
21. Szulc, J.; Wiznerowicz, M.; Sauvain, M. O.; Trono, D.; Aebischer, P. A versatile tool for conditional gene expression and knockdown. *Nat Methods* **2006**, 3, (2), 109-16.
22. Liu, J.; Volkers, L.; Jangsangthong, W.; Bart, C. I.; Engels, M. C.; Zhou, G.; Schalij, M. J.; Ypey, D. L.; Pijnappels, D. A.; de Vries, A. A. Generation and primary characterization of iAM-1, a versatile new line of conditionally immortalized atrial myocytes with preserved cardiomyogenic differentiation capacity. *Cardiovasc Res* **2018**, 114, (14), 1848-1859.
23. Neshati, Z.; Liu, J.; Zhou, G.; Schalij, M. J.; de Vries, A. A. Development of a lentivirus vector-based assay for non-destructive monitoring of cell fusion activity. *PloS One* **2014**, 9, (7), e102433.
24. Cannon, B.; Nedergaard, J. Brown adipose tissue: function and physiological significance. *Physiol Rev* **2004**, 84, (1), 277-359.
25. Forest, C.; Doglio, A.; Ricquier, D.; Ailhaud, G. A preadipocyte clonal line from mouse brown adipose tissue. Short- and long-term responses to insulin and beta-adrenergics. *Exp Cell Res* **1987**, 168, (1), 218-32.
26. Liu, X.; Cervantes, C.; Liu, F. Common and distinct regulation of human and mouse brown and beige adipose tissues: a promising therapeutic target for obesity. *Protein Cell* **2017**, 8, (6), 446-454.
27. Markussen, L. K.; Isidor, M. S.; Breining, P.; Andersen, E. S.; Rasmussen, N. E.; Petersen, L. I.; Pedersen, S. B.; Richelsen, B.; Hansen, J. B. Characterization of immortalized human brown and white pre-adipocyte cell models from a single donor. *PloS One* **2017**, 12, (9), e0185624.
28. Rosell, M.; Kaforou, M.; Frontini, A.; Okolo, A.; Chan, Y. W.; Nikolopoulou, E.; Millership, S.; Fenech, M. E.; MacIntyre, D.; Turner, J. O., et al. Brown and white adipose tissues: intrinsic differences in gene expression and response to cold exposure in mice. *Am J Physiol Endocrinol Metab* **2014**, 306, (8), E945-64.
29. Ray, S.; Anderson, M. E.; Tegtmeyer, P. Differential interaction of temperature-sensitive simian virus 40 T antigens with tumor suppressors pRb and p53. *J Virol* **1996**, 70, (10), 7224-7227.
30. Seale, P.; Kajimura, S.; Yang, W.; Chin, S.; Rohas, L. M.; Uldry, M.; Tavernier, G.; Langin, D.; Spiegelman, B. M. Transcriptional control of brown fat determination by PRDM16. *Cell Metab* **2007**, 6, (1), 38-54.
31. Seale, P. Transcriptional regulatory circuits controlling brown fat development and activation. *Diabetes* **2015**, 64, (7), 2369-75.
32. Ohno, H.; Shinoda, K.; Spiegelman, B. M.; Kajimura, S. PPARγ agonists induce a white-to-brown fat conversion through stabilization of PRDM16 protein. *Cell Metab* **2012**, 15, (3), 395-404.
33. Nagano, G.; Ohno, H.; Oki, K.; Kobuke, K.; Shiwa, T.; Yoneda, M.; Kohno, N. Activation

of classical brown adipocytes in the adult human perirenal depot is highly correlated with PRDM16–EHMT1 complex expression. *PloS One* **2015**, 10, (3), e0122584.

34. Chatzispyrou, I. A.; Held, N. M.; Mouchiroud, L.; Auwerx, J.; Houtkooper, R. H. Tetracycline antibiotics impair mitochondrial function and its experimental use confounds research. *Cancer Res* **2015**, 75, (21), 4446-9.
35. Moullan, N.; Mouchiroud, L.; Wang, X.; Ryu, D.; Williams, E. G.; Mottis, A.; Jovaisaite, V.; Frochaux, M. V.; Quiros, P. M.; Deplancke, B., et al. Tetracyclines Disturb Mitochondrial Function across Eukaryotic Models: A Call for Caution in Biomedical Research. *Cell Rep* **2015**.
36. Cherington, V.; Morgan, B.; Spiegelman, B. M.; Roberts, T. M. Recombinant retroviruses that transduce individual polyoma tumor antigens: effects on growth and differentiation. *Proc Natl Acad Sci U S A* **1986**, 83, (12), 4307-11.
37. Higgins, C.; Chatterjee, S.; Cherington, V. The block of adipocyte differentiation by a C-terminally truncated, but not by full-length, simian virus 40 large tumor antigen is dependent on an intact retinoblastoma susceptibility protein family binding domain. *J Virol* **1996**, 70, (2), 745-52.
38. Moreno-Navarrete, J. M.; Petrov, P.; Serrano, M.; Ortega, F.; Garcia-Ruiz, E.; Oliver, P.; Ribot, J.; Ricart, W.; Palou, A.; Bonet, M. L., et al. Decreased RB1 mRNA, protein, and activity reflect obesity-induced altered adipogenic capacity in human adipose tissue. *Diabetes* **2013**, 62, (6), 1923-31.
39. Berk, A. J.; Sharp, P. A. Spliced early mRNAs of simian virus 40. *Proc Natl Acad Sci U S A* **1978**, 75, (3), 1274-78.
40. Zerrahn, J.; Knippschild, U.; Winkler, T.; Deppert, W. Independent expression of the transforming amino-terminal domain of SV40 large I antigen from an alternatively spliced third SV40 early mRNA. *EMBO J* **1993**, 12, (12), 4739-46.
41. Pallas, D. C.; Shahrik, L. K.; Martin, B. L.; Jaspers, S.; Miller, T. B.; Brautigan, D. L.; Roberts, T. M. Polyoma small and middle T antigens and SV40 small t antigen form stable complexes with protein phosphatase 2A. *Cell* **1990**, 60, (1), 167-76.
42. Pallas, D. C.; Weller, W.; Jaspers, S.; Miller, T.; Lane, W.; Roberts, T. The third subunit of protein phosphatase 2A (PP2A), a 55-kilodalton protein which is apparently substituted for by T antigens in complexes with the 36-and 63-kilodalton PP2A subunits, bears little resemblance to T antigens. *J Virol* **1992**, 66, (2), 886-93.
43. Kroon, J.; Koorneef, L. L.; van den Heuvel, J. K.; Verzijl, C. R.; van de Velde, N. M.; Mol, I. M.; Sips, H. C.; Hunt, H.; Rensen, P. C.; Meijer, O. C. Selective glucocorticoid receptor antagonist CORT125281 activates brown adipose tissue and alters lipid distribution in male mice. *Endocrinology* **2017**, 159, (1), 535-546.
44. Okamatsu-Ogura, Y.; Fukano, K.; Tsubota, A.; Nio-Kobayashi, J.; Nakamura, K.; Morimatsu, M.; Sakaue, H.; Saito, M.; Kimura, K. Cell-cycle arrest in mature adipocytes impairs BAT development but not WAT browning, and reduces adaptive thermogenesis in mice. *Sci Rep* **2017**, 7, (1), 6648.
45. Fukano, K.; Okamatsu-Ogura, Y.; Tsubota, A.; Nio-Kobayashi, J.; Kimura, K. Cold Exposure Induces Proliferation of Mature Brown Adipocyte in a ß3-Adrenergic Receptor-Mediated Pathway. *PloS One* **2016**, 11, (11), e0166579.

SUPPLEMENTARY APPENDIX

Supplementary Materials and Methods

Construction of plasmids

DNA constructions were carried out with enzymes from Fermentas (Thermo Fisher Scientific, Breda, the Netherlands) or from New England Biolabs (Bioké, Leiden, the Netherlands) and with oligodeoxyribonucleotides from Sigma-Aldrich (Zwijndrecht, the Netherlands) using established procedures or following the instructions provided with specific reagents.

To generate pLV.iHsEEF1A1.LT-*ts*A58.WHVPRE, plasmid pAT153.SV40ori(-)*ts*A58, which codes for the temperature-sensitive mutant of the oncogenic SV40 LT antigen designated *ts*A58 [1], was used as template in a polymerase chain reaction (PCR) with VELOCITY DNA polymerase (GC Biotech, Alphen a/d Rijn, the Netherlands) and primers 5′ AAGGATCC-GTGCACCATGGATAAAGTTTTAAACAGAGAGGA 3′ and 5′ CCGAATTCTTTATGTTTCAG-GTTCAGGG 3′ (the LT initiation codon and the complement of its termination codon are underlined). The resulting PCR fragment was inserted into plasmid pJET1.2/blunt using the CloneJET PCR cloning kit (Thermo Fisher Scientific) to generate pJet1.2.LT-*ts*A58. pJet1.2.LT-*ts*A58 was incubated with BamHI and EcoRI and the 2.5-kb digestion product was combined with the 11.5-kb BamHI×EcoRI fragment of SIN-LV shuttle plasmid pLVET.tTS.dEcoRI to generate pLV.iHsEEF1A1.LT-*ts*A58. pLVET.tTS.dEcoRI is a derivative of pLVET-tTR-KRAB [2] (Addgene, Cambridge, MA; plasmid number: 116444). It was made by digestion of pLVET-tTR-KRAB with EcoRI and NheI and ligation of the resulting 1.6-kb fragment encoding the encephalomyocarditis virus internal ribosomal entry site and the tetracycline-controlled transrepressor protein TetR-KRAB [3] to the 10.8-kb EcoRI×BcuI fragment of pLVET-tTR-KRAB.

pLV.ihUBC.LT-*ts*A58.WHVPRE is a derivative of pLV.iHsEEF1A1.LT-*ts*A58.WHVPRE. It was generated by replacing the human eukaryotic translation elongation factor 1A1 gene promoter in pLV.iHsEEF1A1.LT-*ts*A58.WHVPRE by the promoter of the human ubiquitin C gene.

Immunocytology

Cells were processed for immunostaining as previously described [4]. Detection of LT was done with the same primary antibody as used for the analysis of LT expression by western blotting. Actively replicating cells were detected using polyclonal rabbit anti-Ki-67 antibodies (Abcam, Cambridge, United Kingdom; catalogue number: ab15580). The primary antibodies were diluted 1:200 in PBS containing 0.1% normal donkey serum (Sigma-Aldrich) and incubated overnight at 4°C. Bound antigens were detected using Alexa 488-conjugated donkey anti-rabbit IgG (H+L) (Thermo Fisher Scientific; catalogue

number: A21206) and Alexa 568-coupled donkey anti-mouse IgG (H+L) (Thermo Fisher Scientific; catalogue number: A10037). These secondary antibodies were diluted 1:400 in PBS. Hoechst 33342 (10 µg/µL; Thermo Fisher Scientific) was used to counterstain nuclei. Stained cells were visualized using a digital color camera-equipped fluorescence microscope (Nikon Eclipse 80i; Nikon Instruments Europe, Amstelveen, the Netherlands).

Supplementary table 1. Clinical characteristics of patients whose adipose biopsies were used to isolate human primary BPAs

	Age (year)	Sex	BMI (kg/m^2)
Patient 1	36	M	> 30
Patient 2	65	F	27.3
Patient 3	54	F	< 30
Patient 4	38	F	25.2

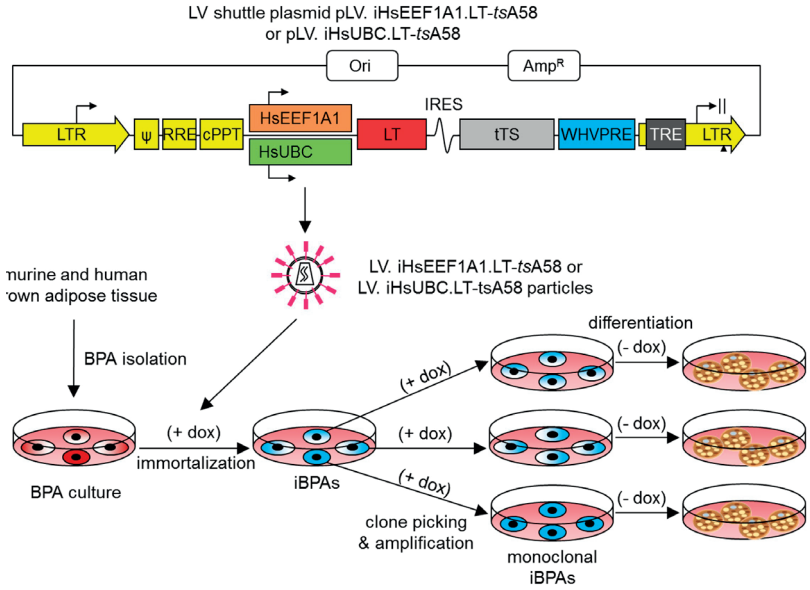

Supplementary figure 1. Schematic representation of LV shuttle plasmids and protocol to generate conditionally immortalized BPAs. Ori, bacterial origin of replication. AmpR, *Escherichia coli* ß-lactamase gene. LTR, human immunodeficiency virus type 1 (HIV1) long terminal repeat. Ψ, HIV1 packaging signal. RRE, HIV1 Rev-responsive element. cPPT, HIV1 central polypurine tract and termination site. HsEEF1A1, human eukaryotic translation elongation factor 1A1 gene promoter. HsUBC, human ubiquitin C gene promoter. LT, coding sequence of the temperature-sensitive mutant LT protein *ts*A58. IRES, encephalomyocarditis virus internal ribosome entry site. tTS, coding sequence of the hybrid tetracycline-controlled transcriptional repressor TetR-KRAB. WHVPRE, woodchuck hepatitis virus posttranscriptional regulatory element. TRE, tetracycline-responsive promoter element consisting of 7 repeats of a 19-nucleotide tetracycline operator (tetO) sequence. LV, lentiviral vector; BPA, brown preadipocyte; iBPAs, conditionally immortalized BPAs.

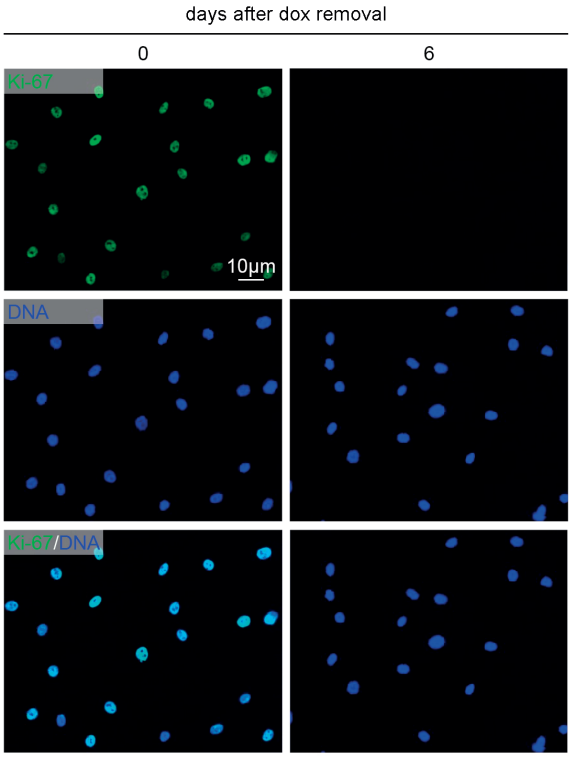

Supplementary figure 2. Dox-inducible proliferation capacity of clone #6 mouse iBPAs. Fluorographs images of iBPAs maintained in growth medium before (0) and 6 days after dox removal immunostained for the proliferation marker Ki-67 (green). Nuclei are visualized with Hoechst 33342 (blue). Dox, doxycycline; iBPA, conditionally immortalized brown preadipocyte.

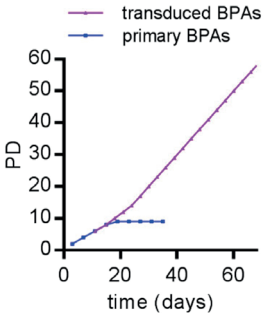

Supplementary figure 3. Growth curves of primary human BPAs and transduced human BPAs. Cells were cultured in the presence of dox. BPA, brown preadipocyte; PD, population doubling.

1. Liu, J.; Volkers, L.; Jangsangthong, W.; Bart, C. I.; Engels, M. C.; Zhou, G.; Schalij, M. J.; Ypey, D. L.; Pijnappels, D. A.; de Vries, A. A. Generation and primary characterization of iAM-1, a versatile new line of conditionally immortalized atrial myocytes with preserved cardiomyogenic differentiation capacity. *Cardiovasc Res* **2018**, 114, (14), 1848-1859.
2. Szulc, J.; Wiznerowicz, M.; Sauvain, M. O.; Trono, D.; Aebischer, P. A versatile tool for conditional gene expression and knockdown. *Nat Methods* **2006**, 3, (2), 109-16.
3. Deuschle, U.; Meyer, W. K.; Thiesen, H. J. Tetracycline-reversible silencing of eukaryotic promoters. *Mol Cell Biol* **1995**, 15, (4), 1907-14.
4. Yu, Z.; Liu, J.; van Veldhoven, J. P.; AP, I. J.; Schalij, M. J.; Pijnappels, D. A.; Heitman, L. H.; de Vries, A. A. Allosteric modulation of Kv11.1 (hERG) channels protects against drug-induced ventricular arrhythmias. *Circ Arrhythm Electrophysiol* **2016**, 9, (4), e003439.

4

IL-37 EXPRESSION REDUCES LEAN BODY MASS IN MICE BY REDUCING FOOD INTAKE

Eline N. Kuipers*,
Andrea D. van Dam*,
Dov B. Ballak, Ellemiek A. de Wit,
Charles A. Dinarello, Rinke Stienstra,
Janna A. van Diepen,
Patrick C.N. Rensen, Mariëtte R. Boon

International Journal of Molecular Sciences (2018); 19: E2264

ABSTRACT

The human cytokine IL-37 is an anti-inflammatory member of the IL-1 family of cytokines. Transgenic expression of IL-37 in mice protects them from diet-induced obesity and associated metabolic complications including dyslipidemia, inflammation and insulin resistance. The precise mechanism of action leading to these beneficial metabolic effects is not entirely known. Therefore, we aimed to assess in detail the effect of transgenic IL-37 expression on energy balance, including food intake and energy expenditure. Feeding homozygous IL-37 transgenic mice and wild-type (WT) control mice a high-fat diet (HFD; 45% kcal palm fat) for 6 weeks showed that IL-37 reduced body weight related to a marked decrease in food intake. Subsequent mechanistic studies in mice with heterozygous IL-37 expression versus WT littermates, fed the HFD for 18 weeks, confirmed that IL-37 reduces food intake, which led to a decrease in lean body mass, but did not reduce fat mass and plasma lipid levels or alterations in energy expenditure independent of lean body mass. Taken together, this suggests that IL-37 reduces lean body mass by reducing food intake.

INTRODUCTION

The worldwide prevalence of obesity, defined as a body mass index (BMI) > 30 kg/m^2, has nearly doubled since 1980 and at least 2.7 million people die each year as a result of obesity [1]. This number is expected to further increase over the next decade. Obesity has a great impact on public health as it leads to disorders such as dyslipidemia, type 2 diabetes and cardiovascular disease [2, 3]. Obesity is caused by a positive energy balance that leads to excessive fat accumulation in adipose tissue, hypertrophy of adipocytes, hypoxia, and in the end cell death. This results in recruitment of inflammatory cells by white adipose tissue (WAT), which eventually leads to adipose tissue dysfunction, preceding dyslipidemia and type 2 diabetes [4, 5].

It has been shown that release of pro-inflammatory cytokines by adipocytes and/or immune cells in adipose tissue, including IL-1β, IL-6, TNFα and CCL2, is higher during obesity compared to the lean state. More specifically, TNFα has been repeatedly shown to hamper insulin signaling and to result in insulin resistance, which may eventually lead to type 2 diabetes (reviewed in [6]). Inhibiting pro-inflammatory cytokines to counteract their disadvantageous metabolic effects is extensively being studied [7, 8]. In contrast, anti-inflammatory cytokines that could potentially ameliorate the inflammatory micro-environment in obesity have been less well studied. IL-37, a cytokine previously known as IL-1 family member 7 (IL-1F7), is a member of the IL-1 family of cytokines that includes amongst others IL-1α, IL-1β, IL-1Ra, IL-18 and IL-33 [9]. The first studies into the function of IL-37 showed that it is a natural suppressor of innate inflammatory and immune responses [10]. In humans, several tissues and cell types express IL-37, including blood monocytes [11, 12], epithelial cells [13], endothelial cells [14] and, importantly, also adipocytes [9, 15]. IL-37 mRNA is degraded in the absence of inflammation, but upon LPS stimulation, *i.e.* a pro-inflammatory stimulus, IL-37 expression increases [16-18]. *In vitro*, it was shown that IL-37 suppresses expression of pro-inflammatory factors in monocytes and macrophages [10, 17]. These studies indicate that IL-37 expression counteracts pro-inflammatory cytokine expression through controlled mechanisms that ensure balance between host defense functions of inflammation and adverse effects [10, 16, 17].

Since a mouse homolog of IL-37 is unknown, *in vivo* studies into IL-37 function have employed a mouse model with transgenic (tg) expression of the most abundant isoform of human IL-37 (IL-37b; IL-37tg mice) [10, 11, 15, 19-21]. IL-37tg mice are protected from LPS-induced shock related to lower levels of inflammatory cytokines upon LPS treatment [10]. Strikingly, IL-37 expression in mice also protects against obesity and obesity-associated inflammation and insulin resistance [15]. IL-37tg mice fed a high-fat diet (HFD) showed a markedly lower gain in body weight and lower plasma lipid levels compared to wild-type (WT) control mice [15]. Although IL-37 was shown to induce metabolic changes in adipocytes and immune cells [15, 22, 23], it is still not entirely

known how the beneficial metabolic effects are instigated. Therefore, the aim of this study was to investigate the effect of IL-37 on energy balance, *i.e.* energy intake and energy expenditure, in more detail. To this end, IL-37tg and WT mice were fed a HFD to induce obesity. Homozygous IL-37tg mice showed lower body weight and food intake. Mechanistic studies in heterozygous mice demonstrated that IL-37 lowers food intake and specifically reduces lean body mass without reducing fat mass or plasma lipid levels. These results suggest that the lower lean body mass in IL-37tg mice is a result of lower food intake.

MATERIALS AND METHODS

Animals and diet

For the first study, male C57Bl/6J mice and IL-37tg mice homozygously overexpressing human IL-37 on a C57Bl/6J background were used. IL-37tg mice were generated as previously described [10], and C57Bl/6J mice were purchased from Jackson Laboratories (Bar Harbor, ME, USA). For the second study, male IL-37tg mice heterozygously expressing human IL-37 and WT littermates (both C57Bl/6J background) were bred. In both studies, mice were individually housed under standard conditions with a 12:12 h light-dark cycle and access to food and water. Animals were approximately 10 weeks of age at the start of high-fat diet (HFD; D12451, of which lard fat was replaced by palm fat, purchased from Ssniff, Soest, The Netherlands and Research Diet Services, Wijk bij Duurstede, The Netherlands) feeding. The HFD contained 45% kcal from palm fat, 20% of kcal derived from protein and 35% kcal derived from carbohydrates and was given for 6 or 18 weeks, as indicated. Mouse experiments were performed in accordance with the Institute for Laboratory Animal Research Guide for the Care and Use of Laboratory Animals and had received approval from the University Ethical Review Boards (DEC 13159, Radboud University Medical Centre, Nijmegen and Leiden University Medical Centre, The Netherlands).

Body weight, body composition and food intake

At indicated time points, body weight and food intake were measured. Body composition was measured using an EchoMRI-100 analyser (EchoMRI, TX, USA). Because IL-37 expression induced hypophagia in the first experiment with IL-37tg homozygous mice, in the second experiment an additional group of C57Bl/6J mice that was pair-fed to the heterozygous IL-37tg group was taken along. To achieve pair-feeding, food intake of the *ad libitum*-fed IL-37tg mice was monitored daily and the pair-fed mice were given the average amount of diet that the IL-37tg mice had consumed the previous day, at the end of the light phase.

Plasma glucose and lipids

At the indicated time points, 6 h-fasted blood samples were collected by tail vein bleeding into chilled capillaries that were coated with paraoxon (Sigma-Aldrich, MO, USA) to prevent ongoing lipolysis [24]. Isolated plasma was assayed for glucose (Instruchemie, Delfzijl, The Netherlands), total cholesterol and triglycerides (Roche Diagnostics, Mannheim, Germany), and free fatty acids (Wako Diagnostics; Instruchemie, Delfzijl, The Netherlands) following the manufacturers' protocols.

Energy metabolism

Heterozygous IL-37tg mice and WT littermates were housed in fully automatic metabolic cages (LabMaster System; TSE Systems, Bad Homburg, Germany) several days before HFD feeding and the first week of HFD-feeding, as indicated. Metabolic cages measured oxygen uptake (V_{O2}) and carbon dioxide production (V_{CO2}). Glucose oxidation and fat oxidation were calculated from V_{O2} and V_{CO2} as described previously [25]. Total energy expenditure was calculated from V_{O2} and V_{CO2} using the Weir equation [26]. Physical activity was measured with infrared sensor frames.

Statistical analysis

All data are expressed as means ± SEM. Differences between groups were determined using a two-tailed unpaired Student's t-test and food intake measurements in the heterozygous IL-37tg mice using a one-tailed unpaired Student's t-test. Statistical analyses were performed using Excel or SPSS 20.0 software package for Windows. Probability values less than 0.05 were considered statistically significant.

RESULTS

IL-37 expression alleviates diet-induced weight gain and reduces food intake

To assess the effect of IL-37 expression on the development of HFD-induced obesity, homozygous IL-37tg mice were fed a HFD for 6 weeks. Body weight of the IL-37tg mice was already 3.6 g lower compared to the WT control mice before initiation of the HFD (**Fig. 1A**) and this difference was magnified during HFD feeding resulting in a body weight difference of 10.5 g after 6 weeks of HFD ($P<0.001$). Even when corrected for body weight at the start of HFD feeding, IL-37tg mice gained substantially less weight compared to WT mice during 6 weeks of HFD (**Fig. 1B**). Next, we measured whether the energy intake in IL-37tg mice was different compared to WT controls. Quite surprisingly, food intake in IL-37tg mice was markedly lower throughout the HFD intervention period (-21 to -32%, $P<0.001$, **Fig. 1C**). This suggests that IL-37tg expression might alleviate diet-induced weight gain by reducing food intake.

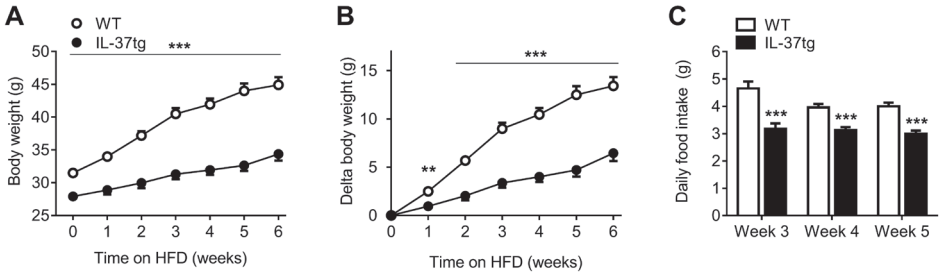

Figure 1. IL-37 expression alleviates diet-induced weight gain and reduces food intake. 10-week old male C57Bl/6J mice and homozygous IL-37tg mice on a C57Bl/6J background were fed a high-fat diet (HFD) for 6 weeks. Body weight (A, B) and food intake (C) were measured at indicated time points. Values represent means ± SEM (n=10 animals per group). **P<0.01, ***P<0.001 vs wild-type (WT).

Reduced food intake in heterozygous IL-37tg mice decreases lean body mass

To further investigate the effect of the reduced food intake in IL-37tg mice on body weight and composition independent of genetic background, a second study was set up that included a group of HFD-fed heterozygous IL-37tg mice and WT littermates that was pair-fed to these IL-37tg mice. Although less pronounced, heterozygous IL-37tg mice also had reduced food intake compared to WT littermates (-8% cumulative food intake after 18 weeks, P<0.05, **Fig. 2A, B**). Compared to homozygous IL-37tg mice, heterozygous IL-37tg mice only showed a tendency towards reduced body weight (**Fig. 2C**). Estimation of body composition by EchoMRI revealed that, while heterozygous IL-37tg mice had similar fat mass compared to WT littermates (**Fig. 2D**), their lean body mass was reduced (-7% after 18 weeks of HFD, P<0.05). Remarkably, lean body mass of the pair-fed group aligned with the WT control group until pair-feeding was started, upon which it dropped towards the lean body mass of the IL-37tg mice (**Fig. 2E**), suggesting that the reduction in food intake underlies the reduced lean body mass. To determine whether heterozygous IL-37 expression affects plasma glucose and lipid levels, blood was drawn after 0, 6 and 18 weeks of HFD feeding. Plasma glucose, total cholesterol, free fatty acids and triglyceride levels did not differ between the groups (**Fig. 3A-D**). These data suggest that heterozygous IL-37 overexpression primarily affects lean body mass *via* reducing food intake without affecting plasma glucose and lipid levels.

IL-37 expression decreases energy expenditure in conjunction with lean body mass reduction

To assess the effect of IL-37 expression on energy metabolism in more depth, energy expenditure, substrate utilization and activity levels were monitored by metabolic cages two days before and during the first week of HFD feeding. IL-37 expression did not affect physical activity levels (Suppl. **Fig. 1A, B**). Fat oxidation during the light period tended to be lower in IL-37tg mice compared to WT littermate controls (-12%, P=0.08, **Fig. 4A, B**).

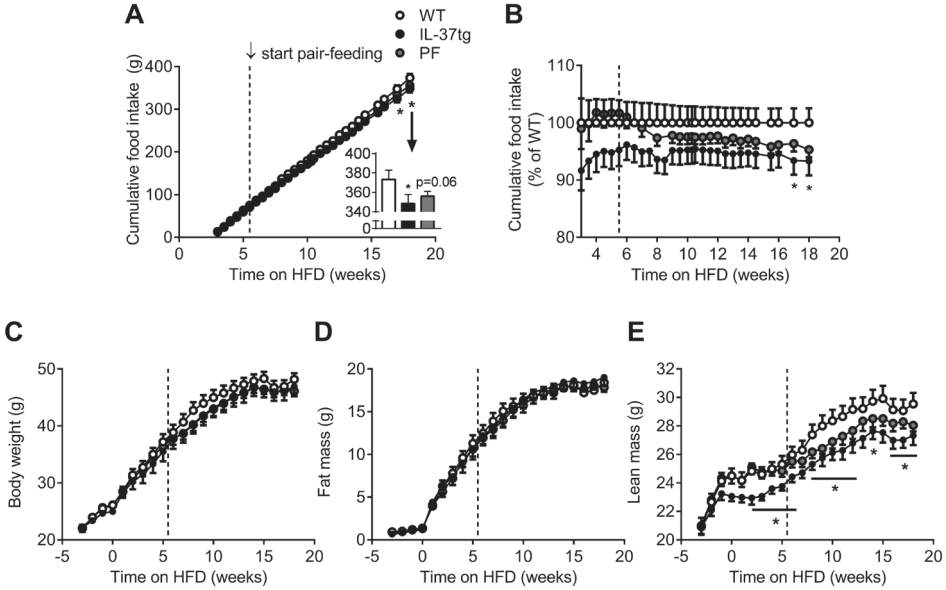

Figure 2. Reduced food intake in heterozygous IL-37tg mice decreases lean mass. 10-week old male C57Bl/6J mice and heterozygous IL-37tg mice on a C57Bl/6J background were fed a high-fat diet (HFD) for 18 weeks. Pair-feeding of wild-type (WT) mice (PF group) was initiated after 5.5 weeks of HFD feeding and is indicated by the dotted line (A-D). Food intake (FI; A, B), body weight (C), fat mass (D) and lean mass (E) were measured at indicated time points. Values represent means ± SEM (n=10 animals per group). *P<0.05 IL-37tg vs wild-type (WT).

Glucose oxidation during the dark period, in which mice are active, was lower in the IL-37tg mice compared to the control group (-12%, P<0.05, **Fig. 4C, D**). Energy expenditure during the light period tended to be lower in IL-37tg mice compared to WT littermate controls (-5%, P=0.07, Suppl. **Fig. 1C, D**). Since IL-37 expression reduced lean body mass, which is an important contributor to energy expenditure, we corrected the fat oxidation, glucose oxidation and total energy expenditure for lean body mass and found that differences in substrate utilization and total energy expenditure lost significance between IL-37tg and WT control mice (**Fig. 4E-H, Suppl. Fig. 1E, F**). These data suggest that heterozygous overexpression of IL-37 decreases glucose oxidation and tends to decrease fat oxidation and energy expenditure as a consequence of reduced lean body mass.

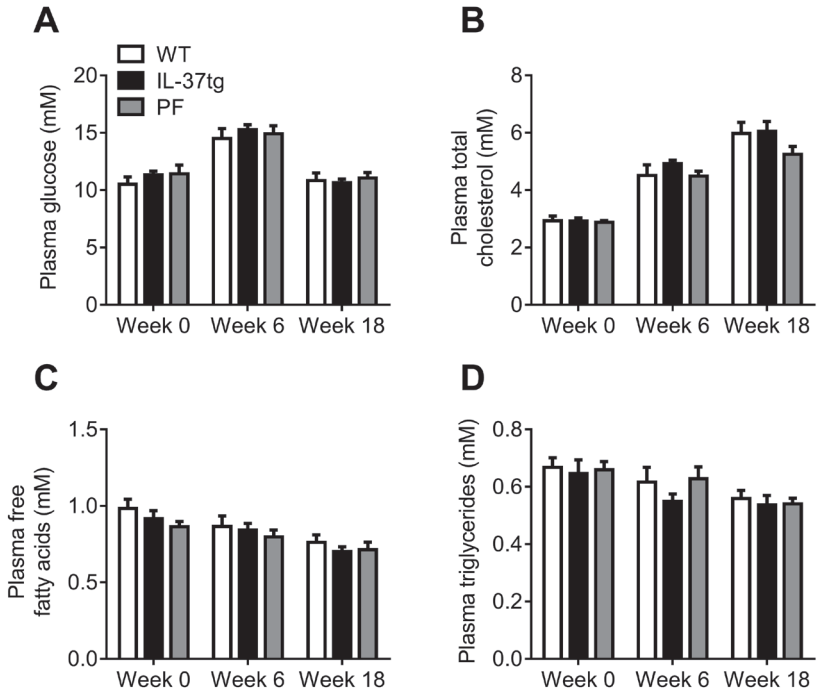

Figure 3. Heterozygous IL-37 expression does not affect plasma glucose and lipid levels. 10-week old male C57Bl/6J mice and heterozygous IL-37tg mice on a C57Bl/6J background were fed a high-fat diet (HFD) for 18 weeks. Pair-feeding of wild-type (WT) mice (PF group) was initiated after 5.5 weeks of HFD feeding. Plasma glucose (A), total cholesterol (B), free fatty acids (C) and triglycerides (D) were measured at indicated time points. Values represent means ± SEM (n=10 animals per group).

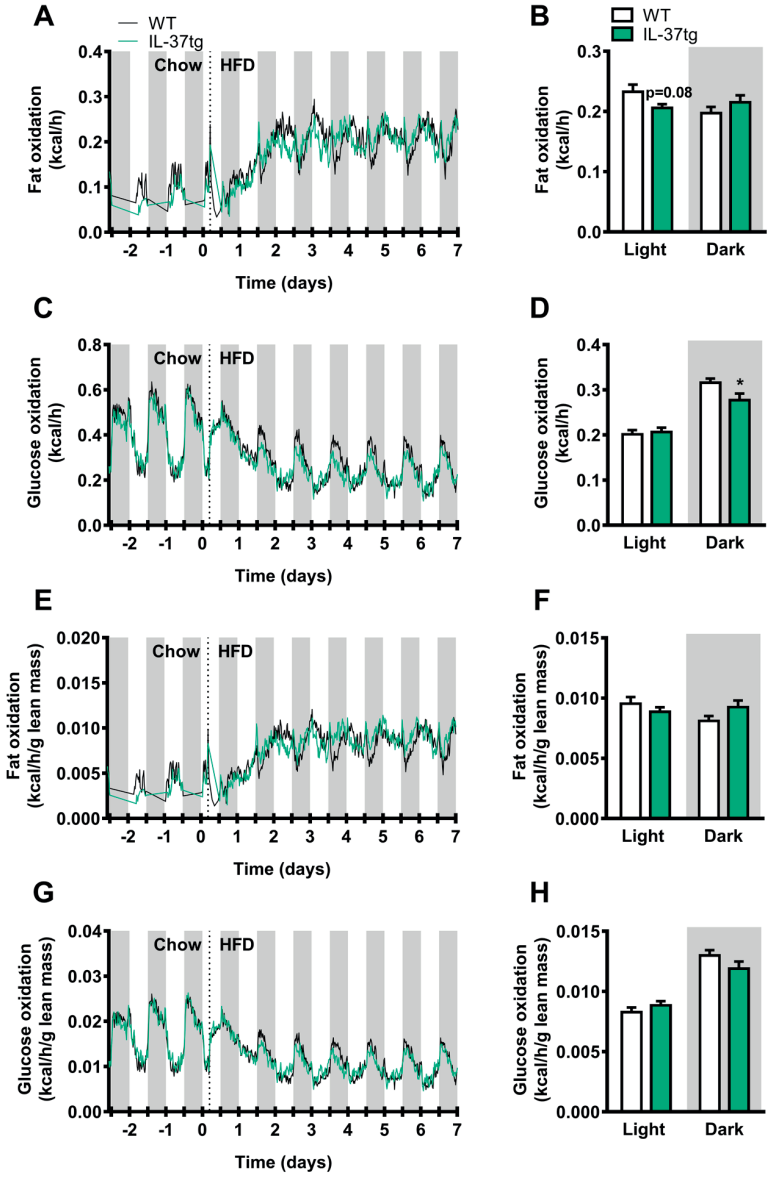

Figure 4. Heterozygous IL-37 expression decreases glucose oxidation in conjunction with lean body mass reduction. 10-week old male C57Bl/6J mice and heterozygous IL-37tg mice on a C57Bl/6J background were fed a high-fat diet (HFD). From 2 days before initiation of HFD until 1 week after the switch to HFD, mice were housed in fully automatic metabolic cages, which measured oxygen uptake (V_{O2}) and carbon dioxide production (V_{CO2}). Fat (A, B) and glucose (C, D) oxidation was calculated and were corrected for lean mass (fat oxidation; E, F; glucose oxidation; G, H). Bar graphs were based on calculations of the mean from day 1.5 to 7. Values represent means (A, C, E, G) and bar graphs represent means ± SEM (B, D, F, H) (n=8 animals per group). *P<0.05 IL-37tg vs wild-type (WT).

DISCUSSION

IL-37 is an anti-inflammatory cytokine of the immune system, and transgenic expression of IL-37 in mice protects them from diet-induced obesity and associated metabolic complications including dyslipidemia, inflammation and insulin resistance [15]. In the current study, we investigated the effect of transgenic IL-37 expression on energy balance in more detail. We confirmed that mice homozygously expressing IL-37 had lower body weight upon HFD feeding, and went on to show that these animals had a marked decrease in food intake. Subsequent mechanistic studies in mice with heterozygous expression showed that IL-37 reduces food intake which led to a decrease in lean body mass, but did not reduce fat mass and plasma lipid levels or alterations in energy expenditure independent of lean body mass. Taken together, this indicates that IL-37 expression lowers lean body mass at least partly *via* reducing food intake.

We found that mice homozygously expressing IL-37 were leaner than WT control mice already before onset of the HFD, and this difference became more evident during HFD feeding for 6 weeks. These body weight curves differ from the course of body weight found previously by Ballak *et al.* [15] for which the exact explanation is currently unknown to us. Despite the fact that the diet, age of the animals and the experimental facility were the same in both studies, IL-37tg and WT control mice in the previous study had a similar weight before onset of the HFD and lower body weight in IL-37tg mice was not evident until 6 weeks of HFD feeding [15]. Strikingly, the previous study reported similar food intake between IL-37tg and WT control mice. The difference in results between our results and the previous experiments published by Ballak *et al.* [15] may be due to differences in methods to monitor food intake. In addition, non-littermates were used in the first experiment in this paper and in the study by Ballak *et al.* [15]. Therefore, the reduction in fat mass and metabolic phenotype that were found initially could also be due to differences in genetic make-up or composition of gut microbiota [27, 28].

For subsequent mechanistic studies into the beneficial metabolic phenotype observed in IL-37tg mice independent of genetic makeup we used heterozygous IL-37tg and WT littermate control animals. The reason we switched to a heterozygous mouse model was because a breeding that generated WT littermate controls was needed and it was impossible to distinguish homozygous from heterozygous mice by PCR, a heterozygous breeding was kept in which heterozygous IL-37tg mice were crossed with WT mice. We observed no obvious difference in behavior between transgenic and WT animals as described before [10]. Although we attempted to investigate whether reduced food intake in IL-37tg animals was causal to the beneficial metabolic phenotype by performing a study in which we included a pair-fed group, we could not reproduce the marked effect on total body weight that we found initially and that was also reported previously [15]. A downside of using this approach is that expression of IL-37 in heterozygous IL-37tg mice

will be lower than in homozygous IL-37tg mice, explaining the reduced effect observed on body weight. Indeed, in heterozygous IL-37tg mice the *IL-37* mRNA expression has shown to be lower and the concomitant beneficial effects milder than the expression and effects of homozygous IL-37tg mice [10, 29]. Since there seems to be a gene dose-dependent effect of IL-37 on food intake and total body weight, and heterozygous IL-37 expression lowers specifically lean body mass, it might be that homozygous IL-37 expression lowers body weight by reducing both fat and lean body mass. Unfortunately, we did not take measures of body composition of the homozygous IL-37tg mice to confirm this. To circumvent the use of transgenic mouse models, an alternative approach for future studies on IL-37 function would be the use of recombinant IL-37 [30].

IL-37 production has been reported to be low and it is mainly induced and detected upon pro-inflammatory stimuli, such as LPS [10] or others that would accumulate during the development of obesity. Even though the animals in our study were fed a pro-inflammatory diet containing palm oil, which may have led to higher LPS exposure in our models [31], heterozygous IL-37 expression might not have been sufficient to counterbalance inflammation upon the pro-inflammatory diet. Nevertheless, heterozygous IL-37tg mice still had a reduction in food intake and less lean body mass. Restricting energy intake in mice with roughly 26%, which is three times higher than the energy restriction in our study, has been shown to decrease lean body mass by about 11% (compared to -7% in our study) without affecting fat mass before [32]. Since in our study the pair-fed mice also showed a reduction in lean body mass from the moment the pair-feeding was initiated, lower lean body mass in IL-37tg mice is probably a result of lower food intake.

How IL-37 might reduce food intake is as yet unknown and would be an interesting subject of future investigation. Extracellular IL-37 interacts with IL-1R8 (SIGIRR) and IL-18Rα. The latter is also the receptor of the pro-inflammatory cytokine IL-18, which is a member of the IL-1 family of cytokines as well [22]. Interestingly, IL-18 deficiency leads to increased food intake and body weight. In addition, intracerebral administration of rIL-18 reduces food intake, suggesting that IL-18 acts centrally [33]. Very recently, Francesconi *et al.* [34] discovered that the IL-18 receptor is highly expressed in the bed nucleus of the stria terminalis, a part of the extended amygdala that is known to influence feeding by projecting on the lateral hypothalamus. It is therefore possible that IL-37 inhibits food intake by acting on the IL-18 receptor in the brain. Furthermore we cannot exclude the possibility that IL-37 modulates the expression of other cytokines and thereby influences food intake.

Whether IL-37 affects food intake in humans, who naturally express IL-37, is unknown. IL-37 gene expression in adipose tissue of humans was found to be higher in subjects with low adipose tissue leptin protein levels [15], which could suggest that high IL-37 expression lowers food intake and consequently reduces levels of the satiety hormone

leptin in adipose tissue. Elevated IL-37 levels in humans are generally found in patients with inflammatory diseases such as nonallergic asthma [35] and systemic lupus erythematosus (SLE) [36]. SLE patients have indeed been reported to have inadequate food intake [37], which would be consistent with higher IL-37, but the complexity and versatility of the immune system makes it challenging to attribute this effect to a specific inflammatory component. Recent genetic studies on body mass index revealed that a majority of the tissues and cell types in which genes near BMI-associated SNPs are highly expressed, are part of the central nervous system [38]. This provides strong support for an important role of the central nervous system, which contains the key sites of central appetite regulation, in obesity susceptibility and therefore highlights the importance of research into factors that influence appetite, such as IL-37. Future studies for therapeutics in humans will focus on recombinant IL-37 linked to the Fc domain of mouse IgG1 (fusion protein), in order to increase the *in vivo* efficacy of IL-37 on inflammatory and immune-mediated diseases.

In conclusion, IL-37 expression in mice reduces food intake, which may underlie the beneficial metabolic effects including fat mass reduction that have previously been reported in IL-37 transgenic mice. The mechanisms behind these findings and the pathophysiological significance of these findings in obesity in humans remain to be determined.

ACKNOWLEDGEMENTS

The authors are grateful to Lisa Hoving, Maaike Schilperoort, Kevin Brewster, Isabel Mol, Hetty Sips, Trea Streefland and Chris van der Bent (all from Leiden University Medical Center, The Netherlands) for their valuable technical assistance.

FUNDING

R. Stienstra was supported by a Vidi grant from the Netherlands Organization for Scientific Research. J.A. van Diepen was supported by the Dutch Diabetes Research Foundation (2013.81.1674) and a Veni Grant of the Netherlands Organization for Scientific Research (91616083). D. B. Ballak was supported by a Glenn/AFAR postdoctoral fellowship and R21 (NIH) 1R21AG053804-01. M.R. Boon is supported by a research grant from the Rembrandt Institute of Cardiovascular Science and by a grant from the Dutch Diabetes Research Foundation (2015.81.1808).

REFERENCES

1. Afshin, A.; Forouzanfar, M. H.; Reitsma, M. B.; Sur, P.; Estep, K.; Lee, A.; Marczak, L.; Mokdad, A. H.; Moradi-Lakeh, M.; Naghavi, M., et al. Health Effects of Overweight and Obesity in 195 Countries over 25 Years. *N Engl J Med* **2017**, 377, (1), 13-27.
2. Berrington de Gonzalez, A.; Hartge, P.; Cerhan, J. R.; Flint, A. J.; Hannan, L.; MacInnis, R. J.; Moore, S. C.; Tobias, G. S.; Anton-Culver, H.; Freeman, L. B., et al. Body-mass index and mortality among 1.46 million white adults. *N Engl J Med* **2010**, 363, (23), 2211-9.
3. Knight, J. A. Diseases and disorders associated with excess body weight. *Ann Clin Lab Sci* **2011**, 41, (2), 107-21.
4. Lumeng, C. N.; Saltiel, A. R. Inflammatory links between obesity and metabolic disease. *J Clin Invest* **2011**, 121, (6), 2111-7.
5. Ouchi, N.; Parker, J. L.; Lugus, J. J.; Walsh, K. Adipokines in inflammation and metabolic disease. *Nat Rev Immunol* **2011**, 11, (2), 85-97.
6. Borst, S. E. The role of TNF-alpha in insulin resistance. *Endocrine* **2004**, 23, (2-3), 177-82.
7. van der Valk, F. M.; van Wijk, D. F.; Stroes, E. S. Novel anti-inflammatory strategies in atherosclerosis. *Curr Opin Lipidol* **2012**, 23, (6), 532-9.
8. Esser, N.; Paquot, N.; Scheen, A. J. Anti-inflammatory agents to treat or prevent type 2 diabetes, metabolic syndrome and cardiovascular disease. *Expert Opin Investig Drugs* **2015**, 24, (3), 283-307.
9. Moschen, A. R.; Molnar, C.; Enrich, B.; Geiger, S.; Ebenbichler, C. F.; Tilg, H. Adipose and liver expression of interleukin (IL)-1 family members in morbid obesity and effects of weight loss. *Mol Med* **2011**, 17, (7-8), 840-5.
10. Nold, M. F.; Nold-Petry, C. A.; Zepp, J. A.; Palmer, B. E.; Bufler, P.; Dinarello, C. A. IL-37 is a fundamental inhibitor of innate immunity. *Nat Immunol* **2010**, 11, (11), 1014-22.
11. Boraschi, D.; Lucchesi, D.; Hainzl, S.; Leitner, M.; Maier, E.; Mangelberger, D.; Oostingh, G. J.; Pfaller, T.; Pixner, C.; Posselt, G., et al. IL-37: a new anti-inflammatory cytokine of the IL-1 family. *Eur Cytokine Netw* **2011**, 22, (3), 127-47.
12. Rudloff, I.; Cho, S. X.; Lao, J. C.; Ngo, D.; McKenzie, M.; Nold-Petry, C. A.; Nold, M. F. Monocytes and dendritic cells are the primary sources of interleukin 37 in human immune cells. *J Leukoc Biol* **2017**, 101, (4), 901-911.
13. Imaeda, H.; Takahashi, K.; Fujimoto, T.; Kasumi, E.; Ban, H.; Bamba, S.; Sonoda, H.; Shimizu, T.; Fujiyama, Y.; Andoh, A. Epithelial expression of interleukin-37b in inflammatory bowel disease. *Clin Exp Immunol* **2013**, 172, (3), 410-6.
14. Yang, T.; Lin, Q.; Zhao, M.; Hu, Y.; Yu, Y.; Jin, J.; Zhou, H.; Hu, X.; Wei, R.; Zhang, X., et al. IL-37 Is a Novel Proangiogenic Factor of Developmental and Pathological Angiogenesis. *Arterioscler Thromb Vasc Biol* **2015**, 35, (12), 2638-46.
15. Ballak, D. B.; van Diepen, J. A.; Moschen, A. R.; Jansen, H. J.; Hijmans, A.; Groenhof, G. J.; Leenders, F.; Bufler, P.; Boekschoten, M. V.; Muller, M., et al. IL-37 protects against obesity-induced inflammation and insulin resistance. *Nat Commun* **2014**, 5, 4711.
16. Bufler, P.; Gamboni-Robertson, F.; Azam, T.; Kim, S. H.; Dinarello, C. A. Interleukin-1 homologues IL-1F7b and IL-18 contain functional mRNA instability elements within the coding region responsive to lipopolysaccharide. *Biochem J* **2004**, 381, (Pt 2), 503-10.
17. Sharma, S.; Kulk, N.; Nold, M. F.; Graf, R.; Kim, S. H.; Reinhardt, D.; Dinarello, C. A.; Bufler, P. The IL-1 family member 7b translocates to the nucleus and down-regulates proinflammatory cytokines. *J Immunol* **2008**, 180, (8), 5477-82.

18. Bulau, A. M.; Nold, M. F.; Li, S.; Nold-Petry, C. A.; Fink, M.; Mansell, A.; Schwerd, T.; Hong, J.; Rubartelli, A.; Dinarello, C. A., et al. Role of caspase-1 in nuclear translocation of IL-37, release of the cytokine, and IL-37 inhibition of innate immune responses. *Proc Natl Acad Sci U S A* **2014**, 111, (7), 2650-5.
19. Coll-Miro, M.; Francos-Quijorna, I.; Santos-Nogueira, E.; Torres-Espin, A.; Bufler, P.; Dinarello, C. A.; Lopez-Vales, R. Beneficial effects of IL-37 after spinal cord injury in mice. *Proc Natl Acad Sci U S A* **2016**, 113, (5), 1411-6.
20. Bulau, A. M.; Fink, M.; Maucksch, C.; Kappler, R.; Mayr, D.; Wagner, K.; Bufler, P. In vivo expression of interleukin-37 reduces local and systemic inflammation in concanavalin A-induced hepatitis. *ScientificWorldJournal* **2011**, 11, 2480-90.
21. van de Veerdonk, F. L.; Gresnigt, M. S.; Oosting, M.; van der Meer, J. W.; Joosten, L. A.; Netea, M. G.; Dinarello, C. A. Protective host defense against disseminated candidiasis is impaired in mice expressing human interleukin-37. *Front Microbiol* **2014**, 5, 762.
22. Nold-Petry, C. A.; Lo, C. Y.; Rudloff, I.; Elgass, K. D.; Li, S.; Gantier, M. P.; Lotz-Havla, A. S.; Gersting, S. W.; Cho, S. X.; Lao, J. C., et al. IL-37 requires the receptors IL-18Ralpha and IL-1R8 (SIGIRR) to carry out its multifaceted anti-inflammatory program upon innate signal transduction. *Nat Immunol* **2015**, 16, (4), 354-65.
23. Cavalli, G.; Justice, J. N.; Boyle, K. E.; D'Alessandro, A.; Eisenmesser, E. Z.; Herrera, J. J.; Hansen, K. C.; Nemkov, T.; Stienstra, R.; Garlanda, C., et al. Interleukin 37 reverses the metabolic cost of inflammation, increases oxidative respiration, and improves exercise tolerance. *Proc Natl Acad Sci U S A* **2017**, 114, (9), 2313-2318.
24. Zambon, A.; Hashimoto, S. I.; Brunzell, J. D. Analysis of techniques to obtain plasma for measurement of levels of free fatty acids. *J Lipid Res* **1993**, 34, (6), 1021-8.
25. Van Klinken, J. B.; van den Berg, S. A.; Havekes, L. M.; Willems Van Dijk, K. Estimation of activity related energy expenditure and resting metabolic rate in freely moving mice from indirect calorimetry data. *PLoS One* **2012**, 7, (5), e36162.
26. Weir, J. B. New methods for calculating metabolic rate with special reference to protein metabolism. *J Physiol* **1949**, 109, (1-2), 1-9.
27. Holmdahl, R.; Malissen, B. The need for littermate controls. *Eur J Immunol* **2012**, 42, (1), 45-7.
28. Heiss, C. N.; Olofsson, L. E. Gut Microbiota-Dependent Modulation of Energy Metabolism. *J Innate Immun* **2017**.
29. Luo, Y.; Cai, X.; Liu, S.; Wang, S.; Nold-Petry, C. A.; Nold, M. F.; Bufler, P.; Norris, D.; Dinarello, C. A.; Fujita, M. Suppression of antigen-specific adaptive immunity by IL-37 via induction of tolerogenic dendritic cells. *Proc Natl Acad Sci U S A* **2014**, 111, (42), 15178-83.
30. Ballak, D. B.; Li, S.; Cavalli, G.; Stahl, J. L.; Tengesdal, I. W.; van Diepen, J. A.; Kluck, V.; Swartzwelter, B.; Azam, T.; Tack, C. J., et al. Interleukin-37 Treatment of Mice with Metabolic Syndrome Improves Insulin Sensitivity and Reduces Pro-inflammatory Cytokine Production in Adipose Tissue. *J Biol Chem* **2018**.
31. Laugerette, F.; Furet, J. P.; Debard, C.; Daira, P.; Loizon, E.; Geloen, A.; Soulage, C. O.; Simonet, C.; Lefils-Lacourtablaise, J.; Bernoud-Hubac, N., et al. Oil composition of high-fat diet affects metabolic inflammation differently in connection with endotoxin receptors in mice. *Am J Physiol Endocrinol Metab* **2012**, 302, (3), E374-86.
32. Wang, S. J.; Birtles, S.; de Schoolmeester, J.; Swales, J.; Moody, G.; Hislop, D.; O'Dowd, J.; Smith, D. M.; Turnbull, A. V.; Arch, J. R. Inhibition of 11beta-hydroxysteroid dehydrogenase type 1 reduces food intake and weight gain but maintains energy

expenditure in diet-induced obese mice. *Diabetologia* **2006**, 49, (6), 1333-7.

33. Netea, M. G.; Joosten, L. A.; Lewis, E.; Jensen, D. R.; Voshol, P. J.; Kullberg, B. J.; Tack, C. J.; van Krieken, H.; Kim, S. H.; Stalenhoef, A. F., et al. Deficiency of interleukin-18 in mice leads to hyperphagia, obesity and insulin resistance. *Nat Med* **2006**, 12, (6), 650-6.
34. Francesconi, W.; Sanchez-Alavez, M.; Berton, F.; Alboni, S.; Benatti, C.; Mori, S.; Nguyen, W.; Zorrilla, E.; Moroncini, G.; Tascedda, F., et al. The Proinflammatory Cytokine Interleukin 18 Regulates Feeding by Acting on the Bed Nucleus of the Stria Terminalis. *J Neurosci* **2016**, 36, (18), 5170-80.
35. Raedler, D.; Ballenberger, N.; Klucker, E.; Bock, A.; Otto, R.; Prazeres da Costa, O.; Holst, O.; Illig, T.; Buch, T.; von Mutius, E., et al. Identification of novel immune phenotypes for allergic and nonallergic childhood asthma. *J Allergy Clin Immunol* **2015**, 135, (1), 81-91.
36. Wu, G. C.; Li, H. M.; Wang, J. B.; Leng, R. X.; Wang, D. G.; Ye, D. Q. Elevated plasma interleukin-37 levels in systemic lupus erythematosus patients. *Lupus* **2016**, 25, (12), 1377-80.
37. Borges, M. C.; dos Santos Fde, M.; Telles, R. W.; Lanna, C. C.; Correia, M. I. Nutritional status and food intake in patients with systemic lupus erythematosus. *Nutrition* **2012**, 28, (11-12), 1098-103.
38. Locke, A. E.; Kahali, B.; Berndt, S. I.; Justice, A. E.; Pers, T. H.; Day, F. R.; Powell, C.; Vedantam, S.; Buchkovich, M. L.; Yang, J., et al. Genetic studies of body mass index yield new insights for obesity biology. *Nature* **2015**, 518, (7538), 197-206.

SUPPLEMENTARY APPENDIX

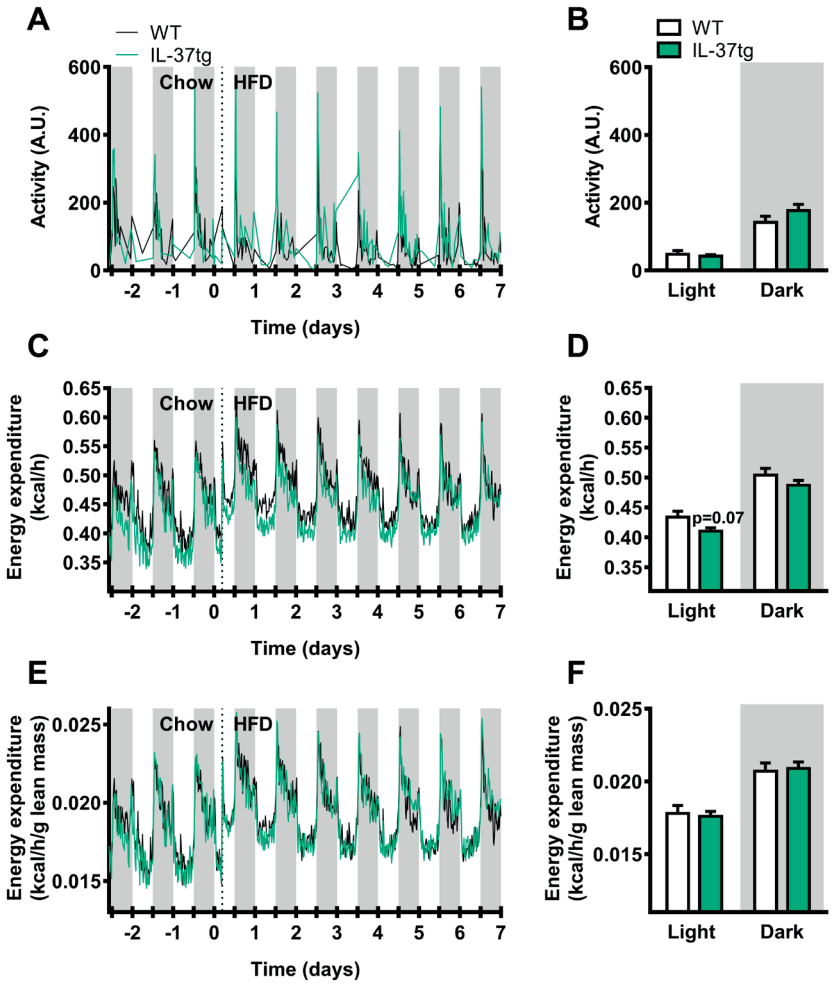

Supplementary figure 1. Heterozygous IL-37 expression decreases energy expenditure in conjunction with lean mass reduction. 10-week old male C57Bl/6J mice and heterozygous IL-37tg mice on a C57Bl/6J background were fed a high-fat diet (HFD). From 2 days before initiation of HFD until 1 week after the switch to HFD, mice were housed in fully automatic metabolic cages, which measured oxygen uptake (V_{O2}) and carbon dioxide production (V_{CO2}). Physical activity (A, B) was measured with infrared sensor frames. Total energy expenditure (C, D) and the energy expenditure were corrected for lean mass (E, F) was calculated from V_{O2} and V_{CO2} using the Weir equation. Bar graphs were based on calculations of the mean from day 1.5 to 7. Values represent means (A, C, E) and bar graphs represent means ± SEM (B, D, F) (n=8 animals per group).

5

A SINGLE DAY OF HIGH FAT DIET FEEDING INDUCES LIPID ACCUMULATION AND INSULIN RESISTANCE IN BROWN ADIPOSE TISSUE IN MICE

Eline N. Kuipers*, Ntsiki M. Held*,
Wietse in het Panhuis,
Melanie Modder,
Philip M. M. Ruppert, Sander Kersten,
Sander Kooijman, Bruno Guigas,
Riekelt H. Houtkooper,
Patrick C.N. Rensen, Mariëtte R. Boon

Submitted

ABSTRACT

Brown adipose tissue (BAT) catabolizes glucose and fatty acids to produce heat and thereby contributes to energy expenditure. Long-term high fat diet (HFD) feeding results in so-called 'whitening' of BAT characterized by increased lipid deposition, mitochondrial dysfunction and reduced fat oxidation. The aim of the current study was to unravel the rate and related mechanisms by which HFD induces BAT whitening and insulin resistance. Wild-type mice were fed a HFD for 0, 1, 3 or 7 days. Within one day of HFD BAT weight and lipid content were increased. HFD also immediately reduced insulin-stimulated glucose uptake by BAT, indicating rapid induction of insulin resistance. This was accompanied by a tendency towards a reduced uptake of triglyceride-derived fatty acids by BAT after 1 day of HFD. Mitochondrial mass and *Ucp1* expression were unaltered, while after 3 days of HFD markers of mitochondrial dynamics suggested induction of a more fused mitochondrial network. In addition, HFD also increased macrophage markers in BAT after 3 days of HFD. Counterintuitively, the switch to HFD was accompanied by an acute rise in core body temperature. In conclusion, we showed that a single day of HFD feeding is sufficient to induce the first signs of whitening and insulin resistance in BAT, which reduces the uptake of glucose and triglyceride-derived fatty acids. BAT whitening and insulin resistance is likely sustained by reduced mitochondrial oxidation due to changes in mitochondrial dynamics and macrophage infiltration, respectively. Likely, the switch to HFD swiftly induces thermogenesis in other metabolic organs, which allows attenuation of BAT thermogenesis.

INTRODUCTION

Obesity results from an imbalance between energy intake and energy expenditure, with energy intake exceeding expenditure. In the case of such a positive energy balance, excess fatty acids (FA) are initially stored in the form of triglycerides (TG) in white adipose tissue, and eventually also in other organs such as the liver and skeletal muscles. Especially ectopic fat deposition is thought to be an important link between obesity and the development of whole-body insulin resistance and, eventually, type 2 diabetes (T2D) [1].

About a decade ago, energy-combusting brown adipose tissue (BAT) was discovered to be present and active in adult humans [2-4]. BAT is seen as a new therapeutic target to combat adiposity and T2D because of its large capacity to take up and combust glucose and FA for heat production [5-7]. Physiologically, BAT is activated by cold stimulation, which results in intracellular lipolysis and release of FA from lipid stores in brown adipocytes [6]. These FA enter the mitochondria where they are broken down and used to generate the proton gradient which is dissipated as heat by the action of uncoupling protein 1 (UCP-1). The depleted intracellular lipid stores need to be replenished by the uptake of TG-derived FA and glucose from the circulation [6] for which insulin signaling is required [8]. The proof-of-principle that activation of BAT is indeed capable of reducing body fat comes from studies in which healthy lean humans were acclimated to cold (~16°C) for 2-6 weeks [9, 10], resulting in recruitment and higher activity of BAT, accompanied by increased energy expenditure and lowered fat mass. Interestingly, in subjects with obesity and/or type 2 diabetes, uptake of the glucose tracer ^{18}F-fluorodeoxyglucose (FDG) by BAT as visualized by PET-CT scan is consistently lower when compared to the glucose uptake in lean subjects, suggesting development of BAT insulin resistance and possibly BAT dysfunction in obesity [4, 11].

Indeed, in mice, long-term high fat diet (HFD) feeding results in insulin resistance [12], and whitening of BAT [13]. BAT whitening characteristics include increased lipid deposition, fewer and dysfunctional mitochondria and reduced fat oxidation [14, 15]. Moreover, HFD-fed mice have reduced ability to maintain their body temperature when exposed to cold. Interestingly, we previously found that during diet-induced obesity (DIO) development, BAT weight and BAT lipid content are elevated [16]. However, the speed at which BAT whitening and insulin resistance occurs, and what the related mechanisms are, have not been extensively studied yet. Therefore, we aimed to study the acute effects of FA overload on BAT lipid metabolism and insulin signaling, in a model of short-term HFD feeding in mice.

MATERIALS AND METHODS

Animals and diet

Male wild-type (WT) C57Bl/6J mice (Charles River Laboratories, Wilmington, MA, USA), all 15-weeks old at sacrifice, were housed under standard conditions in conventional cages. Animals were housed in groups of two or three mice per cage in a 12:12 h light:dark cycle with *ad libitum* access to food and water. Based on body weight, mice were randomized into 4 groups, that received 0, 1, 3 or 7 days of high fat diet (HFD). Thus, at the age of 14 weeks, the first group of mice received an HFD (45% kcal fat, 35% kcal carbohydrate, 20% kcal protein, Special Diets Services, Witham, UK), other groups still remained on a chow diet. The remaining groups started the HFD 3 days or 1 day prior to sacrifice or remained on a chow diet (control group). At the day of sacrifice, after 4 hours of fasting, the mice were sacrificed by means of cervical dislocation after either an injection with radiolabeled lipoprotein-like TG-rich emulsion particles (n=10 mice per dietary treatment group) or an injection with insulin and radiolabeled 2-deoxy-D-glucose (n=7-8 mice per dietary treatment group) (experimental details described below). An additional 3 male C57Bl/6J mice (8-weeks old) underwent surgery for placement of a dual-lead telemetry transmitter (Stellar Telemetry; TSE Systems Inc.; details explained below). In all analyses the interscapular BAT depots were used for analysis unless stated otherwise.

Whole body Toll-like receptor 4 knockout mice ($TLR4^{-/-}$), also on a C57Bl/6J background (The Jackson Laboratory, Bar Harbor, Maine, USA), were bred locally (LUMC). Male $TLR4^{-/-}$ and WT mice were housed under standard conditions as described above and randomized into 4 groups based on body weight to receive 0 or 7 days of HFD (n=7-8 mice per group). At the day of sacrifice, after 4 hours of fasting the mice were sacrificed by means of cervical dislocation and BAT was isolated.

All mouse experiments were performed in accordance with the Institute for Laboratory Animal Research Guide for the Care and Use of Laboratory Animals and have received approval from the Departmental Ethical Review Board (Leiden University Medical Center, Leiden, the Netherlands).

Body weight and food intake

Body weight was determined before the dietary intervention for randomization and at the end of the experiment. Food intake was assessed by daily weighing of the food that was added versus left in the cages.

Plasma parameters

Blood was drawn after 4 hours of fasting in paraoxon (Sigma, St. Louis, MO) coated capillaries. Capillaries were immediately placed on ice and centrifuged. Plasma glucose was measured using an enzymatic kit from Instruchemie (Delfzijl, the Netherlands) and

insulin levels were measured in plasma by ELISA (Crystal Chem Inc., Downers grove, IL, USA), following manufacturers' protocols. The homeostasis model assessment of insulin resistance (HOMA-IR) adjusted to rodents was calculated as: ([glucose (mg/dL)/18] × [insulin (ng/mL)/0.0347])/108.24.

Histology

BAT and subcutaneous white adipose tissue (sWAT) were dissected and immediately fixed in 4% paraformaldehyde for 24 h, overnight dehydrated, embedded in paraffin blocks and cut in sections. Hematoxylin-eosin (H-E) staining was performed and the area of intracellular lipid droplets in BAT and sWAT was quantified using ImageJ (National Institutes of Health). To determine sympathetic activation of BAT, a tyrosine hydroxylase (TH) staining was performed. First, sections were rehydrated and incubated with 10 mM citrate buffer for 15 min (pH 6.0) at 120°C for antigen retrieval. Next, sections were blocked with 5% (wt/vol) BSA/PBS followed by overnight incubation with anti-TH antibody (1:2000, AB-112; Abcam) at 4°C. The following day, sections were incubated with a secondary antibody (anti-rabbit antibody, DAKO enVision), stained with NovaRed and counterstained with Mayer's hematoxylin. Percentage of area positive for TH staining was quantified using ImageJ software.

In vivo glucose uptake upon insulin stimulation

Mice were fasted for 4 h and injected *via* the tail vein with 1 µCi 2-[1-^{14}C]-deoxy-D-glucose (Perkin Elmer) and 0.5 U/kg body weight insulin (NovoRapid, Novo Nordisk). After 15 min, mice were sacrificed by cervical dislocation and liver, BAT, gonadal WAT (gWAT), sWAT and quadriceps muscle were isolated. Organs were dissolved overnight at 60°C in Solvable (Perkin Elmer, Waltham, MA, USA), and the uptake of [^{14}C]-2-deoxyglucose-derived radioactivity was quantified and expressed per gram wet tissue weight.

Protein isolation and western blot

Snap-frozen BAT samples were lysed in ice-cold buffer containing 50 mmol/L HEPES (pH 7.6), 50 mmol/L KCl, 50 mmol/L NaF, 5 mmol/L NaPPi, 1 mmol/L EDTA, 1 mmol/L EGTA, 1 mmol/L dithiothreitol, 5 mmol/L β-glycerophosphate, 1 mmol/L vanadate, 1% NP40 and protease inhibitors cocktail (cOmplete; Roche). LPL western blots were performed using 8 µg of protein/lane as described previously [17]. For western blots of the mitochondrial dynamics markers, 20 µg protein/lane were separated on a 10% SDS-PAGE gel and transferred onto nitrocellulose blotting membranes by means of Trans-Blot Turbo blotting (Bio-Rad). Blotting membranes were blocked with 5% BSA for the pDRP1^{Ser637} antibody and with 5% milk powder for the LPL, MFN2, OPA1, and FIS1 antibodies. After overnight incubation with primary antibodies at 4°C, blots were incubated with the secondary antibody (anti-rabbit IgG HRP conjugate; 1:5,000; Promega; 1:5000 rabbit

anti-goat secondary Ab (LPL)) for 1 h at room temperature. SuperSignal Western Blot Enhancer (Thermo Scientific) was added and proteins band were visualized using a Bio-Rad Imaging system (ChemiDoc Touch, Bio-Rad). Analysis was performed using Bio-Rad Image Lab v5.2 software.

Lysates of 0.8 mg/mL protein extracted from BAT samples obtained after insulin injection were used for western blot using the Wes ProteinSimple apparatus to determine PKB, $pPKB^{Ser473}$, PDHE1α and $pPDHE1α^{Ser232}$ content according to manufacturer's protocol. Data were normalized to GAPDH or Tubulin. The primary antibodies used are given in **Table 1**.

Table 1. Primary antibodies for western blot

Primary antibody	Residue	Supplier	Reference	Dilution
FIS1	-	Atlas Antibodies	HPA017430	1:1000
GAPDH	-	Santa Cruz	#25778	1:50 (Wes ProteinSimple) 1:1000 (Western blot)
MFN2	-	Cell Signaling	#9482	1:1000
OPA1	-	Cell Signaling	#67589	1:1000
PDHE1α	-	Abcam	#ab67592	1:50
pPDHE1α	Ser232	Calbiochem	AP1063	1:50
pDRP1	Ser637	Cell Signaling	#6319	1:1000
PKB	-	Millipore	#07-416	1:50
pPKB	Ser473	Cell Signaling	#9271	1:100
α/β Tubulin		Cell Signaling	#2148	1:1000
LPL	-	Kind gift from André Bensadoun	-	1:5000

In vivo clearance of radiolabeled lipoprotein-like emulsion particles

Lipoprotein-like particles (80 nm) labeled with glycerol tri[^{3}H]oleate (Perkin Elmer, Waltham, MA, USA) were prepared and characterized as described previously [18]. To study the *in vivo* clearance of the lipoprotein-like particles, mice were fasted for 4 h (from 8.00 to 12.00h) and injected *via* the tail vein with 200 µL of emulsion particles (1.0 mg TG per mouse). After 15 minutes, mice were cervically dislocated and perfused with ice-cold PBS with 10 U/mL heparin *via* the heart for 5 min. Subsequently, the liver, heart, spleen, quadriceps muscle, gastrocnemius muscle, gWAT, sWAT, and BAT were collected. Organs were dissolved overnight at 60°C in Solvable (Perkin Elmer, Waltham, MA, USA), and the uptake of glycerol tri[^{3}H]oleate-derived radioactivity was quantified and expressed per gram wet tissue weight.

RNA isolation and RT-PCR analysis

Tissue and cells were lysed in TriPure (Roche) for RNA isolation. For cDNA synthesis, 1 µg of RNA was reverse-transcribed using Promega solutions kit (Promega). Real-time PCR

(RT-PCR) was carried out on a CFX96 PCR machine (Bio-Rad) using SYBR green (Promega). mRNA expression was normalized to *Beta2-microglobulin* (*B2m*) as housekeeping gene and expressed as a fold change compared to the 0 days of HFD (control) group using the ΔΔCT method. The primer sequences are listed in **Table 2**.

Table 2. Primer sequences of forward and reverse primers for RT-PCR

Gene	Forward primer	Reverse primer
Acaca	AACGTGCAATCCGATTTGTT	GAGCAGTTCTGGGAGTTTCG
Acacb	AGATGGCCGATCAGTACGTC	GGGGACCTAGGAAAGCAATC
Angptl4	GGAAAGAGGCTTCCCAAGAT	TCCCAGGACTGGTTGAAGTC
Atgl	ACAGTGTCCCCATTCTCAGG	TTGGTTCAGTAGGCCATTCC
B2m	TGACCGGCTTGTATGCTATC	CAGTGTGAGCCAGGATATAG
Cd36	GCAAAGAACAGCAGCAAAATC	CAGTGAAGGCTCAAAGATGG
Cd68	ATCCCCACCTGTCTCTCTCA	TTGCATTTCCACAGCAGAAG
Cpt1a	GAGACTTCCAACGCATGACA	ATGGGTTGGGGTGATGTAGA
Dnm1l	TGACCAAAGTACCTGTAGGCG	GCATCAGTACCCGCATCCAT
F4/80	CTTTGGCTATGGGCTTCCAGTC	GCAAGGAGGACAGAGTTTATCGTG
Fasn	GCGCTCCTCGCTTGTCGTCT	TAGAGCCCAGCCTTCCATCTCCTG
Fis1	TGAAGGGTTACAGTGTTGCGT	TTCAAAATTCCTTGCAGCTTCGT
Slc2a4	CAGCGCCTGAGTCTTTTCTT	GGCATTGATAACCCCAATGT
Hk1	CGCGCAACTACTGGCATATTAC	GCAATGAAATCCCCCTTTTCTGAG
Hsl	AGACACCAGCCAACGGATAC	ATCACCCTCGAAGAAGAGCA
Lpl	CCCTAAGGACCCCTGAAGAC	GGCCCGATACAACCAGTCTA
Mfn2	CCAGCTAGAAACTTCTCCTCTGT	TGACGGTGACGATGGAGTTG
Opa1	CCTGTGCATCCAAGACGGAT	TGGGAAGAGCTTGCCTTCAA
Ppargc1a	TGCTAGCGGTTCTCACAGAG	AGTGCTAAGACCGCTGCATT
Srebp1c	CTGGCTGAGGCGGGATGA	TACGGGCCACAAGAAGTAGA
Tlr4 (Fig 4*A*)	TCAGAACTTCAGTGGCTGGA	GAGGCCAATTTTGTCTCCAC
Tlr4 (Suppl. Fig. 2)	ACCTGGCTGGTTTACACGTC	CTGCCAGAGACATTGCAGAA
Ucp1	TCAGGATTGGCCTCTACGAC	TGCATTCTGACCTTCACGAC

Citrate synthase activity measurement

Subscapular BAT was homogenized by sonication in ice cold PBS and diluted to 0.3 mg/mL protein (using Pierce BCA Protein Assay Kit, Thermo Scientific). Citrate synthase activity was determined using a colorimetric assay, in which citrate synthase catalyzes the formation of citric acid and CoA-SH from acetyl CoA and oxaloacetic acid. The formation of CoA-SH is coupled to a chemical reaction with DTNB which is spectrophotometrically measured at 412 nm. The absorbance intensity is proportional to the citrate synthase activity. Reactions were performed at 37°C using Tecan Freedom EVO100 and a Tecan Infinite 200 PRO plate reader. The reaction mix contained 10-30 µg/mL sample, 100 mM Tris-HCl

pH 7.6, 100 mM KCl, 100 µM DTNB, 200 µM Acetyl-CoA and 0.1% (w/v) Triton X-100 and was started by the addition of 200 µM oxaloacetic acid, reaching the final reaction volume of 250 µL. Citrate synthase activity expressed in mmol/min/mg was calculated based on Lambert-Beer's law using the slope of the reaction (*i.e.* absorbance change per minute).

Determination of mtDNA/nDNA ratio

Total DNA was isolated from BAT with QIAamp DNA Mini Kit (no. 51306; Qiagen, Hilden Germany) following the provided manufacturer's protocol. The PCR reaction was performed in a LightCycler 480 (Roche). The reaction mix contained 500 pg DNA, 1.25 µM forward and reverse primer, and 4 µL 2x SYBR green master mix (Roche) in a final volume of 8 µL. *16S* and *Cox2* were used as mitochondrial encoded genes, *Hk2* and *Ucp2* for nuclear encoded genes. Primer sequences are listed in **Table 3**. Data were analyzed with LightCycler software release 1.5.0 (Roche). The mean PCR efficiency was calculated to assess gene expression levels using LinRegPCR program version 12.17 [19].

Table 3. DNA primer sequences of forward and reverse primers for PCR

Gene	Forward primer	Reverse primer
16S	CCGCAAGGGAAAGATGAAAGAC	TCGTTTGGTTTCGGGGTTTC
Cox2	GTTGATAACCGAGTCGTTCTGC	CCTGGGATGGCATCAGTTTT
Hk2	TCTGGCTCTGAGATCCATCTTCA	CCGGCCTCTTAACCACATTCC
Ucp2	CTACAGATGTGGTAAAGGTCCGC	GCAATGGTCTTGTAGGCTTCG

Telemetry measurements

WT mice were pre-operatively anaesthetized and a midline incision was made to expose the abdominal cavity after which a dual-lead telemetry transmitter (Stellar Telemetry; TSE Systems Inc.) was subcutaneously inserted. The first lead was inserted in the abdominal cavity and an additional incision was made between the shoulder blades to be able to insert the second lead below the left lobe of the interscapular BAT and sutured to the surrounding tissue. Both incisions were sutured before the anesthetics were antagonized. After a recovery period of one week, a one-day baseline measurement was performed. Subsequently, mice were fed a HFD for 7 days while core body temperature and BAT temperature were being registered with a sampling duration of 6 seconds and a frequency of 200 Hz at an interval of 15 min in AcqKnowledge software (Biopac Systems Inc.).

Statistical analysis

Data are presented as means ± SEM. Differences between the 1, 3, 7 days HFD groups compared the 0 days HFD (control) group in WT mice were determined using ANOVA with Dunnett's *post hoc* test. Differences between 0 and 7 days HFD in TLR4$^{-/-}$ and WT mice were determined using a two-tailed unpaired Student's t-test in each genotype.

Data analysis was performed with SPSS v20 software package for Windows (SPSS, Chicago, USA). Differences at P values < 0.05 were considered statistically significant.

RESULTS

HFD feeding increases BAT weight and lipid content within 1 day

To investigate the short-term effect of HFD feeding on lipid accumulation in BAT, WT mice were fed a HFD for 0, 1, 3 or 7 days. HFD feeding markedly increased fat mass, reaching statistical significance after 7 days (+99%, P<0.001, **Fig. 1A**), while lean mass was not affected. Even though HFD did not significantly increase plasma glucose levels (**Fig. 1B**), it transiently increased insulin levels and HOMA-IR which peaked after 1 day of HFD feeding (+84%, P<0.001, **Fig. 1C** and +115%, P<0.001, **Fig. 1D**, respectively). Also within 1 day of HFD feeding, BAT weight increased (+29%, P<0.05, **Fig. 1E**) and remained elevated up to 7 days of HFD. Histological sections of BAT showed that the increase in

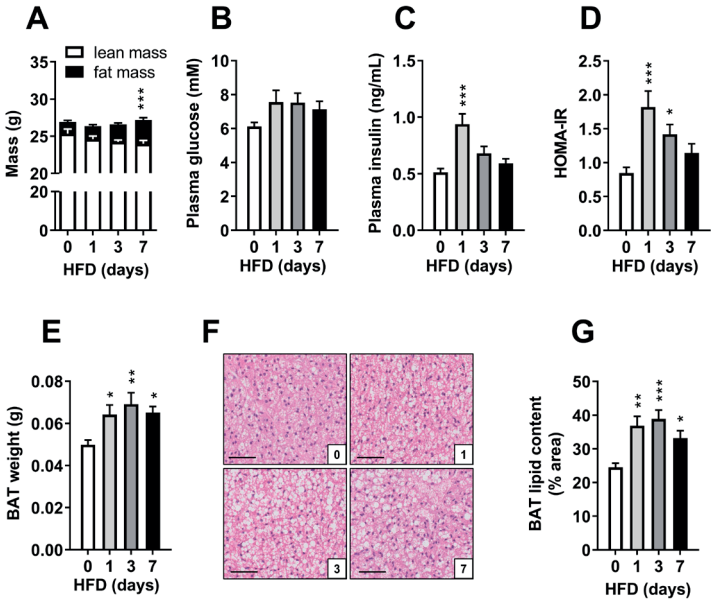

Figure 1. High fat diet feeding rapidly increases plasma insulin, BAT weight and BAT lipid content. Male wild-type mice were fed a HFD for 0, 1, 3 or 7 days to study the short-term effect of a HFD on brown fat. Body composition (*i.e.* lean and fat mass, g) was measured at the end of the dietary interventions (A). Plasma glucose (B) and insulin (C) were measured after a four hour fast and used to calculate HOMA-IR (D). BAT weight (E) was determined at the end of the dietary intervention. Representative pictures of BAT stained with hematoxylin and eosin are shown (F, bars indicate 50 µm) and BAT lipid content (G) was quantified by use of ImageJ. Values are mean ± SEM (n=9-10). * P<0.05, ** P<0.01 and *** P<0.001 compared to the control group. BAT, brown adipose tissue; HFD, high fat diet; HOMA-IR, homeostasis model assessment of insulin resistance.

BAT weight was due to increased lipid content (+35%, P<0.01, **Fig. 1F, G**) already after 1 day. Besides BAT, short-term HFD also increased weight of other metabolic organs, including liver (Suppl. **Fig. 1A**), gWAT (Suppl. **Fig. 1B**) as well as lipid content in sWAT (Suppl. **Fig. 1C**).

HFD feeding rapidly decreases insulin-stimulated glucose uptake by BAT

Accumulation of intracellular lipids can directly interfere with insulin signaling [20]. To determine whether short-term HFD feeding impairs insulin signaling, we injected WT mice that were fed a HFD for 0, 1, 3 or 7 days with insulin and 2-[1-^{14}C]-deoxy-D-glucose and measured the uptake of the radiolabel in various metabolic organs. Interestingly, HFD feeding markedly decreased the insulin-stimulated uptake of 2-[1-^{14}C]-deoxy-D-glucose by BAT after 1 day of HFD feeding (-61%, P<0.001, **Fig. 2A**). We next determined protein content of insulin-induced phosphorylation of protein kinase B (PKB) and pPKB^{Ser473} tended to increase after 1 day HFD and thereafter tended to decrease compared to the

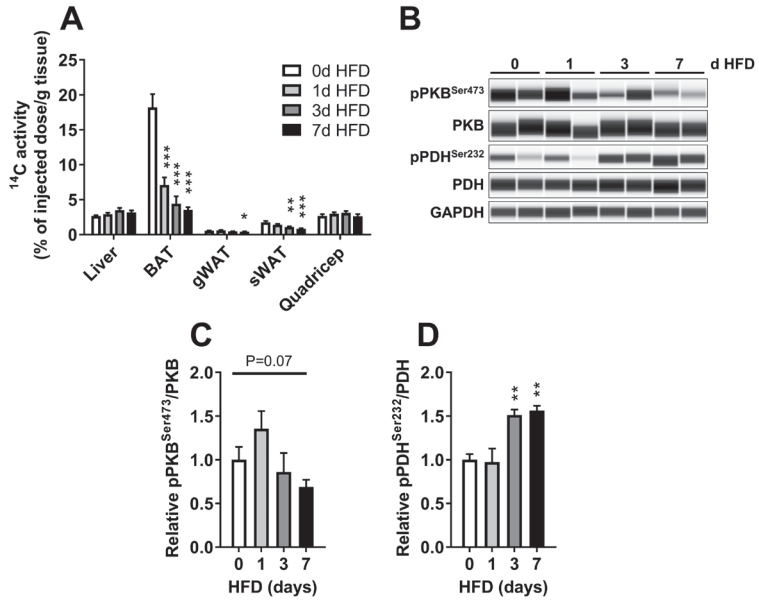

Figure 2. High fat diet feeding rapidly decreases insulin-stimulated glucose uptake by BAT. Mice were fasted for four hours and injected with insulin and 2-[1-^{14}C]-deoxy-D-glucose and uptake per gram organ (A) was determined by [^{14}C]-activity analysis. Protein levels of PKB, phosphorylation (p) state of Ser473-PKB, PDH and phosphorylation (p) state of Ser232-PDH were determined in insulin stimulated BAT and were normalized to GAPDH (B). The phosphorylated-to-total ratios of pPKB^{Ser473}/PKB (C) and pPDH^{Ser232}/PDH (D) were calculated and expressed as fold change relative to the 0 days of HFD group. Values are mean ± SEM (A, F; n=9-10, B-E; n=6-8); * P<0.05, ** P<0.01 and *** P<0.001 compared to the control group. HFD, high fat diet; BAT, brown adipose tissue; gWAT, gonadal white adipose tissue; PDH, pyruvate dehydrogenase; PKB, protein kinase B; sWAT, subcutaneous white adipose tissue.

chow fed group (**Fig. 2B, C**). Because we recently showed that pyruvate dehydrogenase (PDH) plays a central role in glucose utilization during brown adipocyte activation [21], we determined protein content of PDH and its inactive phosphorylated form pPDH^{Ser232}. We found increased pPDH^{Ser232}/PDH after 3 days of HFD (+51%, P<0.01, **Fig. 2B, D**). These data point towards a rapid reduction in BAT insulin sensitivity upon HFD feeding.

HFD feeding tends to decrease TG-derived FA uptake by BAT

A recent study revealed that insulin signaling is required for TG-derived FA uptake by BAT [8]. Therefore, we next studied lipid uptake by BAT by injecting 4h fasted mice with glycerol tri[^{3}H]oleate-labeled lipoprotein-like particles. The HFD fed groups showed a tendency towards a decreased uptake of [^{3}H]oleate by BAT (P=0.067, **Fig. 3A**). BAT *Cd36* expression increased after 3 days of HFD feeding (+66%, P<0.001, **Fig. 3B**), while *Lpl* expression remained unchanged (**Fig. 3B**). In line with the decreased uptake of TG-derived FA by BAT, expression of the LPL inhibitor *Angptl4* progressively increased upon HFD feeding (up to +138% at 7 days, P<0.01, **Fig. 3B**), and protein content of LPL in BAT decreased (**Fig 3C**).

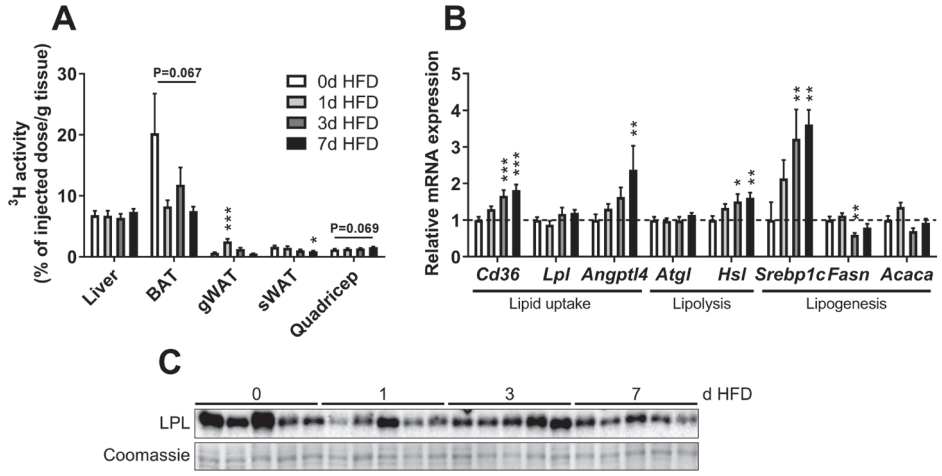

Figure 3. High fat diet feeding tends to decrease TG-derived FA uptake by BAT, accompanied by decreased LPL in BAT. Mice were fasted for 4 hours, injected with glycerol tri[^{3}H]oleate-labeled lipoprotein-like particles, and after 15 min uptake of ^{3}H was determined per gram organ (A). Also, expression in BAT was determined of genes involved in lipid uptake (*Cd36*, *Lpl*, *Angptl4*), lipolysis (*Atgl*, *Hsl*) and lipogenesis (*Srebp1c*, *Fasn* and *Acaca*) (B) and expressed as fold change relative to the 0 days of HFD group. Protein levels of LPL were determined in BAT by western blot (C). Coomassie Blue staining served as loading control. Values are mean ± SEM (n=9-10 in A-B; n=5 in C); expression of genes was corrected for the housekeeping gene *β2m*, * P<0.05, ** P<0.01 and *** P<0.001 compared to the control group. BAT, brown adipose tissue; gWAT, gonadal white adipose tissue; HFD, high fat diet; LPL, lipoprotein lipase; sWAT, subcutaneous white adipose tissue.

We reasoned that the increased lipid accumulation in BAT upon short-term HFD feeding could be the result of, or sustained by, several processes. These include (a) decreased intracellular lipolysis, (b) increased lipogenesis and/or (c) decreased oxidation of lipids due to decreased BAT activity. Therefore, we next determined gene expression of adipose TG lipase (*Atgl*) and hormone-sensitive lipase (*Hsl*), both involved in intracellular lipolysis in BAT. We found an increased rather than decreased *Hsl* expression, up to +61% after 7 days of HFD (P<0.01, **Fig. 3B**). The expression of genes involved in *de novo* lipogenesis were not consistently up- or downregulated except for an increased expression of sterol regulatory element -binding protein 1c (*Srebp1c*) from 3 days HFD onwards (+222%, P<0.01, **Fig. 3B**). Fatty acid synthase (*Fasn*) expression was downregulated after 3 days of 3B). Thus, the rapid increase in BAT lipid content upon HFD is unlikely to be explained by increased uptake of TG-derived FA by BAT, decreased intracellular lipolysis or increased lipogenesis.

HFD feeding increases mitochondrial dynamics markers

We next investigated whether decreased mitochondrial functional capacity could contribute to the increased lipid content in BAT. The expression of *Ucp1* remained unchanged while expression of the mitochondrial biogenesis gene *Ppargc1a* was markedly downregulated after 3 and 7 days HFD (up to -77%, P<0.01, **Fig 4A**). To determine whether the decreased *Ppargc1a* expression resulted in a decreased mitochondrial content, we next determined citrate synthase activity (**Fig. 4B**) and mtDNA/nDNA ratio (**Fig. 4C**), both of which were unchanged. Instead, we hypothesized that mitochondrial network morphology might be altered given that insulin resistance affects mitochondrial dynamics [22-24]. Mitochondrial fusion genes *Mfn2* and *Opa1* increased up to +117% and +51% and the mitochondrial fragmentation gene *Fis1* increased up to + 59% after 7 days of HFD (**Fig. 4D**). Furthermore, we found increased protein content of the pro-fusion long form of OPA1 (top band, +40% after 7 days of HFD, P<0.05, **Fig. 4E**, Suppl. **Fig. 2A**), whereas OPA1 short form remained unchanged (lower band, **Fig. 4F**). The phosphorylated form of DRP1 that inhibits mitochondrial fission (pDRP1^{Ser637}) increased up to +40% (P<0.01, **Fig. 3G, Suppl. Fig. 2A**) after 7 days of HFD. Protein content of MFN2 and FIS1 was unaltered by the HFD (**Suppl. Fig. 2B-D**). Mitochondrial dynamics has also been shown to be influenced by sympathetic nervous system activation of BAT [25], therefore we studied whether sympathetic outflow towards BAT was changed. To this end, we stained BAT slices for tyrosine hydroxylase (TH), the rate limiting enzyme in the synthesis of norepinephrine and found no difference in TH levels upon HFD (**Suppl. Fig. 3A-C**). These data imply that short term HFD does not affect mitochondrial content but rather alters the mitochondrial network morphology to a more fused state which might underlie a decreased activity of BAT with respect to FA oxidation (FAO). Therefore, we next determined the expression of acetyl-CoA carboxylase 2 (*Acacb*) and

carnitine palmitoyltransferase 1A (*Cpt1a*), both involved in FAO, and glucose transporter type 4 (*Slc2a4*) and hexokinase 1 (*Hk1*), both involved in carbohydrate oxidation (CHO). Counterintuitively, after 1 day HFD *Cpt1a* expression and *Hk1* expression were increased (+51%, P<0.01, and +49%, P<0.01, respectively, **Fig. 4H**). These data suggest that whitening causes a compensatory upregulation of genes involved in nutrient oxidation.

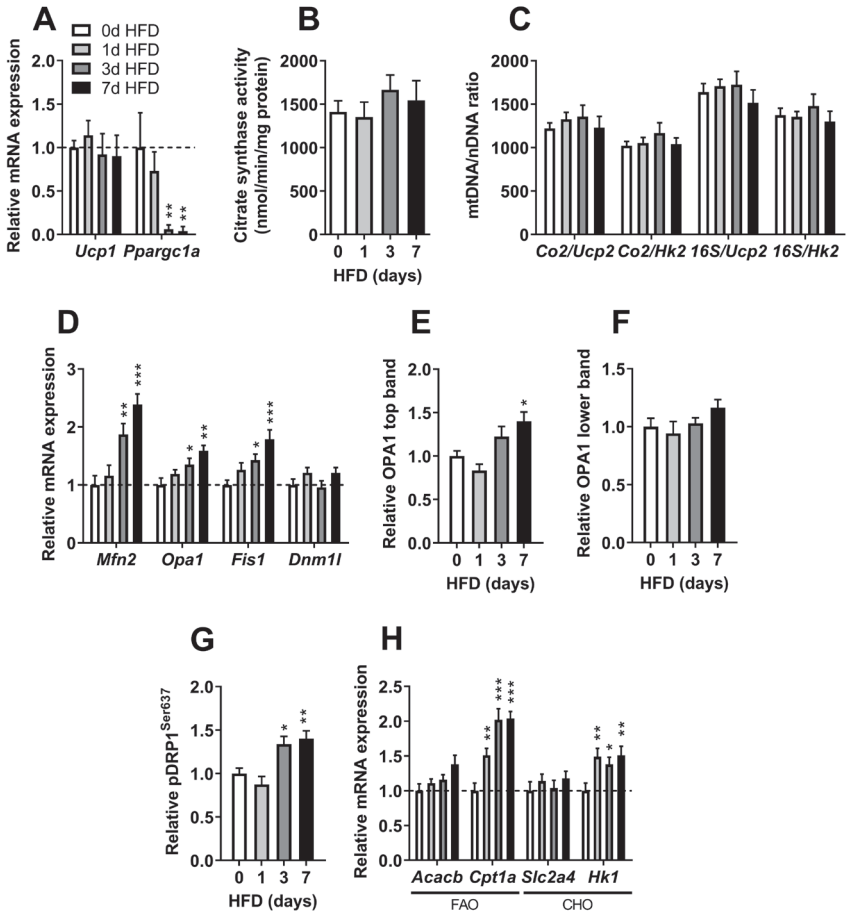

Figure 4. High fat diet feeding increases mitochondrial dynamics markers in BAT. In BAT, expression was determined of *Ucp1*, *Ppargc1a* (A), *Mfn2*, *Opa1*, *Fis1*, *Dnm1l* (D), *Acacb*, *Cpt1a*, *Slc2a4*, and *Hk1* (H), and expressed as fold change relative to the control group. Citrate synthase activity (B) and mitochondrial DNA (mtDNA) versus nuclear DNA (nDNA) ratio (C) was determined in BAT. Protein levels of OPA1 top band (E), OPA1 lower band (F) and pDRP1^{Ser637} (G) in BAT were normalized to GAPDH and expressed relative to the 0 days of HFD group. Values are mean ± SEM (n=9-10 in A-H); expression of genes was corrected for the housekeeping gene *β2m*, * P<0.05, ** P<0.01 and *** P<0.001 compared to the control group. CHO, carbohydrate oxidation; FAO, fatty acid oxidation; HFD, high fat diet; mtDNA, mitochondrial DNA; nDNA, nuclear DNA.

HFD induced lipid accumulation in BAT is not prevented by the absence of TLR4

HFD feeding results in an overload of FA that are not only able to induce lipid accumulation but also able to induce local inflammation, which is associated with reduced function of several organs including muscle and liver, and possibly also BAT [26]. Therefore, we next assessed inflammatory markers in BAT and found increased expression of the macrophage markers *F4/80* and *Cd68* from 3 days HFD feeding on (up to +57%, P<0.01 and +51%, P<0.05, respectively, **Fig. 5A**). Furthermore, the gene encoding toll-like receptor 4 (*Tlr4*), involved in several inflammatory pathways in cells, was increased in BAT (up to +112% after 7 days; P<0.001, **Fig. 5A**). To assess whether intact TLR4 signaling is a prerequisite for HFD induced lipid accumulation in BAT, both WT and TLR4$^{-/-}$ mice were placed on either a chow or HFD for 7 days. We reproduced that *Tlr4* expression was

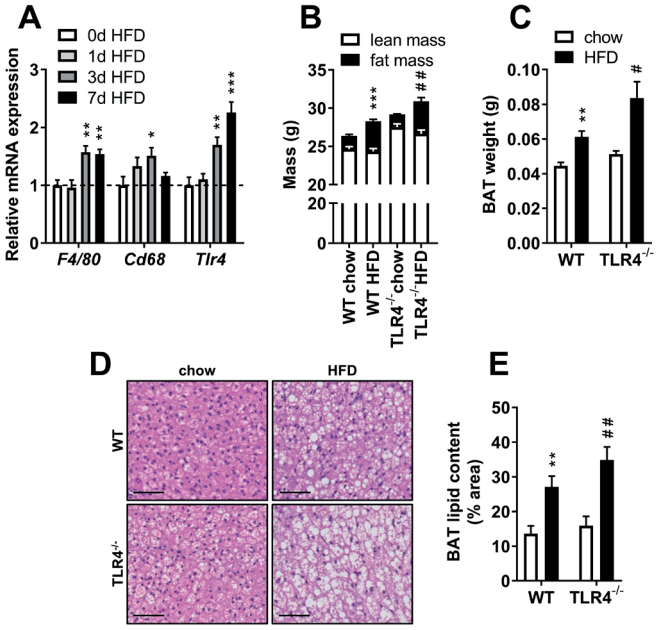

Figure 5. High fat diet feeding rapidly increases the expression of macrophage markers and *Tlr4* in BAT however, the absence of TLR4 does not protect from high fat diet induced lipid deposition in BAT. Gene expression in BAT was determined of *F4/80*, *Cd68* and *Tlr4* (A) and expressed as fold change relative to the 0 days of HFD group. Wild-type (WT) and TLR4$^{-/-}$ mice were fed a chow or a HFD for 7 days to study the involvement of TLR4 in the effect of a HFD on BAT. Body composition (B) in lean and fat mass (g) and BAT weight (C) (g) were measured at the end of the dietary intervention. Representative pictures of BAT stained with hematoxylin and eosin are shown (D, bars indicate 50 μm) and BAT lipid content (E) was quantified by use of ImageJ. Values are mean ± SEM (A; n=9-10, B-E; n=7-8). Expression of genes was corrected for the housekeeping gene *B2m* * P<0.05, ** P<0.01 and *** P<0.001 indicates significant differences between chow and HFD fed in WT mice. # P<0.05 and ## P<0.01 indicated significant differences between chow and HFD fed in TLR4$^{-/-}$ mice. BAT, brown adipose tissue; HFD, high fat diet; TLR4, toll-like receptor 4; WT, wild-type.

increased in WT mice upon HFD whereas *Tlr4* was undetectable in TLR4$^{-/-}$ mice (**Suppl. Fig. 4**). In both genotypes, 7 days of HFD feeding increased total fat mass (**Fig. 5B**), BAT weight (**Fig 5C**) and BAT lipid content (**Fig 5D, E**) compared to the chow diet fed groups. These data imply that the HFD-induced lipid accumulation in BAT is not mediated by TLR4.

HFD feeding immediately increases core body temperature

Next, we determined core body and BAT temperature simultaneously using a dual lead telemetry system in WT mice. Temperature was recorded during 1 day on a chow diet after which the animals were switched to a HFD for 7 days (**Fig. 6**). Core body temperature showed a clear circadian rhythm. After the switch to the HFD, the body temperature increased, most pronounced during the light phase, and amplitude of the oscillation slightly decreased for 3 days (**Fig. 6**). Counterintuitively, BAT temperature accurately followed the core body temperature. Since whitening and insulin resistance of BAT and the fused mitochondrial network within BAT all suggest lowered BAT activity, the increase in core body temperature after the switch to HFD is probably caused by increased whole-body thermogenesis, which indirectly increases the temperature measured in BAT.

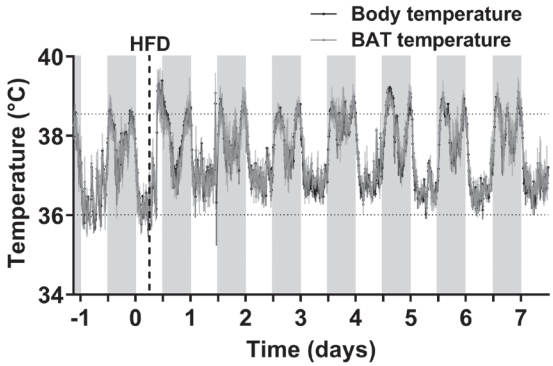

Figure 6. High fat diet feeding immediately increases core body temperature. Mice were implanted with a dual-lead telemetry transmitter and core body temperature (black line) and BAT temperature (gray line) were measured during 1 day before and 7 days after a switch from chow to a HFD. Values are mean ± SEM (n=3). BAT, brown adipose tissue; HFD, high fat diet.

DISCUSSION

Long-term HFD feeding has been shown to result in BAT dysfunction associated with tissue-specific whitening, impaired insulin sensitivity, reduced functional mitochondria, and disturbed thermoregulation [12, 13]. In this study, we showed that the first signs of BAT whitening occur already within a single day of HFD feeding, accompanied by insulin resistance of BAT with respect to uptake of glucose and FA. Secondarily, HFD feeding

increases mitochondrial fusion markers and influx of macrophages, both contributing to a sustained reduced BAT functionality and accumulation of lipids within BAT.

One of the most striking findings of the current study is the rapid lipid accumulation within BAT that occurred upon only one day of HFD feeding. It is likely that the initial whitening is caused by an initial rapid influx of FA into metabolic organs including BAT upon HFD feeding. We recently showed that lipid deposition in BAT rapidly drives the synthesis of endocannabinoids, with increased expression of endocannabinoid synthesis enzymes within one week [16]. Even though we now observed that HFD does not affect sympathetic outflow to BAT, as TH levels were unchanged, locally synthesized endocannabinoids might inhibit noradrenergic signaling in brown adipocytes [27]. Reduced noradrenergic signaling probably sustains whitening by inhibiting the liberation of intracellular FA from lipid droplets for FAO and thermogenesis [28]. Whitening was associated with a rapid and marked decrease in insulin-stimulated glucose uptake by BAT, suggesting impaired insulin sensitivity already after one day of HFD feeding. Rapid insulin resistance is probably caused by intracellular accumulation of lipids that interfere with the insulin signaling cascade [20]. Recently, proper insulin signaling appeared to be also crucial for the uptake of TG-derived FA uptake by BAT [8]. Indeed, we now showed that the uptake of TG-derived FA by BAT after a bolus of injected TG-rich lipoproteins is rapidly reduced (**Fig. 7**). In line with this, we observed an increased *Angptl4* expression and decreased LPL content in BAT after HFD feeding. Taken together, HFD feeding likely causes immediate lipid accumulation in BAT, which probably drives endocannabinoid synthesis by and insulin resistance in BAT, as a consequence of which the uptake of circulating glucose and TG-derived FA by BAT is decreased.

Besides whitening, we obtained evidence for altered mitochondrial function in BAT after HFD feeding. While we did not observe an effect of HFD on mitochondrial mass, we did show an increased expression of *Mfn2* and *Opa1*, accompanied by an increased long form OPA1 and pDRP1^{Ser637}, suggesting a more fused mitochondrial network [29, 30] after three days of HFD feeding (**Fig. 7**). Interestingly, BAT activation usually results in fragmentation of the mitochondrial network [25, 31]. In fact, *in vitro* experiments with brown adipocytes showed that mitochondrial fragmentation is a prerequisite for norepinephrine-induced uncoupling of mitochondrial oxidative phosphorylation [25]. Norepinephrine-induced BAT mitochondrial fission is hypothesized to increase mitochondrial sensitivity to FA, thereby increasing BAT uncoupling potential [32]. On the other hand, long-term HFD feeding of mice results in less and dysfunctional mitochondria in BAT, rendering mice less cold tolerant [13]. Thus, in the short-term HFD fed condition as applied in our study, a higher degree of fused mitochondrial network might contribute to decreased mitochondrial surface area and BAT activity, leading to a sustained intracellular accumulation of TG within lipid droplets.

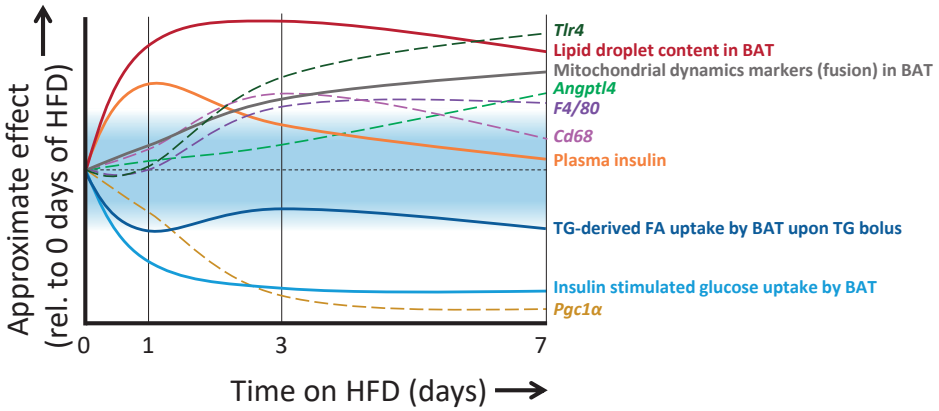

Figure 7. Schematic representation of the high fat diet induced effects in time. Different measures represented as approximate effects relative to 0 days of HFD feeding over the time course of 7 days. Dashed lines indicate gene expression patterns in BAT, solid lines indicate either measures in BAT or plasma insulin levels. The blue area around the middle line indicates non-significant effects compared to the control group. BAT, brown adipose tissue; FA, fatty acid; HFD, high fat diet; TG, triglyceride.

After three days of HFD feeding, we observed increased *F4/80* and *Cd68* expression in BAT, which might indicate an influx of monocyte-derived macrophages into the tissue. This is consistent with data of a mouse model showing that hyperlipidemia promotes the infiltration of monocytes into peripheral tissues [33], by lipid-induced monocyte activation and/or increased tissue expression of chemotactic factors. Likewise, ingestion of a high fat, high caloric diet by humans for only five days increases macrophage markers in muscle [34]. Infiltration of macrophages in BAT is known to induce insulin resistance *via* the secretion of inflammatory cytokines [12]. Roberts-Toler *et al.* [12] showed that insulin resistance is associated with decreased uptake of insulin-stimulated glucose in HFD fed mice accompanied by decreased BAT insulin signaling *via* PKB. In contrast, cold induced BAT activation leads to increased $pPKB^{Ser473}$ levels and subsequent glucose uptake by BAT [35]. We found that HFD feeding tended to increase the insulin-stimulated $pPKB^{Ser473}$ after one day and thereafter its content tended to decrease in BAT. Therefore, reduced PKB activity might have added to a lower glucose uptake after three days HFD. However, in the present study the rise in macrophage markers expression in BAT occurred only after the onset of reduction in insulin-stimulated glucose uptake. This suggests that the initial reduction in insulin sensitivity is not due to enhanced local inflammation, but that the inflammation is rather involved in sustained insulin resistance (**Fig. 7**). This is in agreement with previous findings of Shimobayashi *et al.* [36], who recently showed that obesity-mediated insulin resistance precedes WAT inflammation. The hypothesis that inflammation is not involved in the immediate lipid accumulation and insulin resistance is further corroborated by the fact that an intact TLR4 axis was not required for the lipid accumulation by BAT since $TLR4^{-/-}$ mice also showed whitening of BAT upon short-term

HFD feeding. Although TLR4 plays an important role between immunity and insulin resistance [37], the initial lipid accumulation in BAT is thus unlikely to involve increased local inflammation.

Despite the fact that HFD rapidly inactivates BAT, we found that core body temperature immediately increased after the switch to a HFD. This is in line with previously observed rapid increases in core body temperature [38, 39] and energy expenditure [40] after switching to HFD feeding. A switch to HFD feeding not only leads to a high flux of FA to BAT, but also to other metabolic tissues including intestine and liver. Indeed, we observed that liver weight was increased already after one day of HFD. It should be realized that, in contrast to intestinal absorption of glucose, absorption of TG requires breakdown in 2-monoacylglycerol and FA, which are re-esterified within enterocytes and packed into chylomicrons. These in turn deliver FA to extrahepatic tissues after LPL-mediated breakdown to glycerol and FA, and to the liver where TG are broken down and partly reassembled [41, 42]. All of these combined catabolic and anabolic reactions are exothermic processes generating heat [43]. The fact that both telemetry-leads, in the abdominal cavity and in BAT, measured similar increased temperatures might thus be the result of thermogenesis through exothermic processes in organs other than BAT (*e.g.* in intestine and liver) coupled to delivery of blood with increased temperature to BAT *via* efficient perfusion. Although the increase in body temperature is relatively small, the slightly higher temperature of the blood perfusing BAT might decrease activation of temperature sensitive transient receptor potential (TRP) channels in BAT thereby decreasing BAT activity [44]. In fact, locally produced endocannabinoids might also partly deactivate BAT *via* TRP channels of the vanilloid subfamily [45].

In conclusion, HFD feeding rapidly induces whitening and insulin resistance of BAT within one day, accompanied by decreased uptake of glucose and TG-derived FA. Secondarily, HFD feeding promotes a fused BAT mitochondrial network, an influx of macrophages and heat production by other metabolic organs, all contributing to a sustained reduced BAT functionality and accumulation of lipids within BAT.

ACKNOWLEDGEMENTS

The authors thank Andrea van Dam, Geerte Hoeke, Maaike Schilperoort, Amanda Pronk, Isabel Mol, Lianne van der Wee–Pals, Hetty Sips, Trea Streefland and Chris van der Bent (LUMC, Internal Medicine, Div. Endocrinology) and Jos Ruiter (AMC, Laboratory of Genetic Metabolic Diseases) for their valuable technical assistance. The contribution of Margreet de Vries (LUMC, Dept. of Vascular Surgery) by providing the TLR4$^{-/-}$ mice is highly appreciated.

FUNDING

This work was supported by a research grant from the Rembrandt Institute of Cardiovascular Science to M.R. Boon and R.H. Houtkooper. P.C.N. Rensen is an Established Investigator of the Netherlands Heart Foundation (grant 2009T087). M.R. Boon is supported by a grant from the Dutch Diabetes Foundation (2015.81.1808). Furthermore, we acknowledge the support from the Netherlands Cardiovascular Research Initiative: an initiative with support of the Dutch Heart Foundation (CVON2014-02 ENERGISE).

REFERENCES

1. Tchernof, A.; Despres, J. P. Pathophysiology of human visceral obesity: an update. *Physiol Rev* **2013,** 93, (1), 359-404.
2. Cypess, A. M.; Lehman, S.; Williams, G.; Tal, I.; Rodman, D.; Goldfine, A. B.; Kuo, F. C.; Palmer, E. L.; Tseng, Y. H.; Doria, A., et al. Identification and importance of brown adipose tissue in adult humans. *N Engl J Med* **2009,** 360, (15), 1509-17.
3. Virtanen, K. A.; Lidell, M. E.; Orava, J.; Heglind, M.; Westergren, R.; Niemi, T.; Taittonen, M.; Laine, J.; Savisto, N. J.; Enerback, S., et al. Functional brown adipose tissue in healthy adults. *N Engl J Med* **2009,** 360, (15), 1518-25.
4. van Marken Lichtenbelt, W. D.; Vanhommerig, J. W.; Smulders, N. M.; Drossaerts, J. M.; Kemerink, G. J.; Bouvy, N. D.; Schrauwen, P.; Teule, G. J. Cold-activated brown adipose tissue in healthy men. *N Engl J Med* **2009,** 360, (15), 1500-8.
5. Bartelt, A.; Bruns, O. T.; Reimer, R.; Hohenberg, H.; Ittrich, H.; Peldschus, K.; Kaul, M. G.; Tromsdorf, U. I.; Weller, H.; Waurisch, C., et al. Brown adipose tissue activity controls triglyceride clearance. *Nat Med* **2011,** 17, (2), 200-5.
6. Khedoe, P. P.; Hoeke, G.; Kooijman, S.; Dijk, W.; Buijs, J. T.; Kersten, S.; Havekes, L. M.; Hiemstra, P. S.; Berbee, J. F.; Boon, M. R., et al. Brown adipose tissue takes up plasma triglycerides mostly after lipolysis. *J Lipid Res* **2015,** 56, (1), 51-9.
7. Ruiz, J. R.; Martinez-Tellez, B.; Sanchez-Delgado, G.; Osuna-Prieto, F. J.; Rensen, P. C. N.; Boon, M. R. Role of Human Brown Fat in Obesity, Metabolism and Cardiovascular Disease: Strategies to Turn Up the Heat. *Prog Cardiovasc Dis* **2018,** 61, (2), 232-245.
8. Heine, M.; Fischer, A. W.; Schlein, C.; Jung, C.; Straub, L. G.; Gottschling, K.; Mangels, N.; Yuan, Y.; Nilsson, S. K.; Liebscher, G., et al. Lipolysis Triggers a Systemic Insulin Response Essential for Efficient Energy Replenishment of Activated Brown Adipose Tissue in Mice. *Cell Metab* **2018,** 28, (4), 644-655.e4.
9. Yoneshiro, T.; Aita, S.; Matsushita, M.; Kayahara, T.; Kameya, T.; Kawai, Y.; Iwanaga, T.; Saito, M. Recruited brown adipose tissue as an antiobesity agent in humans. *J Clin Invest* **2013,** 123, (8), 3404-8.
10. van der Lans, A. A.; Hoeks, J.; Brans, B.; Vijgen, G. H.; Visser, M. G.; Vosselman, M. J.; Hansen, J.; Jorgensen, J. A.; Wu, J.; Mottaghy, F. M., et al. Cold acclimation recruits human brown fat and increases nonshivering thermogenesis. *J Clin Invest* **2013,** 123, (8), 3395-403.
11. Blondin, D. P.; Labbe, S. M.; Noll, C.; Kunach, M.; Phoenix, S.; Guerin, B.; Turcotte, E. E.; Haman, F.; Richard, D.; Carpentier, A. C. Selective Impairment of Glucose but Not Fatty Acid or Oxidative Metabolism in Brown Adipose Tissue of Subjects With Type 2 Diabetes. *Diabetes* **2015,** 64, (7), 2388-97.
12. Roberts-Toler, C.; O'Neill, B. T.; Cypess, A. M. Diet-induced obesity causes insulin resistance in mouse brown adipose tissue. *Obesity (Silver Spring)* **2015,** 23, (9), 1765-70.
13. Shimizu, I.; Aprahamian, T.; Kikuchi, R.; Shimizu, A.; Papanicolaou, K. N.; MacLauchlan, S.; Maruyama, S.; Walsh, K. Vascular rarefaction mediates whitening of brown fat in obesity. *J Clin Invest* **2014,** 124, (5), 2099-112.
14. Shimizu, I.; Walsh, K. The Whitening of Brown Fat and Its Implications for Weight Management in Obesity. *Curr Obes Rep* **2015,** 4, (2), 224-9.
15. Cinti, S. Transdifferentiation properties of adipocytes in the adipose organ. *Am J Physiol Endocrinol Metab* **2009,** 297, (5), E977-86.
16. Kuipers, E. N.; Kantae, V.; Maarse, B. C. E.; van den Berg, S. M.; van Eenige, R.; Nahon,

K. J.; Reifel-Miller, A.; Coskun, T.; de Winther, M. P. J.; Lutgens, E., et al. High Fat Diet Increases Circulating Endocannabinoids Accompanied by Increased Synthesis Enzymes in Adipose Tissue. *Front Physiol* **2019,** 9, (1913).

17. Dijk, W.; Ruppert, P. M. M.; Oost, L. J.; Kersten, S. Angiopoietin-like 4 promotes the intracellular cleavage of lipoprotein lipase by PCSK3/furin in adipocytes. *J Biol Chem* **2018,** 293, (36), 14134-14145.
18. Rensen, P. C.; van Dijk, M. C.; Havenaar, E. C.; Bijsterbosch, M. K.; Kruijt, J. K.; van Berkel, T. J. Selective liver targeting of antivirals by recombinant chylomicrons--a new therapeutic approach to hepatitis B. *Nat Med* **1995,** 1, (3), 221-5.
19. Ruijter, J. M.; Ramakers, C.; Hoogaars, W. M.; Karlen, Y.; Bakker, O.; van den Hoff, M. J.; Moorman, A. F. Amplification efficiency: linking baseline and bias in the analysis of quantitative PCR data. *Nucleic Acids Res* **2009,** 37, (6), e45.
20. Samuel, V. T.; Petersen, K. F.; Shulman, G. I. Lipid-induced insulin resistance: unravelling the mechanism. *Lancet* **2010,** 375, (9733), 2267-77.
21. Held, N. M.; Kuipers, E. N.; van Weeghel, M.; van Klinken, J. B.; Denis, S. W.; Lombes, M.; Wanders, R. J.; Vaz, F. M.; Rensen, P. C. N.; Verhoeven, A. J., et al. Pyruvate dehydrogenase complex plays a central role in brown adipocyte energy expenditure and fuel utilization during short-term beta-adrenergic activation. *Sci Rep* **2018,** 8, (1), 9562.
22. Toledo, F. G.; Watkins, S.; Kelley, D. E. Changes induced by physical activity and weight loss in the morphology of intermyofibrillar mitochondria in obese men and women. *J Clin Endocrinol Metab* **2006,** 91, (8), 3224-7.
23. Bach, D.; Pich, S.; Soriano, F. X.; Vega, N.; Baumgartner, B.; Oriola, J.; Daugaard, J. R.; Lloberas, J.; Camps, M.; Zierath, J. R., et al. Mitofusin-2 determines mitochondrial network architecture and mitochondrial metabolism. A novel regulatory mechanism altered in obesity. *J Biol Chem* **2003,** 278, (19), 17190-7.
24. Tol, M. J.; Ottenhoff, R.; van Eijk, M.; Zelcer, N.; Aten, J.; Houten, S. M.; Geerts, D.; van Roomen, C.; Bierlaagh, M. C.; Scheij, S., et al. A PPARgamma-Bnip3 Axis Couples Adipose Mitochondrial Fusion-Fission Balance to Systemic Insulin Sensitivity. *Diabetes* **2016,** 65, (9), 2591-605.
25. Wikstrom, J. D.; Mahdaviani, K.; Liesa, M.; Sereda, S. B.; Si, Y.; Las, G.; Twig, G.; Petrovic, N.; Zingaretti, C.; Graham, A., et al. Hormone-induced mitochondrial fission is utilized by brown adipocytes as an amplification pathway for energy expenditure. *EMBO J* **2014,** 33, (5), 418-36.
26. Heydemann, A. An Overview of Murine High Fat Diet as a Model for Type 2 Diabetes Mellitus. *J Diabetes Res* **2016,** 2016, 2902351.
27. Quarta, C.; Mazza, R.; Obici, S.; Pasquali, R.; Pagotto, U. Energy balance regulation by endocannabinoids at central and peripheral levels. *Trends Mol Med* **2011,** 17, (9), 518-26.
28. Cannon, B.; Nedergaard, J. Brown adipose tissue: function and physiological significance. *Physiol Rev* **2004,** 84, (1), 277-359.
29. Guillery, O.; Malka, F.; Landes, T.; Guillou, E.; Blackstone, C.; Lombes, A.; Belenguer, P.; Arnoult, D.; Rojo, M. Metalloprotease-mediated OPA1 processing is modulated by the mitochondrial membrane potential. *Biol Cell* **2008,** 100, (5), 315-25.
30. Liesa, M.; Palacin, M.; Zorzano, A. Mitochondrial dynamics in mammalian health and disease. *Physiol Rev* **2009,** 89, (3), 799-845.
31. Schilperoort, M.; van Dam, A. D.; Hoeke, G.; Shabalina, I. G.; Okolo, A.; Hanyaloglu, A. C.; Dib, L. H.; Mol, I. M.; Caengprasath, N.; Chan, Y. W., et al. The GPR120 agonist TUG-891 promotes metabolic health by

stimulating mitochondrial respiration in brown fat. *EMBO Mol Med* **2018,** 10, (3).

32. Gao, A. W.; Houtkooper, R. H. Mitochondrial fission: firing up mitochondria in brown adipose tissue. *EMBO J* **2014,** 33, (5), 401-2.
33. Saja, M. F.; Baudino, L.; Jackson, W. D.; Cook, H. T.; Malik, T. H.; Fossati-Jimack, L.; Ruseva, M.; Pickering, M. C.; Woollard, K. J.; Botto, M. Triglyceride-Rich Lipoproteins Modulate the Distribution and Extravasation of Ly6C/Gr1(low) Monocytes. *Cell Rep* **2015,** 12, (11), 1802-15.
34. Boon, M. R.; Bakker, L. E.; Haks, M. C.; Quinten, E.; Schaart, G.; Van Beek, L.; Wang, Y.; Van Schinkel, L.; Van Harmelen, V.; Meinders, A. E., et al. Short-term high-fat diet increases macrophage markers in skeletal muscle accompanied by impaired insulin signalling in healthy male subjects. *Clin Sci (Lond)* **2015,** 128, (2), 143-51.
35. Albert, V.; Svensson, K.; Shimobayashi, M.; Colombi, M.; Munoz, S.; Jimenez, V.; Handschin, C.; Bosch, F.; Hall, M. N. mTORC2 sustains thermogenesis via Akt-induced glucose uptake and glycolysis in brown adipose tissue. *EMBO Mol Med* **2016,** 8, (3), 232-46.
36. Shimobayashi, M.; Albert, V.; Woelnerhanssen, B.; Frei, I. C.; Weissenberger, D.; Meyer-Gerspach, A. C.; Clement, N.; Moes, S.; Colombi, M.; Meier, J. A., et al. Insulin resistance causes inflammation in adipose tissue. *J Clin Invest* **2018,** 128, (4), 1538-1550.
37. Shi, H.; Kokoeva, M. V.; Inouye, K.; Tzameli, I.; Yin, H.; Flier, J. S. TLR4 links innate immunity and fatty acid-induced insulin resistance. *J Clin Invest* **2006,** 116, (11), 3015-25.
38. Qiao, L.; Lee, S.; Nguyen, A.; Hay, W. W., Jr.; Shao, J. The Regulatory Effects of Brown Adipose Tissue Thermogenesis on Maternal Metabolic Adaptation, Placental Efficiency, and Fetal Growth in Mice. *Am J Physiol Endocrinol Metab* **2018**.
39. So, M.; Gaidhu, M. P.; Maghdoori, B.; Ceddia, R. B. Analysis of time-dependent adaptations in whole-body energy balance in obesity induced by high-fat diet in rats. *Lipids Health Dis* **2011,** 10, 99.
40. Kuipers, E. N.; van Dam, A. D.; Ballak, D. B.; de Wit, E. A.; Dinarello, C. A.; Stienstra, R.; van Diepen, J. A.; Rensen, P. C. N.; Boon, M. R. IL-37 Expression Reduces Lean Body Mass in Mice by Reducing Food Intake. *Int J Mol Sci* **2018,** 19, (8).
41. Iqbal, J.; Hussain, M. M. Intestinal lipid absorption. *Am J Physiol Endocrinol Metab* **2009,** 296, (6), E1183-94.
42. Sanders, F. W.; Griffin, J. L. De novo lipogenesis in the liver in health and disease: more than just a shunting yard for glucose. *Biol Rev Camb Philos Soc* **2016,** 91, (2), 452-68.
43. Abumrad, N. A. The Liver as a Hub in Thermogenesis. *Cell Metab* **2017,** *26*, (3), 454-455.
44. Gao, P.; Yan, Z.; Zhu, Z. The role of adipose TRP channels in the pathogenesis of obesity. *J Cell Physiol* **2019**.
45. Di Marzo, V. New approaches and challenges to targeting the endocannabinoid system. *Nat Rev Drug Discov* **2018,** 17, (9), 623-639.

SUPPLEMENTARY APPENDIX

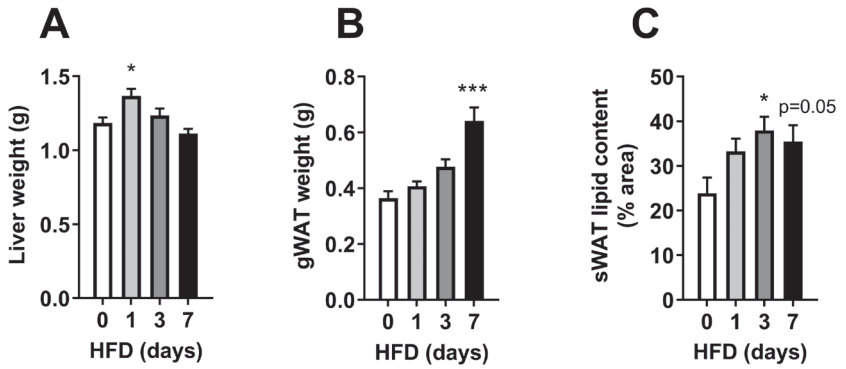

Supplementary figure 1. High fat diet feeding increases liver weight, gWAT weight and sWAT lipid content. Weight (g) of the liver (A) and gWAT (B) was measured at the end of the dietary interventions. sWAT sections were stained with hematoxylin and used to quantify lipid content (C) by use of ImageJ. Values are mean ± SEM (n=9-10); * P<0.05 and *** P<0.001 compared to the control group. HFD, high fat diet; gWAT, gonadal white adipose tissue; sWAT, subcutaneous white adipose tissue.

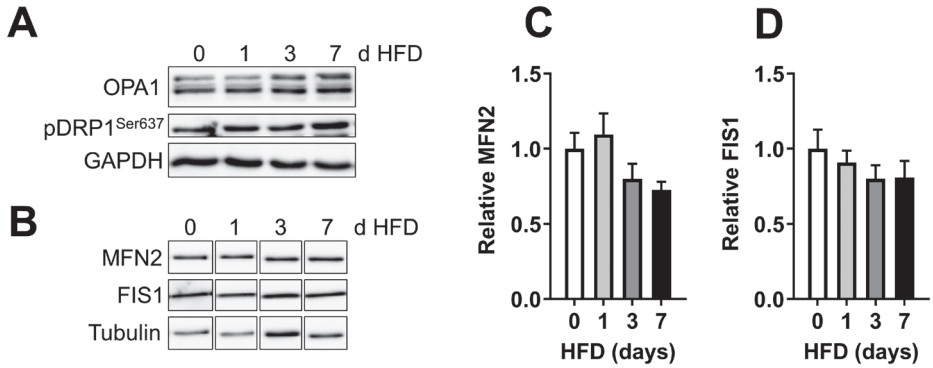

Supplementary figure 2. High fat diet feeding does not affect MFN2 and FIS1 protein content in BAT. Protein levels of OPA1, pDRP1^{Ser637}, GAPDH (A), MFN2, FIS1 and tubulin (B) in BAT were determined and representative bands are shown. Protein levels of MFN2 (C), FIS1 (D) were normalized to tubulin and shown as relative to the control group. Values are mean ± SEM (n=9-10); HFD, high fat diet.

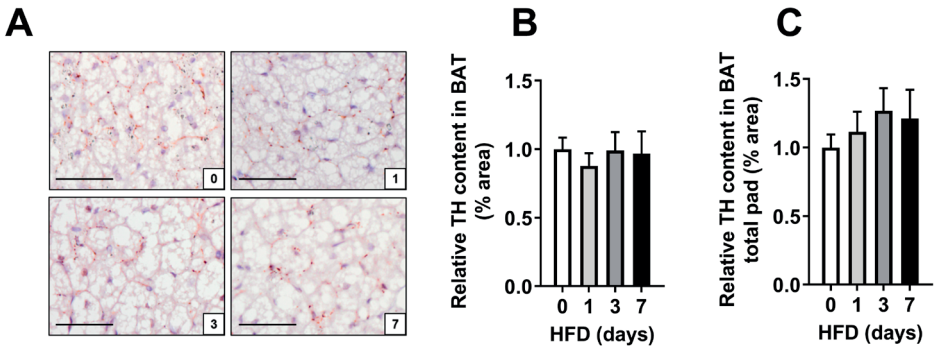

Supplementary figure 3. High fat diet feeding does not affect sympathetic outflow to BAT. BAT sections were stained for tyrosine hydroxylase (TH). Representative pictures are shown (A, bar indicates 50µm). Stained sections were quantified using ImageJ and shown as percentage staining per area (B) and per whole BAT pad (C) relative to the control group. Values are mean ± SEM (n=9-10). HFD, high fat diet; BAT, brown adipose tissue; TH, tyrosine hydroxylase.

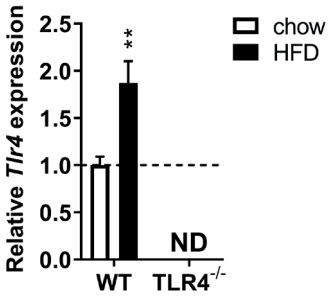

Supplementary figure 4. *Tlr4* expression is absent in TLR$^{-/-}$ mice and increased upon high fat diet feeding in wild-type mice. Wild-type and TLR4$^{-/-}$ mice were fed a chow or a HFD for 7 days to study the involvement of TLR4 in the effect of a HFD on brown fat. *Tlr4* expression in BAT was determined. Values are mean ± SEM (n=7-8). Gene expression was corrected for the housekeeping gene *B2m*. ** P<0.01 indicates significant differences between chow and HFD fed in WT mice. HFD, high fat diet; ND, not detectable; TLR4, toll-like receptor 4; WT, wild-type.

6

HIGH FAT DIET INCREASES CIRCULATING ENDOCANNABINOIDS ACCOMPANIED BY INCREASED SYNTHESIS ENZYMES IN ADIPOSE TISSUE

Eline N. Kuipers*, Vasudev Kantae*,
Boukje C. Eveleens Maarse,
Susan M. van den Berg,
Robin van Eenige, Kimberly J. Nahon,
Anne Reifel-Miller, Tamer Coskun,
Menno P. J. de Winther,
Esther Lutgens, Sander Kooijman,
Amy C. Harms, Thomas Hankemeier,
Mario van der Stelt,
Patrick C. N. Rensen, Mariëtte R. Boon

Frontiers in Physiology (2019); 9:1913

ABSTRACT

The endocannabinoid system (ECS) controls energy balance by regulating both energy intake and energy expenditure. Endocannabinoid levels are elevated in obesity suggesting a potential causal relationship. This study aimed to elucidate the rate of dysregulation of the ECS, and the metabolic organs involved, in diet-induced obesity. Eight groups of age-matched male C57Bl/6J mice were randomized to receive a chow diet (control) or receive a high fat diet (HFD, 45% of calories derived from fat) ranging from 1 day up to 18 weeks before euthanasia. Plasma levels of the endocannabinoids 2-AG and AEA, and related *N*-acylethanolamines, were quantified by UPLC-MS/MS and gene expression of components of the ECS was determined in liver, muscle, white adipose tissue (WAT) and brown adipose tissue (BAT) during the course of diet-induced obesity development. HFD feeding gradually increased 2-AG (+132% within 4 weeks, $P<0.05$), accompanied by upregulated expression of its synthesizing enzymes *Dagla* and *ß* in WAT and BAT. HFD also rapidly increased AEA (+81% within 1 week, $P<0.01$), accompanied by increased expression of its synthesizing enzyme *Nape-pld*, specifically in BAT. Interestingly, *Nape-pld* expression in BAT correlated with plasma AEA levels ($R^2=0.171$, $\beta=0.276$, $P<0.001$). We conclude that a HFD rapidly activates adipose tissue depots to increase the synthesis pathways of endocannabinoids that may aggravate the development of HFD-induced obesity.

INTRODUCTION

Obesity is becoming a global epidemic and the need for development of novel therapeutic interventions is high. The endocannabinoid system (ECS) is regarded as a potential therapeutic target since it regulates energy balance by influencing appetite [1, 2], intracellular lipolysis and energy expenditure (reviewed in [3, 4]). The ECS consists of cannabinoid receptors, their endogenous ligands, the endocannabinoids, and the enzymes that synthesize and degrade the endocannabinoids. The cannabinoid receptors are G-protein-coupled receptors, comprising the cannabinoid receptor type 1 (CB1R) and cannabinoid receptor type 2 (CB2R). The CB1R is expressed centrally and in peripheral metabolic tissues including white adipose tissue (WAT), brown adipose tissue (BAT), liver, skeletal muscle and the pancreas. In contrast, the CB2R is mainly expressed in immune cells [5].

The two main circulating endocannabinoids are anandamide (*N*-arachidonoyl-ethanolamine, AEA) and 2-arachidonoylglycerol (2-AG). Although they are both derived from cell membrane arachidonic acid derivatives, the levels of these endocannabinoids are differentially regulated. AEA can be generated via hydrolysis of *N*-acyl-phosphatidylethanolamines (NAPE) by a NAPE-specific phospholipase D (NAPE-PLD) and its degradation is primarily regulated by fatty acid amide hydrolase (FAAH). 2-AG levels are regulated by the biosynthesis enzymes diacylglycerol lipase α and β (DAGL-α and β) and the degradation enzyme mono-acylglycerol lipase (MAGL) [6-8].

Activation of the CB1R in peripheral tissues inhibits fatty acid oxidation resulting in a positive energy balance and thus development of obesity in mice [9-11]. In addition, an increased tone of the ECS is associated with obesity in humans [12, 13]. Efforts have been made to reverse obesity by blocking the CB1R by small molecules such as the inverse agonist rimonabant [14]. Albeit that rimonabant was effective in humans as evident from sustained weight loss and reduction of dyslipidemia, centrally mediated side effects resulted in removal from the market [15, 16]. Nevertheless, blocking the actions of the ECS is still regarded a potent therapeutic strategy (reviewed in [17, 18]).

To develop novel therapeutics that target specific aspects of the ECS, it is crucial to obtain more insight in how fast and in which organs the dysregulation of the ECS sets off. In this study, we aimed at elucidating these questions by exposing mice to a high fat diet (HFD) ranging from one day up to 18 weeks, which finally causes diet-induced obesity (DIO). We analyzed endocannabinoid levels in plasma as well as the expression of enzymes involved in endocannabinoid synthesis and breakdown in several metabolic organs.

MATERIALS AND METHODS

Animals and diet

Eighty-six 7-week old male C57B1/6J mice (Charles River Laboratories, USA) were obtained. All mice were group housed (3-4 mice per cage) under a 12h:12h light-dark cycle with *ad libitum* access to food and water. During the course of the experiment 7 out of 8 groups of mice were switched from a regular chow diet (Special Diets Services, UK) to a high fat diet (HFD; 45% kcal fat, 35% kcal carbohydrate, 20% kcal protein, Special Diets Services, UK) in such a way that all mice were 25 weeks of age at the time of euthanasia. In total, the study consisted of 8 groups receiving HFD for 0 days (control group, remaining on a regular chow diet), 1 day, 3 days, 1, 2, 4, 10 and 18 weeks (n=10-11 per group). At the end of the study, mice were fasted overnight and subsequently euthanized by an injection with 0.25 mg ketamine and 0.05 mg xylazine per gram body weight. Blood was collected *via* a cardiac puncture with EDTA filled syringes and several organs (liver, quadriceps muscle, gonadal WAT and interscapular BAT) were isolated. The organs were immediately snap frozen in liquid nitrogen and stored at -80℃ until further analysis. For BAT, a small piece was fixated for histological analysis. A second experiment was performed in which 14-week old male C57Bl/6J mice (Charles River Laboratories, USA) were fed 0 days or 1 week HFD (n=8 per group) prior to euthanasia. Mice were fasted for 4 hours and euthanized by CO_2 suffocation. Blood was collected *via* cardiac puncture with EDTA filled syringes as described above. These studies were carried out in accordance with the recommendations of the animal experimentation guidelines of Amsterdam Medical Center (n=86 experiment) and Leiden University Medical Center (n=16 experiment) and approved by the local ethical review boards on animal experimentation.

Endocannabinoid plasma levels

A liquid-liquid extraction using methyl tert-butyl ether as an organic solvent was used to extract endocannabinoids from plasma. Levels of endocannabinoids (AEA, 2-AG), *N*-acylethanolamines (NAEs), and arachidonic acid (AA) were measured by ultra-performance liquid chromatography coupled tandem mass spectrometry (UPLC-MS/MS, AB Sciex 6500 QTRAP) in 25 µL plasma samples. From the pool of individual study samples, quality controls (QCs) were used to generate calibration curves. Additionally, all samples were randomized and each batch of study samples included calibration samples, an even distribution of QC samples and blanks. The sample extraction procedure and method has been described in detail previously [19].

RNA isolation and RT-PCR analysis

RNA of liver and muscle was isolated using TriPure Isolation reagent (Roche, the Netherlands) and 1 µg of RNA was reverse transcribed using Moloney Murine Leukemia Virus

Reverse Transcriptase (Promega, the Netherlands). For WAT and BAT, RNA was isolated using Trizol (Invitrogen, USA) and cDNA was synthesized using an iScript cDNA synthesis kit (Bio-Rad, The Netherlands). RT-PCR was carried out on a CFX96 PCR machine (Bio-Rad) using IQ SYBR-Green Supermix (Promega). mRNA expression was normalized to *Hprt* and *36b4* as household genes for liver, BAT and WAT; for muscle mRNA expression was normalized to the expression of *36b4* only. Changes in gene expression relative to basal expression levels were only calculated if the average expression of at least the control group were Ct < 32. Primer sequences are listed in **Table 1**.

Table 1 List of primer sequences for RT-PCR

Gene	Forward primer	Reverse primer
Abhd4	ATCCTCCAGTGTCTCCAGAACAA	GGGTCCCTTGGGAATGTTGG
Cd68	ATCCCCACCTGTCTCTCTCA	TTGCATTTCCACAGCAGAAG
Dagla	TATCTTCCTCTTCCTGCT	CCATTTCGGCAATCATAC
Daglβ	GGGTCTTTTGAGCTGTTC	AAGGAGGACTATCAGGTA
Faah	CAGCTACAAGGGCCATGCT	TTCCACGGGTTCATGGTCTG
Gde1	AAGGATTTTGTCTCCCCGGAC	ATGTAGCTGGACCCAAGGTG
Hprt	TTGCTCGAGATGTCATGAAGGA	AGCAGGTCAGCAAAGAACTTATAG
Mgll	CAGAGAGGCCAACCTACTTT	ATGCGCCCCAAGGTCATATTT
Nape-pld	AAAACATCTCCATCCCGAA	CGTCCATTTCCACCATCA
Pla/at1	CGGTAAATGATTGCTTCAGT	CCACAACATCCTTCAAAAGC
Pla/at5	CCTGGAGACCTGATTGAGA	GGTTGCTGAAGATAGAGGTG
36b4	GGACCCGAGAAGACCTCCTT	GCACATCACTCAGAATTTCAATGG

Histology and determination of lipid droplet content in BAT

After dissection, a small piece of interscapular BAT was immediately fixated in 4% paraformaldehyde, subsequently dehydrated and embedded in paraffin. A Hematoxylin and Eosin staining was performed on paraffin sections using standard protocols. Intracellular lipid content was quantified with ImageJ (version 1.49).

Statistical analysis

All data are expressed as mean ± SEM. Data analysis was performed with an IBM SPSS Statistics 23 software package. Analysis between multiple groups was done by a one-way ANOVA with Dunnett's *post hoc* test. For the analysis of plasma 2-AG in the second experiment we used an unpaired two-sided t-test. Furthermore, linear regression analysis computed by Pearson's correlation was used to determine correlations. Significant differences are expressed relative to the chow-fed (0 weeks HFD) control group.

RESULTS

HFD feeding rapidly increases plasma 2-AG and AEA levels in mice

To investigate the time course of the dysregulation of the ECS in the development of DIO, C57B1/6J mice were fed a HFD for 1 day up to 18 weeks. As expected, dietary intervention increased body weight (up to +51% after 18 weeks, P<0.001, **Table 2**). Blood glucose levels rapidly increased in response to the HFD (+88% after one day of HFD, P<0.001), whereas plasma TG levels increased more gradually (+155% after two weeks of HFD, P<0.01) (**Table 2**).

Table 2. General characteristics of the mice during diet-induced obesity development

	Duration of HFD (weeks), mean ± SEM							
	0	**1/7**	**3/7**	**1**	**2**	**4**	**10**	**18**
N=	11	11	10	10	11	11	11	11
Body weight (g)	27.3 ± 0.6	29.5 ± 0.6	31.1 ± 0.8~	31.5 ± 0.5*	34.4 ± 0.9***	36.5 ± 1.2***	38.1 ± 0.9***	41.3 ± 2.0***
Glucose (mg/dL)	69 ± 3	130 ± 15***	118 ± 7***	123 ± 4***	104 ± 5*	91 ± 4	112 ± 9**	124 ± 7***
Triglycerides (mM)	0.20 ± 0.02	0.25 ± 0.05	0.41 ± 0.09~	0.34 ± 0.06	0.51 ± 0.07**	0.81 ± 0.08***	0.54 ± 0.03**	0.60 ± 0.05***

Values are indicated in mean ± SEM. ~P<0.1; *P<0.05; **P<0.01; ***P<0.001 compared to the control group. These data were previously published elsewhere [20].

First, we assessed plasma levels of the two main endocannabinoids in the course of DIO development (**Fig. 1**). HFD feeding gradually increased 2-AG levels, which reached significance after 4 weeks (+132%, P<0.05) and further increased up to 18 weeks (+201%; P<0.001) (**Fig. 1A**). Of note, in a few samples of the control group we observed extremely high 2-AG levels (>100 pmol/mL) that masked an initial increase in 2-AG levels upon HFD. To determine whether these high levels would represent (biological) outliers, we determined plasma 2-AG levels in a separate cohort of mice fed a HFD for 0 or 7 days. Indeed these values lie more than 6 standard deviations away from the average of the repeated control animals and could therefore be regarded as biological outliers. Importantly, we observed a trend towards elevated 2-AG plasma levels in the 7 days HFD fed group (+34%, P=0.055, not shown) compared to the 0 day group in the repeated experiment. Therefore, we excluded the mice of the control group with extremely high plasma 2-AG levels from calculation of the means of all endocannabinoids and related metabolites, and instead indicated these data in grey (**Fig. 1, A-I**). HFD feeding also rapidly increased levels of AEA, the other main endocannabinoid, which reached significance after one week (+81%, P<0.01) and further increased up to 18 weeks (+165%, P<0.001) (**Fig. 1B**). Next, we determined whether plasma endocannabinoid levels were related to body weight. Linear regression analysis on all data combined showed that body weight cor-

related weakly but positively with 2-AG levels (R^2=0.073, β=1.447, P=0.017, **Fig. 1C**) and much more strongly with AEA levels (R^2=0.654, β=0.041, P<0.001, **Fig. 1D**).

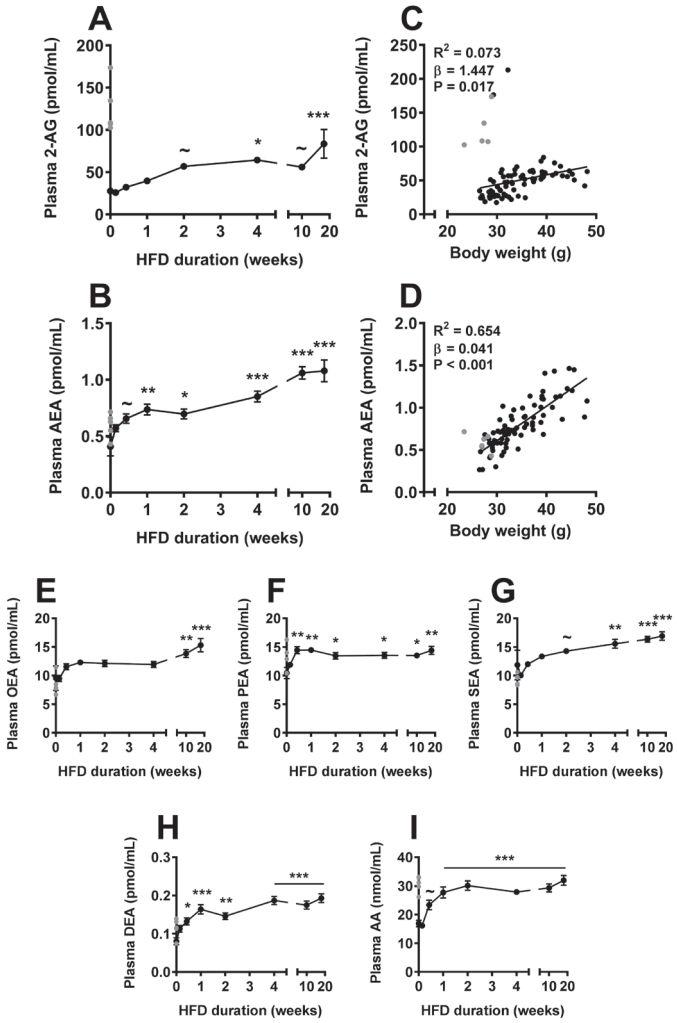

Figure 1. High fat diet feeding time-dependently increases plasma levels of 2-AG and AEA in mice. Liquid chromatography coupled with tandem mass spectrometry (LC-MS/MS) was used to determine plasma levels of 2-AG (A), AEA (B), OEA (E), PEA (F), SEA (G), DEA (H) and AA (I). Data are mean ± SEM (n=10-11). Error bars were too small to be visible for several data points (in A, E, F, G and I). ~P<0.1; *P<0.05; **P<0.01; ***P<0.001 compared to the control (0 weeks of HFD) group analyzed by one-way ANOVA with Dunnett's *post hoc* test. In addition, linear regression analysis was performed on correlations between body weight and plasma levels of 2-AG (C) or AEA (D), for all samples depicted in black (n=81). Samples depicted in grey were regarded as biological outliers based on 2-AG and AA levels and therefore excluded from plasma data analyses.

NAPE-PLD does not only produce AEA, but generates a whole family of *N*-acylethanolamines (NAEs), including *N*-oleoylethanolamine (OEA), *N*-palmitoylethanolamine (PEA), *N*-stearoylethanolamine (SEA), and *N*-docosatetraenoylethanolamine (DEA). Similar to AEA, plasma concentrations of these non-cannabinoid fatty acid amides were raised in response to HFD feeding, albeit with different kinetics (**Fig. 1, E-H**). Plasma levels of arachidonic acid (AA), the precursor and degradation product of 2-AG and AEA [21], also rapidly increased in the first 2 weeks of HFD after which a plateau was reached (+89% after 18 weeks, P<0.001, **Fig. 1I**). Of note, the samples of the control group with extremely high 2-AG levels (**Fig. 1A**) also showed elevated AA levels (**Fig. 1I**).

HFD feeding increases expression of 2-AG synthesis and degradation enzymes in WAT and BAT

Next, we assessed gene expression of the enzymes responsible for the synthesis (*Dagla* and *Daglβ*) and degradation (*Mgll*) of 2-AG in liver, muscle, WAT and BAT (**Fig. 2**; an overview of all relative gene expressions of the enzymes involved in synthesis and degradation is shown in Suppl. **Table 1**). HFD feeding transiently increased *Dagla* expression in WAT after 3 days (+57%, P<0.05, **Fig. 2A**) and increased *Dagla* expression in BAT after 1 and 4 weeks of HFD (**Fig. 2B**). HFD feeding also induced *Daglβ* expression in WAT (**Fig. 2C**) and BAT (**Fig. 2D**), especially towards the end of the intervention (*i.e.* +246% in WAT and +38% in BAT after 18 weeks). Linear regression analyses between the expression levels of DAG lipases in adipose tissues and plasma 2-AG levels showed inconclusive data (**Suppl. Fig. 1**). HFD feeding also transiently increased *Mgll* expression in WAT reaching a peak after 1 week of HFD (+75%, P<0.001), which normalized towards the end of HFD intervention (**Fig. 2E**). In contrast, HFD induced a sustained increase in *Mgll* expression levels in BAT from 1 day on (+28%, P<0.05, **Fig. 2F**). HFD feeding did not persistently affect gene expression of synthesis and degradation enzymes in liver and muscle. It only temporarily increased *Dagla* expression in muscle (at 2 weeks), increased *Daglβ* expression (at 3 days) and decreased *Mgll* expression (at 1 day) in liver (data in **Suppl. Table 1**). Collectively, these data show that the rise in 2-AG levels during DIO development coincided with enhanced expression of synthesis and degradation enzymes specifically in WAT and BAT.

HFD feeding increases *Nape-pld* expression in WAT and BAT

We next assessed gene expression of the enzyme responsible for AEA and NAEs synthesis (*Nape-pld*) in the various metabolic organs. HFD feeding tended to increase *Nape-pld* expression in WAT after 3 days, although expression levels normalized thereafter and were decreased after 18 weeks (-41%, P<0.01, **Fig 3A**). Surprisingly, linear regression analysis showed a small, but significant, negative correlation between *Nape-pld* expression in WAT and plasma AEA levels (R^2=0.124, β=-0.235, P=0.002, **Fig. 3B**). Interestingly,

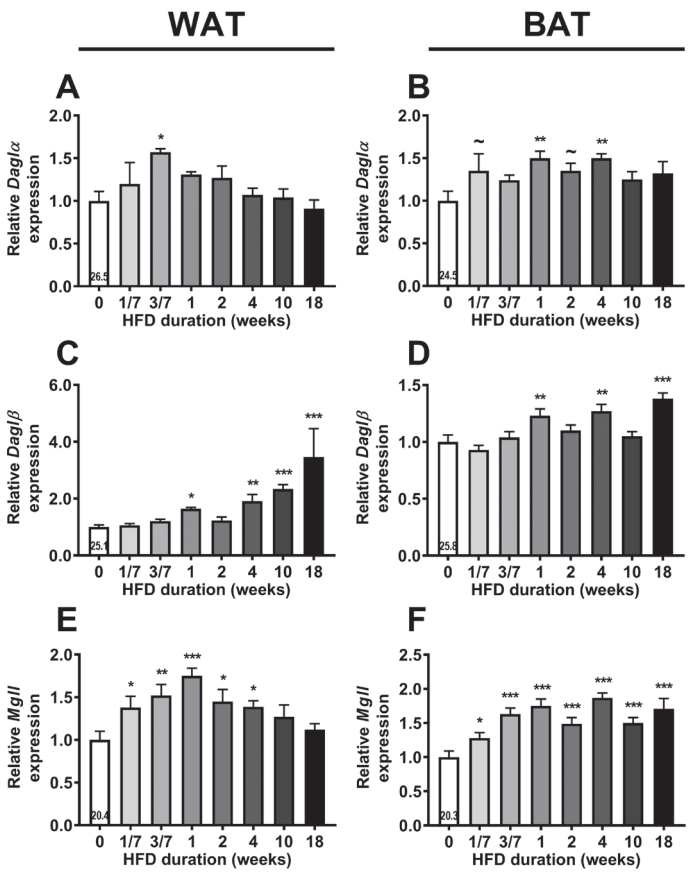

Figure 2. HFD feeding increases the expression of 2-AG synthesis and degradation enzymes in WAT and BAT. Relative gene expression of 2-AG synthesis enzymes *Dagla* (A, B), *Daglβ* (C, D), and degradation enzyme *Mgll* (E, F) in WAT (A, C, E) and in BAT (B, D, F). The number in the column of the 0 weeks of HFD group indicates the average CT value of that treatment group for that gene. Data are mean + upper SEM (n=10-11) ~P<0.1; *P<0.05; **P<0.01; ***P<0.001 compared to the control (0 weeks of HFD) group analysed by one-way ANOVA with Dunnett's *post hoc* test.

HFD feeding increased *Nape-pld* expression in BAT starting at 3 days (+102%, P<0.001, **Fig. 3C**), after which levels reached a plateau. Moreover, *Nape-pld* expression in BAT positively correlated with plasma AEA levels (R^2=0.171, β=0.276, P<0.001, **Fig. 3D**), supporting a contribution of BAT *Nape-pld* expression to circulating AEA levels. HFD feeding decreased the expression of *Nape-pld* in muscle reaching significance from 4 weeks onwards and did not affect *Nape-pld* expression in de liver (data in **Suppl. Table 1**). We also determined the potential contribution of the expression of genes involved in the phospholipase A/acyltransferase (PLA/AT) family, which can produce NAPE in a Ca^{2+}-independent manner, in the increase in AEA levels in DIO [22]. However, expression

of the PLA/AT (HRAS-like suppressor) gene family was either too low to detect (*Pla/at1* in liver, WAT, BAT and *Pla/at5* in liver) or did not show a clear or persistent rise in expression levels that could explain the rise in AEA levels (not shown). Alpha/beta hydrolase domain containing-4 (ABHD4) and glycerophosphodiesterase-1 (GDE1) have been suggested to be involved in AEA synthesis by BAT [23]. However, time-dependent expression levels of *Abhd4* and *Gde1* in BAT did not coincide with the HFD-induced rise in AEA and NAEs (not shown).

Next, we determined gene expression levels of *Faah*, the enzyme involved in AEA and NAEs degradation. HFD feeding decreased *Faah* expression levels in the liver after 18 weeks (-41%, P<0.01, **Suppl. Table 1**). Expression levels of *Faah* in muscle, WAT and BAT were too low to be detected. Altogether, these data show that HFD robustly increased

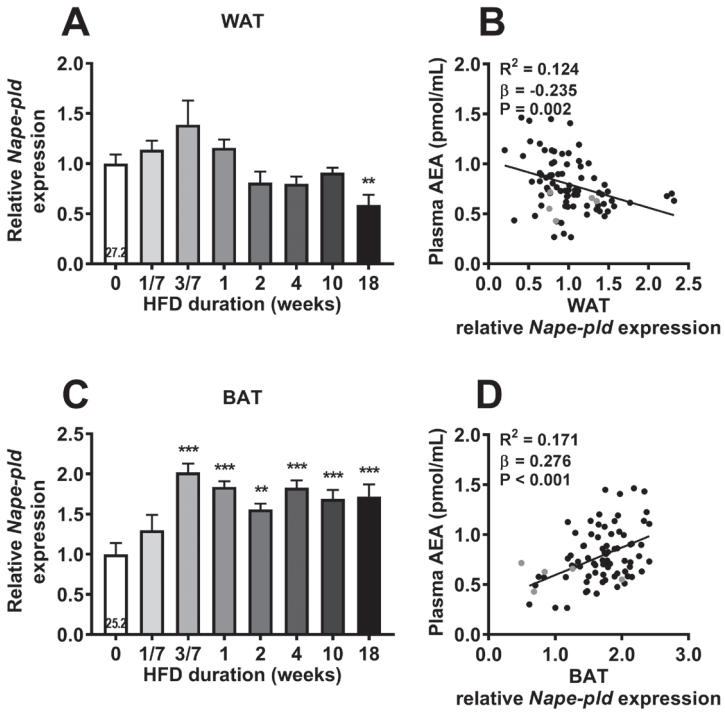

Figure 3. HFD feeding upregulates *Nape-pld* expression in WAT and in BAT. Relative gene expression of AEA synthesis enzyme *Nape-pld* in WAT (A) and BAT (C). The number in the column of the 0 weeks of HFD group indicates the average CT value of that treatment group for that gene. Data are mean + upper SEM (n=10-11). **P<0.01; ***P<0.001 compared to the control (0 weeks of HFD) group analysed by one-way ANOVA with Dunnett's *post hoc* test. In addition, linear regression analysis was performed on correlations between *Nape-pld* expression relative to 0 weeks of HFD in WAT (B) or in BAT (D) and plasma levels of AEA, for all samples depicted in black (n=81). Samples depicted in grey were regarded as biological outliers based on 2-AG and AA levels and therefore excluded from linear regression analyses.

the expression of *Nape-pld* in BAT, suggesting that this tissue may contribute to the increased plasma AEA and NAE levels during DIO development.

Plasma AEA levels positively correlate with lipid content of BAT

Next, we aimed to gain more insight into the cell types within BAT that may have contributed to the robust increased *Nape-pld* expression and plasma AEA levels in DIO development. Because macrophages have been shown to produce AEA [24], we first determined gene expression levels of the macrophage marker *Cd68* in BAT. Linear regression analysis showed a weak positive correlation between *Cd68* expression and *Nape-pld* expression in BAT (R^2=0.113, β=0.170, P=0.002, **Fig. 4A**) and plasma AEA levels (R^2=0.088, β=0.088, P=0.009, **Fig. 4B**). Besides macrophages, brown adipocytes might also be involved. Since intracellular lipid droplets have been shown to co-localize with intracellular AEA [25], we quantified BAT lipid droplet content in H&E stained BAT sections (**Suppl. Fig.**

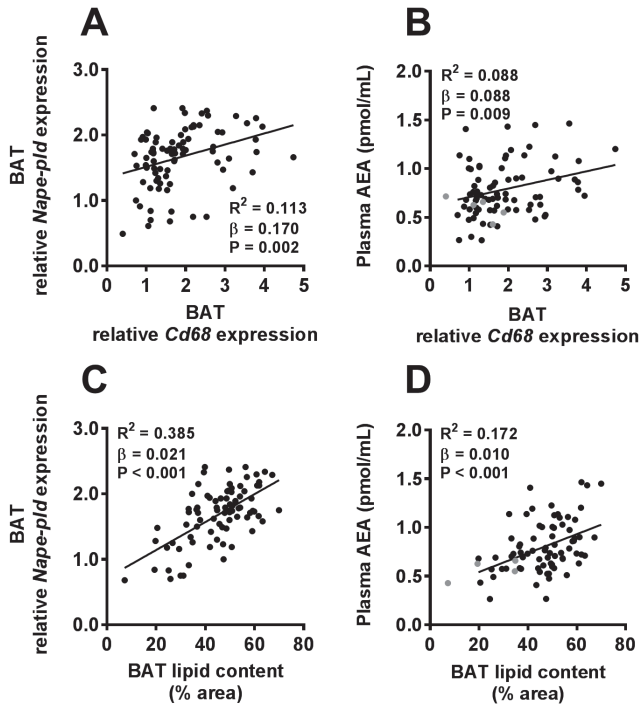

Figure 4. Both macrophage marker expression in BAT and lipid content of BAT positively correlate with plasma AEA levels. Linear regression analysis was performed on correlations between *Cd68* expression relative to 0 weeks of HFD in BAT and *Nape-pld* expression in BAT (A) or plasma levels of AEA (B). Also, linear regression analysis was performed on correlations between lipid content of BAT and *Nape-pld* expression relative to 0 weeks of HFD in BAT (C) or plasma levels of AEA (D). Correlations are shown for all samples depicted in black (n=86 in A, C and n=81 in B, D). Samples depicted in grey were regarded as biological outliers based on 2-AG and AA levels and therefore excluded from linear regression analyses.

2). Compared to *Cd68*, BAT lipid droplet content showed a more pronounced positive correlation with *Nape-pld* expression levels in BAT (R^2=0.385, β=0.021, P<0.001, **Fig. 4C**) as well as plasma AEA levels (R^2=0.172, β=0.010, P<0.001, **Fig. 4D**).

DISCUSSION

In this study, we demonstrated that HFD feeding increases circulating levels of endocannabinoids, with a rapid initial increase in AEA and a more gradual increase in 2-AG, in the course of DIO development. These changes were accompanied by increased gene expression of the synthesis and degradation enzymes of 2-AG in both WAT and BAT, and with increased expression of the AEA synthesis enzyme *Nape-pld* in BAT. Taken together, these data indicate that the dysregulation of the ECS in the development of obesity occurs rapidly and that WAT and BAT might contribute to these effects.

The observed increases in endocannabinoids in the development of DIO are in agreement with previous studies in mice that showed increased plasma 2-AG and AEA levels after 9 weeks [26] and 36 weeks [27] of HFD feeding and increased plasma AEA levels in a model for glucocorticoid induced obesity [28]. These data also are concordant with data in humans, since obese individuals have higher 2-AG levels compared to lean individuals [12, 13, 29]. It was somewhat surprising that a subset of the control group that were not fed a HFD showed very high 2-AG levels in addition to AA levels, the reason of which is currently unclear to us. By performing a second study in mice we confirmed that HFD feeding induced an initial rise rather than decrease in 2-AG levels. Thus, although the reason for the very high 2-AG levels in a subgroup is intriguing, we regarded those mice as biological outliers. Besides 2-AG and AEA, HFD feeding also increased the plasma levels of AA. Since AA is constituent and degradation product of 2-AG and AEA, elevated AA levels may either be a cause or consequence of the increased levels. HFD feeding also increased plasma levels of other *N*-acylethanolamines, including OEA, PEA, SEA and DEA. These NAEs have other biological targets involved in controlling the energy balance, such as peroxisome proliferator-activated receptors-α (PPARα), PPARγ and G protein-coupled receptor 119 [30].

Currently, it is unknown which organs contribute to the increased plasma endocannabinoid levels in HFD-induced obesity [31]. We showed that body weight positively correlates with plasma endocannabinoid levels, albeit that the correlation with AEA (R^2=0.654) is stronger than with 2-AG (R^2=0.073). Since body weight differences in the range of approximately 30-50 g, as observed in this study, are mainly caused by differences in body fat [32], it was considered likely that engulfment of lipids by adipocytes and/or expansion of the adipocyte pool would contribute to the increase in endocannabinoids. Insulin resistance, which is closely linked to increased intracellular lipid

deposition [33] is also associated with a dysregulated ECS [34]. By performing gene expression analysis in metabolically active organs, we could demonstrate that expression of enzymes involved in endocannabinoid synthesis increased in WAT as well as BAT. This is in full agreement with a previous study in which 3 and 8 weeks of HFD feeding, with a diet closely resembling the HFD used in our experiments, resulted in increased local levels of endocannabinoids (AEA and 2-AG) in BAT [35]. The increase in plasma 2-AG coincided with increased gene expression of DAGLα and DAGLβ in both WAT and BAT. Given the different time-course of expression, where the increase in *Dagla* seems to precede the increase in *Daglβ*, we postulate that DAGLα may be responsible for the initial rise in 2-AG, while DAGLβ may mediate the late increase in 2-AG. Similarly, the increase in plasma AEA coincided with increased gene expression of its synthesizing enzyme NAPE-PLD in BAT. Moreover, plasma AEA correlated positively with *Nape-pld* expression in BAT but not in WAT. It is therefore likely that BAT rather than WAT contributes to the rise in AEA levels. In this respect, it is interesting that expression of *Nape-pld* is higher in BAT than in WAT, as evident from lower Ct values. The expression levels of most of the enzymes showed a sharp increase in the first week of HFD feeding, which coincided with the timing of the largest increase in lipid deposition in BAT. In BAT, ABHD4 and GDE1 were shown to also be involved in AEA synthesis and their expression respond to BAT activating agents [23], although we did not find the expression levels of these enzymes to coincide with the increase in circulating AEA and NAEs levels with prolonged HFD feeding. Of note, expression of the endocannabinoid degradation enzymes *Faah* and *Mgll* in the adipose tissues were either undetectable or increased. Although we have not been able to measure actual enzyme activities due to technical reasons, it is tempting to speculate that net whole body endocannabinoid synthesis exceeds degradation since circulating levels increase in the course of DIO. Synthesis enzymes of 2-AG in liver and skeletal muscle were only transiently increased, and the synthesis enzyme of AEA was decreased in skeletal muscle. Thus, although we cannot exclude the contribution of other organs as source for plasma endocannabinoid levels (*e.g.* brain and intestine), our data suggest that WAT and BAT are likely important organs that release 2-AG and AEA levels in HFD-induced obesity.

It is interesting to speculate on the cellular source within the adipose tissue depots that is involved in endocannabinoid synthesis. HFD-induced development of DIO causes accumulation of macrophages in WAT [32] as well as BAT (Van den Berg S.M., unpublished). Macrophages are able to produce AEA [24], and we found a positive correlation between macrophage marker *Cd68* and *Nape-pld* expression in BAT as well as with AEA levels in plasma. However, the concentration of macrophages in adipose tissue is relatively low, even in obesity, and stronger positive correlations were found between the lipid content in BAT and both *Nape-pld* expression and plasma AEA levels. Therefore, adipocytes likely contribute substantially more to the circulating endocannabinoid pool than

macrophages. This hypothesis is corroborated by previous findings that AEA co-localizes with adiposomes or lipid droplets *in vitro* [25] and that specific deletion of NAPE-PLD in adipocytes of mice decreased levels of PEA, OEA and SEA in WAT, despite increased inflammation and influx of macrophages [36]. In our study, HFD feeding increases the cellular mRNA levels of the synthesizing enzymes in adipose tissue. In addition, expansion of the total number of adipocytes in the time course of DIO further increases whole body expression of these enzymes. The rapid increases in gene expression in BAT may be explained by the rapid whitening of BAT as induced by HFD feeding [37]. Indeed, BAT lipid droplet content positively correlated with *Nape-pld* expression and AEA plasma levels. Furthermore, these data are in line with the recent observation that acute activation of BAT decreases *Nape-pld* expression [23]. Interestingly, the concentration of 2-AG and AEA is higher in BAT than WAT [23], suggesting at least a role of BAT in determining circulating endocannabinoid levels. Collectively, it is likely that lipid-filled adipocytes rather than macrophages within the adipose tissues contribute to circulating plasma endocannabinoid levels.

In our study, we found no evidence for a contribution of decreased degradation pathways of 2-AG and AEA in adipose tissues determining plasma levels of endocannabinoids. Specifically, we were unable to detect any expression of AEA degradation enzyme *Faah* in WAT, BAT and muscle, and found decreased liver *Faah* expression after 18 weeks of HFD feeding. This is in line with the fact that FAAH was reported to play an important role in obesity. Notably, a missense polymorphism in the FAAH gene is associated with obesity in humans [38] and FAAH deficient mice have increased AEA levels in *e.g.* the liver and show increased fat mass and body weight [39]. On the other hand, Bartelt and colleagues [40] found that HFD feeding for 16 weeks in mice caused a decrease in *Faah* expression and FAAH enzymatic activity in WAT which was accompanied by increased AEA in this tissue. To what extend catabolism of AEA and 2-AG by adipose tissue determines circulating levels of these endocannabinoids warrants further study.

It is tempting to speculate on the biological role of the increases of 2-AG and AEA in the time course of HFD-induced obesity. Endocannabinoids are known to decrease insulin sensitivity [34] and to reduce sympathetic responses by inhibiting noradrenergic signaling [23, 41], and thereby decrease lipolysis in WAT and thermogenesis in BAT. Possibly, in case of acute lipid overload, as mimicked by a switch from regular chow to a HFD, initial accumulation of lipids in WAT and BAT drives the synthesis pathways of endocannabinoids that can have autocrine and even paracrine effects on these organs to inhibit sympathetic signaling. This sequence of events reduces intracellular lipolysis in BAT and WAT, thereby resulting in reduced thermogenesis in BAT and increased triglyceride storage in WAT. Such as a feed-forward mechanism may thus allow the body to store excess lipids effectively in adipose tissues. Interestingly, we have shown that inhibition of endocannabinoid signaling by strictly peripheral CB1R antagonism activates BAT and

reduces adiposity in HFD-fed mice [42]. In theory, HFD induced lipid accumulation can lead to increased endocannabinoid synthesis which attenuates BAT and WAT activity and results in a positive energy balance.

In conclusion, in the time course of HFD-induced obesity plasma endocannabinoid levels rapidly rise as most probably explained by increased synthesis pathways in adipose tissue depots. We speculate that this sequence of events may attenuate sympathetic signaling in these tissues by CB1R agonism, which would result in reduced thermogenesis and increased storage of excess lipids in WAT. Given the fact that strictly peripheral CB1R antagonism activates BAT and reduces adiposity in mice, we anticipate that strategies inhibiting CB1R selectively on (brown) adipocytes or reducing endocannabinoid synthesis by adipocytes may be a worthwhile strategy to pursue in combating obesity and associated disorders.

ACKNOWLEDGEMENTS

The authors thank T.C.M. Streefland (Dept. of Medicine, Div. of Endocrinology, LUMC, Leiden), A.C.M. van Esbroeck-Weevers and E.D. Mock (Dept. of Molecular Physiology, Leiden Institute of Chemistry, Leiden) for their valuable technical support.

FUNDING

This project received support from the Faculty of Science ("Profiling programme: Endocannabinoids"), Leiden University (V. Kantae, M. van der Stelt, T. Hankemeier). P.C.N. Rensen is an Established Investigator of the Dutch Heart Foundation (grant 2009T038), and is supported a Lilly Research Award Program (LRAP) Award. M.R. Boon is supported by a research grant from the Rembrandt Institute of Cardiovascular Science and by a grant from the Dutch Diabetes Foundation (2015.81.1808). Furthermore, we acknowledge the support from the Netherlands Cardiovascular Research Initiative: an initiative with support of the Dutch Heart Foundation (CVON2014-02 ENERGISE).

REFERENCES

1. Jamshidi, N.; Taylor, D. A. Anandamide administration into the ventromedial hypothalamus stimulates appetite in rats. *Br J Pharmacol* **2001,** 134, (6), 1151-4.
2. Foltin, R. W.; Fischman, M. W.; Byrne, M. F. Effects of smoked marijuana on food intake and body weight of humans living in a residential laboratory. *Appetite* **1988,** 11, (1), 1-14.
3. Cota, D. CB1 receptors: emerging evidence for central and peripheral mechanisms that regulate energy balance, metabolism, and cardiovascular health. *Diabetes Metab Res Rev* **2007,** 23, (7), 507-17.
4. Mazier, W.; Saucisse, N.; Gatta-Cherifi, B.; Cota, D. The Endocannabinoid System: Pivotal Orchestrator of Obesity and Metabolic Disease. *Trends Endocrinol Metab* **2015,** 26, (10), 524-37.
5. Howlett, A. C.; Barth, F.; Bonner, T. I.; Cabral, G.; Casellas, P.; Devane, W. A.; Felder, C. C.; Herkenham, M.; Mackie, K.; Martin, B. R., et al. International Union of Pharmacology. XXVII. Classification of cannabinoid receptors. *Pharmacol Rev* **2002,** 54, (2), 161-202.
6. Bisogno, T.; Maccarrone, M. Endocannabinoid signaling and its regulation by nutrients. *Biofactors* **2014,** 40, (4), 373-80.
7. Muccioli, G. G. Endocannabinoid biosynthesis and inactivation, from simple to complex. *Drug Discov Today* **2010,** 15, (11-12), 474-83.
8. Baggelaar, M. P.; Maccarrone, M.; van der Stelt, M. 2-Arachidonoylglycerol: A signaling lipid with manifold actions in the brain. *Prog Lipid Res* **2018,** 71, 1-17.
9. Ravinet Trillou, C.; Arnone, M.; Delgorge, C.; Gonalons, N.; Keane, P.; Maffrand, J. P.; Soubrie, P. Anti-obesity effect of SR141716, a CB1 receptor antagonist, in diet-induced obese mice. *Am J Physiol Regul Integr Comp Physiol* **2003,** 284, (2), R345-53.
10. Osei-Hyiaman, D.; DePetrillo, M.; Pacher, P.; Liu, J.; Radaeva, S.; Batkai, S.; Harvey-White, J.; Mackie, K.; Offertaler, L.; Wang, L., et al. Endocannabinoid activation at hepatic CB1 receptors stimulates fatty acid synthesis and contributes to diet-induced obesity. *J Clin Invest* **2005,** 115, (5), 1298-305.
11. Arrabal, S.; Lucena, M. A.; Canduela, M. J.; Ramos-Uriarte, A.; Rivera, P.; Serrano, A.; Pavon, F. J.; Decara, J.; Vargas, A.; Baixeras, E., et al. Pharmacological Blockade of Cannabinoid CB1 Receptors in Diet-Induced Obesity Regulates Mitochondrial Dihydrolipoamide Dehydrogenase in Muscle. *PLoS One* **2015,** 10, (12), e0145244.
12. Bluher, M.; Engeli, S.; Kloting, N.; Berndt, J.; Fasshauer, M.; Batkai, S.; Pacher, P.; Schon, M. R.; Jordan, J.; Stumvoll, M. Dysregulation of the peripheral and adipose tissue endocannabinoid system in human abdominal obesity. *Diabetes* **2006,** 55, (11), 3053-60.
13. Engeli, S.; Bohnke, J.; Feldpausch, M.; Gorzelniak, K.; Janke, J.; Batkai, S.; Pacher, P.; Harvey-White, J.; Luft, F. C.; Sharma, A. M., et al. Activation of the peripheral endocannabinoid system in human obesity. *Diabetes* **2005,** 54, (10), 2838-43.
14. Sam, A. H.; Salem, V.; Ghatei, M. A. Rimonabant: From RIO to Ban. *J Obes* **2011,** 2011, 432607.
15. Despres, J. P.; Golay, A.; Sjostrom, L. Effects of rimonabant on metabolic risk factors in overweight patients with dyslipidemia. *N Engl J Med* **2005,** 353, (20), 2121-34.
16. Pi-Sunyer, F. X.; Aronne, L. J.; Heshmati, H. M.; Devin, J.; Rosenstock, J. Effect of rimonabant, a cannabinoid-1 receptor blocker, on weight and cardiometabolic risk factors in overweight or obese patients: RIO-North America: a randomized controlled trial. *JAMA* **2006,** 295, (7), 761-75.
17. Simon, V.; Cota, D. MECHANISMS IN ENDOCRINOLOGY: Endocannabinoids and

metabolism: past, present and future. *Eur J Endocrinol* **2017,** 176, (6), R309-r324.
18. O'Keefe, L.; Simcocks, A. C.; Hryciw, D. H.; Mathai, M. L.; McAinch, A. J. The cannabinoid receptor 1 and its role in influencing peripheral metabolism. *Diabetes Obes Metab* **2014,** 16, (4), 294-304.
19. Kantae, V.; Nahon, K. J.; Straat, M. E.; Bakker, L. E. H.; Harms, A. C.; van der Stelt, M.; Hankemeier, T.; Jazet, I. M.; Boon, M. R.; Rensen, P. C. N. Endocannabinoid tone is higher in healthy lean South Asian than white Caucasian men. *Sci Rep* **2017,** 7, (1), 7558.
20. van den Berg, S. M.; Seijkens, T. T.; Kusters, P. J.; Beckers, L.; den Toom, M.; Smeets, E.; Levels, J.; de Winther, M. P.; Lutgens, E. Diet-induced obesity in mice diminishes hematopoietic stem and progenitor cells in the bone marrow. *FASEB J* **2016,** 30, (5), 1779-88.
21. Piomelli, D. The molecular logic of endocannabinoid signalling. *Nat Rev Neurosci* **2003,** 4, (11), 873-84.
22. Hussain, Z.; Uyama, T.; Tsuboi, K.; Ueda, N. Mammalian enzymes responsible for the biosynthesis of N-acylethanolamines. *Biochim Biophys Acta* **2017**.
23. Krott, L. M.; Piscitelli, F.; Heine, M.; Borrino, S.; Scheja, L.; Silvestri, C.; Heeren, J.; Di Marzo, V. Endocannabinoid regulation in white and brown adipose tissue following thermogenic activation. *J Lipid Res* **2016,** 57, (3), 464-73.
24. Di Marzo, V.; De Petrocellis, L.; Sepe, N.; Buono, A. Biosynthesis of anandamide and related acylethanolamides in mouse J774 macrophages and N18 neuroblastoma cells. *Biochem J* **1996,** 316 (Pt 3*)*, 977-84.
25. Oddi, S.; Fezza, F.; Pasquariello, N.; De Simone, C.; Rapino, C.; Dainese, E.; Finazzi-Agro, A.; Maccarrone, M. Evidence for the intracellular accumulation of anandamide in adiposomes. *Cell Mol Life Sci* **2008,** 65, (5), 840-50.
26. D'Eon, T. M.; Pierce, K. A.; Roix, J. J.; Tyler, A.; Chen, H.; Teixeira, S. R. The role of adipocyte insulin resistance in the pathogenesis of obesity-related elevations in endocannabinoids. *Diabetes* **2008,** 57, (5), 1262-8.
27. Pati, S.; Krishna, S.; Lee, J. H.; Ross, M. K.; de La Serre, C. B.; Harn, D. A., Jr.; Wagner, J. J.; Filipov, N. M.; Cummings, B. S. Effects of high-fat diet and age on the blood lipidome and circulating endocannabinoids of female C57BL/6 mice. *Biochim Biophys Acta* **2018,** 1863, (1), 26-39.
28. Bowles, N. P.; Karatsoreos, I. N.; Li, X.; Vemuri, V. K.; Wood, J. A.; Li, Z.; Tamashiro, K. L.; Schwartz, G. J.; Makriyannis, A. M.; Kunos, G., et al. A peripheral endocannabinoid mechanism contributes to glucocorticoid-mediated metabolic syndrome. *Proc Natl Acad Sci U S A* **2015,** 112, (1), 285-90.
29. Cote, M.; Matias, I.; Lemieux, I.; Petrosino, S.; Almeras, N.; Despres, J. P.; Di Marzo, V. Circulating endocannabinoid levels, abdominal adiposity and related cardiometabolic risk factors in obese men. *Int J Obes (Lond)* **2007,** 31, (4), 692-9.
30. Fezza, F.; Bari, M.; Florio, R.; Talamonti, E.; Feole, M.; Maccarrone, M. Endocannabinoids, related compounds and their metabolic routes. *Molecules* **2014,** *19*, (11), 17078-106.
31. Hillard, C. J. Circulating Endocannabinoids: From Whence Do They Come and Where are They Going? *Neuropsychopharmacology* **2018,** 43, (1), 155-172.
32. van Beek, L.; van Klinken, J. B.; Pronk, A. C.; van Dam, A. D.; Dirven, E.; Rensen, P. C.; Koning, F.; Willems van Dijk, K.; van Harmelen, V. The limited storage capacity of gonadal adipose tissue directs the development of metabolic disorders in male C57Bl/6J mice. *Diabetologia* **2015,** 58, (7), 1601-9.
33. Tchernof, A.; Despres, J. P. Pathophysiology of human visceral obesity: an update. *Physiol Rev* **2013,** 93, (1), 359-404.
34. Gruden, G.; Barutta, F.; Kunos, G.; Pacher, P. Role of the endocannabinoid system in

diabetes and diabetic complications. *Br J Pharmacol* **2016,** 173, (7), 1116-27.

35. Matias, I.; Petrosino, S.; Racioppi, A.; Capasso, R.; Izzo, A. A.; Di Marzo, V. Dysregulation of peripheral endocannabinoid levels in hyperglycemia and obesity: Effect of high fat diets. *Mol Cell Endocrinol* **2008,** 286, (1-2 Suppl 1), S66-78.
36. Geurts, L.; Everard, A.; Van Hul, M.; Essaghir, A.; Duparc, T.; Matamoros, S.; Plovier, H.; Castel, J.; Denis, R. G.; Bergiers, M., et al. Adipose tissue NAPE-PLD controls fat mass development by altering the browning process and gut microbiota. *Nat Commun* **2015,** 6, 6495.
37. Shimizu, I.; Aprahamian, T.; Kikuchi, R.; Shimizu, A.; Papanicolaou, K. N.; MacLauchlan, S.; Maruyama, S.; Walsh, K. Vascular rarefaction mediates whitening of brown fat in obesity. *J Clin Invest* **2014,** 124, (5), 2099-112.
38. Sipe, J. C.; Waalen, J.; Gerber, A.; Beutler, E. Overweight and obesity associated with a missense polymorphism in fatty acid amide hydrolase (FAAH). *Int J Obes (Lond)* **2005,** 29, (7), 755-9.
39. Tourino, C.; Oveisi, F.; Lockney, J.; Piomelli, D.; Maldonado, R. FAAH deficiency promotes energy storage and enhances the motivation for food. *Int J Obes (Lond)* **2010,** 34, (3), 557-68.
40. Bartelt, A.; Orlando, P.; Mele, C.; Ligresti, A.; Toedter, K.; Scheja, L.; Heeren, J.; Di Marzo, V. Altered endocannabinoid signalling after a high-fat diet in Apoe(-/-) mice: relevance to adipose tissue inflammation, hepatic steatosis and insulin resistance. *Diabetologia* **2011,** 54, (11), 2900-10.
41. Quarta, C.; Mazza, R.; Obici, S.; Pasquali, R.; Pagotto, U. Energy balance regulation by endocannabinoids at central and peripheral levels. *Trends Mol Med* **2011,** 17, (9), 518-26.
42. Boon, M. R.; Kooijman, S.; van Dam, A. D.; Pelgrom, L. R.; Berbee, J. F.; Visseren, C. A.; van Aggele, R. C.; van den Hoek, A. M.; Sips, H. C.; Lombes, M., et al. Peripheral cannabinoid 1 receptor blockade activates brown adipose tissue and diminishes dyslipidemia and obesity. *FASEB J* **2014,** 28, (12), 5361-75.

Supplementary table 1. Relative gene expression levels of synthesis and degradation enzymes *Dagla*, *Daglβ*, *Mgll* (of the 2-AG pathway) and *Nape-pld* and *Faah* (of the AEA pathway)

		HFD intervention (weeks)								
		0	1/7	3/7	1	2	4	10	18	*P*-value
Liver	*Dagla*	1.00 (0.93, 1.08)	0.93 (0.86, 1.00)	1.16 (1.05, 1.29)	1.16 (0.99, 1.34)	0.96 (0.85, 1.09)	1.24 (1.14, 1.35)	1.14 (1.05, 1.23)	1.20 (1.14, 1.27)	0.266
	Daglβ	1.00 (0.96, 1.05)	1.09 (1.04, 1.15)	1.21* (1.17, 1.25)	0.96 (0.93, 0.98)	0.97 (0.93, 1.01)	0.95 (0.91, 0.99)	0.96 (0.90, 1.03)	0.93 (0.90, 0.96)	0.001
	Mgll	1.00 (0.93, 1.08)	0.65*** (0.59, 0.71)	1.03 (0.96, 1.10)	0.79 (0.79, 0.80)	1.05 (1.00, 1.10)	0.99 (0.94, 1.05)	0.91 (0.86, 0.98)	0.86 (0.80, 0.92)	<0.001
	Nape-pld	1.00 (0.89, 1.12)	0.92 (0.81, 1.06)	1.16 (1.06, 1.27)	1.12 (1.04, 1.22)	1.21 (1.06, 1.37)	1.09 (1.00, 1.19)	1.20 (1.10, 1.30)	1.11 (0.88, 1.40)	0.792
	Faah	1.00 (0.94, 1.06)	1.10 (1.04, 1.16)	1.30 (1.21, 1.40)	0.93 (0.82, 1.06)	1.20 (1.12, 1.28)	0.87 (0.77, 0.99)	0.94 (0.82, 1.08)	0.59** (0.49, 0.70)	<0.001
Muscle	*Dagla*	1.00 (0.76, 1.32)	1.41 (1.16, 1.71)	1.43 (1.32, 1.56)	1.45 (1.38, 1.53)	1.82** (1.72, 1.93)	1.39 (1.30, 1.49)	1.47 (1.40, 1.53)	1.00 (0.89, 1.14)	0.009
	Daglβ	1.00 (0.86, 1.16)	0.95 (0.84, 1.08)	1.03 (1.00, 1.07)	1.02 (0.99, 1.05)	1.24 (1.17, 1.30)	1.15 (1.10, 1.20)	1.14 (1.09, 1.20)	0.97 (0.92, 1.01)	0.073
	Mgll	1.00 (0.76, 1.32)	0.79 (0.66, 0.95)	1.48 (1.21, 1.81)	1.06 (0.91, 1.23)	1.45 (1.27, 1.66)	1.24, (1.10, 1.40)	1.20 (1.10, 1.30)	0.89 (0.79, 1.00)	0.060
	Nape-pld	1.00 (0.91, 1.09)	0.72 (0.61, 0.85)	0.86 (0.75, 0.98)	0.71 (0.65, 0.78)	0.88 (0.81, 0.97)	0.58** (0.55, 0.60)	0.67~ (0.64, 0.71)	0.62* (0.55, 0.71)	0.010
	Faah	ND								

Supplementary table 1. Relative gene expression levels of synthesis and degradation enzymes *Dagla*, *Daglβ*, *Mgll* (of the 2-AG pathway) and *Nape-pld* and *Faah* (of the AEA pathway) (*continued*)

		HFD intervention (weeks)								
		0	1/7	3/7	1	2	4	10	18	*P*-value
WAT	*Dagla*	1.00 (0.90, 1.11)	1.20 (0.99, 1.45)	1.57* (1.53, 1.61)	1.31 (1.28, 1.34)	1.27 (1.14, 1.41)	1.07 (1.00, 1.15)	1.04 (0.95, 1.14)	0.91 (0.83, 1.01)	0.028
	Daglβ	1.00 (0.93, 1.07)	1.06 (1.00, 1.12)	1.21 (1.15, 1.27)	1.64* (1.59, 1.69)	1.23 (1.12, 1.35)	1.91** (1.70, 2.14)	2.34*** (2.19, 2.49)	3.46*** (2.68, 4.46)	<0.001
	Mgll	1.00 (0.91, 1.10)	1.38* (1.26, 1.51)	1.52** (1.41, 1.65)	1.75*** (1.67, 1.84)	1.45* (1.33, 1.59)	1.39* (1.32, 1.46)	1.27 (1.14, 1.41)	1.12 (1.06, 1.19)	<0.001
	Nape-pld	1.00 (0.92, 1.09)	1.14 (1.05, 1.23)	1.39 (1.18, 1.63)	1.16 (1.08, 1.24)	0.81 (0.72, 0.92)	0.80 (0.73, 0.87)	0.91 (0.87, 0.96)	0.59** (0.51, 0.69)	<0.001
	Faah	ND								
BAT	*Dagla*	1.00 (0.90, 1.11)	1.35~ (1.17, 1.55)	1.24 (1.19, 1.30)	1.50** (1.43, 1.58)	1.35~ (1.27, 1.44)	1.50** (1.45, 1.55)	1.25 (1.17, 1.34)	1.32 (1.19, 1.46)	0.030
	Daglβ	1.00 (0.95, 1.06)	0.93 (0.90, 0.97)	1.04 (1.00, 1.09)	1.23** (1.17, 1.29)	1.10 (1.05, 1.15)	1.27** (1.22, 1.33)	1.05 (1.00, 1.09)	1.38*** (1.33, 1.43)	<0.001
	Mgll	1.00 (0.92, 1.09)	1.28* (1.20, 1.36)	1.63*** (1.54, 1.72)	1.75*** (1.66, 1.85)	1.49*** (1.42, 1.58)	1.87*** (1.81, 1.94)	1.50*** (1.43, 1.58)	1.71*** (1.57, 1.86)	<0.001
	Nape-pld	1.00 (0.88, 1.14)	1.30 (1.14, 1.49)	2.02*** (1.92, 2.13)	1.84*** (1.77, 1.91)	1.56** (1.49, 1.63)	1.83*** (1.74, 1.92)	1.69*** (1.59, 1.80)	1.72*** (1.59, 1.87)	<0.001
	Faah	ND								

Data are mean (with lower, upper SEM) (n=10-11). ND (not detected) indicates the average CT values were >32. ~P<0.1; *P<0.05; **P<0.01; ***P<0.001 compared to the control (0 weeks of HFD) group analyzed by one-way ANOVA with Dunnett's *post hoc* test.

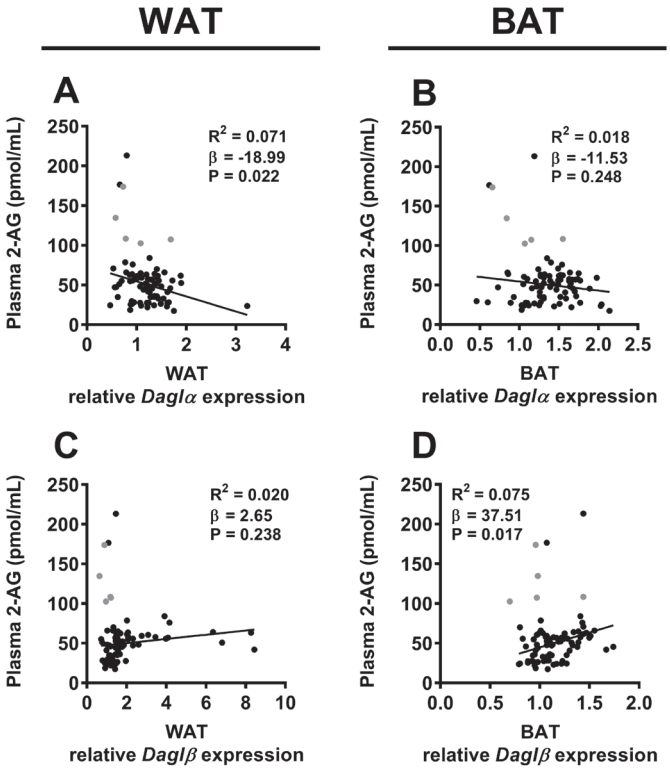

Supplementary figure 1. Linear regression analysis was performed on correlations between DAG lipase expression in the adipose tissues and plasma 2-AG levels. Linear regression analysis for *Daglα* expression relative to 0 weeks of HFD in WAT (A) and BAT (B) and 2-AG levels and linear regression analysis for *Daglβ* expression relative to 0 weeks of HFD in WAT (C) and BAT (D) and 2-AG levels. Correlations are shown for all samples depicted in black (n=81). Samples depicted in grey were regarded as biological outliers based on 2-AG and AA levels and therefore excluded from linear regression analyses.

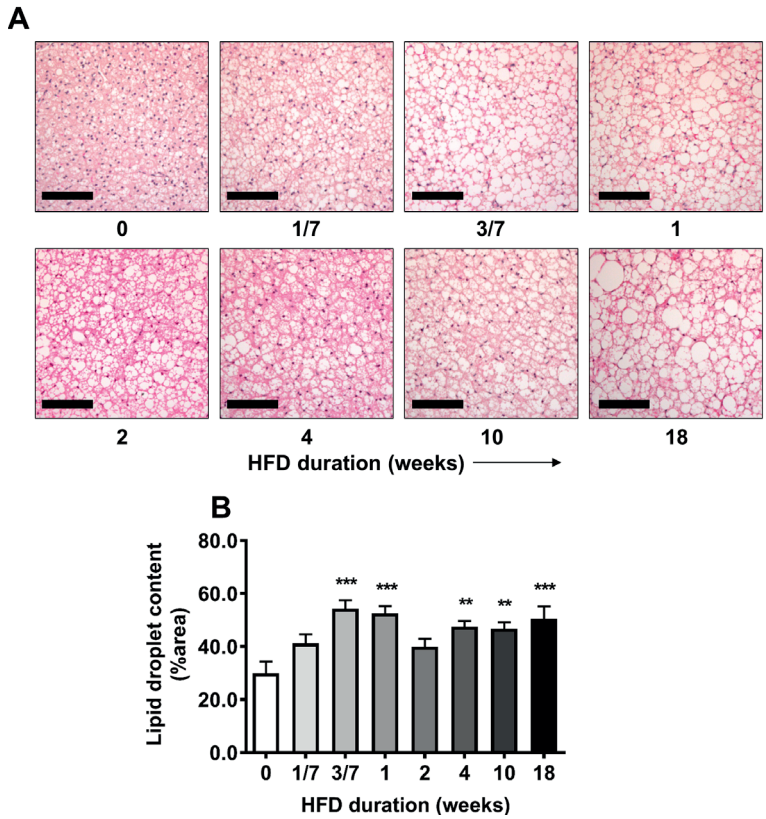

Supplementary figure 2. BAT sections were stained for H&E and representative images are shown (A). Pictures were analyzed in ImageJ to determine the lipid droplet content (B). Data are represented as mean ± SEM (n=9-11) **P<0.01; ***P<0.001 compared to the control (0 weeks of HFD) group analyzed by one-way ANOVA with Dunnett's *post hoc* test. Bars (A) indicate 100 µm.

7

QUERCETIN LOWERS PLASMA TRIGLYCERIDES ACCOMPANIED BY WHITE ADIPOSE TISSUE BROWNING IN DIET-INDUCED OBESE MICE

Eline N. Kuipers, Andrea D. van Dam,
Ntsiki M. Held, Isabel M. Mol,
Riekelt H. Houtkooper,
Patrick C.N. Rensen, Mariëtte R. Boon

International Journal of Molecular Sciences (2018); 19: E1786

ABSTRACT

Obesity and dyslipidemia are major risk factors for the development of cardiovascular diseases (CVD). Quercetin, a natural flavonoid, lowers plasma triglycerides (TG) in human intervention studies and its intake is associated with lower CVD risk. The aim of this study was to elucidate the mechanism by which quercetin lowers plasma TG levels in diet-induced obesity. C57Bl/6J mice received a high-fat diet (45% of calories derived from fat) with or without quercetin (0.1% w/w) for 12 weeks. Quercetin decreased plasma TG levels from 9 weeks onwards (-19%, $P<0.05$), without affecting food intake, body composition or energy expenditure. Mechanistically, quercetin did not reduce intestinal fatty acid (FA) absorption. Rather, quercetin induced a slight reduction in liver *Apob* expression (-13%, $P<0.05$), which suggests decreased VLDL-TG production. Interestingly, quercetin also markedly increased uptake of [^{3}H]oleate derived from glycerol tri[^{3}H]oleate-labeled lipoprotein-like particles by subcutaneous white adipose tissue (sWAT, +60%, $P<0.05$) together with markedly increased mRNA expression of *Ucp1* (+229%, $P<0.05$) and *Elovl3* (+138%, $P<0.05$) specifically in sWAT. Accordingly, only quercetin-treated animals showed UCP-1 protein-positive cells in sWAT, which is fully compatible with increased browning. Taken together, the TG-lowering effect of quercetin may, at least in part, be due to increased TG-derived FA uptake by sWAT as a consequence of browning.

INTRODUCTION

Cardiovascular diseases (CVD) are the number one cause of death worldwide. Obesity and dyslipidemia are major risk factors for developing CVD [1-3]. Super foods and other natural products including flavonoids have become increasingly popular as potential strategies to target these risk factors. Quercetin is a naturally occurring flavonoid that is present in fruits and vegetables [4]. Interestingly, epidemiological studies show that increased quercetin intake is associated with a reduced risk for developing CVD [5]. In a preclinical study quercetin supplementation indeed reduced atherosclerosis development [6]. Furthermore, quercetin supplementation attenuates body weight gain [7-9] and lipid deposition in the liver [10, 11] as well as white adipose tissue depots [12] of animals on a high fat diet. In addition, quercetin lowers plasma triglyceride (TG) levels in mice [7, 9, 13] and in humans [14] thereby targeting another risk factor for CVD.

The exact mechanism underlying the TG-lowering effect of quercetin and the organs involved have not yet been elucidated. Interestingly, a recent *in vitro* study showed that quercetin induces browning of 3T3-L1 white adipocytes [15], as they adapted a more brown-like phenotype including higher mRNA expression of the uncoupling protein 1 (UCP-1) [16]. Of note, we recently showed that browned white adipose tissue (WAT) depots increase their uptake of TG-derived fatty acids (FA) from the circulation compared to the same WAT depots in mice that lack the browning stimulus [17, 18]. In addition, brown adipose tissue (BAT) is a major contributor to TG metabolism [19, 20]. When activated by *e.g.* cold, BAT enhances oxidation of intracellular FA in both mice [17] and humans [21], which causes rapid depletion of intracellular TG stores. As a consequence, BAT takes up large amounts of TG-derived FA in a lipoprotein lipase (LPL) dependent manner and combusts these to generate heat in a process dependent on mitochondrial UCP-1 [20, 22].

Whether BAT and (browned) WAT are involved in the beneficial effects of quercetin with respect to reduction of plasma TG remains to be determined. Therefore, in the current study, we aimed at elucidating the mechanism by which quercetin lowers plasma TG levels by studying whole body lipid metabolism with the focus on BAT and WAT in diet-induced obese mice.

MATERIALS AND METHODS

Animals and diet

Male C57Bl/6J mice (n=18, Charles River Laboratories, USA), 9 weeks of age, were placed on a run-in high fat diet (HFD, 45% of calories derived from fat, D12451, Research Diets) for three weeks. Next, mice were randomized based on body weight and plasma TG

levels to receive a HFD with or without quercetin (0.1% w/w) for 12 weeks. Mice were housed individually under standard conditions with *ad libitum* access to food and water. Mouse experiments were performed in accordance with the Institute for Laboratory Animal Research Guide for the Care and Use of Laboratory Animals and have received approval from the University Ethical Review Board (Leiden University Medical Center, Leiden, the Netherlands).

Body weight, body composition and food intake

Body weight and body composition were determined weekly by using an EchoMRI-100 analyzer (EchoMRI, TX, USA). Food intake was measured weekly by subtracting the amount of food that was left in the cage from the amount given at the previous weighing.

Plasma parameters

Before randomization and every three weeks thereafter, mice were fasted for four hours and blood was drawn from the tail vein. Blood was collected in paraoxon (Sigma, St. Louis, MO) coated capillaries that were immediately placed on ice and centrifuged to obtain plasma. TG, total cholesterol (TC) and glucose were determined using commercially available enzymatic kits (Roche Diagnostics, Mannheim, Germany for TG and TC and Instruchemie, Delfzijl the Netherlands for glucose). FFA were measured using NEFA C kit (Wako Diagnostics, Instruchemie, Delfzijl, the Netherlands).

Lipoprotein profiles

Plasma samples obtained after 12 weeks of intervention were pooled to determine cholesterol distribution over plasma lipoproteins by fast performance liquid chromatography (FPLC). Plasma was placed onto a Superose 6 column (ÄKTA System, Amersham Pharmacia Biotech, Piscataway, NJ, USA) and eluted at a constant flow of 50 µL/min with PBS pH 7.4. Individual fractions were measured for TC as described above.

Indirect calorimetry and physical activity

During the third week of treatment, mice (n=8 per group) were placed in fully automatic metabolic cages (LabMaster System, TSE Systems, Bad Homburg, Germany) to assess energy expenditure and physical activity levels. After 20 h acclimatization, oxygen uptake (V_{O2}) and carbon dioxide production (V_{CO2}) were measured for 5 consecutive days. Total energy expenditure (EE) was calculated from V_{O2} and V_{CO2} using the Weir equation [23]. Fat and glucose oxidation rates were calculated from V_{O2} and V_{CO2} as described previously [24]. Physical activity was measured using infrared sensor frames.

Feces collection and fecal FFA concentration

After two and ten weeks of intervention, feces was collected by placing the mice in cages with new bedding and removing feces 24 hours later. Feces was then dried and weighed, approx. 30 mg was ground, and fecal FFA were determined after methyl esterification using the NEFA C kit (Wako Diagnostics) as described previously [25].

RNA isolation and RT-PCR analysis

Total RNA was isolated using TriPure Isolation reagent (Roche, the Netherlands) following the manufacturer's protocol. cDNA was made using Moloney Murine Leukemia Virus Reverse Transcriptase (Promega, The Netherlands). Real-time PCR (RT-PCR) was performed with SYBR green (Promega) on a CFX96 PCR Machine (Bio-Rad, Veenendaal, The Netherlands). mRNA expression levels were normalized to *β2-microglobulin* or glyceraldehyde-3-phosphate dehydrogenase (*Gapdh*) and hypoxanthine guanine phosphoribosyl transferase (*Hprt*) as reference genes. Primer sequences are listed in **Table 1**.

Table 1 List of primer sequences for RT-PCR

Gene	Forward primer	Reverse primer
β2-microglobulin	TGACCGGCTTGTATGCTATC	CAGTGTGAGCCAGGATATAG
Angptl4	GGAAAGAGGCTTCCCAAGAT	TCCCAGGACTGGTTGAAGTC
Apob	GCCCATTGTGGACAAGTTGATC	CCAGGACTTGGAGGTCTTGGA
Acc2	AGATGGCCGATCAGTACGTC	GGGGACCTAGGAAAGCAATC
Acsl1	TGCCAGAGCTGATTGACATTC	GGCATACCAGAAGGTGGTGAG
Cd36	GCAAAGAACAGCAGCAAAATC	CAGTGAAGGCTCAAAGATGG
Cidea	CTCGGCTGTCTCAATGTCAA	CCGCATAGACCAGGAACTGT
Cyp3a11	CTTTCCTTCACCCTGCATTCC	CTCATCCTGCAGTTTTTTCTGGAT
Elovl3	GGATGACGCCGTAGTCAGTA	GACAGAATGGACGCCAAAGT
Gapdh	GGGGCTGGCATTGCTCTCAA	TTGCTCAGTGTCCTTGCTGGGG
Hprt	TTGCTCGAGATGTCATGAAGGA	AGCAGGTCAGCAAAGAACTTATAG
Lpl	CCCTAAGGACCCCTGAAGAC	GGCCCGATACAACCAGTCTA
Mttp	CTCTTGGCAGTGCTTTTTCTCT	GAGCTTGTATAGCCGCTCATT
Pgc1a	TGCTAGCGGTTCTCACAGAG	AGTGCTAAGACCGCTGCATT
Prdm16	ACTTTGGATGGGAGCAGATG	CTCCAGGCTCGATGTCCTTA
Pxr	GAGCGGAGAAGACGGCAGCATC	CCCAGGTTCCCGTTTCCGTGTC
Ucp1	TCAGGATTGGCCTCTACGAC	TGCATTCTGACCTTCACGAC

In vivo clearance of radiolabeled lipoprotein-like particles

Lipoprotein-like particles (80 nm) labeled with glycerol tri[^{3}H]oleate (triolein, [^{3}H]TO) were prepared and characterized as described previously [26]. Mice were fasted for 4 h and injected (t = 0) with 200 µL of [^{3}H]TO-labeled lipoprotein-like particles (1.0 mg TG

per mouse) *via* the tail vein. Blood samples were taken 2, 5, 10 and 15 min after injection to determine the plasma decay of [^{3}H]TO (using calculations described in [27]). Next, mice were sacrificed by means of cervical dislocation and perfused with ice-cold heparin solution (0.1% v/v in PBS) *via* the heart. Organs were harvested, weighed and the uptake of [^{3}H]TO-derived radioactivity was quantified and expressed per gram or whole organ wet tissue weight.

Histology

Interscapular BAT (iBAT), gonadal WAT (gWAT), subcutaneous WAT (sWAT), visceral WAT (vWAT) and liver were removed and directly placed in 4% paraformaldehyde, dehydrated and embedded in paraffin. Hematoxylin and Eosin staining was performed using standard protocols. An overview of the studied fat depots can be found in **Suppl. Fig. 1**. Relative cell size and intracellular lipid content was quantified using ImageJ (version 1.49). UCP-1 staining on sWAT and BAT were performed as described before [27].

Quantification of lipid content in liver

Liver samples (approx. 50 mg) were homogenized in 10 µL of ice-cold methanol per mg tissue. Lipids were extracted as described before [27]. Hepatic TG, TC and PL concentrations were measured using commercial kits (as explained in Plasma parameters). Liver lipids were expressed per milligram of protein, which was determined using Pierce BCA protein assay kit (Thermo Scientific, Rockford, IL, USA).

Protein isolation and western blot

sWAT samples were lysed in buffer containing 50 mM HEPES (pH 7.6), 50 mM NaF, 50 mM KCl, 5 mM NaPPi, 1 mM EDTA, 1 mM EGTA, 1 mM DTT, 5 mM β-glycerophosphate, 1 mM sodium vanadate, 1% Nonidet P-40, and protease inhibitors using cocktail tablets (Roche). Protein concentration was determined using the Pierce BCA Protein Assay kit (Thermo Scientific) and extracts were diluted in Laemli buffer. Next, 10 µg protein of sWAT was separated on a 10% polyacrylamide gel (#456-8035, Bio-Rad) by electrophoresis and turbo-blotted on nitrocellulose membranes (#170-4159, Trans-blot Turbo, Bio-Rad). Membranes were blocked for 1 h at room temperature in Tween-20 buffer with 5% non-fat dry milk. Next membranes were incubated overnight with 1:1000 or 1:5000 (only for UCP-1 in BAT) diluted specific primary antibodies. Primary antibodies specific for AMPKα (#2532), p-AMPKα (Thr172, #2535) and α/β-Tubulin (#2148) were purchased from Cell Signalling Technology (Leiden, The Netherlands) and the antibody specific for UCP-1 (#U6382) was purchased from Sigma (St. Louis, MO). A primary antibody specific for GAPDH was purchased from Santa Cruz Biotechnology (Heidelberg, Germany). Membranes were incubated with horseradish peroxidase-conjugated secondary antibodies for 1 h. Super Signal West Pico Chemiluminescent Substrate (Thermo Scientific, Rock-

ford, IL, USA) was used to visualize bands on the ChemiDocTM Touch imaging system (Bio-Rad). The images were analyzed with Image lab software (version 5.2, Bio-Rad) and protein content was corrected for GAPDH (housekeeping protein).

Determination of mtDNA/nDNA ratio

Total DNA was isolated from sWAT with QIAamp DNA Mini Kit (no. 51306; Qiagen, Hilden Germany) following the provided manufacturer's protocol. The PCR reaction was performed in a LightCycler 480 (Roche). The reaction mix contained 500 pg DNA, 1.25 µM forward and reverse primer, and 4 µL 2x SYBR green master mix (Roche) in a final volume of 8 µL. *16S* and *Cox2* were used as mitochondrial encoded genes, *Hk2* and *Ucp2* for nuclear encoded genes. Primer sequences are listed in **Table 2**. Data were analyzed with LightCycler software release 1.5.0 (Roche). The mean PCR efficiency was calculated to assess gene expression levels using LinRegPCR program version 12.17 [28].

Table 2. List of PCR primer sequences

Gene	Forward primer	Reverse primer
16S	CCGCAAGGGAAAGATGAAAGAC	TCGTTTGGTTTCGGGGTTTC
Cox2	GTTGATAACCGAGTCGTTCTGC	CCTGGGATGGCATCAGTTTT
Hk2	TCTGGCTCTGAGATCCATCTTCA	CCGGCCTCTTAACCACATTCC
Ucp2	CTACAGATGTGGTAAAGGTCCGC	GCAATGGTCTTGTAGGCTTCG

Statistical analysis

All data are expressed as mean ± SEM. Statistical analysis was performed with an IBM SPSS Statistics 23 software package and Microsoft Excel 2010. Differences between control and quercetin was determined using an unpaired two-tailed t-test. Plasma decay in the clearance was analyzed using repeated measurements ANOVA with Sidak's *post hoc* test. A P-value < 0.05 was considered statistically significant.

RESULTS

Quercetin reduces plasma triglyceride levels without affecting body composition, food intake and energy expenditure

In order to assess the effect of quercetin on body composition, plasma lipids and energy balance, C57Bl/6J mice were fed a high fat diet (HFD) with or without 0.1% (w/w) quercetin for 12 weeks. Quercetin neither affected body weight (mean body weight after 12 weeks 45.2±2.5 g in control and 47.4±3.3 g in quercetin treated animals; **Fig. 1A**) nor body composition with respect to lean and fat mass (**Fig. 1B**). In line with these data, organ weight of spleen, gWAT and iBAT at necropsy were unaffected by quercetin.

We only found liver weight to be increased (+13%, P<0.05; **Suppl. Fig. 2A**). Of note, quercetin lowered plasma TG levels from 9 weeks onwards (up to -19%, P<0.05; **Fig. 1C**). Furthermore, quercetin treatment increased plasma total cholesterol levels, which was mainly due to increased cholesterol in the HDL fraction (**Suppl. Fig. 2B, C**), decreased plasma free FA (FFA) levels, and did not affect plasma glucose (**Suppl. Fig. 2D, E**). The lowering in plasma TG levels by quercetin could not be explained by a lower daily food intake, since daily food intake was not persistently affected by quercetin (**Fig. 1D**) and cumulative food intake was not different between the two groups (data not shown). To determine whether quercetin influenced whole body energy expenditure and substrate utilization, mice were placed in metabolic cages in the third week of treatment. Quercetin did not affect total energy expenditure (EE), fat or glucose oxidation (**Fig. 1E-G**). Respiratory exchange ratio (RER) and physical activity were also unaltered (**Suppl. Fig.**

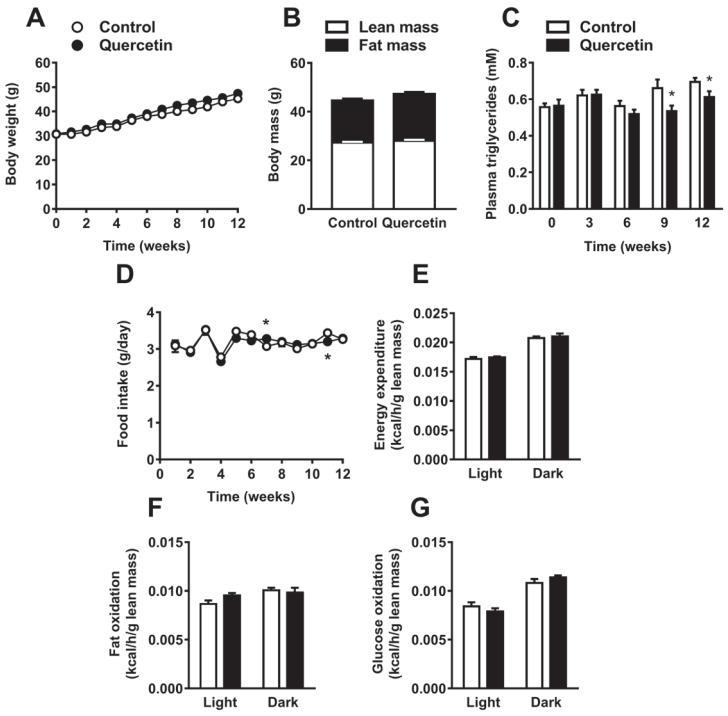

Figure 1. Quercetin reduces plasma triglyceride levels without affecting body composition, food intake and energy expenditure. C57Bl/6J mice were fed a high-fat diet (HFD) +/- quercetin (0.1% w/w) for 12 weeks. Body weight was measured weekly (A). Body composition was determined (B). Plasma triglycerides were determined before and every 3 weeks during de intervention (C). Food intake was determined weekly (D). In the third week of treatment, animals were placed in fully automatic metabolic cages for assessment of total energy expenditure (E), fat oxidation (F) and glucose oxidation (G). Data are represented as mean ± SEM (n=8-10), *P<0.05 versus control.

2F, G). Taken together, quercetin reduced plasma TG without affecting body weight, body composition, food intake and energy expenditure.

Quercetin reduces hepatic *ApoB* expression and increases uptake of TG-derived FA by sWAT

Plasma TG levels are determined by the balance between intestinal TG uptake, hepatic VLDL-TG production and VLDL-TG clearance by LPL-expressing peripheral organs. We first assessed total fecal output, measured over 24 h, which was unaltered after 2 and 10 weeks of quercetin treatment (**Fig. 2A**). Interestingly, FFA content in feces was reduced after 10 weeks of quercetin treatment (-39%, $P<0.05$; **Fig. 2B**), suggesting enhanced rather than decreased intestinal TG absorption. We next focused on the effect of quercetin on liver lipid metabolism. Albeit that quercetin increased liver weight (**Suppl. Fig. 2A**), quercetin did not affect liver lipid content (**Suppl. Fig. 3A, B**). Activation of xenobiotic sensing nuclear receptor pregnane X receptor (PXR), as underlying cause for the increased liver weight, was excluded since *Pxr* expression and the expression of the PXR target gene *Cyp3a11* remained unchanged (**Suppl. Fig. 3C**). Hepatic expression of lipid synthesis and oxidation marker acyl-CoA synthetase long-chain family member 1 (*Acsl1*) was unaffected and lipid synthesis marker acetyl-CoA carboxylase 2 (*Acc2*) tended to be increased after quercetin treatment (**Fig. 2C**).

To assess the effect of quercetin on VLDL-TG production, we determined the mRNA expression of hepatic microsomal triglyceride transfer protein (*Mttp*) and apolipoprotein B (*Apob*), both involved in hepatic VLDL assembly and secretion (**Fig. 2C**). Of note, quercetin decreased *Apob* expression (-13%, $P<0.05$; **Fig. 2C**), which may indicate lower VLDL production.

To investigate whether quercetin reduced plasma TG levels due to increased clearance of TG-rich lipoproteins, we determined the kinetics of intravenous injected [^{3}H]TO labeled TG-rich lipoprotein-like particles, and studied the plasma clearance of [^{3}H]TO and organ uptake of [^{3}H]TO-derived [^{3}H]oleate in mice treated with quercetin for 12 weeks. The plasma clearance of [^{3}H]TO was slightly accelerated in the quercetin treated group (**Fig. 2D**). The uptake of ^{3}H per gram organ was decreased in the liver (-22%, $P<0.05$), but this effect disappeared when data were corrected for whole organ weight (**Suppl. Fig. 3D**). Interestingly, quercetin markedly increased (+60%, $P<0.05$; **Fig. 2E**) the uptake of ^{3}H per gram organ by sWAT, while the uptake by the two studied classical BAT depots (interscapular and subscapular) were not changed. All in all, our data suggest that quercetin decreases plasma TG levels by decreasing VLDL-TG production and increasing TG-derived FA uptake by sWAT.

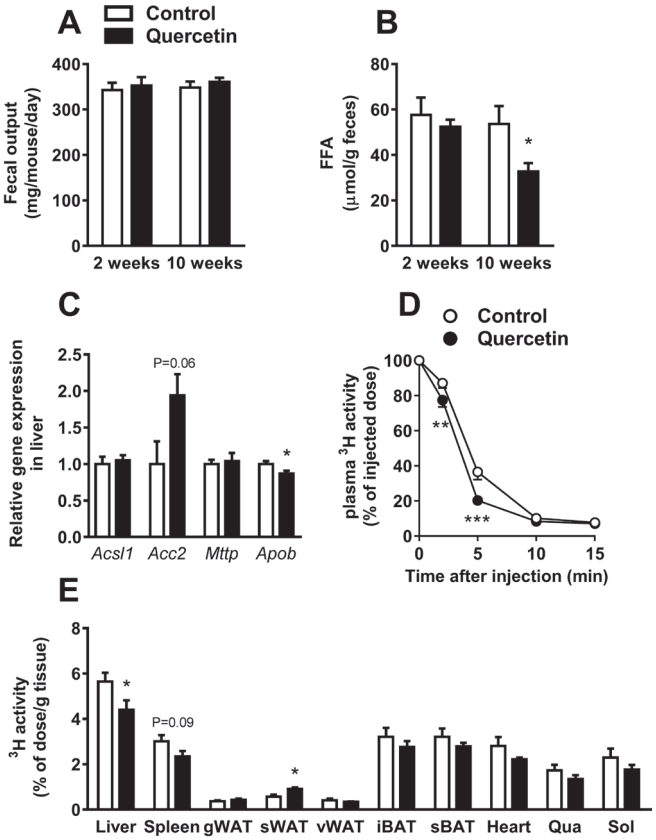

Figure 2. Quercetin reduces hepatic *Apob* expression and increases uptake of TG-derived FA by subcutaneous white adipose tissue. In week 2 and week 10 of the intervention, 24 hours feces was collected (A) and used to determine fecal free fatty acid (FFA) concentration (B). Gene expression in the liver was determined by qRT-PCR for *Acsl1*, *Acc2*, *Mttp* and *Apob* (C). After 12 weeks, mice were injected with glycerol tri[^{3}H]oleate-labeled lipoprotein-like particles and clearance from plasma (D) and uptake per gram organ (E) were determined by ^{3}H-activity analysis. Data are represented as mean ± SEM (n=8-10); expression of genes was corrected for the reference gene *β2-microglobulin*, *P<0.05 versus control. (g,s,v)WAT, gonadal, subcutaneous, visceral white adipose tissue; (i,s)BAT, interscapular, subscapular brown adipose tissue; qua, quadriceps muscle; sol, soleus muscle.

Quercetin increases *Ucp1* gene expression specifically in sWAT

Since increased uptake of TG-derived FA by sWAT might point to increased browning of this depot [17, 18], we next determined whether quercetin had induced browning of sWAT. Indeed, quercetin markedly increased the expression of *Ucp1* in sWAT (+229%, P<0.05) as well as the brown fat marker fatty acid elongase 3 (*Elovl3*, +138%, P<0.05, **Fig. 3A**). Expression of other markers of BAT-like metabolism, including the transcriptional coregulators PR domain containing 16 (*Prdm16*) and Cell Death-inducing DFFA-like Effector A (*Cidea*), the central inducer of mitochondrial biogenesis peroxisome proliferator-

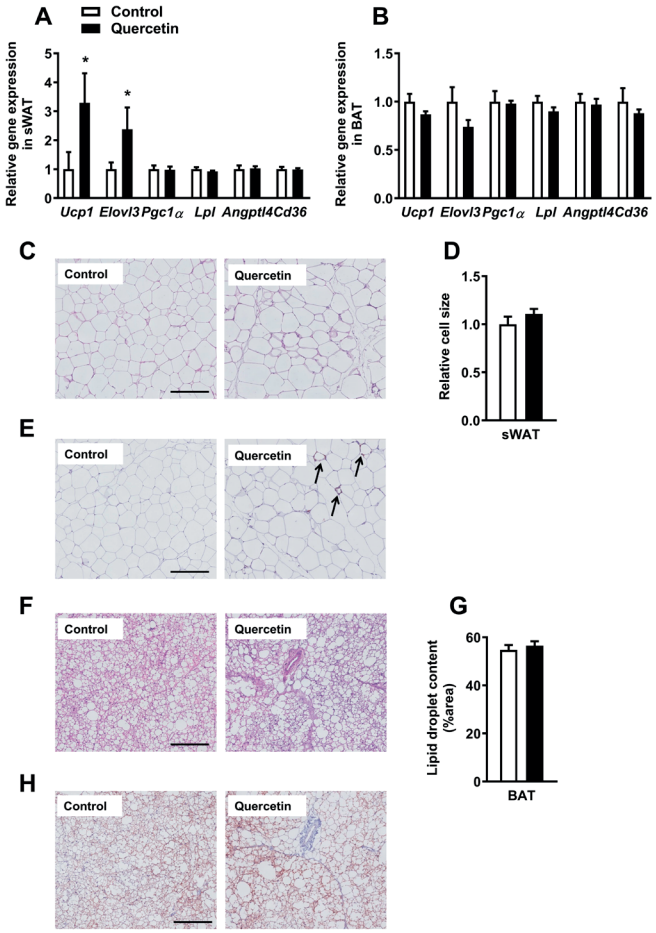

Figure 3. Quercetin increases *Ucp1* gene expression specifically in subcutaneous white adipose tissue. Gene expression in sWAT (A) and BAT (B) was determined by qRT-PCR. H&E staining was performed on paraffin embedded sWAT sections and representative pictures are shown (C). Pictures were analyzed in ImageJ to determine the relative cell size (D). sWAT sections were stained for UCP-1 (E) as well. BAT sections were stained for H&E (F) and used to quantify lipid droplet content in ImageJ (G). BAT sections were also stained for UCP-1 (H). Data are represented as mean ± SEM (n=8-10); expression of genes was corrected for the reference gene *β2-microglobulin* (sWAT), *Gapdh* and *Hprt* (BAT), *P<0.05 versus control. Bars (C, E, F, H) indicate 200 μm.

activated receptor γ coactivator 1 (*Pgc1α*) and markers involved in lipid uptake, including lipoprotein lipase (*Lpl*), the LPL regulator angiopoietin like 4 (*Angptl4*) and fatty acid translocase (*Cd36*) were unaltered in sWAT (**Fig. 3A**). Also, p-AMPK (Thr172)/AMPK ratio in sWAT did not differ between quercetin and the control group (**Suppl. Fig. 4A**). Furthermore, quercetin did not increase expression of *Ucp1*, *Elvol3*, *Pgc1a*, *Lpl*, *Angptl4* and *Cd36* in BAT (**Fig. 3B**), gWAT (**Suppl. Fig. 5A**) and visceral WAT (vWAT, **Suppl. Fig. 5B**). To

verify browning on a morphological level, sWAT sections were stained with H&E (**Fig. 3C**) and for UCP-1 (**Fig. 3E**). While relative cell size did not differ between the two treatment groups (**Fig. 3D**), quercetin did induce the presence of UCP-1 positive cells (indicated by the arrows) while these were completely absent in the control animals (**Fig. 3E**). We also attempted to measure UCP-1 content in sWAT *via* western blot, but the content appeared too low to draw conclusions (data not shown). Quercetin did not increase mitochondrial abundance since only the mitochondrial DNA versus nuclear DNA ratio of *16s*/*Hk2* tended to be increased (P=0.08, **Suppl. Fig. 4B**) in the quercetin treated animals while *Cox2*/*Ucp2*, *Cox2*/*Hk2* and *16S*/*Hk2* were unaffected. In line with the qRT-PCR data, quercetin did not affect histological appearance and lipid droplet content of BAT (**Fig. 3F, G**), gWAT (**Suppl. Fig. 5C, D**), and vWAT (**Suppl. Fig. 5E, F**). Also, quercetin did not affect UCP-1 content in BAT (**Fig. 3H**) or UCP-1 protein content as measured *via* western blot (data not shown). All in all, our data shows that quercetin increases expression of BAT markers and UCP-1 content specifically in sWAT.

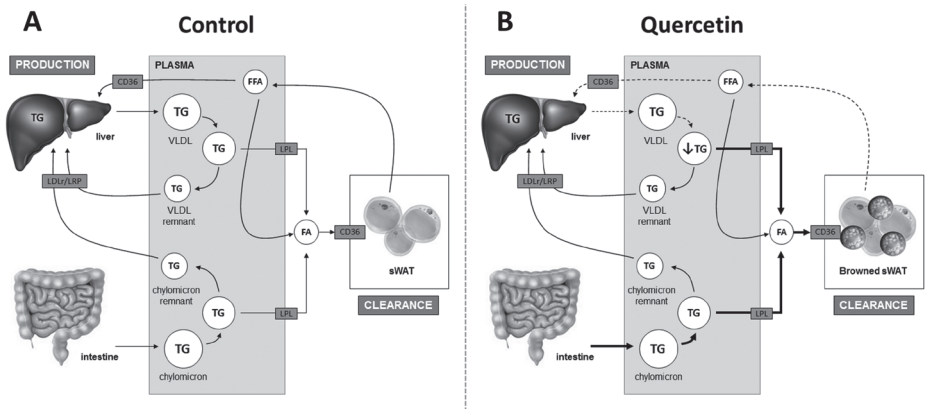

Figure 4. Proposed mechanism by which quercetin lowers plasma triglycerides (TG). Plasma TG levels are regulated by intestinal TG absorption, hepatic VLDL-TG production and the clearance of TG-derived fatty acids (FA) by peripheral organs such as sWAT in a process that is dependent on lipoprotein lipase (LPL) (left). Quercetin induces browning of sWAT resulting in increased uptake of TG-derived FA by sWAT. This may contribute to lowering of plasma TG levels. Moreover, quercetin may also lower lipolysis from (s)WAT, which may contribute to lower plasma free FA (FFA) levels and lower VLDL-TG production by the liver, also contributing to lower plasma TG levels. Lastly, quercetin increases uptake of lipids by the intestine, which apparently does not counteract the reduction in plasma TG levels (right). Bold arrows indicate increased flux, dashed arrows indicate decreased flux. LDLr, low density lipoprotein receptor; LRP, low density lipoprotein receptor-related protein.

DISCUSSION

Previous studies in humans and animals have shown that quercetin is a possible new agent to improve metabolic health, since it lowers plasma TG levels [7, 13, 14]. The organs involved in the TG-lowering effect of quercetin remained obscure so far. In the current study, we demonstrated that quercetin reduces plasma TG as well as FA levels accompanied by increased flux of TG-derived FA towards sWAT, but not BAT, and induction of browning of this depot. Quercetin probably lowers VLDL-TG production as indicated by lower *Apob* expression. We conclude that the TG-lowering effect of quercetin may, at least in part, be due to increased TG-derived FA uptake by sWAT as a consequence of browning (**Fig. 4**).

Our finding that quercetin lowers plasma TG levels has been repeatedly shown by others [7, 11, 13, 29]. Of note, in all of these studies quercetin lowers plasma TG levels even though different concentrations (ranging from 0.025% to 0.33% w/w) of quercetin were added to a high fat and/or high fructose diet. This indicates that quercetin is a potent modulator of plasma TG levels and exerts metabolically beneficial effects at a wide dose range. In contrast to our study, several of these studies also reported a reduction in body weight following quercetin treatment, again in a dose range [7, 11]. This discrepancy might be explained by a difference in age of the animals at the start of the intervention. Studies that describe weight reduction after quercetin treatment used animals of 4-5 weeks of age, which are not yet developed into adult mice and might therefore be more susceptible to body weight changes caused by the intervention compared to the 9 week old animals as used in this study.

To gain insight into the mechanism underlying the TG-lowering effect of quercetin, we determined the effect of quercetin on several metabolic organs and performed kinetic studies to assess FA fluxes. To assess whether quercetin affected intestinal FA absorption, we measured fecal FA output. A previous study in Caco-2 cells, which mimic human intestinal epithelial cells, shows that quercetin increases ^{3}H-FA uptake, but only when initial ^{3}H-FA uptake was reduced under conditions of oxidative stress [30]. However, fecal FA in our study was lower rather than higher in the quercetin treated group. This suggests higher rather than lower intestinal FA absorption, which therefore cannot explain the observed reduction in plasma TG levels. Interestingly, we found that quercetin reduced liver *Apob* expression, which might indicate lower VLDL production. In support of this hypothesis, Gnoni *et al.* [31] found that stimulation of isolated rat hepatocytes with quercetin decreases TG synthesis and VLDL-TG formation due to lower ACC and diacylglycerol acyltransferase activity. A lower VLDL-TG production might underlie the increase in liver weight in the quercetin treated animals by inducing a trend towards higher TG accumulation. Of note, this is in contrast to previous literature in which liver weight was shown to be unaffected [32] or even decreased, due to a reduction in liver

TG [11]. Next to a direct effect of quercetin on hepatocytes, a lower VLDL production *in vivo* might also be the consequence of lower FA flux towards the liver due to reduced FA liberation by lipolysis in WAT. In line with this, we showed that quercetin lowered plasma FFA levels, although we did not find any effect of quercetin on expression of markers of lipolysis in white adipose tissue (not shown). Rather, others have shown that quercetin increases lipolysis in white adipocytes [15, 33]. Alternatively, lower plasma FFA levels might also be a consequence of increased FFA uptake by adipose depots, since not only TG-derived FA but also FFA can be taken up by BAT [34] and possibly also by browned white adipose tissue.

Our kinetic study using labeled lipoprotein-like TG-rich particles showed that quercetin increases the uptake of TG-derived FA specifically by sWAT, the depot that is especially prone to browning [35]. This metabolic effect along with increased *Ucp1* and *Elovl3* expression and the presence of UCP-1 positive cells in sWAT, is fully compatible with increased browning. In agreement with our results, Lee and colleagues [15] recently showed that onion peel, with quercetin as a main component, induces *Ucp1* expression in white adipose tissue of mice. In that study, effects on plasma TG levels were not reported. Of note, we found that quercetin solely increased *Ucp1* expression and TG-derived FA uptake in sWAT and did not affect uptake by BAT in our study. Adipose depot-specific responses to intervention have been observed before. For instance, mice with genetically increased levels of bone morphogenetic protein 4 are protected from obesity due to a phenotype with sWAT browning despite the fact that BAT accumulates lipids and adapts a beige/brite phenotype [36]. It can be questioned whether adipose tissue browning has the capacity to reduce plasma TG levels, also since the UCP-1 content in sWAT is quite low. Interestingly, inactivating the classical BAT depot by selective inhibition of lipid droplet lipolysis induces WAT browning and lowers TG levels in peripheral organs, which indeed demonstrates the potency of browning per se to affect TG distribution [37] and possibly also to reduce plasma TG levels. Our data thus suggest that quercetin induces browning that could, at least in part, be responsible for the improved plasma TG levels (**Fig. 4**). Future studies are evidently needed to clarify the extent to which adipose tissue browning contributes to the metabolically beneficial effects induced by quercetin.

How quercetin might induce browning of sWAT has not yet been fully elucidated. Lee *et al.* [15] propose a mechanism by which quercetin acts directly on the adipocyte and induces browning at least in part *via* the AMP-activated protein kinase (AMPK)/SIRT1/PGC1α pathway. Activation of this pathway results in increased *Pgc1α* expression, suggesting to increase mitochondrial biogenesis. Although quercetin tended to slightly increase one of the four mtDNA/nDNA ratios in sWAT in our study, quercetin did not affect sWAT p-AMPK/AMPK ratio and *Pgc1α* expression. Interestingly, quercetin is known as a phytoestrogen because of its binding capacity to the estrogen receptor (ER) [38].

Pharmacological activation of the ER subtype β (ER-β) in mice reduces body weight and adiposity with concomitant enhanced oxygen consumption and elevated core body temperature [39]. Moreover, ER-β ligand LY3201 induces browning of sWAT by modulating the sympathetic ganglia and the adipocytes directly [40]. The mechanism underlying the quercetin induced browning of specifically sWAT and possible involvement of the ER-β remains to be determined and is an interesting avenue to pursue in future studies. In addition, whether quercetin induces browning in humans, and whether this mediates the improvement of TG metabolism, remains to be studied.

In conclusion, our study shows that quercetin induces browning of sWAT, which results in an increased flux of TG-derived FA towards sWAT and which may, at least in part, underlie the TG-lowering effect of quercetin (**Fig. 4**). The mechanism behind these effects and the ability of quercetin to induce browning in humans remains to be determined.

ACKNOWLEDGEMENTS

The authors thank Kevin Brewster, Lianne van der Wee-Pals and Trea Streefland (LUMC, Dept. Medicine, Div. Endocrinology) for their valuable technical assistance.

FUNDING

This work was supported by a research grant from the Rembrandt Institute of Cardiovascular Science to M.R. Boon and R.H. Houtkooper. M.R. Boon is supported by a grant from the Dutch Diabetes Foundation (2015.81.1808). Furthermore, we acknowledge the support from the Netherlands Cardiovascular Research Initiative: an initiative with support of the Dutch Heart Foundation (CVON2014-02 ENERGISE).

REFERENCES

1. Knight, J. A. Diseases and disorders associated with excess body weight. *Ann Clin Lab Sci* **2011**, 41, (2), 107-21.
2. Nordestgaard, B. G.; Benn, M.; Schnohr, P.; Tybjaerg-Hansen, A. Nonfasting triglycerides and risk of myocardial infarction, ischemic heart disease, and death in men and women. *JAMA* **2007**, 298, (3), 299-308.
3. Nordestgaard, B. G. Triglyceride-Rich Lipoproteins and Atherosclerotic Cardiovascular Disease: New Insights From Epidemiology, Genetics, and Biology. *Circ Res* **2016**, 118, (4), 547-63.
4. Manach, C.; Scalbert, A.; Morand, C.; Remesy, C.; Jimenez, L. Polyphenols: food sources and bioavailability. *Am J Clin Nutr* **2004**, 79, (5), 727-47.
5. Peterson, J. J.; Dwyer, J. T.; Jacques, P. F.; McCullough, M. L. Associations between flavonoids and cardiovascular disease incidence or mortality in European and US populations. *Nutr Rev* **2012**, 70, (9), 491-508.
6. Shen, Y.; Ward, N. C.; Hodgson, J. M.; Puddey, I. B.; Wang, Y.; Zhang, D.; Maghzal, G. J.; Stocker, R.; Croft, K. D. Dietary quercetin attenuates oxidant-induced endothelial dysfunction and atherosclerosis in apolipoprotein E knockout mice fed a high-fat diet: a critical role for heme oxygenase-1. *Free Radic Biol Med* **2013**, 65, 908-15.
7. Kobori, M.; Masumoto, S.; Akimoto, Y.; Oike, H. Chronic dietary intake of quercetin alleviates hepatic fat accumulation associated with consumption of a Western-style diet in C57/BL6J mice. *Mol Nutr Food Res* **2011**, 55, (4), 530-40.
8. Kobori, M.; Takahashi, Y.; Sakurai, M.; Akimoto, Y.; Tsushida, T.; Oike, H.; Ippoushi, K. Quercetin suppresses immune cell accumulation and improves mitochondrial gene expression in adipose tissue of diet-induced obese mice. *Mol Nutr Food Res* **2016**, 60, (2), 300-12.
9. Porras, D.; Nistal, E.; Martinez-Florez, S.; Pisonero-Vaquero, S.; Olcoz, J. L.; Jover, R.; Gonzalez-Gallego, J.; Garcia-Mediavilla, M. V.; Sanchez-Campos, S. Protective effect of quercetin on high-fat diet-induced non-alcoholic fatty liver disease in mice is mediated by modulating intestinal microbiota imbalance and related gut-liver axis activation. *Free Radic Biol Med* **2016**, 102, 188-202.
10. Kim, C. S.; Kwon, Y.; Choe, S. Y.; Hong, S. M.; Yoo, H.; Goto, T.; Kawada, T.; Choi, H. S.; Joe, Y.; Chung, H. T., et al. Quercetin reduces obesity-induced hepatosteatosis by enhancing mitochondrial oxidative metabolism via heme oxygenase-1. *Nutr Metab (Lond)* **2015**, 12, 33.
11. Jung, C. H.; Cho, I.; Ahn, J.; Jeon, T. I.; Ha, T. Y. Quercetin reduces high-fat diet-induced fat accumulation in the liver by regulating lipid metabolism genes. *Phytother Res* **2013**, 27, (1), 139-43.
12. Panchal, S. K.; Poudyal, H.; Brown, L. Quercetin ameliorates cardiovascular, hepatic, and metabolic changes in diet-induced metabolic syndrome in rats. *J Nutr* **2012**, 142, (6), 1026-32.
13. Hoek-van den Hil, E. F.; Keijer, J.; Bunschoten, A.; Vervoort, J. J.; Stankova, B.; Bekkenkamp, M.; Herreman, L.; Venema, D.; Hollman, P. C.; Tvrzicka, E., et al. Quercetin induces hepatic lipid omega-oxidation and lowers serum lipid levels in mice. *PLoS One* **2013**, 8, (1), e51588.
14. Sahebkar, A. Effects of quercetin supplementation on lipid profile: A systematic review and meta-analysis of randomized controlled trials. *Crit Rev Food Sci Nutr* **2017**, 57, (4), 666-676.
15. Lee, S. G.; Parks, J. S.; Kang, H. W. Quercetin, a functional compound of onion peel, remodels white adipocytes to brown-like adipocytes. *J Nutr Biochem* **2017**, 42, 62-71.

16. Rosell, M.; Kaforou, M.; Frontini, A.; Okolo, A.; Chan, Y. W.; Nikolopoulou, E.; Millership, S.; Fenech, M. E.; MacIntyre, D.; Turner, J. O., et al. Brown and white adipose tissues: intrinsic differences in gene expression and response to cold exposure in mice. A*m J Physiol Endocrinol Metab* **2014**, 306, (8), E945-64.
17. Berbee, J. F.; Boon, M. R.; Khedoe, P. P.; Bartelt, A.; Schlein, C.; Worthmann, A.; Kooijman, S.; Hoeke, G.; Mol, I. M.; John, C., et al. Brown fat activation reduces hypercholesterolaemia and protects from atherosclerosis development. *Nat Commun* **2015**, 6, 6356.
18. Kooijman, S.; Wang, Y.; Parlevliet, E. T.; Boon, M. R.; Edelschaap, D.; Snaterse, G.; Pijl, H.; Romijn, J. A.; Rensen, P. C. Central GLP-1 receptor signalling accelerates plasma clearance of triacylglycerol and glucose by activating brown adipose tissue in mice. *Diabetologia* **2015**, 58, (11), 2637-46.
19. Laplante, M.; Festuccia, W. T.; Soucy, G.; Blanchard, P. G.; Renaud, A.; Berger, J. P.; Olivecrona, G.; Deshaies, Y. Tissue-specific postprandial clearance is the major determinant of PPARgamma-induced triglyceride lowering in the rat. *Am J Physiol Regul Integr Comp Physiol* **2009**, 296, (1), R57-66.
20. Khedoe, P. P.; Hoeke, G.; Kooijman, S.; Dijk, W.; Buijs, J. T.; Kersten, S.; Havekes, L. M.; Hiemstra, P. S.; Berbee, J. F.; Boon, M. R., et al. Brown adipose tissue takes up plasma triglycerides mostly after lipolysis. *J Lipid Res* **2015**, 56, (1), 51-9.
21. Bakker, L. E.; Boon, M. R.; van der Linden, R. A.; Arias-Bouda, L. P.; van Klinken, J. B.; Smit, F.; Verberne, H. J.; Jukema, J. W.; Tamsma, J. T.; Havekes, L. M., et al. Brown adipose tissue volume in healthy lean south Asian adults compared with white Caucasians: a prospective, case-controlled observational study. *Lancet Diabetes Endocrinol* **2014**, 2, (3), 210-7.
22. Cannon, B.; Nedergaard, J. Brown adipose tissue: function and physiological significance. *Physiol Rev* **2004**, 84, (1), 277-359.
23. Weir, J. B. New methods for calculating metabolic rate with special reference to protein metabolism. *J Physiol* **1949**, 109, (1-2), 1-9.
24. Van Klinken, J. B.; van den Berg, S. A.; Havekes, L. M.; Willems Van Dijk, K. Estimation of activity related energy expenditure and resting metabolic rate in freely moving mice from indirect calorimetry data. *PLoS One* **2012**, 7, (5), e36162.
25. van Dam, A. D.; Nahon, K. J.; Kooijman, S.; van den Berg, S. M.; Kanhai, A. A.; Kikuchi, T.; Heemskerk, M. M.; van Harmelen, V.; Lombes, M.; van den Hoek, A. M., et al. Salsalate activates brown adipose tissue in mice. *Diabetes* **2015**, 64, (5), 1544-54.
26. Rensen, P. C.; van Dijk, M. C.; Havenaar, E. C.; Bijsterbosch, M. K.; Kruijt, J. K.; van Berkel, T. J. Selective liver targeting of antivirals by recombinant chylomicrons--a new therapeutic approach to hepatitis B. *Nat Med* **1995**, 1, (3), 221-5.
27. Boon, M. R.; Kooijman, S.; van Dam, A. D.; Pelgrom, L. R.; Berbee, J. F.; Visseren, C. A.; van Aggele, R. C.; van den Hoek, A. M.; Sips, H. C.; Lombes, M., et al. Peripheral cannabinoid 1 receptor blockade activates brown adipose tissue and diminishes dyslipidemia and obesity. *FASEB J* **2014**, 28, (12), 5361-75.
28. Ruijter, J. M.; Ramakers, C.; Hoogaars, W. M.; Karlen, Y.; Bakker, O.; van den Hoff, M. J.; Moorman, A. F. Amplification efficiency: linking baseline and bias in the analysis of quantitative PCR data. *Nucleic Acids Res* **2009**, 37, (6), e45.
29. Porras, A.; Alvarez, A. M.; Valladares, A.; Benito, M. TNF-alpha induces apoptosis in rat fetal brown adipocytes in primary culture. *FEBS Lett* **1997**, 416, (3), 324-8.
30. Couto, M. R.; Goncalves, P.; Catarino, T.; Araujo, J. R.; Correia-Branco, A.; Martel, F. The effect of oxidative stress upon the in-

testinal uptake of folic acid: in vitro studies with Caco-2 cells. *Cell Biol Toxicol* **2012**, 28, (6), 369-81.

31. Gnoni, G. V.; Paglialonga, G.; Siculella, L. Quercetin inhibits fatty acid and triacylglycerol synthesis in rat-liver cells. *Eur J Clin Invest* **2009**, 39, (9), 761-8.
32. Arias, N.; Macarulla, M. T.; Aguirre, L.; Miranda, J.; Portillo, M. P. Liver delipidating effect of a combination of resveratrol and quercetin in rats fed an obesogenic diet. *J Physiol Biochem* **2015**, 71, (3), 569-76.
33. Arias, N.; Macarulla, M. T.; Aguirre, L.; Milton, I.; Portillo, M. P. The combination of resveratrol and quercetin enhances the individual effects of these molecules on triacylglycerol metabolism in white adipose tissue. *Eur J Nutr* **2016**, 55, (1), 341-8.
34. Labbe, S. M.; Caron, A.; Bakan, I.; Laplante, M.; Carpentier, A. C.; Lecomte, R.; Richard, D. In vivo measurement of energy substrate contribution to cold-induced brown adipose tissue thermogenesis. *FASEB J* **2015**, 29, (5), 2046-58.
35. Bargut, T. C. L.; Souza-Mello, V.; Aguila, M. B.; Mandarim-de-Lacerda, C. A. Browning of white adipose tissue: lessons from experimental models. *Horm Mol Biol Clin Investig* **2017**, 31, (1).
36. Hoffmann, J. M.; Grunberg, J. R.; Church, C.; Elias, I.; Palsdottir, V.; Jansson, J. O.; Bosch, F.; Hammarstedt, A.; Hedjazifar, S.; Smith, U. BMP4 Gene Therapy in Mature Mice Reduces BAT Activation but Protects from Obesity by Browning Subcutaneous Adipose Tissue. *Cell Rep* **2017**, 20, (5), 1038-1049.
37. Shin, H.; Ma, Y.; Chanturiya, T.; Cao, Q.; Wang, Y.; Kadegowda, A. K. G.; Jackson, R.; Rumore, D.; Xue, B.; Shi, H., et al. Lipolysis in brown adipocytes is not essential for cold-induced thermogenesis in mice. *Cell Metab* **2017**, 26, (5), 764-777.e5.
38. Kuiper, G. G.; Lemmen, J. G.; Carlsson, B.; Corton, J. C.; Safe, S. H.; van der Saag, P. T.; van der Burg, B.; Gustafsson, J. A. Interaction of estrogenic chemicals and phytoestrogens with estrogen receptor beta. *Endocrinology* **1998**, 139, (10), 4252-63.
39. Ponnusamy, S.; Tran, Q. T.; Harvey, I.; Smallwood, H. S.; Thiyagarajan, T.; Banerjee, S.; Johnson, D. L.; Dalton, J. T.; Sullivan, R. D.; Miller, D. D., et al. Pharmacologic activation of estrogen receptor beta increases mitochondrial function, energy expenditure, and brown adipose tissue. *FASEB J* **2017**, 31, (1), 266-281.
40. Miao, Y. F.; Su, W.; Dai, Y. B.; Wu, W. F.; Huang, B.; Barros, R. P.; Nguyen, H.; Maneix, L.; Guan, Y. F.; Warner, M., et al. An ERbeta agonist induces browning of subcutaneous abdominal fat pad in obese female mice. *Sci Rep* **2016**, 6, 38579.

SUPPLEMENTARY APPENDIX

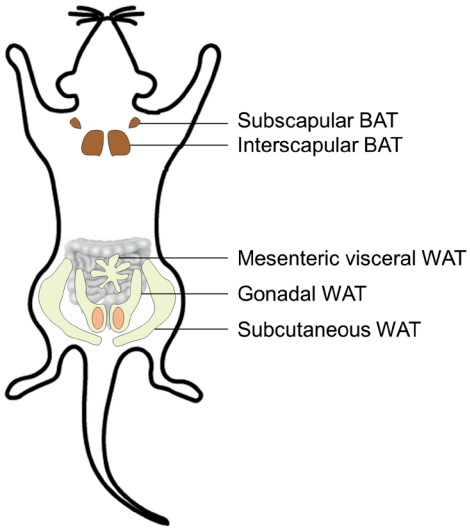

Supplementary figure 1. Schematic overview of studied fat depots. Subscapular BAT (sBAT), interscapular BAT (iBAT), mesenteric visceral WAT (vWAT), gonadal WAT (gWAT) and subcutaneous WAT (sWAT).

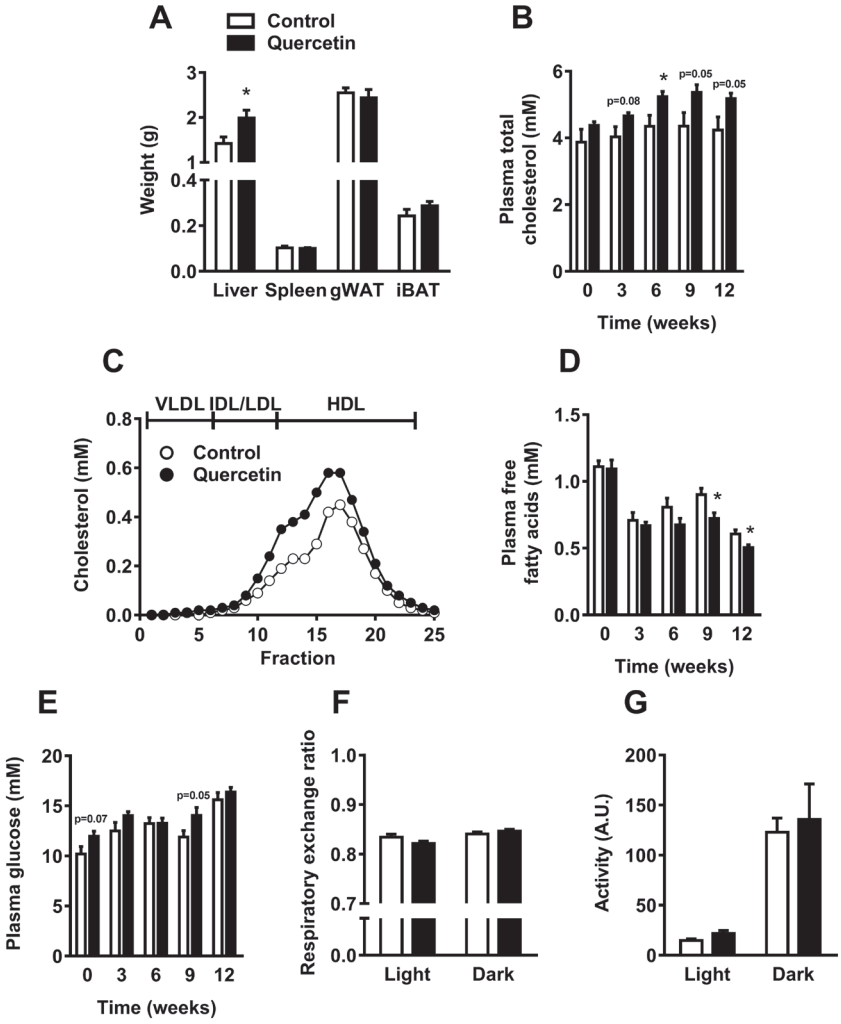

Supplementary figure 2. Quercetin increases liver weight, plasma total cholesterol and decreases plasma free fatty acids. Organ weight of liver, spleen, iBAT and gWAT (A) was determined at the end of the intervention. Plasma total cholesterol (B), free fatty acids (D) and glucose (E) were analyzed at the indicated time points. Cholesterol distribution over lipoproteins after separation from pooled plasma after 12 weeks of treatment was assessed by FPLC (C). In the third week of treatment, animals were placed in fully automatic metabolic cages and respiratory exchange ratio (F) and activity (G) were determined. Data are represented as mean ± SEM (n=8-10), *P<0.05 versus control.

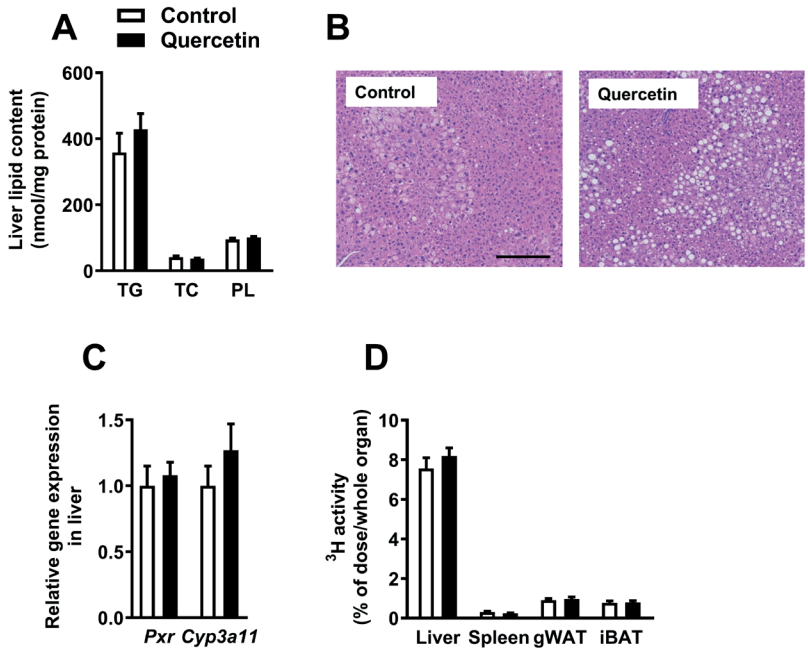

Supplementary figure 3. Quercetin does not affect liver lipids or whole liver TG-derived FA uptake. Liver was analyzed for content of triglyceride (TG), total cholesterol (TC) and phospholipid (PL) (A). Representative pictures of liver sections stained for H&E from control and quercetin treated animals (B, bar indicates 200µm). Gene expression in the liver was determined by qRT-PCR (C). After 12 weeks, mice were injected with glycerol tri[^{3}H]oleate-labeled lipoprotein-like particles and uptake was determined by ^{3}H-activity corrected for whole organ weight (D). Data are represented as mean ± SEM (n=8-10); expression of genes was corrected for the reference gene *β2-microglobulin*.

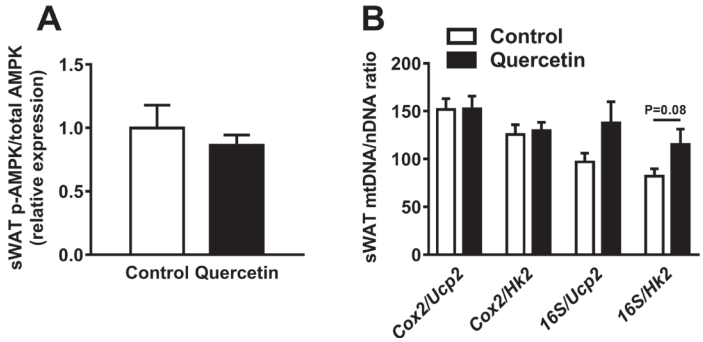

Supplementary figure 4. Quercetin does not affect the p-AMPK/total AMPK ratio and tends to increase the *16s*/*Hk2* ratio in subcutaneous white adipose tissue. Protein levels were determined by western blot in sWAT (A). Total DNA was isolated from sWAT and primers for mitochondrial and nuclear encoded genes were used to determine the mitochondrial DNA versus nuclear DNA ratio (mtDNA/nDNA, C) by PCR. Data are represented as mean ± SEM (n=8-10); protein content was corrected for the reference protein GAPDH.

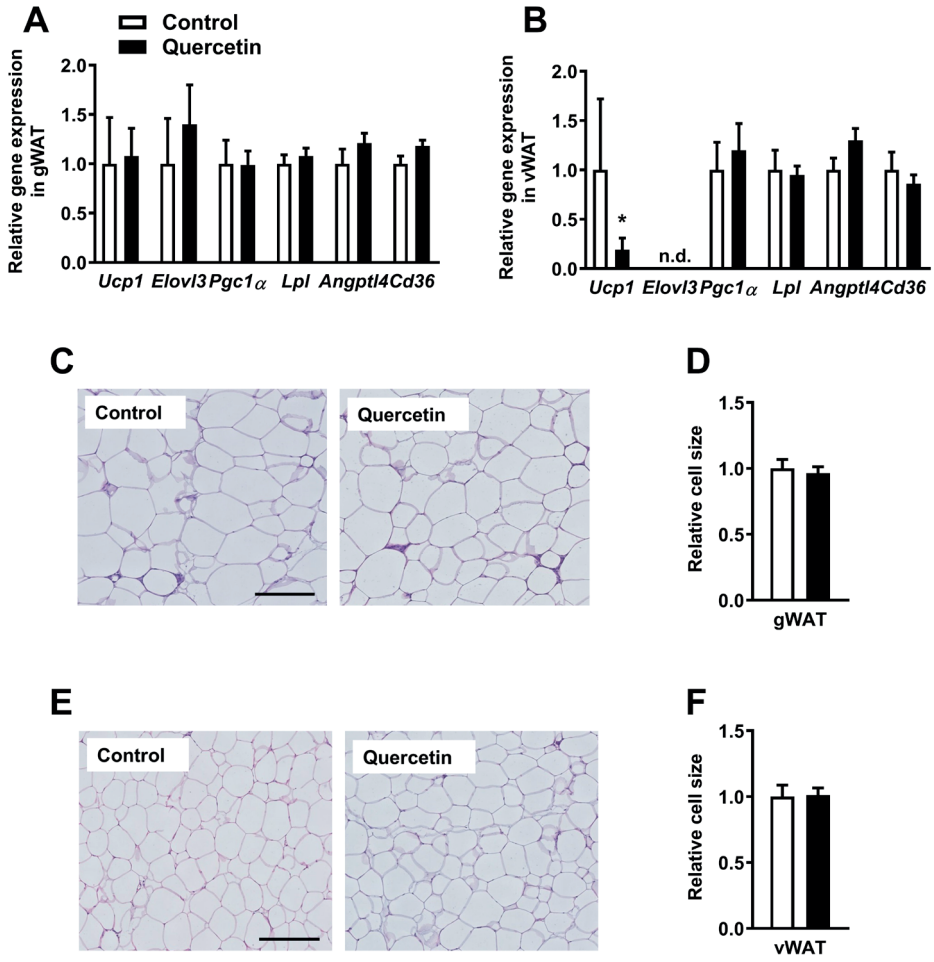

Supplementary figure 5. Quercetin does not affect browning markers in gonadal and visceral white adipose tissue. Gene expression was determined by qRT-PCR in gWAT (A) and vWAT (B). H&E staining was performed on sections of gWAT (C) and vWAT (E) from control and quercetin treated animals and representative pictures are shown and all pictures were used to determined relative cell size in gWAT (D) and vWAT (F) in ImageJ. Data are represented as mean ± SEM (n=8-10); expression of genes was corrected for the reference gene *β2-microglobulin*. ND (not detected) indicates the average CT values were >32. *p<0.05 versus control. Bars (A and E) indicate 200 μm.

8

GENERAL DISCUSSION AND FUTURE PERSPECTIVES

The current worldwide obesity epidemic demands the development of novel preventive and curative approaches that aim at reducing obesity and its related diseases including type 2 diabetes (T2D) and cardiovascular diseases (CVD). Obesity is a multifactorial disease initiated by an energy imbalance where energy intake exceeds expenditure. Energy-combusting brown adipose tissue (BAT) has been identified as an important player in energy balance, at least in rodents and likely also in humans.

In this thesis, we first describe substrate flux experiments that were conducted in a currently available murine brown adipocyte cell line. Furthermore, we generated new *in vitro* brown adipocyte models for mice and humans, with the aim to better understand energy metabolism of brown adipocytes and potential species differences. Since obesity and the subsequent development of T2D and CVD are closely linked to systemic inflammation, strategies aimed at inhibiting pro-inflammatory cytokines are extensively studied for their therapeutic effectiveness. To gain more insight in the potential role of the anti-inflammatory cytokine IL-37, we studied the effect of IL-37 on the energy balance. Next, we investigated the effect of diet-induced obesity (DIO) development on BAT function in relation to yet another important regulator of the energy balance, the endocannabinoid system (ECS). Finally, we studied the therapeutic potential of the dietary compound quercetin on triglyceride metabolism.

From this thesis, novel insights into the pathophysiology of obesity have arisen, with the emphasis on BAT and white adipose tissue (WAT), which will be discussed in this final chapter. Furthermore, therapeutic implications, translational limitations and future perspectives will be addressed.

SUBSTRATE USE BY BROWN ADIPOCYTES

Lessons from *in vitro* and *in vivo* studies

From *in vivo* studies it is known that brown adipocytes take up both glucose, free fatty acids (FA) and triglyceride-derived FA. While activated BAT primarily burns FA to produce heat, it also takes up large amounts of glucose. In fact, glucose uptake by BAT as visualized by positron emission tomography-computed tomography (PET/CT) scan is the current 'gold' standard to determine BAT activity in humans (discussed below). However, why brown adipocytes take up a substantial amount of glucose upon activation is not entirely known. Therefore, one of our objectives was to better understand brown adipocyte metabolism by studying how activated brown adipocytes handle glucose and free FA. In **Chapter 2** we studied the metabolic fluxes of glucose, FA and glutamine in differentiated T37i brown adipocytes after activation with the β3-adrenergic receptor (AR) agonist CL316,243 (**Fig. 1** of this discussion). By measuring oxygen consumption of T37i brown adipocytes in the presence of specific substrate inhibitors, we confirmed

that FA were the main substrate for oxidation, both in resting and activated conditions. Besides FA, T37i brown adipocytes simultaneously oxidize glucose and glucose is also utilized for alternative metabolic pathways such as glycerol synthesis. This indicated that although FA are the main substrate for activated brown adipocytes, glucose also has a central role in their energy metabolism. In fact, Albert *et al.* [1], showed that glucose uptake is essential for BAT thermogenesis in mice since defective glucose uptake and glycolysis through inactivation of the kinase mTOR Complex 2 in adipose tissue results in cold intolerance. Restoration of glucose uptake, by overexpression of the glycolysis enzyme hexokinase II, also restores cold tolerance. Pyruvate dehydrogenase (PDH) is a central regulator in intracellular glucose metabolism. Active PDH, as rapidly induced in brown adipocytes after β3-AR activation in **Chapter 2**, couples glycolysis in the cytosol to oxidative metabolism by forming acetyl-CoA from pyruvate which can support the tricarboxylic acid (TCA) cycle in mitochondria [2]. In addition, the generated acetyl-CoA can also be used for lipogenesis. Indeed, we found that glucose not only directly contributed to uncoupled respiration, but also ended up in the glycerol backbone of triglycerides and not in the FA. In contrast, others have reported that glucose taken up

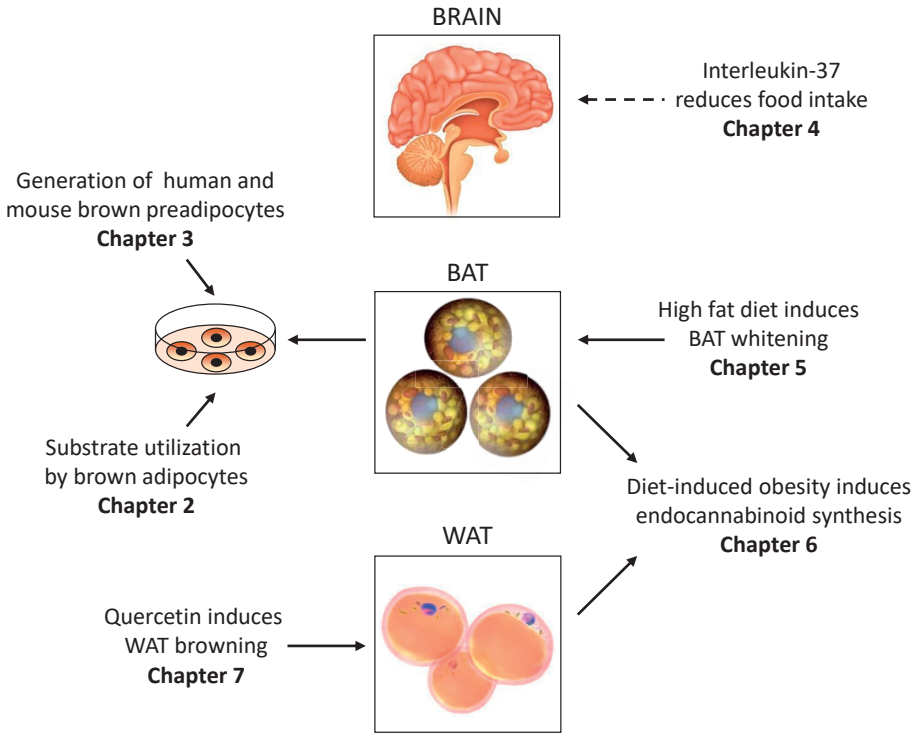

Figure 1. Dietary modulation of adipose tissue and energy balance. See text for explanation. BAT, brown adipose tissue; WAT, white adipose tissue.

by primary brown adipocytes and immortalized murine BAT cells, is primarily used to generate *de novo* FA which are used to generate triglycerides [3]. This discrepancy might be the result of differences in experimental set-up (*i.e.* brown adipocyte model, glucose concentration, intracellular lipid content). Taken together, we provided evidence that besides FA also glucose contributes to uncoupled respiration in activated T37i brown adipocytes *in vitro* and, at least in these brown adipocytes, also to glycerol synthesis for triglyceride production. To evaluate substrate use by brown adipocytes in absence of proliferation pressure and to reveal potential species differences, future studies on substrate use in our newly developed differentiated brown preadipocytes (BPAs) from murine and human origin (**Chapter 3**) are warranted.

BAT activation not only enhances glucose and FA catabolism, but also increases the expression of glycogen synthesis genes [4, 5]. Glycogen is a glucose polymer and is, besides triglycerides, another form of long-term energy storage in the body. Although glycogen is primarily found in the liver and skeletal muscle, it can thus also be found in BAT. Already 20 years ago, Farkas *et al.* [6] showed that cold exposure of rats led to an initial decrease of the glycogen content in BAT followed by glycogen accumulation in the recovery period. This compensation in glycogen storage is also observed in muscle upon exercise [7]. Increased glycogenesis after BAT activation has been proposed to provide a readily available pool of glucose to ensure avid glycolysis and acetyl-CoA turnover [4] and is therefore probably an indirect consequence of BAT activation. However, the exact role of glycogen in BAT metabolism is still elusive and would be interesting to further explore in future studies.

It should be noted that *in vivo*, the total influx of FA into BAT is highly regulated by lipoprotein lipase (LPL) [8, 9]. Functionally, LPL liberates FA from triglyceride-rich lipoproteins, which can subsequently be taken up by BAT *via* FA transporters cluster of differentiation 36 (CD36) and FA binding protein (FABP). Although brown adipocytes express LPL, *in vivo* translocation and anchoring of LPL to the luminal side of capillary endothelium by the protein glycosylphosphatidylinositol-anchored high-density lipoprotein-binding protein 1 (GPIHBP1) is required [10, 11]. By studying monocultures of brown adipocytes, LPL will be released from the cells as inactive LPL monomers. Therefore, by using monocultures of brown adipocytes the uptake of FA is likely highly underestimated, as triglyceride-derived FA uptake does not occur. To better mimic the physiological *in vivo* situation, future studies should preferably study nutrient handling using organ-on-chip models of BAT, in which *e.g.* differentiated BPAs as described in this thesis are co-cultured with endothelial cells. Such a dual cell culture system will probably also enable studying the pathophysiology of a fatty acid overload, as in DIO, on brown adipocytes in more detail. Furthermore, since LPL-activating strategies are currently being developed to lower TG and reduce cardiovascular disease risk, such 'BAT-on-chip'

models may be valuable to screen small molecules for LPL-activating properties, which can become leads for development of new drugs to combat CVD.

Assessment of BAT activity *in vivo*

Nutrient uptake by BAT is currently used as an indirect assessment of BAT activity in mice and humans. The most used technique to determine BAT activity in humans is by means of [^{18}F]fluorodeoxyglucose ([^{18}F]FDG) uptake measured by PET/CT. However, this technique has several limitations. The fact that the uptake of glucose heavily relies on proper insulin signaling, hampers its applicability in insulin resistant persons. Moreover, the primary energy source for brown adipocyte thermogenesis is FA rather than glucose (**Chapter 2** and [4]), and a major fraction of the injected [^{18}F]FDG ends up in the brain. As an alternative, the FA tracer 14(R,S)-[^{18}F]fluoro-6-thia-heptadecanoid acid (FTHA) has been used to detect BAT [12]. Although uptake by the brain is prevented, [^{18}F]FTHA binds to albumin in the blood and is largely taken up by the liver, which limits potential uptake of [^{18}F]FTHA by BAT and at the same time results in a large background signal in PET/CT scans. Moreover, our previous mouse studies have shown that BAT primarily and specifically takes up triglyceride-derived FA [13], without uptake by brain and only low uptake by liver, and we have no reason to doubt this is also the case in humans. Although the uptake of triglyceride-derived FA by BAT may also, at least partly, be dependent on insulin signaling, future studies are thus warranted to investigate the applicability of an ^{18}F-labeled FA incorporated into triglycerides that are packed inside reconstituted triglyceride-rich lipoproteins [14] to specifically determine triglyceride-derived FA uptake by BAT also in humans. Such a novel radiotracer will enable studying lipoprotein kinetics and uptake by BAT similar to our rodent studies (**Chapter 5** and **7**), without having to take biopsies of the tissues or collect tissues post mortem. Another, possibly even more appropriate method to determine overall BAT activity determines the oxidative metabolism of tissue, rather than the substrate uptake, by making use of a [^{11}C]acetate tracer for oxidative metabolism by PET/CT [15]. However, all of these PET/CT techniques make use of radioactive tracers and the resulting radioactive exposure limits repeated measurements, while multiple measurements would be needed to monitor the effect of an intervention.

Another non-invasive indirect imaging method that is being developed for assessing BAT activity is magnetic resonance imaging (MRI). A main advantage of MRI over PET/CT is that it does not involve radioactive exposure and it can therefore be repeatedly used. MRI makes use of water-fat separation to determine the fat fraction and this enables to discriminate between BAT with a low fat fraction and WAT with a higher fat fraction [16]. By determining the fat fraction before and after cold exposure, which induces intracellular lipolysis and FA combustion [17], the decrease in fat fraction might be a suitable measure for BAT activity [18]. However, replenishment of the lipid stores with nutrients from

the circulation [13] will most likely rapidly compensate for the decreased fat fraction and thereby underestimate the BAT activity when only assessing fat fraction using MRI. MRI can also be used to observe blood flow [16]. Since BAT activation increases blood flow to BAT [19], monitoring perfusion might provide additional insight into the activation state of the tissue, possibly in relation with nutrient uptake as discussed above.

Since the primary function of active BAT is to produce heat, in many rodent studies rectal or core body temperature have been registered as a more direct approach to assess BAT activity [20-22]. Transponders, that locally measure temperature within or in the vicinity of the BAT depot, have also been used in different studies [23-25]. Although higher rectal temperature, core body temperature or even the temperature near BAT in a BAT-stimulated setting compared to a control situation might suggest increased BAT activity, contribution of other organs or tissues to the increase in temperature cannot be excluded. In **Chapter 5**, we used a dual-lead telemetry transmitter to simultaneously measure interscapular BAT temperature and core body temperature, and observed that both leads measured similar temperatures. Hence, this method of assessing BAT temperature might be less specific for BAT thermogenesis and more sensitive to temperature changes caused by blood flow, providing BAT with blood of higher temperature. This may be a mouse-specific phenomenon, as in humans BAT activation does increase skin temperature in the supraclavicular area without affecting the core body temperature [26], which may be related to substantial differences in metabolic rate between humans and mice (*i.e.* heart rate is 10-fold higher in mice than humans).

Another promising and non-invasive approach to assess BAT activity is infrared thermography (IRT) which has been used in rodent [27] and human [28] studies. Cold exposing healthy lean human subjects increases supraclavicular skin temperature, as measured with IRT, which positively correlates with the uptake of [^{18}F]FDG by BAT measured by PET/CT [28]. Although IRT is a promising and non-invasive method, IRT is restricted to detecting surface temperature only. More research should be conducted to assess the applicability of IRT in measuring BAT activity in overweight and obese individuals who have more insulation as a result of subcutaneous WAT in the supraclavicular area. Another approach to measure (supraclavicular) skin temperature is by the use of iButtons [29, 30]. However, a drawback of the use of either IRT or iButtons is vasodilation following heat production by active BAT as this might interfere with IRT and iButtons measurements.

Aside from imaging techniques, many labs are searching for easily accessible circulating biomarkers for BAT activity. We showed that pre-cooling serum lysophosphatidylcholine (lysoPC)-acyl C16:0 levels correlate with BAT volume and metabolic activity assessed by [^{18}F]FDG PET/CT in healthy lean men [31]. However, we [31] as well as Lynes *et al.* [32] found no increase in lysoPC-acyl C16:0 levels in plasma in a small cohorts of healthy lean humans upon cold exposure. BAT excretes small lipid vesicles called 'exosomes' that con-

tain *e.g.* lipids, proteins, messenger RNAs and micro RNAs (miRNAs), which are used for cell-to-cell communication [33]. Interestingly, cold exposed and CL316,243 treated mice had lower miRNA miR-92a levels when compared with controls, and miR-92a showed a modest negative correlation with BAT activity in humans. This suggests that less miR-92a is released by BAT upon activation, but additional studies in larger cohorts are needed to confirm this finding. As a third example, cold exposure increases fibroblast growth factor 21 (FGF21) levels in mice [34] and men [35, 36]. A challenge is to determine whether the biomarker is exclusively expressed and secreted by active BAT. For instance, FGF21 is also expressed and secreted by the liver [37]. The recently developed technique of microdialysis [38], which enables the measurement of arterio-interstitial differences in substrates and intermediates in human BAT, will be a valuable tool to advance the search for suitable BAT biomarkers. However, a major downside of this technique is the invasive nature and the radiation exposure from PET/CT scanning which is needed for correct placement of the catheter. Finding a specific BAT activity biomarker is however relevant as it can also help to decipher the relative contribution of BAT and the muscle in thermogenesis and whether we are activating BAT maximally (discussed below). Also, biomarkers will be valuable tools to select those individuals with low BAT activity who will probably benefit most of BAT-activating strategies, and to monitor the success of BAT activation.

In conclusion, as yet there is no optimal measure for BAT activity *in vivo*. The various currently used approaches as discussed above hold several limitations. Finding a (set of) BAT specific biomarkers is of great scientific interest and the most promising avenue to pursue. In the meantime, the use of IRT and developing triglyceride-rich lipoproteins with a radiolabeled FA incorporated into a triglyceride to determine BAT activity seem promising alternatives.

MODIFIERS OF BAT FUNCTION AND CARDIOMETABOLIC HEALTH

The endocannabinoid system

Many endogenous factors have been shown to modulate energy metabolism by regulating BAT activity. For example, BAT is activated by hormones such as norepinephrine, T3, FGF21, and secretin [39, 40]. In addition, BAT activity is modulated by the endocannabinoid system (ECS), consisting of the endocannabinoids anandamide (*N*-arachidonoyl-ethanolamine, AEA) and 2-arachidonoylglycerol (2-AG), their receptors cannabinoid 1 receptor (CB1R) and cannabinoid 2 receptor (CB2R) and the enzymes that synthesize and degrade the endocannabinoids. In fact, the ECS modulates energy balance at several levels; it regulates appetite, lipogenesis in adipose tissue and energy expenditure [41, 42]. An overactive ECS has been associated with obesity and T2D [43-

45]. Interestingly, the inverse CB1R antagonist rimonabant profoundly reduced fat mass and dyslipidemia in clinical trials [46-48], although psychiatric side effects unfortunately prevented further development as a weight loss drug. Of note, previous studies from our group showed that rimonabant activates BAT in lean as well as DIO mice [49].

We now aimed to gain more insight into the derailment of the ECS towards overactivity in obesity development, as such information could be used to develop *e.g.* tissue-specific inhibitors of endocannabinoid synthesis to improve energy metabolism without adverse effects in the brain as was induced by rimonabant. Therefore, in **Chapter 6**, we fed different groups of mice a high fat diet (HFD) for a duration of 1 day up to 18 weeks as a model to study the effects of DIO development on the ECS. We found increased plasma levels of the two endocannabinoids AEA and 2-AG, within 1-2 weeks of HFD feeding. Increased circulating endocannabinoid levels in obesity have also been reported in mice [50, 51] and men [43, 44, 52] by others. However, it remained unclear which organs contribute to the increased plasma endocannabinoid levels. We found rapidly increased expression of endocannabinoid synthesis enzymes *N*-acylphosphatidylethanolamine-phospholipase D (NAPE-PLD) and diacylglycerol lipase-α/β (DAGLA/B) in WAT and BAT, suggesting that at least these two organs are involved in enhanced endocannabinoid synthesis in the development of obesity (**Fig. 1**). Since endocannabinoids are lipid derivatives [53], it is likely that the increased flux of HFD-derived fatty acids to adipocytes induces the synthesis of endocannabinoids, which are then secreted from adipocytes and accumulate in plasma. The increased production of endocannabinoids in the development of DIO is most likely the reason why systemic, but also strictly peripheral, CB1R antagonism is effective in reducing fat mass and dyslipidemia [49, 54, 55].

Besides antagonism of CB1R, an alternative promising approach to target the ECS in obesity treatment is to modulate the activity of the enzymes involved in the endocannabinoid biosynthesis and degradation. Based on results presented in **Chapter 6**, inhibiting biosynthesis enzymes NAPE-PLD and DAGLA/B in WAT and BAT might be a worthwhile strategy to pursue. The last couple of years several DAGLA/B inhibitors have been generated [56], which thus have high potential for treating metabolic disorders such as obesity and diabetes. It should however be noted that endocannabinoids have a wide range of effects. Besides their role in the regulation of the energy balance, they are also involved in regulating pain and inflammation. Actually, inhibitors of the endocannabinoid degradation enzymes fatty acid amide hydrolase (FAAH) and monoacylglycerol lipase (MAGL) are being tested for the treatment of inflammatory pain and anxiety disorders [57]. Because of the wide-range of processes in which the ECS is involved, modulating endocannabinoid synthesis and degradation to counteract the increased endocannabinoid levels as observed in obesity will thus probably require a tissue-specific approach. Based on the notion that hepatocyte-specific downregulation of gene expression can already be achieved in the clinic using asialoglycoprotein

receptor-targeted short interfering RNA [58], WAT/BAT-specific silencing of genes involved in endocannabinoid synthesis can probably be achieved in a similar way once tissue-specific targetable cell surface receptors have been identified.

BAT mitochondrial dynamics

Long-term HFD feeding of mice results in insulin resistance and whitening of BAT [23, 59]. Interestingly, in the time course of HFD feeding the largest increase in lipid content in BAT was observed already in the first week of HFD feeding after which intracellular lipid levels reached a plateau. Hence, we studied the effect of one week HFD feeding on BAT in more detail in **Chapter 5**. We found increased lipid deposition in BAT, one of the characteristics of BAT whitening, already after a single day of HFD feeding (**Fig. 1**). Mechanistically, HFD feeding immediately induced BAT insulin resistance resulting in decreased uptake of both glucose and triglyceride-derived FA by this tissue. We also observed alterations in the BAT mitochondrial morphology markers upon HFD feeding in **Chapter 5**. Mitochondria are dynamic organelles, and as a part of their mitochondrial quality control pathways, fuse and fragment based on the energy status of the cell. In fact, the name mitochondrion is inspired by their heterogeneous morphology; *mitos* means 'thread' and *chondrion* means 'granule' [60]. Fusion of mitochondria is regulated by mitofusins (MFN1 and MFN2) and optic-atrophy gene 1 (OPA1 or mitochondrial dynamin like GTPase) and fission or fragmentation of mitochondria is mediated by fission 1 protein (FIS1) and dynamin-related protein 1 (DRP1). Activation of BAT, *e.g.* by cold or G-protein coupled receptor (GPR)-120 agonism, is associated with mitochondrial fragmentation [61, 62], in which DRP1 mediated fission is required for mitochondrial uncoupling and energy expenditure [61]. Forced mitochondrial fragmentation in brown adipocytes, by knocking down MFN2, did not affect the norepinephrine-stimulated energy expenditure but did increase the ability of FFA to increase energy expenditure [61]. As such, *in vivo* knock out of MFN2 in BAT [63] and in total adipose tissue [64] led to BAT dysfunction resulting in impaired cold tolerance, while insulin sensitivity upon HFD feeding was, surprisingly, improved in both models. Boutant *et al*. [64] proposed that MFN2 is important for mediating interaction between mitochondria and lipid droplets; MFN2 deletion results in impaired FA catabolism and, as a result, in increased glucose uptake and glycolysis. In **Chapter 5**, we found indications for a more fused mitochondrial network after three days of HFD feeding, with increased levels of OPA1 and phosphorylated DRP1 that inhibits mitochondrial fission. Since fragmentation is associated with enhanced BAT function, a more fused mitochondrial network might indicate an attenuation of BAT function. Although the role of mitochondrial dynamics in BAT has only recently become topic of investigations, various studies underscore the importance of this process in BAT function [61-64]. Further studies are evidently needed to determine whether mitochondrial fragmentation can be promoted specifically in BAT, for instance

by using antisense oligonucleotides against MFN2 and OPA1 or a pharmacological approach, in order to increase BAT uncoupling potential and improve insulin sensitivity. In addition, electron microscopy imaging techniques, such as serial block face scanning electron microscopy [65], may be helpful in future studies to visualize the effects of BAT activation on the mitochondrial network morphology of BAT.

Receptor involvement in the activation of BAT

Generation of the murine and human BPA cell lines (**Chapter 3**) also enabled us to study species differences in the activation of brown adipocytes. In mice, it has become clear that the β3-AR is predominantly involved in cold-induced BAT activation [17]. BAT activation with the highly selective β3-AR agonist CL316,243 increases energy expenditure, prevents fat accumulation, improves dyslipidemia and attenuates atherosclerosis development in mice [66]. Human studies, so far, have been less conclusive. Cypess *et al.* [67] showed that a single dose of 200 mg of mirabegron, a moderately selective β3-AR agonist, led to increased [^{18}F]FDG uptake by BAT as measured by PET/CT imaging accompanied by an increased resting energy expenditure (REE). However, a dose of 50 mg mirabegron, which is the pharmacological dose to activate the β3-AR and prescribed to patients with an overactive bladder, appeared insufficient to activate BAT and increase REE [68]. In addition, the high dose of mirabegron also increased heart rate and blood pressure [67] [Nahon *et al*., submitted], which suggests cross reactivity of mirabegron with other β-ARs such as β1-AR that is expressed by the heart. Unexpectedly, upon incubation of the murine and the human BPAs generated in **Chapter 3** with either vehicle, CL316,243 or the non-specific agonist norepinephrine, only the murine cells responded to CL316,243 with enhanced intracellular lipolysis and increased oxygen consumption (OCR) compared to vehicle [Blondin, Kuipers *et al.*, unpublished]. In contrast, norepinephrine activated BPAs of both species. Since this indicates that human brown adipocytes are unresponsive to the β3-AR agonist CL316,243, it seems likely that another receptor, such as the β1-AR or the β2-AR, is involved in human BAT activation. Indeed, the human BPAs showed increased intracellular lipolysis and *UCP1* expression upon stimulation with the β2-AR agonist formoterol. Moreover, treatment of human BPAs with the β2-AR antagonist ICI118,551 almost completely abolished the effects of formoterol, norepinephrine and mirabegron. Based on these *in vitro* data, it is likely that the high dose of mirabegron required to activate human BAT acts *via* activating the β2-AR rather than the β3-AR. Although this finding warrants studying the effect of a specific β2-AR agonist on BAT activity in humans, therapeutic application may be hampered because of effects of β2-AR activation on the cardiovascular and pulmonary system.

Anti-inflammatory strategies

Obesity, T2D and CVD are associated with inflammation. Several pro-inflammatory cytokines are upregulated in obesity, including interleukin-1β (IL-1β), IL-6 and tumor necrosis factor-α (TNF-α) and have been targeted in preclinical studies to assess therapeutic applicability to combat metabolic diseases. Salsalate, by inhibiting NF-κB, inhibits transcription of many pro-inflammatory cytokines and exerts beneficial metabolic effects such as improved glucose and lipid levels and increased energy expenditure in humans [69, 70]. Furthermore, tocilizumab, a humanized monoclonal antibody against the IL-6 receptor, improved glucose metabolism as evidenced by decreased glycated hemoglobin (HbA1c) levels in a small cohort of rheumatoid arthritis patients with T2D [71]. However, IL-6 targeting is complex because IL-6 appears to be a pleiotropic cytokine that functions as a pro-inflammatory cytokine involved in obesity-associated insulin resistance as well as a myokine involved in insulin-sensitizing effects [72]. The different effects of IL-6 are mediated *via* different routes of IL-6 signaling, therefore therapeutic intervention should rather focus on specifically inhibiting the deleterious signaling route of signaling rather than merely targeting the upstream signaling such as circulating IL-6 levels [73].

In contrast to pro-inflammatory cytokines, the anti-inflammatory cytokines such as IL-10 and IL-37 are less well studied. IL-10 overexpression has beneficial effects on body weight and insulin sensitivity in mice when fed a HFD [74]. However, clinical studies on the association between IL-10 levels and clinical outcomes in terms of cardiovascular morbidity and mortality are less consistent [75, 76]. Another, potentially more interesting, anti-inflammatory cytokine is IL-13. IL-13 circulating levels are lower in T2D patients [77] and mouse studies show that IL-13 has a direct role in maintaining glucose homeostasis during obesity [78]. Transgenic overexpression of yet another anti-inflammatory cytokine, IL-37, protects mice from DIO and associated dyslipidemia, inflammation and insulin resistance [79]. To decipher underlying mechanisms, in **Chapter 4** we showed that transgenic overexpression of IL-37 reduced food intake in mice (**Fig. 1**). Based on our data, it is thus likely that a part of the described beneficial effects of IL-37 are mediated *via* induction of satiety. Interestingly, intracerebral infusion of recombinant pro-inflammatory IL-18 reduces food intake [80], and both IL-37 and IL-18 bind to the IL-18Rα. Therefore, the effects of IL-37 on food intake may well be mediated *via* IL-18Rα. It would thus be interesting to investigate the effects of centrally administered recombinant IL-37 on food intake and other metabolic parameters, and to elucidate the potential mediating role of IL-18Rα. Mediators of satiety are valuable for the clinic, especially since one of the major reasons for the low adherence to dietary interventions is drive to eat [81]. Humans naturally express IL-37, however, whether targeting IL-37 in humans to induce satiety has therapeutic potential requires further investigation.

To conclude, targeting inflammation will most likely improve cardiometabolic disorders. In fact, a landmark study recently showed that a monoclonal antibody targeting IL-1β lowered the rate of recurrent cardiovascular events independent of lipid lowering [82]. Targeting anti-inflammatory cytokines as a therapy in cardiometabolic disease requires more clinical investigation. Currently, salsalate seems to be the most promising option as it is already prescribed in the clinic, with favorable metabolic outcome.

ORGAN CROSSTALK IN THERMOGENESIS

The function of active BAT is to produce heat and is therefore part of the body's thermoregulation. There are several thermoregulatory processes involved in maintaining temperature homeostasis in mammals, such as vasodilation/constriction, sweating and (non)shivering thermogenesis. When core body temperature drops, extra heat must be generated to maintain temperature homeostasis. This heat is produced by contraction of muscles resulting in thermogenesis due to shivering, and the initiation of nonshivering thermogenesis in muscles and BAT [83]. In neonates, nonshivering thermogenesis in BAT is particularly important because they have a relatively large body surface area to lose heat and little capacity to shiver as a result of underdeveloped muscles [17].

As with every homeostatic mechanism, also body temperature regulation relies on feedback/forward loops [84]. Studies in rodents from which interscapular BAT was removed, which leads to reduced capacity for nonshivering thermogenesis [85], showed that the body compensates by increasing browning of WAT [86] and increasing thermogenesis by other BAT depots [87]. In addition, impaired bone morphogenic protein (BMP) signaling in mice, by genetic ablation of type 1A BMP receptor, results in severely impaired BAT thermogenesis, with thermogenic capacity being restored by subsequent browning of WAT [88]. Conversely, during exercise, which is a heat generating process, BAT is hypothesized to be hypoactive because there is a decreased necessity for BAT derived heat [17]. The concept that cross-talk exists between tissues involved in thermogenesis has also been demonstrated in humans. Blondin *et al.* [89] showed that reducing BAT activity during cold exposure, by preventing triglyceride hydrolysis in adipose tissue using nicotinic acid, resulted in earlier shivering and with increased intensity. In **Chapter 5**, we observed that core body temperature immediately increased upon switching mice from chow to HFD feeding, while BAT became inactivated. It is thus conceivable that induction of thermogenesis elsewhere in the body, in this case by the metabolic organs that process the excess of dietary lipids (*i.e.* intestine and liver), inactivates BAT by a negative feedforward mechanism. Thus, thermoregulation is a multifactorial process where the loss or production of heat by a certain thermogenic system is compensated for by another system.

Central in thermoregulation are the temperature sensitive receptors such as transient receptor potential (TRP) channels. Cold stimulates TRP channels of the subfamily melastatin 8 (TRPM8) present on sensory nerves in the skin [90], which signal to the hypothalamus. The TRP channels of the melastatin subtype [91], but also the TRP vanilloid (TRPV) subtype [92, 93] are present on several peripheral organs including BAT (reviewed in [94]). The TRPM8 agonist menthol induces a brown-like phenotype in white adipocytes *in vitro* [95] and menthol mixed through the diet activates BAT thermogenesis *in vivo* [91]. In contrast to TRPM channels which are activated by cold, TRPV channels are activated by heat. Activation of TRPV1 by dietary compound capsaicin most likely activates and recruits human BAT (reviewed in [96]). In addition, TRPV2 KO mice are cold intolerant, have impaired BAT thermogenesis and are prone to develop obesity when fed a HFD [92]. The fact that endocannabinoids, which have profound effects on energy metabolism as outlined above, are able to bind to TRP channels makes these receptors even more interesting for future research into BAT function specifically and systemic thermoregulation in general [97].

Thus, in the search for tools to increase energy expenditure as a potential target for therapy of adiposity and related cardiometabolic disorders, BAT activation might be even more beneficial when combined with activation of other thermogenic processes, *e.g.* in skeletal muscles to prevent potentially negative feedforward loops.

THERAPEUTIC EFFECTIVENESS OF BROWN(ING) ADIPOSE TISSUE

Many attempts are being made to activate BAT by cold exposure or pharmacologic intervention, however the therapeutic applicability of BAT activation in cardiometabolic disease in humans is still a matter of debate. Beneficial effects of cold-induced BAT activation on plasma glucose and lipid levels have been shown in animal models [8, 17, 66, 98] and in humans [99-102]. In mice, BAT activation also results in reduced body weight. Although BAT activation by means of cold acclimation in humans did reduce fat mass to a modest extent [99], cold exposure did not result in weight loss [101, 103, 104]. This can be explained by either a modest effect of BAT activation to total energy expenditure or by compensatory increased energy intake.

A main contributor to the different effects of BAT activation between mice and humans is the relative amount of BAT in the body. While mice have a relatively large BAT depot in the interscapular area resembling that of human newborns, human adults probably have much smaller relative amounts of BAT [105], although quantifying BAT volume in humans is challenging due to limitations of the imaging techniques as discussed above. In mice prolonged cold exposure or β3-AR agonism not only activates BAT but also induces browning of WAT [66] and thereby increases the total number of energy dissipat-

ing adipocytes. On the other hand, we showed that browning can contribute to lower plasma triglyceride levels in mice (**Chapter 7**). Considering the fact that metabolically compromised humans often have large amounts of WAT, and strategies to convert white adipocytes into beige adipocytes are actively searched for, inducing browning could be of high value to combat metabolic disorders in humans. As a highly interesting example of nature, extreme browning of visceral fat in patients with a catecholamine-secreting paraganglioma highly increases energy expenditure and leads to weight loss [106]. Whether such an extent of browning can be achieved in humans by cold acclimation or pharmacological intervention, is still controversial and requires further study [105].

In my opinion, activating BAT, and inducing browning of WAT *via* for instance dietary compounds, as discussed below, still holds potential to combat adiposity and related diseases. Small shifts in energy balance that are sustained over time can have major effects on health [105]. Thus, inducing a sustained negative energy balance with slightly increased energy expenditure, due to activation of BAT or browning, can certainly exert beneficial effects. Indeed, moderate (5%) weight loss in obese patients already has considerable health benefits including increased insulin sensitivity [107], probably related to a decrease in ectopic fat. Since long-term cold exposure is probably not a suitable treatment option for most metabolically compromised individuals, alternative treatment modalities such as dietary compounds or pharmacological strategies to activate BAT and induce browning of WAT are wanted. Combining BAT activation and/or browning with attempts to also counteract compensatory increases in energy intake will probably further increase beneficial effects of BAT activation and browning. However it must be noted that promoting a healthy lifestyle, rather than pharmacological approaches, should always be the first line of treatment and the cornerstone of for the prevention and treatment of obesity and related metabolic diseases.

DIETARY MODULATION

As stated above, central in the therapeutic approaches to combat obesity is lifestyle modification of which adapting a healthy diet is an important part. Several studies have focused on elucidating which dietary measures are most effective in ameliorating or preventing metabolic diseases. Comparing the effects of low-carbohydrate interventions with low-fat-diet interventions in overweight individuals (BMI 28-40) without T2D, showed that both diets induced weight loss after 12 months to a similar degree [108]. On the other hand, in T2D patients low carbohydrate diets improve glycemic control [109] and low-carbohydrate interventions are slightly better than low-fat diets [110]. Short-term consumption of a low-carbohydrate diet led to a greater decrease in HbA1c in T2D patients, than consumption of a low-fat diet [110]. However, on the long-term

this difference between diets disappeared most likely due to limited long-term adherence to the dietary inventions. Collectively, in T2D patients reduction in carbohydrate consumption may thus be favorable compared to reduction in fat consumption, but also the sort of fat or carbohydrate matters. Intake of trans fats is strongly associated with higher mortality rates whereas intake of polyunsaturated FA was associated with lower mortality rates [111]. Also refined grains and sugar as a carbohydrate source should probably be replaced by carbohydrates from whole grains, fruits or vegetables in order to decrease the risk of developing T2D and CVD [112-114]. Very recently, Willet *et al.* [115] estimated that transformation to a healthy diet, where red meat and sugars are replaced by nuts, fruits and vegetables, will avert around 11 million premature deaths per year.

Increasing consumption of fruits and vegetables will increase the ingestion of dietary fibers and a series of systematic reviews and meta-analyses convincingly show that fiber intake is dose-dependently associated with reduced incidence and mortality from T2D and CVD [114]. Dietary fibers are fermented by gut bacteria to produce short chain FA including butyrate. Oral butyrate administration prevents DIO, hyperinsulinemia and hypertriglyceridemia in mice [116]. This is attributed to reduced food intake, in addition to increased BAT activity by increased sympathetic outflow [116]. Butyrate consumption stimulates the production of glucagon-like peptide 1 (GLP-1) by intestinal L cells [117] [Li, Rensen *et al.*, unpublished], and GLP-1 signaling is likely involved in these beneficial metabolic effects. Also in T2D patients, dietary fibers increase short chain FA-producing gut microbiota and improve HbA1c levels, at least partly *via* increased GLP-1 secretion [118]. Activating the GLP-1 pathway with GLP-1 receptor agonists (*i.e.* liraglutide and exenatide) is a strategy that is already widely used for the treatment of T2D [119] and shown to reduce CVD [120]. In fact, a recent study showed that treating obese individuals with a dual GLP1 receptor and glucose-dependent insulinotropic polypeptide (GIP) receptor agonist results in massive weight loss at least similar to that observed with rimonabant [121]. However, as dietary approaches to combat metabolic disorders are preferred over pharmacological approaches, highly increasing the intake of dietary fibers may be a promising strategy to pursue in the fight against obesity and related cardiometabolic diseases.

In addition to fibers, fruits and vegetables also contain polyphenols, to which beneficial metabolic effects have been attributed [122]. The polyphenol resveratrol induces browning of WAT [123], improves lipid profiles and reduces atherosclerosis development in mice [124]. Although clinical studies on resveratrol are less consistent, trials with T2D patients show that resveratrol improves glycemic control [125]. Quercetin, a dietary compound that belongs to the polyphenol subclass of flavonoids, lowers plasma triglyceride levels in mice [126, 127] and men [128] and thereby targets one of the risk factors for developing CVD [129, 130]. In **Chapter 7** we now revealed that the quercetin-

induced lowering of plasma triglyceride levels could at least in part be due to browning of WAT (**Fig. 1**). Since we did not find a stimulatory effect of quercetin on BAT, this suggests that WAT browning is able to reduce plasma triglyceride levels by increasing the utilization of triglyceride-derived FA by this tissue. Indeed, BAT inactivation by selective inhibition of lipid droplet lipolysis induces WAT browning and lowers triglyceride levels in peripheral tissues [131]. Although not reported, this strategy likely also decreased plasma triglycerides. Future studies are needed to determine whether WAT browning is also involved in the triglyceride lowering effects of quercetin in humans. However, since the relative amounts of polyphenols like resveratrol and quercetin in fruits and vegetables are small, they should probably be administered as dietary supplements to be metabolically effective.

These data reveal that adapting a healthy diet, with a high intake of fruits and vegetables, is able to improve metabolic health, at least partly *via* increased fiber intake. However, it is unlikely that a single dietary regime will be effective for every person, *e.g.* since responses in blood glucose to an identical meal show great interindividual variability [132]. In conclusion, while lifestyle modification should be central in the treatment of metabolic disorders, with adapting a healthy diet as central intervention, the formula of this modification likely requires a personalized approach.

CONCLUDING REMARKS AND FUTURE PERSPECTIVES

Obesity and related T2D and cardiovascular diseases are multifactorial diseases that lead to high morbidity and mortality. Since current treatment options for obesity are either not effective on the long-term, invasive or reported to give adverse effects, new treatment options are needed. BAT activation is a promising tool because of its ability to combust nutrients and thereby improving lipid and glucose metabolism and increasing energy expenditure. However, in order to develop drugs aimed at activating BAT, we need to better understand the pathophysiology of DIO on BAT function and whole body metabolism.

This thesis has provided novel insights into the metabolism of brown adipocytes and the pathophysiology of DIO. Generating cell lines for mouse and human BPAs will enable us to investigate species differences. These cell lines also provide opportunities for future studies into the involvement of various receptors in BAT activation (*e.g.* TRP channels or β-ARs), and uptake of triglyceride-derived FA, especially when cocultured with endothelial cells in a BAT-on-chip setting. Moreover, we identified the endocannabinoid synthesis enzymes in adipose tissue as potential leads for therapeutic intervention. Strikingly, besides affecting the ECS, HFD feeding also rapidly affected BAT by inducing lipid accumulation, insulin resistance and alterations in mitochondrial dynamics

markers. Future studies into for instance endocannabinoid modulation, TRP channels and mitochondrial dynamics are needed determine whether these avenues are able to enhance BAT activation. However, in order to determine the effectiveness and degree of BAT activation we need to improve our methods for detecting BAT activation. Therefore, novel FA tracers incorporated in triglyceride-rich lipoprotein-like particles and non-invasive methods such as IRT and biomarkers need further study.

BAT activation will probably only be beneficial when there is no compensatory decrease in energy-consuming processes, or increase in energy intake. Based on currently available data, therapeutic modalities that target these different aspects of the energy balance, such as GLP-1 pathway activators, are of special interest and hold great therapeutic potential. Besides pharmacological therapy, also dietary modulation (*i.e.* increased ingestion of dietary fibers and possibly polyphenols derived from fruits and vegetables) has many beneficial effects on food intake, BAT activation, browning of WAT and cardiometabolic disease as a whole. The greatest challenge in life-style modulation is long-term adherence to these programs, therefore to prolong the beneficial effects of dietary modulation more research should be conducted into personalized dietary interventions and ways to sustain adherence.

REFERENCES

1. Albert, V.; Svensson, K.; Shimobayashi, M.; Colombi, M.; Munoz, S.; Jimenez, V.; Handschin, C.; Bosch, F.; Hall, M. N. mTORC2 sustains thermogenesis via Akt-induced glucose uptake and glycolysis in brown adipose tissue. *EMBO Mol Med* **2016**, 8, (3), 232-46.
2. Gray, L. R.; Tompkins, S. C.; Taylor, E. B. Regulation of pyruvate metabolism and human disease. *Cell Mol Life Sci* **2014**, 71, (14), 2577-604.
3. Irshad, Z.; Dimitri, F.; Christian, M.; Zammit, V. A. Diacylglycerol acyltransferase 2 links glucose utilization to fatty acid oxidation in the brown adipocytes. *J Lipid Res* **2017**, 58, (1), 15-30.
4. Labbe, S. M.; Caron, A.; Bakan, I.; Laplante, M.; Carpentier, A. C.; Lecomte, R.; Richard, D. In vivo measurement of energy substrate contribution to cold-induced brown adipose tissue thermogenesis. *FASEB J* **2015**, 29, (5), 2046-58.
5. Hao, Q.; Yadav, R.; Basse, A. L.; Petersen, S.; Sonne, S. B.; Rasmussen, S.; Zhu, Q.; Lu, Z.; Wang, J.; Audouze, K., et al. Transcriptome profiling of brown adipose tissue during cold exposure reveals extensive regulation of glucose metabolism. *Am J Physiol Endocrinol Metab* **2015**, 308, (5), E380-92.
6. Farkas, V.; Kelenyi, G.; Sandor, A. A dramatic accumulation of glycogen in the brown adipose tissue of rats following recovery from cold exposure. *Arch Biochem Biophys* **1999**, 365, (1), 54-61.
7. Bergstrom, J.; Hultman, E. Muscle glycogen synthesis after exercise: an enhancing factor localized to the muscle cells in man. *Nature* **1966**, 210, (5033), 309-10.
8. Bartelt, A.; Bruns, O. T.; Reimer, R.; Hohenberg, H.; Ittrich, H.; Peldschus, K.; Kaul, M. G.; Tromsdorf, U. I.; Weller, H.; Waurisch, C., et al. Brown adipose tissue activity controls triglyceride clearance. *Nat Med* **2011**, 17, (2), 200-5.
9. van den Berg, R.; Kooijman, S.; Noordam, R.; Ramkisoensing, A.; Abreu-Vieira, G.; Tambyrajah, L. L.; Dijk, W.; Ruppert, P.; Mol, I. M.; Kramar, B., et al. A Diurnal Rhythm in Brown Adipose Tissue Causes Rapid Clearance and Combustion of Plasma Lipids at Wakening. *Cell Rep* **2018**, 22, (13), 3521-3533.
10. Beigneux, A. P.; Davies, B. S.; Gin, P.; Weinstein, M. M.; Farber, E.; Qiao, X.; Peale, F.; Bunting, S.; Walzem, R. L.; Wong, J. S., et al. Glycosylphosphatidylinositol-anchored high-density lipoprotein-binding protein 1 plays a critical role in the lipolytic processing of chylomicrons. *Cell Metab* **2007**, 5, (4), 279-91.
11. Davies, B. S.; Beigneux, A. P.; Barnes, R. H., 2nd; Tu, Y.; Gin, P.; Weinstein, M. M.; Nobumori, C.; Nyren, R.; Goldberg, I.; Olivecrona, G., et al. GPIHBP1 is responsible for the entry of lipoprotein lipase into capillaries. *Cell Metab* **2010**, 12, (1), 42-52.
12. Blondin, D. P.; Labbe, S. M.; Noll, C.; Kunach, M.; Phoenix, S.; Guerin, B.; Turcotte, E. E.; Haman, F.; Richard, D.; Carpentier, A. C. Selective Impairment of Glucose but Not Fatty Acid or Oxidative Metabolism in Brown Adipose Tissue of Subjects With Type 2 Diabetes. *Diabetes* **2015**, 64, (7), 2388-97.
13. Khedoe, P. P.; Hoeke, G.; Kooijman, S.; Dijk, W.; Buijs, J. T.; Kersten, S.; Havekes, L. M.; Hiemstra, P. S.; Berbee, J. F.; Boon, M. R., et al. Brown adipose tissue takes up plasma triglycerides mostly after lipolysis. *J Lipid Res* **2015**, 56, (1), 51-9.
14. Rensen, P. C.; van Dijk, M. C.; Havenaar, E. C.; Bijsterbosch, M. K.; Kruijt, J. K.; van Berkel, T. J. Selective liver targeting of antivirals by recombinant chylomicrons--a new therapeutic approach to hepatitis B. *Nat Med* **1995**, 1, (3), 221-5.
15. Ouellet, V.; Labbe, S. M.; Blondin, D. P.; Phoenix, S.; Guerin, B.; Haman, F.; Turcotte,

E. E.; Richard, D.; Carpentier, A. C. Brown adipose tissue oxidative metabolism contributes to energy expenditure during acute cold exposure in humans. *J Clin Invest* **2012**, 122, (2), 545-52.

16. Chen, Y. C.; Cypess, A. M.; Chen, Y. C.; Palmer, M.; Kolodny, G.; Kahn, C. R.; Kwong, K. K. Measurement of human brown adipose tissue volume and activity using anatomic MR imaging and functional MR imaging. *J Nucl Med* **2013**, 54, (9), 1584-7.
17. Cannon, B.; Nedergaard, J. Brown adipose tissue: function and physiological significance. *Physiol Rev* **2004**, 84, (1), 277-359.
18. Stahl, V.; Maier, F.; Freitag, M. T.; Floca, R. O.; Berger, M. C.; Umathum, R.; Berriel Diaz, M.; Herzig, S.; Weber, M. A.; Dimitrakopoulou-Strauss, A., et al. In vivo assessment of cold stimulation effects on the fat fraction of brown adipose tissue using DIXON MRI. *J Magn Reson Imaging* **2017**, 45, (2), 369-380.
19. Orava, J.; Nuutila, P.; Lidell, M. E.; Oikonen, V.; Noponen, T.; Viljanen, T.; Scheinin, M.; Taittonen, M.; Niemi, T.; Enerback, S., et al. Different metabolic responses of human brown adipose tissue to activation by cold and insulin. *Cell Metab* **2011**, 14, (2), 272-9.
20. van Dam, A. D.; Nahon, K. J.; Kooijman, S.; van den Berg, S. M.; Kanhai, A. A.; Kikuchi, T.; Heemskerk, M. M.; van Harmelen, V.; Lombes, M.; van den Hoek, A. M., et al. Salsalate activates brown adipose tissue in mice. *Diabetes* **2015**, 64, (5), 1544-54.
21. Okla, M.; Wang, W.; Kang, I.; Pashaj, A.; Carr, T.; Chung, S. Activation of Toll-like receptor 4 (TLR4) attenuates adaptive thermogenesis via endoplasmic reticulum stress. *J Biol Chem* **2015**, 290, (44), 26476-90.
22. Heine, M.; Fischer, A. W.; Schlein, C.; Jung, C.; Straub, L. G.; Gottschling, K.; Mangels, N.; Yuan, Y.; Nilsson, S. K.; Liebscher, G., et al. Lipolysis Triggers a Systemic Insulin Response Essential for Efficient Energy Replenishment of Activated Brown Adipose Tissue in Mice. *Cell Metab* **2018**, 28, (4), 644-655.e4.
23. Shimizu, I.; Aprahamian, T.; Kikuchi, R.; Shimizu, A.; Papanicolaou, K. N.; MacLauchlan, S.; Maruyama, S.; Walsh, K. Vascular rarefaction mediates whitening of brown fat in obesity. *J Clin Invest* **2014**, 124, (5), 2099-112.
24. Mills, E. L.; Pierce, K. A.; Jedrychowski, M. P.; Garrity, R.; Winther, S.; Vidoni, S.; Yoneshiro, T.; Spinelli, J. B.; Lu, G. Z.; Kazak, L., et al. Accumulation of succinate controls activation of adipose tissue thermogenesis. *Nature* **2018**, 560, (7716), 102-106.
25. Bajzer, M.; Olivieri, M.; Haas, M. K.; Pfluger, P. T.; Magrisso, I. J.; Foster, M. T.; Tschop, M. H.; Krawczewski-Carhuatanta, K. A.; Cota, D.; Obici, S. Cannabinoid receptor 1 (CB1) antagonism enhances glucose utilisation and activates brown adipose tissue in diet-induced obese mice. *Diabetologia* **2011**, 54, (12), 3121-31.
26. Boon, M. R.; Bakker, L. E.; van der Linden, R. A.; Pereira Arias-Bouda, L.; Smit, F.; Verberne, H. J.; van Marken Lichtenbelt, W. D.; Jazet, I. M.; Rensen, P. C. Supraclavicular skin temperature as a measure of 18F-FDG uptake by BAT in human subjects. *PLoS One* **2014**, 9, (6), e98822.
27. Crane, J. D.; Mottillo, E. P.; Farncombe, T. H.; Morrison, K. M.; Steinberg, G. R. A standardized infrared imaging technique that specifically detects UCP1-mediated thermogenesis in vivo. *Mol Metab* **2014**, 3, (4), 490-4.
28. Law, J.; Morris, D. E.; Izzi-Engbeaya, C.; Salem, V.; Coello, C.; Robinson, L.; Jayasinghe, M.; Scott, R.; Gunn, R.; Rabiner, E., et al. Thermal Imaging Is a Noninvasive Alternative to PET/CT for Measurement of Brown Adipose Tissue Activity in Humans. *J Nucl Med* **2018**, 59, (3), 516-522.
29. van Marken Lichtenbelt, W. D.; Daanen, H. A.; Wouters, L.; Fronczek, R.; Raymann, R. J.; Severens, N. M.; Van Someren, E. J. Evaluation of wireless determination of skin

temperature using iButtons. *Physiol Behav* **2006**, 88, (4-5), 489-97.
30. Martinez-Tellez, B.; Sanchez-Delgado, G.; Acosta, F. M.; Alcantara, J. M. A.; Boon, M. R.; Rensen, P. C. N.; Ruiz, J. R. Differences between the most used equations in BAT-human studies to estimate parameters of skin temperature in young lean men. *Sci Rep* **2017**, 7, (1), 10530.
31. Boon, M. R.; Bakker, L. E. H.; Prehn, C.; Adamski, J.; Vosselman, M. J.; Jazet, I. M.; Arias-Bouda, L. M. P.; van Lichtenbelt, W. D. M.; van Dijk, K. W.; Rensen, P. C. N., et al. LysoPC-acyl C16:0 is associated with brown adipose tissue activity in men. *Metabolomics* **2017**, 13, (5), 48.
32. Lynes, M. D.; Shamsi, F.; Sustarsic, E. G.; Leiria, L. O.; Wang, C. H.; Su, S. C.; Huang, T. L.; Gao, F.; Narain, N. R.; Chen, E. Y., et al. Cold-Activated Lipid Dynamics in Adipose Tissue Highlights a Role for Cardiolipin in Thermogenic Metabolism. *Cell Rep* **2018**, 24, (3), 781-790.
33. Chen, Y.; Buyel, J. J.; Hanssen, M. J.; Siegel, F.; Pan, R.; Naumann, J.; Schell, M.; van der Lans, A.; Schlein, C.; Froehlich, H., et al. Exosomal microRNA miR-92a concentration in serum reflects human brown fat activity. *Nat Commun* **2016**, 7, 11420.
34. Hondares, E.; Iglesias, R.; Giralt, A.; Gonzalez, F. J.; Giralt, M.; Mampel, T.; Villarroya, F. Thermogenic activation induces FGF21 expression and release in brown adipose tissue. *J Biol Chem* **2011**, 286, (15), 12983-90.
35. Hanssen, M. J.; Broeders, E.; Samms, R. J.; Vosselman, M. J.; van der Lans, A. A.; Cheng, C. C.; Adams, A. C.; van Marken Lichtenbelt, W. D.; Schrauwen, P. Serum FGF21 levels are associated with brown adipose tissue activity in humans. *Sci Rep* **2015**, 5, 10275.
36. Lee, P.; Linderman, J. D.; Smith, S.; Brychta, R. J.; Wang, J.; Idelson, C.; Perron, R. M.; Werner, C. D.; Phan, G. Q.; Kammula, U. S., et al. Irisin and FGF21 are cold-induced endocrine activators of brown fat function in humans. *Cell Metab* **2014**, 19, (2), 302-9.
37. Badman, M. K.; Pissios, P.; Kennedy, A. R.; Koukos, G.; Flier, J. S.; Maratos-Flier, E. Hepatic fibroblast growth factor 21 is regulated by PPARalpha and is a key mediator of hepatic lipid metabolism in ketotic states. *Cell Metab* **2007**, 5, (6), 426-37.
38. Weir, G.; Ramage, L. E.; Akyol, M.; Rhodes, J. K.; Kyle, C. J.; Fletcher, A. M.; Craven, T. H.; Wakelin, S. J.; Drake, A. J.; Gregoriades, M. L., et al. Substantial Metabolic Activity of Human Brown Adipose Tissue during Warm Conditions and Cold-Induced Lipolysis of Local Triglycerides. *Cell Metab* **2018**, 27, (6), 1348-1355.e4.
39. Villarroya, F.; Vidal-Puig, A. Beyond the sympathetic tone: the new brown fat activators. *Cell Metab* **2013**, 17, (5), 638-43.
40. Li, Y.; Schnabl, K.; Gabler, S. M.; Willershauser, M.; Reber, J.; Karlas, A.; Laurila, S.; Lahesmaa, M.; M, U. D.; Bast-Habersbrunner, A., et al. Secretin-Activated Brown Fat Mediates Prandial Thermogenesis to Induce Satiation. *Cell* **2018**, 175, (6), 1561-1574. e12.
41. Cota, D. CB1 receptors: emerging evidence for central and peripheral mechanisms that regulate energy balance, metabolism, and cardiovascular health. *Diabetes Metab Res Rev* **2007**, 23, (7), 507-17.
42. Mazier, W.; Saucisse, N.; Gatta-Cherifi, B.; Cota, D. The Endocannabinoid System: Pivotal Orchestrator of Obesity and Metabolic Disease. *Trends Endocrinol Metab* **2015**, 26, (10), 524-37.
43. Engeli, S.; Bohnke, J.; Feldpausch, M.; Gorzelniak, K.; Janke, J.; Batkai, S.; Pacher, P.; Harvey-White, J.; Luft, F. C.; Sharma, A. M., et al. Activation of the peripheral endocannabinoid system in human obesity. *Diabetes* **2005**, 54, (10), 2838-43.
44. Bluher, M.; Engeli, S.; Kloting, N.; Berndt, J.; Fasshauer, M.; Batkai, S.; Pacher, P.; Schon, M. R.; Jordan, J.; Stumvoll, M. Dysregulation

of the peripheral and adipose tissue endocannabinoid system in human abdominal obesity. *Diabetes* **2006**, 55, (11), 3053-60.
45. Gruden, G.; Barutta, F.; Kunos, G.; Pacher, P. Role of the endocannabinoid system in diabetes and diabetic complications. *Br J Pharmacol* **2016**, 173, (7), 1116-27.
46. Van Gaal, L. F.; Rissanen, A. M.; Scheen, A. J.; Ziegler, O.; Rossner, S. Effects of the cannabinoid-1 receptor blocker rimonabant on weight reduction and cardiovascular risk factors in overweight patients: 1-year experience from the RIO-Europe study. *Lancet* **2005**, 365, (9468), 1389-97.
47. Despres, J. P.; Golay, A.; Sjostrom, L. Effects of rimonabant on metabolic risk factors in overweight patients with dyslipidemia. *N Engl J Med* **2005**, 353, (20), 2121-34.
48. Pi-Sunyer, F. X.; Aronne, L. J.; Heshmati, H. M.; Devin, J.; Rosenstock, J. Effect of rimonabant, a cannabinoid-1 receptor blocker, on weight and cardiometabolic risk factors in overweight or obese patients: RIO-North America: a randomized controlled trial. *JAMA* **2006**, 295, (7), 761-75.
49. Boon, M. R.; Kooijman, S.; van Dam, A. D.; Pelgrom, L. R.; Berbee, J. F.; Visseren, C. A.; van Aggele, R. C.; van den Hoek, A. M.; Sips, H. C.; Lombes, M., et al. Peripheral cannabinoid 1 receptor blockade activates brown adipose tissue and diminishes dyslipidemia and obesity. *FASEB J* **2014**, 28, (12), 5361-75.
50. D'Eon, T. M.; Pierce, K. A.; Roix, J. J.; Tyler, A.; Chen, H.; Teixeira, S. R. The role of adipocyte insulin resistance in the pathogenesis of obesity-related elevations in endocannabinoids. *Diabetes* **2008**, 57, (5), 1262-8.
51. Pati, S.; Krishna, S.; Lee, J. H.; Ross, M. K.; de La Serre, C. B.; Harn, D. A., Jr.; Wagner, J. J.; Filipov, N. M.; Cummings, B. S. Effects of high-fat diet and age on the blood lipidome and circulating endocannabinoids of female C57BL/6 mice. *Biochim Biophys Acta* **2018**, 1863, (1), 26-39.
52. Cote, M.; Matias, I.; Lemieux, I.; Petrosino, S.; Almeras, N.; Despres, J. P.; Di Marzo, V. Circulating endocannabinoid levels, abdominal adiposity and related cardiometabolic risk factors in obese men. *Int J Obes (Lond)* **2007**, 31, (4), 692-9.
53. Hillard, C. J. Circulating Endocannabinoids: From Whence Do They Come and Where are They Going? *Neuropsychopharmacology* **2018**, 43, (1), 155-172.
54. Tam, J.; Cinar, R.; Liu, J.; Godlewski, G.; Wesley, D.; Jourdan, T.; Szanda, G.; Mukhopadhyay, B.; Chedester, L.; Liow, J. S., et al. Peripheral cannabinoid-1 receptor inverse agonism reduces obesity by reversing leptin resistance. *Cell Metab* **2012**, 16, (2), 167-79.
55. Tam, J.; Vemuri, V. K.; Liu, J.; Batkai, S.; Mukhopadhyay, B.; Godlewski, G.; Osei-Hyiaman, D.; Ohnuma, S.; Ambudkar, S. V.; Pickel, J., et al. Peripheral CB1 cannabinoid receptor blockade improves cardiometabolic risk in mouse models of obesity. *J Clin Invest* **2010**, 120, (8), 2953-66.
56. Janssen, F. J.; van der Stelt, M. Inhibitors of diacylglycerol lipases in neurodegenerative and metabolic disorders. *Bioorg Med Chem Lett* **2016**, 26, (16), 3831-7.
57. Di Marzo, V. New approaches and challenges to targeting the endocannabinoid system. *Nat Rev Drug Discov* **2018**, 17, (9), 623-639.
58. Springer, A. D.; Dowdy, S. F. GalNAc-siRNA Conjugates: Leading the Way for Delivery of RNAi Therapeutics. *Nucleic Acid Ther* **2018**, 28, (3), 109-118.
59. Roberts-Toler, C.; O'Neill, B. T.; Cypess, A. M. Diet-induced obesity causes insulin resistance in mouse brown adipose tissue. *Obesity (Silver Spring)* **2015**, 23, (9), 1765-70.
60. Benda, C. Ueber dier Spermatogenese de Verbebraten und höherer Evertebraten, II. Theil: Die Histiogenese der Spermien. *Arch Anat Physiol* **1898**, 73, 393-398.

61. Wikstrom, J. D.; Mahdaviani, K.; Liesa, M.; Sereda, S. B.; Si, Y.; Las, G.; Twig, G.; Petrovic, N.; Zingaretti, C.; Graham, A., et al. Hormone-induced mitochondrial fission is utilized by brown adipocytes as an amplification pathway for energy expenditure. *EMBO J* **2014**, 33, (5), 418-36.
62. Schilperoort, M.; van Dam, A. D.; Hoeke, G.; Shabalina, I. G.; Okolo, A.; Hanyaloglu, A. C.; Dib, L. H.; Mol, I. M.; Caengprasath, N.; Chan, Y. W., et al. The GPR120 agonist TUG-891 promotes metabolic health by stimulating mitochondrial respiration in brown fat. *EMBO Mol Med* **2018**, 10, (3).
63. Mahdaviani, K.; Benador, I. Y.; Su, S.; Gharakhanian, R. A.; Stiles, L.; Trudeau, K. M.; Cardamone, M.; Enriquez-Zarralanga, V.; Ritou, E.; Aprahamian, T., et al. Mfn2 deletion in brown adipose tissue protects from insulin resistance and impairs thermogenesis. *EMBO Rep* **2017**, 18, (7), 1123-1138.
64. Boutant, M.; Kulkarni, S. S.; Joffraud, M.; Ratajczak, J.; Valera-Alberni, M.; Combe, R.; Zorzano, A.; Canto, C. Mfn2 is critical for brown adipose tissue thermogenic function. *EMBO J* **2017**, 36, (11), 1543-1558.
65. Hughes, L.; Hawes, C.; Monteith, S.; Vaughan, S. Serial block face scanning electron microscopy--the future of cell ultrastructure imaging. *Protoplasma* **2014**, 251, (2), 395-401.
66. Berbee, J. F.; Boon, M. R.; Khedoe, P. P.; Bartelt, A.; Schlein, C.; Worthmann, A.; Kooijman, S.; Hoeke, G.; Mol, I. M.; John, C., et al. Brown fat activation reduces hypercholesterolaemia and protects from atherosclerosis development. *Nat Commun* **2015**, 6, 6356.
67. Cypess, A. M.; Weiner, L. S.; Roberts-Toler, C.; Franquet Elia, E.; Kessler, S. H.; Kahn, P. A.; English, J.; Chatman, K.; Trauger, S. A.; Doria, A., et al. Activation of human brown adipose tissue by a beta3-adrenergic receptor agonist. *Cell Metab* **2015**, 21, (1), 33-8.
68. Baskin, A. S.; Linderman, J. D.; Brychta, R. J.; McGehee, S.; Anflick-Chames, E.; Cero, C.; Johnson, J. W.; O'Mara, A. E.; Fletcher, L. A.; Leitner, B. P., et al. Regulation of Human Adipose Tissue Activation, Gallbladder Size, and Bile Acid Metabolism by a beta3-Adrenergic Receptor Agonist. *Diabetes* **2018**, 67, (10), 2113-2125.
69. Goldfine, A. B.; Silver, R.; Aldhahi, W.; Cai, D.; Tatro, E.; Lee, J.; Shoelson, S. E. Use of salsalate to target inflammation in the treatment of insulin resistance and type 2 diabetes. *Clin Transl Sci* **2008**, 1, (1), 36-43.
70. Meex, R. C.; Phielix, E.; Moonen-Kornips, E.; Schrauwen, P.; Hesselink, M. K. Stimulation of human whole-body energy expenditure by salsalate is fueled by higher lipid oxidation under fasting conditions and by higher oxidative glucose disposal under insulin-stimulated conditions. *J Clin Endocrinol Metab* **2011**, 96, (5), 1415-23.
71. Ogata, A.; Morishima, A.; Hirano, T.; Hishitani, Y.; Hagihara, K.; Shima, Y.; Narazaki, M.; Tanaka, T. Improvement of HbA1c during treatment with humanised anti-interleukin 6 receptor antibody, tocilizumab. *Ann Rheum Dis* **2011**, 70, (6), 1164-5.
72. Esser, N.; Paquot, N.; Scheen, A. J. Anti-inflammatory agents to treat or prevent type 2 diabetes, metabolic syndrome and cardiovascular disease. *Expert Opin Investig Drugs* **2015**, 24, (3), 283-307.
73. Qu, D.; Liu, J.; Lau, C. W.; Huang, Y. IL-6 in diabetes and cardiovascular complications. *Br J Pharmacol* **2014**, 171, (15), 3595-603.
74. Gao, M.; Zhang, C.; Ma, Y.; Bu, L.; Yan, L.; Liu, D. Hydrodynamic delivery of mIL10 gene protects mice from high-fat diet-induced obesity and glucose intolerance. *Mol Ther* **2013**, 21, (10), 1852-61.
75. Malarstig, A.; Eriksson, P.; Hamsten, A.; Lindahl, B.; Wallentin, L.; Siegbahn, A. Raised interleukin-10 is an indicator of poor outcome and enhanced systemic inflam-

mation in patients with acute coronary syndrome. *Heart* **2008**, 94, (6), 724-9.

76. Heeschen, C.; Dimmeler, S.; Hamm, C. W.; Fichtlscherer, S.; Boersma, E.; Simoons, M. L.; Zeiher, A. M. Serum level of the antiinflammatory cytokine interleukin-10 is an important prognostic determinant in patients with acute coronary syndromes. *Circulation* **2003**, 107, (16), 2109-14.
77. Jiang, L. Q.; Franck, N.; Egan, B.; Sjogren, R. J.; Katayama, M.; Duque-Guimaraes, D.; Arner, P.; Zierath, J. R.; Krook, A. Autocrine role of interleukin-13 on skeletal muscle glucose metabolism in type 2 diabetic patients involves microRNA let-7. *Am J Physiol Endocrinol Metab* **2013**, 305, (11), E1359-66.
78. Stanya, K. J.; Jacobi, D.; Liu, S.; Bhargava, P.; Dai, L.; Gangl, M. R.; Inouye, K.; Barlow, J. L.; Ji, Y.; Mizgerd, J. P., et al. Direct control of hepatic glucose production by interleukin-13 in mice. *J Clin Invest* **2013**, 123, (1), 261-71.
79. Ballak, D. B.; van Diepen, J. A.; Moschen, A. R.; Jansen, H. J.; Hijmans, A.; Groenhof, G. J.; Leenders, F.; Bufler, P.; Boekschoten, M. V.; Muller, M., et al. IL-37 protects against obesity-induced inflammation and insulin resistance. *Nat Commun* **2014**, 5, 4711.
80. Netea, M. G.; Joosten, L. A.; Lewis, E.; Jensen, D. R.; Voshol, P. J.; Kullberg, B. J.; Tack, C. J.; van Krieken, H.; Kim, S. H.; Stalenhoef, A. F., et al. Deficiency of interleukin-18 in mice leads to hyperphagia, obesity and insulin resistance. *Nat Med* **2006**, 12, (6), 650-6.
81. Gibson, A. A.; Sainsbury, A. Strategies to Improve Adherence to Dietary Weight Loss Interventions in Research and Real-World Settings. *Behav Sci (Basel)* **2017**, 7, (3).
82. Ridker, P. M.; Everett, B. M.; Thuren, T.; MacFadyen, J. G.; Chang, W. H.; Ballantyne, C.; Fonseca, F.; Nicolau, J.; Koenig, W.; Anker, S. D., et al. Antiinflammatory Therapy with Canakinumab for Atherosclerotic Disease. *N Engl J Med* **2017**, 377, (12), 1119-1131.
83. Blondin, D. P.; Haman, F. Shivering and nonshivering thermogenesis in skeletal muscles. *Handb Clin Neurol* **2018**, 156, 153-173.
84. Romanovsky, A. A. The thermoregulation system and how it works. *Handb Clin Neurol* **2018**, 156, 3-43.
85. Heldmaier, G.; Buchberger, A. Sources of heat during nonshivering thermogenesis in Djungarian hamsters: a dominant role of brown adipose tissue during cold adaptation. *J Comp Physiol B* **1985**, 156, (2), 237-45.
86. Piao, Z.; Zhai, B.; Jiang, X.; Dong, M.; Yan, C.; Lin, J.; Jin, W. Reduced adiposity by compensatory WAT browning upon iBAT removal in mice. *Biochem Biophys Res Commun* **2018**, 501, (3), 807-813.
87. Rothwell, N. J.; Stock, M. J. Surgical removal of brown fat results in rapid and complete compensation by other depots. *Am J Physiol* **1989**, 257, (2 Pt 2), R253-8.
88. Schulz, T. J.; Huang, P.; Huang, T. L.; Xue, R.; McDougall, L. E.; Townsend, K. L.; Cypess, A. M.; Mishina, Y.; Gussoni, E.; Tseng, Y. H. Brown-fat paucity due to impaired BMP signalling induces compensatory browning of white fat. *Nature* **2013**, 495, (7441), 379-83.
89. Blondin, D. P.; Frisch, F.; Phoenix, S.; Guerin, B.; Turcotte, E. E.; Haman, F.; Richard, D.; Carpentier, A. C. Inhibition of Intracellular Triglyceride Lipolysis Suppresses Cold-Induced Brown Adipose Tissue Metabolism and Increases Shivering in Humans. *Cell Metab* **2017**, 25, (2), 438-447.
90. Bautista, D. M.; Siemens, J.; Glazer, J. M.; Tsuruda, P. R.; Basbaum, A. I.; Stucky, C. L.; Jordt, S. E.; Julius, D. The menthol receptor TRPM8 is the principal detector of environmental cold. *Nature* **2007**, 448, (7150), 204-8.
91. Ma, S.; Yu, H.; Zhao, Z.; Luo, Z.; Chen, J.; Ni, Y.; Jin, R.; Ma, L.; Wang, P.; Zhu, Z., et al. Activation of the cold-sensing TRPM8 channel triggers UCP1-dependent thermogenesis

and prevents obesity. *J Mol Cell Biol* **2012**, 4, (2), 88-96.

92. Sun, W.; Uchida, K.; Suzuki, Y.; Zhou, Y.; Kim, M.; Takayama, Y.; Takahashi, N.; Goto, T.; Wakabayashi, S.; Kawada, T., et al. Lack of TRPV2 impairs thermogenesis in mouse brown adipose tissue. *EMBO Rep* **2016**, 17, (3), 383-99.
93. Baskaran, P.; Krishnan, V.; Fettel, K.; Gao, P.; Zhu, Z.; Ren, J.; Thyagarajan, B. TRPV1 activation counters diet-induced obesity through sirtuin-1 activation and PRDM-16 deacetylation in brown adipose tissue. *Int J Obes (Lond)* **2017**, 41, (5), 739-749.
94. Gao, P.; Yan, Z.; Zhu, Z. The role of adipose TRP channels in the pathogenesis of obesity. *J Cell Physiol* **2019**.
95. Rossato, M.; Granzotto, M.; Macchi, V.; Porzionato, A.; Petrelli, L.; Calcagno, A.; Vencato, J.; De Stefani, D.; Silvestrin, V.; Rizzuto, R., et al. Human white adipocytes express the cold receptor TRPM8 which activation induces UCP1 expression, mitochondrial activation and heat production. *Mol Cell Endocrinol* **2014**, 383, (1-2), 137-46.
96. Ruiz, J. R.; Martinez-Tellez, B.; Sanchez-Delgado, G.; Osuna-Prieto, F. J.; Rensen, P. C. N.; Boon, M. R. Role of Human Brown Fat in Obesity, Metabolism and Cardiovascular Disease: Strategies to Turn Up the Heat. *Prog Cardiovasc Dis* **2018**, 61, (2), 232-245.
97. De Petrocellis, L.; Nabissi, M.; Santoni, G.; Ligresti, A. Actions and Regulation of Ionotropic Cannabinoid Receptors. *Adv Pharmacol* **2017**, 80, 249-289.
98. Stanford, K. I.; Middelbeek, R. J.; Townsend, K. L.; An, D.; Nygaard, E. B.; Hitchcox, K. M.; Markan, K. R.; Nakano, K.; Hirshman, M. F.; Tseng, Y. H., et al. Brown adipose tissue regulates glucose homeostasis and insulin sensitivity. *J Clin Invest* **2013**, 123, (1), 215-23.
99. Yoneshiro, T.; Aita, S.; Matsushita, M.; Kayahara, T.; Kameya, T.; Kawai, Y.; Iwanaga, T.; Saito, M. Recruited brown adipose tissue as an antiobesity agent in humans. *J Clin Invest* **2013**, 123, (8), 3404-8.
100. Iwen, K. A.; Backhaus, J.; Cassens, M.; Waltl, M.; Hedesan, O. C.; Merkel, M.; Heeren, J.; Sina, C.; Rademacher, L.; Windjager, A., et al. Cold-Induced Brown Adipose Tissue Activity Alters Plasma Fatty Acids and Improves Glucose Metabolism in Men. *J Clin Endocrinol Metab* **2017**, 102, (11), 4226-4234.
101. Hanssen, M. J.; Hoeks, J.; Brans, B.; van der Lans, A. A.; Schaart, G.; van den Driessche, J. J.; Jorgensen, J. A.; Boekschoten, M. V.; Hesselink, M. K.; Havekes, B., et al. Short-term cold acclimation improves insulin sensitivity in patients with type 2 diabetes mellitus. *Nat Med* **2015**, 21, (8), 863-5.
102. Chondronikola, M.; Volpi, E.; Borsheim, E.; Porter, C.; Annamalai, P.; Enerback, S.; Lidell, M. E.; Saraf, M. K.; Labbe, S. M.; Hurren, N. M., et al. Brown adipose tissue improves whole-body glucose homeostasis and insulin sensitivity in humans. *Diabetes* **2014**, 63, (12), 4089-99.
103. Hanssen, M. J.; van der Lans, A. A.; Brans, B.; Hoeks, J.; Jardon, K. M.; Schaart, G.; Mottaghy, F. M.; Schrauwen, P.; van Marken Lichtenbelt, W. D. Short-term Cold Acclimation Recruits Brown Adipose Tissue in Obese Humans. *Diabetes* **2016**, 65, (5), 1179-89.
104. Lee, P.; Smith, S.; Linderman, J.; Courville, A. B.; Brychta, R. J.; Dieckmann, W.; Werner, C. D.; Chen, K. Y.; Celi, F. S. Temperature-acclimated brown adipose tissue modulates insulin sensitivity in humans. *Diabetes* **2014**, 63, (11), 3686-98.
105. Carpentier, A. C.; Blondin, D. P.; Virtanen, K. A.; Richard, D.; Haman, F.; Turcotte, E. E. Brown Adipose Tissue Energy Metabolism in Humans. *Front Endocrinol (Lausanne)* **2018**, 9, 447.
106. Sondergaard, E.; Gormsen, L. C.; Christensen, M. H.; Pedersen, S. B.; Christiansen, P.; Nielsen, S.; Poulsen, P. L.; Jessen, N. Chronic adrenergic stimulation induces

brown adipose tissue differentiation in visceral adipose tissue. *Diabet Med* **2015**, 32, (2), e4-8.

107. Magkos, F.; Fraterrigo, G.; Yoshino, J.; Luecking, C.; Kirbach, K.; Kelly, S. C.; de Las Fuentes, L.; He, S.; Okunade, A. L.; Patterson, B. W., et al. Effects of Moderate and Subsequent Progressive Weight Loss on Metabolic Function and Adipose Tissue Biology in Humans with Obesity. *Cell Metab* **2016**, 23, (4), 591-601.
108. Gardner, C. D.; Trepanowski, J. F.; Del Gobbo, L. C.; Hauser, M. E.; Rigdon, J.; Ioannidis, J. P. A.; Desai, M.; King, A. C. Effect of Low-Fat vs Low-Carbohydrate Diet on 12-Month Weight Loss in Overweight Adults and the Association With Genotype Pattern or Insulin Secretion: The DIETFITS Randomized Clinical Trial. *JAMA* **2018**, 319, (7), 667-679.
109. Snorgaard, O.; Poulsen, G. M.; Andersen, H. K.; Astrup, A. Systematic review and meta-analysis of dietary carbohydrate restriction in patients with type 2 diabetes. *BMJ Open Diabetes Res Care* **2017**, 5, (1), e000354.
110. van Zuuren, E. J.; Fedorowicz, Z.; Kuijpers, T.; Pijl, H. Effects of low-carbohydrate-compared with low-fat-diet interventions on metabolic control in people with type 2 diabetes: a systematic review including GRADE assessments. *Am J Clin Nutr* **2018**, 108, (2), 300-331.
111. Ludwig, D. S.; Willett, W. C.; Volek, J. S.; Neuhouser, M. L. Dietary fat: From foe to friend? *Science* **2018**, 362, (6416), 764-770.
112. Hu, F. B. Are refined carbohydrates worse than saturated fat? *Am J Clin Nutr* **2010**, 91, (6), 1541-2.
113. Mozaffarian, D.; Hao, T.; Rimm, E. B.; Willett, W. C.; Hu, F. B. Changes in diet and lifestyle and long-term weight gain in women and men. *N Engl J Med* **2011**, 364, (25), 2392-404.
114. Reynolds, A.; Mann, J.; Cummings, J.; Winter, N.; Mete, E.; Te Morenga, L. Carbohydrate quality and human health: a series of systematic reviews and meta-analyses. *Lancet* **2019**, 393, (10170), 434-445.
115. Willett, W.; Rockstrom, J.; Loken, B.; Springmann, M.; Lang, T.; Vermeulen, S.; Garnett, T.; Tilman, D.; DeClerck, F.; Wood, A., et al. Food in the Anthropocene: the EAT-Lancet Commission on healthy diets from sustainable food systems. *Lancet* **2019**, 393, (10170), 447-492.
116. Li, Z.; Yi, C. X.; Katiraei, S.; Kooijman, S.; Zhou, E.; Chung, C. K.; Gao, Y.; van den Heuvel, J. K.; Meijer, O. C.; Berbee, J. F. P., et al. Butyrate reduces appetite and activates brown adipose tissue via the gut-brain neural circuit. *Gut* **2018**, 67, (7), 1269-1279.
117. Tolhurst, G.; Heffron, H.; Lam, Y. S.; Parker, H. E.; Habib, A. M.; Diakogiannaki, E.; Cameron, J.; Grosse, J.; Reimann, F.; Gribble, F. M. Short-chain fatty acids stimulate glucagon-like peptide-1 secretion via the G-protein-coupled receptor FFAR2. *Diabetes* **2012**, 61, (2), 364-71.
118. Zhao, L.; Zhang, F.; Ding, X.; Wu, G.; Lam, Y. Y.; Wang, X.; Fu, H.; Xue, X.; Lu, C.; Ma, J., et al. Gut bacteria selectively promoted by dietary fibers alleviate type 2 diabetes. *Science* **2018**, 359, (6380), 1151-1156.
119. Ahren, B.; Schmitz, O. GLP-1 receptor agonists and DPP-4 inhibitors in the treatment of type 2 diabetes. *Horm Metab Res* **2004**, 36, (11-12), 867-76.
120. Zelniker, T. A.; Wiviott, S. D.; Raz, I.; Im, K.; Goodrich, E. L.; Furtado, R. H. M.; Bonaca, M. P.; Mosenzon, O.; Kato, E. T.; Cahn, A., et al. Comparison of the Effects of Glucagon-Like Peptide Receptor Agonists and Sodium-Glucose Co-Transporter 2 Inhibitors for Prevention of Major Adverse Cardiovascular and Renal Outcomes in Type 2 Diabetes Mellitus: A Systematic Review and Meta-Analysis of Cardiovascular Outcomes Trials. *Circulation* **2019**.
121. Frias, J. P.; Nauck, M. A.; Van, J.; Kutner, M. E.; Cui, X.; Benson, C.; Urva, S.; Gimeno, R. E.; Milicevic, Z.; Robins, D., et al. Efficacy and safety of LY3298176, a novel dual GIP

and GLP-1 receptor agonist, in patients with type 2 diabetes: a randomised, placebo-controlled and active comparator-controlled phase 2 trial. *Lancet* **2018**, 392, (10160), 2180-2193.

122. Mele, L.; Bidault, G.; Mena, P.; Crozier, A.; Brighenti, F.; Vidal-Puig, A.; Del Rio, D. Dietary (Poly)phenols, Brown Adipose Tissue Activation, and Energy Expenditure: A Narrative Review. *Adv Nutr* **2017**, 8, (5), 694-704.
123. Wang, S.; Liang, X.; Yang, Q.; Fu, X.; Rogers, C. J.; Zhu, M.; Rodgers, B. D.; Jiang, Q.; Dodson, M. V.; Du, M. Resveratrol induces brown-like adipocyte formation in white fat through activation of AMP-activated protein kinase (AMPK) alpha1. *Int J Obes (Lond)* **2015**, 39, (6), 967-76.
124. Berbee, J. F.; Wong, M. C.; Wang, Y.; van der Hoorn, J. W.; Khedoe, P. P.; van Klinken, J. B.; Mol, I. M.; Hiemstra, P. S.; Tsikas, D.; Romijn, J. A., et al. Resveratrol protects against atherosclerosis, but does not add to the antiatherogenic effect of atorvastatin, in APOE*3-Leiden.CETP mice. *J Nutr Biochem* **2013**, 24, (8), 1423-30.
125. de Ligt, M.; Timmers, S.; Schrauwen, P. Resveratrol and obesity: Can resveratrol relieve metabolic disturbances? *Biochim Biophys Acta* **2015**, 1852, (6), 1137-44.
126. Kobori, M.; Masumoto, S.; Akimoto, Y.; Oike, H. Chronic dietary intake of quercetin alleviates hepatic fat accumulation associated with consumption of a Western-style diet in C57/BL6J mice. *Mol Nutr Food Res* **2011**, 55, (4), 530-40.
127. Hoek-van den Hil, E. F.; Keijer, J.; Bunschoten, A.; Vervoort, J. J.; Stankova, B.; Bekkenkamp, M.; Herreman, L.; Venema, D.; Hollman, P. C.; Tvrzicka, E., et al. Quercetin induces hepatic lipid omega-oxidation and lowers serum lipid levels in mice. *PLoS One* **2013**, 8, (1), e51588.
128. Sahebkar, A. Effects of quercetin supplementation on lipid profile: A systematic review and meta-analysis of randomized controlled trials. *Crit Rev Food Sci Nutr* **2017**, 57, (4), 666-676.
129. Nordestgaard, B. G.; Benn, M.; Schnohr, P.; Tybjaerg-Hansen, A. Nonfasting triglycerides and risk of myocardial infarction, ischemic heart disease, and death in men and women. *JAMA* **2007**, 298, (3), 299-308.
130. Sarwar, N.; Danesh, J.; Eiriksdottir, G.; Sigurdsson, G.; Wareham, N.; Bingham, S.; Boekholdt, S. M.; Khaw, K. T.; Gudnason, V. Triglycerides and the risk of coronary heart disease: 10,158 incident cases among 262,525 participants in 29 Western prospective studies. *Circulation* **2007**, 115, (4), 450-8.
131. Shin, H.; Ma, Y.; Chanturiya, T.; Cao, Q.; Wang, Y.; Kadegowda, A. K. G.; Jackson, R.; Rumore, D.; Xue, B.; Shi, H., et al. Lipolysis in brown adipocytes is not essential for cold-induced thermogenesis in mice. *Cell Metab* **2017**, 26, (5), 764-777.e5.
132. Zeevi, D.; Korem, T.; Zmora, N.; Israeli, D.; Rothschild, D.; Weinberger, A.; Ben-Yacov, O.; Lador, D.; Avnit-Sagi, T.; Lotan-Pompan, M., et al. Personalized Nutrition by Prediction of Glycemic Responses. *Cell* **2015**, 163, (5), 1079-1094.

9

ADDENDUM

SUMMARY

The 24-hour society we are currently living in with food readily available, together with the fact that we have adapted a more sedentary lifestyle, has led to a dramatic increase in the number of people suffering from obesity. Obesity is a multifactorial disease and has a great impact on society as it contributes to the development of type 2 diabetes (T2D) and cardiovascular diseases (CVD). Current treatment options for obesity, mainly aimed at reducing caloric intake, have proven largely unsuccessful. In the previous decennium, it was discovered that adult humans have functional brown adipose tissue (BAT), which is able to contribute substantially to energy expenditure by combusting glucose and fatty acids upon activation, resulting in dissipation of energy stored in those macronutrients as heat. Since then, increasing energy expenditure *via* activation of BAT is seen as a novel strategy to combat adiposity and its related disorders. In order to develop novel compounds or methods to activate BAT especially in obese humans, a better understanding of the pathophysiology of diet-induced obesity on BAT function and whole body metabolism is required. The research described in this thesis was performed 1) to generate *in vitro* brown adipocyte models for mice and humans to study and better understand nutrient handling by brown adipocytes in relation to their role in energy metabolism, 2) to gain more insight into the effect of the anti-inflammatory cytokine IL-37 on energy balance, 3) to study the effect of diet-induced obesity on BAT function and the endocannabinoid system (ECS), and 4) to study the therapeutic potential of the dietary compound quercetin on triglyceride metabolism. **Chapter 1** gives a broad introduction to the pathophysiology of obesity, the role of the different types of adipose tissue and other organs in the etiology of obesity, and the current treatment options for obesity.

Activated BAT increases the clearance of lipids and glucose from the circulation, but how BAT accommodates the large influx of multiple substrates was not well defined. The aim of **Chapter 2** was to assess the metabolic fluxes in brown adipocytes during β3-adrenergic receptor (β3-AR) activation. T37i murine preadipocytes were differentiated into brown adipocytes and Seahorse respirometry employing a set of specific substrate inhibitors was used in the presence or absence of the β3-AR agonist CL316,243. The main substrate used by these brown adipocytes were fatty acids, which were oxidized equally during activation as well as during resting condition. [U-^{13}C]-glucose tracer-based metabolomics revealed that the flux of glucose through the tricarboxylic acid cycle (TCA) cycle was enhanced upon β3-AR activation, and regulated by pyruvate dehydrogenase (PDH) activity. Based on assessment of incorporation of [U-^{13}C]-glucose-derived radioactivity into lipids, it appeared that some internalized glucose was utilized for glycerol-3-phosphate synthesis to replenish the triglyceride pool while most glucose was oxidized *via* TCA cycle activity. From these data we concluded that while brown

adipocytes mainly use fatty acids as substrate for oxidation, glucose is also oxidized to meet the increased energy demand during short term β3-AR activation and that PDH plays an important role in directing glucose carbons towards oxidation.

Cellular and molecular investigation of BAT in humans is hampered by the limited availability of cell material and the heterogeneity of BAT between and within individuals. In **Chapter 3**, monoclonal lines of conditionally immortalized brown preadipocytes (iBPAs) of both mouse and human origin were generated. Conditional immortalization was achieved by doxycycline-controlled expression of simian virus 40 large T antigen with a Tet-On system. In the presence of doxycycline, both the murine and human cell lines showed long-term proliferation capacity with a cell doubling time of approximately 24 h. Shutdown of large T expression by removal of doxycycline and concomitant exposure to an adipogenic differentiation cocktail, resulted in the acquirement of mature brown adipocyte properties in cells of both species. This was evidenced by the accumulation of multilocular lipid droplets, the upregulation of brown adipocyte markers including uncoupling protein 1 and the induction of lipolysis and oxygen consumption following adrenergic stimulation. Notably, shutdown of large T expression prior to the onset of differentiation appeared to be only critical to induce adipogenesis in the human iBPAs, while their murine counterparts showed adipogenesis upon exposure to the adipogenic differential cocktail regardless of large T expression. We suggest that conditionally iBPAs represent an easy-to-use model for fundamental and applied research into (modulation of) energy metabolism by BAT.

Inflammation plays an important role in the development of obesity-induced insulin resistance. Research has primarily focused on the role of pro-inflammatory cytokines in this pathology and only recently was attention drawn to the anti-inflammatory cytokine IL-37. Transgenic expression of IL-37 in mice protects them from diet-induced obesity and associated metabolic complications including dyslipidemia, inflammation and insulin resistance. The precise mechanism leading to these beneficial metabolic effects was not entirely known. Therefore, in **Chapter 4**, we aimed to assess in detail the effect of transgenic IL-37 expression in mice on energy balance, including food intake and energy expenditure. Feeding homozygous IL-37 transgenic mice and wild-type (WT) control mice a high-fat diet (HFD) for 6 weeks showed that transgenic IL-37 expression reduced body weight related to a marked decrease in food intake. Subsequent mechanistic studies in mice with heterozygous IL-37 expression versus WT littermates, fed the HFD for 18 weeks, confirmed that IL-37 reduces food intake, which led to a decrease in lean body mass, but did not reduce fat mass and plasma lipid levels or alterations in energy expenditure independent of lean body mass. This suggests that IL-37 reduces lean body mass by reducing food intake.

Next, we studied the pathophysiology of diet-induced obesity on BAT and the ECS. Long-term HFD feeding results in so-called 'whitening' of BAT characterized by increased

lipid deposition, mitochondrial dysfunction and reduced fat oxidation. The aim of **Chapter 5** was to unravel the rate and related mechanisms by which HFD induces BAT whitening and insulin resistance. Mice were fed a HFD for 0, 1, 3 or 7 days. Within one day of HFD feeding BAT weight and lipid content were already increased. HFD also immediately reduced insulin-stimulated glucose uptake by BAT, indicating rapid induction of insulin resistance. This was accompanied by reduced uptake of triglyceride-derived fatty acids by BAT after 1 day of HFD. Mitochondrial mass and *Ucp1* expression were unaltered, while after 3 days of HFD markers of mitochondrial dynamics suggested induction of a more fused mitochondrial network. After 3 days of HFD, macrophage markers also increased in BAT. Counterintuitively, the switch to HFD was accompanied by an acute rise in core body temperature. Thus, a single day of HFD feeding is sufficient to induce the first signs of whitening and insulin resistance in BAT, which reduces the uptake of glucose and triglyceride-derived fatty acids. BAT whitening and insulin resistance is likely sustained by reduced mitochondrial oxidation due to changes in mitochondrial dynamics and macrophage infiltration, respectively. Likely, the switch to HFD swiftly induces thermogenesis in other metabolic organs, which allows attenuation of BAT thermogenesis.

The ECS is seen as a potential therapeutic target to combat cardiometabolic diseases because it controls the energy balance by regulating both energy intake and energy expenditure. Moreover, an increased tone of the ECS is associated with obesity. In order to develop novel therapeutics, more insight is needed in how fast and in which organs the dysregulation of the ECS in obesity development sets off. Therefore, the aims of **Chapter 6** were to elucidate the rate of dysregulation of the ECS, and the metabolic organs involved, in diet-induced obesity. Eight groups of mice were randomized to receive a chow diet (control) or a HFD ranging from 1 day up to 18 weeks. Plasma levels of the endocannabinoids 2-arachidonoylglycerol (2-AG) and anandamide (*N*-arachidonoylethanolamine, AEA), and related *N*-acylethanolamines, were quantified and gene expression of components of the ECS was determined in liver, muscle, white adipose tissue (WAT) and BAT during the course of diet-induced obesity development. HFD feeding gradually increased plasma 2-AG, accompanied by upregulated expression of its synthesizing enzymes *Dagla* and *Daglb* in WAT and BAT. HFD feeding also rapidly increased plasma AEA, accompanied by increased expression of its synthesizing enzyme *Nape-pld*, specifically in BAT. Interestingly, *Nape-pld* expression in BAT correlated with plasma AEA levels. Based on these data we concluded that HFD feeding rapidly activates adipose tissue depots to increase the synthesis pathways of endocannabinoids that may aggravate the development of HFD-induced obesity. Future research is required to determine whether inhibiting endocannabinoid signaling specifically in adipose tissue is a worthwhile strategy to pursue in combating obesity and related diseases.

Quercetin is a natural flavonoid which lowers plasma triglycerides in human intervention studies, and its intake is associated with lower CVD risk. The aim of **Chapter 7** was to elucidate the mechanism by which quercetin lowers plasma triglyceride levels in diet-induced obesity. Mice received a HFD with or without quercetin (0.1% w/w) for 12 weeks. Quercetin decreased plasma triglyceride levels from nine weeks onwards, without affecting food intake, body composition, or energy expenditure. Mechanistically, quercetin did not reduce intestinal fatty acid absorption. Rather, quercetin induced a slight reduction in liver *Apob* expression, which suggests decreased very-low density lipoprotein-triglyceride production. Interestingly, quercetin also markedly increased the uptake of triglyceride-derived fatty acids by subcutaneous white adipose tissue (sWAT). Furthermore, quercetin markedly increased mRNA expression of *Ucp1* and *Elovl3*, specifically in sWAT. Accordingly, only quercetin-treated animals showed UCP-1 protein-positive cells in sWAT, which is fully compatible with increased browning. Taken together, the triglyceride-lowering effect of quercetin may, at least in part, be due to increased triglyceride-derived fatty acid uptake by sWAT as a consequence of browning.

To conclude, in **Chapter 8** the results of this thesis were evaluated within context of current literature, and novel insights into the pathophysiology of obesity and T2D were discussed, as well as therapeutic implications and translational challenges. Collectively the studies described in this thesis have increased our insight into brown adipocyte metabolism, the mechanism underlying the beneficial metabolic effects of the anti-inflammatory cytokine IL-37, the pathophysiology of diet-induced obesity and the mechanism underlying the triglyceride-lowering effect of quercetin.

SAMENVATTING

Tegenwoordig leven we in een 24-uurs samenleving, waarin voedsel gemakkelijk en op zijn zachtst gezegd in overvloed beschikbaar is. Samen met het feit dat we een meer zittende levensstijl hebben ontwikkeld waarin we minder bewegen, heeft deze leefomgeving ertoe geleid dat het aantal mensen met obesitas dramatisch is toegenomen. Obesitas is een complexe ziekte en heeft grote impact op onze samenleving, omdat het bijdraagt aan de ontwikkeling van suikerziekte, ook wel diabetes type 2 genoemd, en hart- en vaatziekten. Huidige behandelmethoden voor obesitas zijn voornamelijk gericht op calorische beperking, en zijn op de langer termijn vaak niet effectief. Daarom is onderzoek nodig naar de ontstaansmechanismen van obesitas, om op basis van die kennis nieuwe behandelstrategieën te ontwikkelen en het risico het ontwikkelen van suikerziekte en hart- en vaatziekten te verminderen.

Obesitas ontstaat door een zogenaamde 'positieve energiebalans', waarbij de inname van energie (in de vorm van voedsel) gedurende langere tijd hoger is dan de energie die verbruikt wordt (door bijvoorbeeld beweging). De organen in ons lichaam gebruiken voornamelijk suikers en vetten als energiebron. In het geval van een positieve energiebalans, zullen de overtollige suikers en vetten vanuit het bloed worden opgenomen en opgeslagen in vetweefsel. Er zijn twee typen vetweefsel: wit en bruin vet. De voornaamste functie van wit vet is die opslag van overtollige vetten in de vorm van triglyceriden. Bruin vet daarentegen verbrandt juist suikers en vetten om warmte te produceren en verhoogt daarmee het energieverbruik. In eerste instantie werd aangenomen dat alleen pasgeboren baby's bruin vet hebben, om hun lichaamstemperatuur op peil te houden. Maar iets meer dan tien jaar geleden is ontdekt dat volwassen mensen ook actief bruin vet hebben. Terwijl wit vet vooral in de buik en rond de heupen zit, bevindt bruin vet zich in baby's vooral tussen de schouderbladen en in volwassenen in het gebied boven de sleutelbeenderen en rond de grote lichaamsslagader (de 'aorta'). Sindsdien wordt het verhogen van het energieverbruik door activatie van bruin vet gezien als een nieuwe methode om vetstapeling en de daaraan gerelateerde ziektes aan te pakken. Om nieuwe methoden die bruin vet activeren te kunnen ontwikkelen, is meer inzicht nodig in het effect van obesitas op de functie van bruin vet en op de stofwisseling van het gehele lichaam.

Hoofdstuk 1 geeft een uitgebreide introductie over de verschillende organen en processen die betrokken zijn bij de ontwikkeling van obesitas. Het onderzoek in dit proefschrift werd uitgevoerd om 1) bruin vetcellijnen van muizen en mensen te genereren, die gebruikt kunnen worden voor het bestuderen van het energiemetabolisme van die cellen, 2) meer inzicht te krijgen in het effect van het ontstekingsremmende cytokine interleukine-37 (IL-37) op de energiebalans, 3) het effect van obesitas, dat is ontstaan door teveel vetrijk voedsel te eten, op de functie van bruin vet en het endocannabinoï-

densysteem te onderzoeken, en (4) het onderliggende mechanisme te onderzoeken van het triglyceridenverlagende effect van quercetine dat van nature voorkomt in groenten en fruit.

Zoals eerder aangegeven neemt geactiveerd bruin vet grote hoeveelheden vetten en suikers op uit het bloed, maar wat er vervolgens met deze verschillende macronutriënten gebeurt na opname door bruine vetcellen was nog niet geheel bekend. Daarom hebben we in **Hoofdstuk 2** onderzocht wat er gebeurt met de verschillende macronutriënten in bruine vetcellen na stimulatie door een activator van de β3-adrenerge receptor. Hiertoe zijn T37i cellen, voorlopercellen van bruin vet afkomstig uit muizen, gekweekt en gedifferentieerd tot bruine vetcellen. Met deze gedifferentieerde bruine vetcellen zijn in de aan- en afwezigheid van de β3-adrenerge receptoractivator CL316,243, metingen uitgevoerd aan het zuurstofverbruik als uitleesmaat voor de energiestofwisseling. Hierbij werd gebruik gemaakt van specifieke remmers van de verschillende macronutriënten. We ontdekten dat de bruine vetcellen voornamelijk vetzuren verbranden, zowel in rust als na stimulatie. Door gebruik te maken van radioactief suiker ('glucose') ontdekten we dat gestimuleerde bruine vetcellen glucose gedeeltelijk gebruiken voor het maken van triglyceriden. Glucose bleek echter voornamelijk verbrand te worden via de citroenzuurcyclus waarbij het enzym pyruvaatdehydrogenase een belangrijke rol speelt.

Onderzoek naar bruin vet in mensen vordert gestaag maar relatief langzaam, enerzijds omdat het niet eenvoudig is de activiteit van bruin vet te bepalen en anderzijds doordat zeer weinig bruin vet voor onderzoek beschikbaar is. Daarnaast zijn er veel verschillen in bruin vet tussen verschillende mensen, maar ook binnen een persoon kan het bruin vet tussen de diverse locaties verschillen. Om onderzoek naar bruin vet buiten het lichaam om mogelijk te maken hebben anderen eerder al cellijnen van bruin vet uit muizen en mensen gemaakt. Deze cellen zijn genetisch gemodificeerd om hen 'onsterfelijk' te maken door herhaaldelijk te delen wanneer ze in kweek worden gebracht. Door de genetische aanpassing brengen deze cellen continu een soort tumoreiwit tot expressie, wat ze normaal gesproken niet zouden doen en dit zou mogelijk een negatief effect kunnen hebben op de functie van de vetcellen. Daarom hebben we in **Hoofdstuk 3** voorlopercellen van bruin vet van muizen en mensen genomen en door genetische modificatie ervoor gezorgd dat de cellen alleen deze tumoreiwitten tot expressie brengen wanneer doxycycline aan het kweekmedium wordt toegevoegd. Dit noemen we voorwaardelijke onsterfelijkheid. De bruin vetcellijnen van zowel de muis als mens konden in aanwezigheid van doxycycline langdurig in kweek gehouden worden waarbij het aantal cellen ongeveer elke 24 uur verdubbelde. Door doxycycline uit het kweekmedium weg te halen en door de cellen vervolgens bloot te stellen aan een cocktail van stimulerende stoffen, veranderden de voorlopercellen in volgroeide bruine vetcellen. Dit proces nemen we 'differentiatie'. Deze gedifferentieerde bruine vetcellen toonden de diverse karakteristieke eigenschappen van bruin vet: opstapeling

van vet in diverse kleine vetdruppeltjes, hoge expressie van bruin vetgenen (zoals ontkoppelingseiwit-1, UCP-1) en verhoging van lipolyse en zuurstofverbruik als reactie op activatie van de adrenerge receptor. Daarnaast vonden we dat het wegnemen van het tumoreiwit cruciaal was voor differentiatie van de menselijke voorlopercellen, terwijl de muizenvoorlopercellen ongeacht de expressie van het tumoreiwit differentieerden. In de toekomst kunnen deze nieuwe bruin vetcellijnen van grote betekenis zijn in zowel fundamenteel als toegepast onderzoek rond de energiestofwisseling van bruin vet.

Bij de ontwikkeling van obesitas-gerelateerde insulineresistentie speelt het immuunsysteem een belangrijke rol. In deze context is er tot op heden voornamelijk onderzoek gedaan naar het remmen van de ontstekingsbevorderende cytokines. Recent werd echter de aandacht getrokken door de ontstekingsremmende cytokine IL-37. Eerder onderzoek heeft aangetoond dat transgene muizen die IL-37 tot expressie brengen zijn beschermd tegen de ontwikkeling van overgewicht en de daaraan gerelateerde ontsteking en insulineresistentie. Omdat niet geheel bekend was hoe dit werkte hebben we in **Hoofdstuk 4** het effect van IL-37 op beide kanten van de energiebalans, inname en verbruik, verder onderzocht. Gedurende 6 weken voerden we muizen die IL-37 al dan niet homozygoot tot expressie brengen een vetrijk dieet en ontdekten dat expressie van IL-37 het lichaamsgewicht verlaagde en voedselinname remde. Vervolgens hebben we heterozygote IL-37 transgene muizen en controle muizen, afkomstig uit dezelfde fok als de heterozygote muizen, gedurende 18 weken een vetrijk dieet gevoerd. Wederom vonden we dat de IL-37 transgene muizen minder voedsel aten. Dit leidde tot een verlaging van het vetvrije lichaamsgewicht maar niet tot een verlaging van de vetmassa of bloedvetconcentratie. We vonden ook geen verschillen in het energieverbruik wanneer we corrigeerden voor het vetvrije lichaamsgewicht. Uit deze studie konden we dus concluderen dat IL-37 het vetvrije lichaamsgewicht verlaagt door de voedselinname te verminderen.

Vervolgens hebben we onderzocht wat er met bruin vet en het endocannabinoïdensysteem gebeurt tijdens de ontwikkeling van obesitas, door muizen een vetrijk dieet te eten te geven. Eerdere studies lieten zien dat het voeren van een vetrijk dieet aan muizen gedurende een lange tijd resulteert in zogeheten 'verwitting' van bruin vet, gekarakteriseerd door verhoogde vetafzetting, slecht werkende mitochondriën en verlaagde vetverbranding. Zoals in **Hoofdstuk 5** beschreven hebben we onderzocht hoe snel verwitting van bruin vet optreedt en welke mechanismen daarbij betrokken zijn, door muizen een vetrijk dieet te geven gedurende één, drie of zeven dagen. Het vetrijke dieet deed het gewicht van het bruin vet en de vetstapeling in bruin vet al binnen één dag toenemen. Dit ging samen met een sterk verlaagde insuline-gestimuleerde opname van glucose door bruin vet, wat erop duidt dat het weefsel binnen slechts één dag insulineresistent is geworden. Ook leek de opname van vetzuren vanuit triglyceridenrijke lipoproteïne-achtige deeltjes door bruin vet binnen één dag lager te zijn.

Hoewel het aantal mitochondriën en de genexpressie van UCP-1 niet veranderd waren, zagen we na drie dagen vetrijk dieet een verhoogde expressie van genen en eiwitten die betrokken zijn bij het fuseren en verlengen van het mitochondriële netwerk. Na drie dagen leidde het vetrijk dieet ook tot verhoogde expressie van macrofaaggenen in bruin vet. Onverwachts zagen we dat de omschakeling naar voeren van het vetrijke dieet de lichaamstemperatuur van de muizen acuut deed stijgen. Op basis van deze data concludeerden we dat één dag vetrijk voedsel eten al voldoende is om de eerste tekenen van verwitting en insulineresistentie in bruin vet te veroorzaken, wat ervoor zorgt dat de opname van glucose en vetzuren door bruin vet sterk afneemt. Verlaagde vetzuurverbranding door het gefuseerde mitochondriële netwerk en de aanwezigheid van macrofagen in het bruin vetweefsel zorgen waarschijnlijk voor het in stand houden van de verwitting en insulineresistentie in bruin vet. De omschakeling naar het vetrijke dieet zorgt waarschijnlijk voor warmteproductie in andere organen die betrokken zijn bij de verwerking van het vele vet uit het voedsel, waaronder de dunne darm en de lever, waardoor bruin vet minder actief hoeft te zijn.

Het endocannabinoïdensysteem speelt een belangrijke rol in de energiebalans omdat dit systeem betrokken is bij zowel de energie-inname als het energieverbruik. Om deze redenen wordt het endocannabinoïdensysteem gezien als mogelijk aangrijpingspunt voor nieuwe therapieën om obesitas tegen te gaan. Het was al bekend dat hoge concentraties van endocannabinoïden in het bloed geassocieerd zijn met obesitas. Maar nog onduidelijk was hoe snel het endocannabinoïdensysteem ontregelt en welke organen hieraan bijdragen. Daarom hebben we muizen verdeeld over acht groepen, waarbij één groep een regulier controledieet kreeg en de overige zeven groepen een vetrijk dieet kregen gedurende één dag tot 18 weken om zo de ontwikkeling van obesitas in relatie tot het endocannabinoïdensysteem te kunnen bestuderen. De resultaten hiervan staan beschreven in **Hoofdstuk 6**. We vonden dat de concentratie van de endocannabinoïd 2-arachidonoylglycerol (2-AG) in het bloedplasma geleidelijk steeg en dat dit gepaard ging met verhoging van de genexpressie van DAGLA en DAGLB, betrokken bij de aanmaak van 2-AG, in wit en bruin vet. Daarnaast zagen we dat de concentratie van het endocannabinoïd anandamide (*N*-arachidonoylethanolamine, AEA) in het bloedsplasma snel steeg en dat dit eveneens gepaard ging met een verhoogde genexpressie van NAPE-PLD, betrokken bij de synthese van AEA, maar dan specifiek in bruin vet. Tevens bleek er een positief verband te zijn tussen de plasmaniveaus van AEA en de genexpressie van NAPE-PLD in bruin vet. Op basis van deze resultaten concludeerden we dat het eten van een vetrijk dieet in vetweefsels snel de enzymen activeert die betrokken zijn bij de aanmaak van endocannabinoïden, die vervolgens vetstapeling en daarmee de ontwikkeling van obesitas kunnen verergeren. Het zou interessant zijn om in aanvullende studies te onderzoeken of het specifiek remmen van het endocannabinoïdensysteem

in vetweefsels een mogelijk aangrijpingspunt kan zijn tegen obesitas en de daaraan gerelateerde ziektes als diabetes type 2 en hart- en vaatziekten.

Quercetine is een stofje dat aanwezig is in groente en fruit en waarvan is aangetoond dat het in mensen de triglyceridenconcentratie in het bloedplasma verlaagt. De inname van quercetine is geassocieerd met verlaging van het risico op het ontwikkelen van hart- en vaatziekten. In **Hoofdstuk 7** hebben we onderzocht wat het achterliggende mechanisme is waardoor quercetine triglyceriden in het bloed verlaagt. Hiertoe hebben we muizen 12 weken een vetrijk dieet gevoerd met of zonder quercetine. Zoals verwacht verlaagde quercetine na negen weken de triglyceridenconcentratie in het bloed, zonder effect te hebben op de voedselinname, lichaamssamenstelling of het energieverbruik. We hebben onderzocht of de opname van vetten in de darmen veranderd was door quercetine, maar dit bleek niet het geval. Daarentegen vonden we een lichte verhoging van expressie van het *Apob* gen in de lever, dat betrokken is bij de productie van zeer lage dichtheid lipoproteïnen die rijk zijn aan triglyceriden. Quercetine verhoogde ook aanzienlijk de opname van vetzuren afkomstig van triglyceriden door onderhuids wit vet, het depot dat het meest gevoelig is voor 'verbruining'. Tevens verhoogde quercetine de expressie van de bruin vetgenen *Ucp1* en *Elovl3* specifiek in onderhuids wit vet. Hiermee overeenkomend ontwikkelden alleen de met quercetine behandelde dieren cellen in het onderhuidse wit vetdepot die positief waren voor UCP-1, wat suggereert dat dit wit vetdepot kenmerken heeft gekregen van bruin vet. Het triglyceridenverlagende effect van quercetine kan dus vermoedelijk voor een deel worden verklaard door een hogere opname van vetzuren vanuit deze triglyceriden door het onderhuidse wit vetdepot als gevolg van verbruining.

Tenslotte werden de bevindingen van dit proefschrift bediscussieerd in de context van de huidige kennis beschreven in de wetenschappelijke literatuur in **Hoofdstuk 8**. Daarnaast werden in dit hoofdstuk de door dit proefschrift verkregen inzichten in de ontwikkeling van obesitas en diabetes type 2, de gevolgen voor de klinische praktijk en de uitdagingen in het onderzoek naar bruin vet in relatie tot obesitas behandeld. De studies die beschreven zijn in dit proefschrift hebben ons inzicht vergroot in de energiestofwisseling van de bruine vetcel en de manier waarop de ontstekingsremmende cytokine IL-37 gunstige metabole effecten geeft. Maar ze hebben ook meer inzicht gegeven in de mechanismen die betrokken zijn bij de ontwikkeling van dieet-geïnduceerde obesitas en het mechanisme waardoor quercetine de triglyceridenconcentratie in het bloed verlaagt.

LIST OF PUBLICATIONS

Kooijman S, van den Berg R, Ramkisoensing A, Boon MR, **Kuipers EN**, Loef M, Zonneveld TC, Lucassen EA, Sips HC, Chatzispyrou IA, Houtkooper RH, Meijer JH, Coomans CP, Biermasz NR, Rensen PCN. Prolonged daily light exposure increases body fat mass through attenuation of brown adipose tissue activity. **Proc Natl Acad Sci U S A** 2015; 112:6748-53

Kuipers EN, Dam ADV, Held NM, Mol IM, Houtkooper RH, Rensen PCN, Boon MR. Quercetin lowers plasma triglycerides accompanied by white adipose tissue browning in diet-induced obese mice. **Int J Mol Sci** 2018; 19(6):1786

Kuipers EN*, Held NM*, van Weeghel M, van Klinken JB, Denis SW, Lombès M, Wanders RJ, Vaz FM, Rensen PCN, Verhoeven AJ, Boon MR, Houtkooper RH. Pyruvate dehydrogenase complex plays a central role in brown adipocyte energy expenditure and fuel utilization during short-term beta-adrenergic activation. **Sci Rep** 2018; 8(1):9562

Kuipers EN*, van Dam AD*, Ballak DB, de Wit EA, Dinarello CA, Stienstra R, van Diepen JA, Rensen PCN, Boon MR. IL-37 expression reduces lean body mass in mice by reducing food intake. **Int J Mol Sci** 2018; 19(8):2264

Spaanderman DCE, Nixon M, Buurstede JC, Sips HC, Schilperoort M, **Kuipers EN**, Backer EA, Kooijman S, Rensen PCN, Homer NZM, Walker BR, Meijer OC, Kroon J. Androgens modulate glucocorticoid receptor activity in adipose tissue and liver. **J Endocrinol** 2018; 240(1): 51-63

Kuipers EN*, Kantae V*, Maarse BCE, van den Berg SM, van Eenige R, Nahon KJ, Reifel-Miller A, Coskun T, de Winther MPJ, Lutgens E, Kooijman S, Harms AC, Hankemeier T, van der Stelt M, Rensen PCN, Boon MR. High fat diet increases circulating endocannabinoids accompanied by increased synthesis enzymes in adipose tissue. **Front Physiol** 2019; 9:1913

Kuipers EN*, Held NM*, in het Panhuis W, Modder M, Ruppert PMM, Kersten S, Kooijman S, Guigas B, Houtkooper RH, Rensen PCN, Boon MR. A single day of high fat diet feeding induces lipid accumulation and insulin resistance in brown adipose tissue in mice. S*ubmitted*

Kuipers EN*, Liu J*, Sips HCM, Mariadasan JC, van Dam AD, Christodoulides C, Karpe F, Zhou GQ, Boon MR, Rensen PCN, de Vries AAF, Kooijman S. Generation of conditionally immortalized murine and human brown pre-adipocytes with preserved adipogenic capacity. *In preparation*

Blondin DP, Severinsen MC, **Kuipers EN**, Jensen VH, Miard S, Jespersen NZ, Kooijman S, Boon MR, Fortin M, Phoenix S, Frisch F, Guérin B, Turcotte EE, Haman F, Richard D, Picard F, Rensen PCN, Scheele C, Carpentier AC. Human BAT thermogenesis is stimulated by the β2-adrenergic receptor. *In preparation*

Florijn BW, Klaver M, **Kuipers EN**, Kooijman S, Duijs JMGJ, Sips HCM, Rabelink AJ, van Rijn BB, Rensen PCN, den Heijer M, Bijkerk R, van Zonneveld AJ. Estrogen driven miR-224 and miR-452 expression associates with a prediabetic shift in adipocyte lipolysis, glucose uptake and mitochondrial respiration. *In preparation*

*shared first authorship

CURRICULUM VITAE

Eline Nathalie Kuipers werd op 14 februari 1990 geboren te Groningen. Daar groeide zij op met haar ouders en zus Sandra. Haar VWO diploma behaalde zij in 2008 aan het Zernike College te Haren. In datzelfde jaar begon zij met haar studie Biologie aan de Rijksuniversiteit Groningen, waarvan zij haar bachelorsdiploma in de hoofdvakken Biomedische Wetenschappen en Gedrag- en Neurowetenschappen behaalde in 2012. De bachelorscriptie over de rol van oligodendrocyten in multiple sclerose schreef zij in 2012 onder leiding van Dr. Wia Baron binnen de afdeling Celbiologie van het Universitair Medisch Centrum Groningen. Gedurende haar bachelorstudie was Eline betrokken bij verschillende organisatorische activiteiten bij onder andere het studentendesk van het Rode Kruis en de IFMSA-Groningen.

Na deze periode in Groningen verhuisde zij naar Leiden waar zij startte met haar masteropleiding *Biomedical Sciences* aan de Universiteit Leiden. In het kader van deze masterstudie deed zij twee stages: eerst onderzocht zij het effect van HDL op de activiteit van bruin vet bij de afdeling Interne Geneeskunde van het Leids Universitair Medisch Centrum, onder supervisie van Dr. Sander Kooijman, Dr. Illiana Meurs en Prof. dr. Patrick Rensen. Vervolgens analyseerde zij een *business case* voor het gebruik van de cross-farmaceutische Investigator Databank bij het opzetten van klinische studies bij Janssen Biologics B.V. (onderdeel van Johnson en Johnson) te Leiden onder supervisie van Dr. Danny Hasselbaink en Drs. Erik Coumou. In het kader van de masterstudie nam Eline ook deel aan de avondcursus *Research Based Business* en schreef samen met drie medestudenten het business plan SkinPrint, waarmee zij de *Digital Award* van de *Philips Innovation Awards* en een *Netexplo Award* van UNESCO wonnen. Ook was zij betrokken bij de organisatie van bedrijfsbezoeken aan wetenschappelijk georiënteerde bedrijven, de organisatie van het Biomedical Sciences Symposium in 2013 en was zij één maand vrijwilliger binnen het project iChange in Ho Chi Minh City (Vietnam) via AIESEC. In november 2014 behaalde zij haar masterdiploma voor *Biomedical Sciences* met als specialisatie *Management* (*cum laude*).

Na een periode van reizen keerde Eline in maart 2015 terug naar de afdeling Interne Geneeskunde van het Leids Universitair Medisch Centrum waar zij, onder supervisie van Dr. Mariëtte Boon en Prof. dr. Patrick Rensen, startte met haar promotieonderzoek gefinancierd door het *Rembrandt Institute of Cardiovascular Science* (RICS). Het onderzoek werd uitgevoerd in samenwerking met Ntsiki Held uit de onderzoeksgroep van Prof. dr. Riekelt Houtkooper van het laboratorium voor Genetische Metabole Ziekten in het Amsterdam Universitair Medisch Centrum. Eline presenteerde de resultaten van haar onderzoek tijdens verscheidene (bio)medische (inter)nationale congressen. Het promotieonderzoek, waarvan de resultaten zijn beschreven in dit proefschrift, werd afgerond in maart 2019.

DANKWOORD

Dit proefschrift zou niet tot stand zijn gekomen zonder de hulp van velen. Daarom sluit ik graag af met een woord van dank aan alle mensen die hebben bijgedragen.

In het bijzonder gaat mijn dank uit naar mijn promotor Prof. dr. Rensen en copromotor Dr. Boon. Ik wil jullie bedanken voor de begeleiding, alle inspirerende overleggen en jullie aanstekelijke enthousiasme voor het onderzoek. Beste Patrick, ik heb veel bewondering voor je toewijding en betrokkenheid die je toont in het onderzoek. Daarnaast heb ik mij heel erg op mijn plek gevoeld binnen jouw onderzoeksgroep, dankjewel daarvoor. Beste Mariëtte, dankjewel voor je onuitputtelijke positieve instelling waarmee je mij tijdens onze (bel)meetings weer op weg hielp als ik het even niet meer zag zitten. Ik heb ontzettend veel van jullie geleerd en kijk terug op een fijne samenwerking.

Prof. dr. Houtkooper, beste Riekelt, jou wil ik bedanken voor alle mitochondriële steun die ik kreeg tijdens mijn promotietraject. Ntsiki, bedankt voor alle gezellige uurtjes hangende boven de 384-wells platen, op de congressen en tijdens de koffies bij Amsterdam Zuid. Met al mijn 'metabolic-pathway'-vragen kon ik bij jou terecht. Ik heb veel gehad aan, maar ook genoten van, de samenwerking met jullie, zowel tijdens de verscheidene Rembrandt meetings als het congres in Lausanne.

Mijn directe collega's van de afdeling Endocrinologie wil ik bedanken, met wie ik niet alleen fijn heb samengewerkt maar bovenal veel lol heb gehad op de werkvloer. Andrea en Kimberly, mijn C7-buurvrouwen, bedankt dat ik altijd met mijn vragen bij jullie terecht kon en dat ik aan jullie zijde mocht staan tijdens jullie verdedigingen, die dagen waren heel bijzonder. Geerte, Rosa, Maaike, Lauren, Zhuang en Enchen bedankt voor alle hulp tijdens experimenten, samenwerken met jullie was altijd fijn. Sander, ik wil jou bedanken voor de introductie in het onderzoek tijdens mijn stage, maar ook voor je kritische blik en inventieve hulp tijdens mijn promotietraject. Laura, tijdens onze eindsprints waren de muzikale intermezzo's een fijne afwisseling van het schrijven. Lisanne, dankjewel voor alle tips en trucs die we de afgelopen jaren hebben gedeeld van leesboek tot onderzoek. Jimmy and Yanan, thank you both for sharing your wisdom, inspiration and technical skills with me. Onno, bedankt voor je farmacologische- en hormonale input bij experimenten en werkbesprekingen. Jan en Rob, ik ben blij dat ik jullie altijd kon lastigvallen met onderzoek gerelateerde zaken en mijn woordgrappen. Ook wil ik Huub, Iris, Borja, Lisa, Lisa, Milena, Joost, Anne-Sophie, Wietse, Robin, Eva, Maaike, Jorge, Cong, Zhixiong en Hiroyuki bedanken voor alle gezelligheid en de samenwerking. Zonder goede analisten ben je nergens. Chris, Hetty, Trea, Isabel, Amanda en Lianne, jullie waren onmisbaar en ik ben ontzettend dankbaar voor jullie technische

ondersteuning, het geduld waarmee jullie mij veel hebben geleerd maar ook de gezelligheid in de celkweek, op het lab en tijdens de koffiepauzes. Marjolein en Marianne, dankjulliewel voor alle hulp en ondersteuning de afgelopen jaren. Redouan, bedankt voor de goede zorgen. Natuurlijk ook de studenten die bij mij stage hebben gelopen, Luuk, Boukje, Kevin, Melanie en Jennifa, bedankt voor jullie inzet en voor alles dat jullie mij geleerd hebben.

Collega's van andere afdelingen die hebben bijgedragen aan manuscripten, werkbesprekingen, experimenten en koffiepauzes wil ik tevens bedanken. Ko, Vanessa, Jan, Lisa en Saeed van de Humane Genetica bedankt voor jullie input. Geertje, Marjan en Maaike van de Urologie, bedankt voor de vele gezellige uren in de celkweek. De collega's van de Radiologie, Nierziekten en Hartziekten wil ik bedanken voor de samenwerking op het lab, in het bijzonder Barend, Roel, Jia en Twan. Bruno from Parasitology, thank you for all your input on the insulin and Seahorse related experiments. Ben, Fred, Norma en Silvia en alle andere collega's van het PDC, bedankt voor jullie goede zorgen. Ook wil ik mijn collega's uit de kantoortuin, waaronder Bas, Michiel, Ingrid, Manuela, Friso en Aurelie bedanken voor alle gezelligheid in de pauzes. Vasudev, Amy, Mario and Thomas, thank you for collaborating on the endocannabinoid project. Denis, thank you for collaborating on the β2-AR project. Susan, dankjewel voor de fijne samenwerking en het ter beschikking stellen van jouw zorgvuldig verzamelde samples. Ook collega's van onder andere TNO, Radboud en de WUR, bedankt voor de samenwerking.

Buiten werk hebben ook veel mensen indirect bijgedragen aan mijn promotieonderzoek. Danny, mijn mentor in de wondere wereld van de farmaceutische industrie, dankjewel voor je interesse in mijn onderzoek en enthousiasmering voor jouw werkveld. Mijn 'BW-studiematen': Tessa, Eileen, Paul, Ingmar en Leonard, jullie weten als geen ander wat er bij onderzoek doen komt kijken, bedankt voor jullie 'luisterend oor' maar vooral ook voor de gezelligheid. De meiden van jaarclub Captain en damesdispuut Isis, ik ben dankbaar voor de hechte band die ik met velen van jullie heb. Bedankt voor jullie interesse, steun maar vooral gezelligheid de afgelopen jaren. Mark, ik waardeer onze vriendschap enorm, wij kunnen samen lachen en huilen maar vooral huilen van het lachen.

Tenslotte zou ik graag mijn familie bedanken. Lieve pap en mam, bedankt voor jullie onuitputtelijke steun en vertrouwen in mij. Jullie staan altijd voor me klaar en dat is een hele fijne basis om altijd op terug te kunnen vallen. Lieve oma, de telefoontjes en spelletjes waren een welkome afwisseling. Lieve Sandra, Stefan en Nora, jullie deur staat altijd voor mij open en jullie interesse en steun is hartverwarmend. San, ik kan mij geen fijnere zus voorstellen, dankjewel voor de goede gesprekken, de steuntjes in de rug, de gezelligheid, de vele vakanties en nog veel meer.

Lieve Daan, dankjewel voor je flexibiliteit en onvoorwaardelijke liefde, steun en begrip tijdens dit traject. Als ik het even niet meer zag zitten, was jij degene die mij thuis opving, de zaken relativeert en mij elke keer weer motiveert. Ik geniet van de avonturen die we samen ondernemen en kan niet wachten op de vele die nog komen gaan.